EFFECT OF A POROUS COLLAGEN-GLYCOSAMINOGLYCAN COPOLYMER ON EARLY TENDON HEALING IN A NOVEL ANIMAL MODEL

by

Libby K. Louie

B.S., Materials Science and Engineering
University of California, Berkeley, 1990

Submitted to the Department of Materials Science and Engineering
in Partial Fulfillment of the Requirements for the
Degree of

Doctor of Philosophy in Polymers

at the
Massachusetts Institute of Technology
February 1997

Signature of Author _____
Department of Materials Science and Engineering
January 10, 1997

Certified by _____
Professor Ioannis V. Yannas
Professor of Polymer Science and Engineering
Thesis Supervisor

Accepted by _____
Professor Linn W. Hobbs
John F. Elliott Professor of Materials
Chairman, Departmental Committee on Graduate Students

EFFECT OF A POROUS COLLAGEN-GLYCOSAMINOGLYCAN COPOLYMER ON EARLY TENDON HEALING IN A NOVEL ANIMAL MODEL

by

LIBBY K. LOUIE

Submitted to the Department of Materials Science and Engineering on
January 10, 1997 in Partial Fulfillment of the Requirements for the Degree of
Doctor of Philosophy in Polymers

ABSTRACT

The effects of a collagen-glycosaminoglycan (CG) copolymer on the early healing of transected Achilles tendon were studied. A novel rabbit model that isolates the tendon defect site from surrounding tissue during healing was developed in order to evaluate the effects of implanting the defect site with analogs of extracellular matrix. The objective of this study was to investigate the effect of resorbable (CG) matrices with different pores diameters on the early healing response of Achilles tendon in this animal model.

The animal model consisted of creating a lesion gap of 11±1 mm and isolating it from the surrounding tissue by a silicone tube into which the tendon stumps were inserted. In one group of animals, the tube was empty and, in the other three, it contained a CG matrix with average pore diameter of 25, 60, or 120 μm. The lesion site was protected from mechanical loading in the early stages of healing. Animals were sacrificed at intervals of 1.5, 3, 6 and 12 weeks. Tissue sections were evaluated histomorphometrically, immunohistochemically and ultrastructurally.

The results showed that the tendon stumps induced synthesis of a tissue cable inside the silicone tube in both the presence and absence of CG matrix. Histologically and ultrastructurally, the tissue cable did not appear similar to normal tendon. At 12 weeks, the new tissue in the empty tubes consisted of a dense aggregate of crimped fibers with a wavelength that was significantly shorter that in normal tendon. The average collagen fibril diameter was significantly smaller for the healing tissue compared to normal.

Tubes filled with CG matrix contained a significantly greater volume of tissue at all time periods. The presence of the CG matrix appeared to modify the kinetics of tendon healing. Unlike tissue in the empty tube, by 12 weeks, tissue in the CG-filled tubes did not have a crimp pattern. CG matrices with the 120 μm pore size appeared to have a greater percentage of fibrous tissue than CG matrices with 25 and 60 μm pore sizes. CG matrices were resorbed by 12 weeks.

Thesis Supervisor: Ioannis V. Yannas

Title: Professor of Polymer Science and Engineering

Acknowledgments

I foremost would like to thank Professor Yannas and Professor Spector for their guidance and advice through this whole experience. Thank you for allowing the space to grow as a scientist while knowing wisely when to rein me in.

I would like to also thank Professor Hobbs for being the third member of my thesis committee. It was a challenge to get you guys together but it was all worth it for your useful critiques and suggestions.

This project would absolutely not been possible without the help of Dr. Hsu with the development of the animal model and the surgical implementation of the model.

Many thanks to Sandra and Pat for taking the time to teach me about histology and TEM usage. I will never see the world the same way again.

Thanks to everyone at the Brigham and Women's Hospital Orthopedic Lab, especially Karen and Michelle who were willing to help in time of need. Thanks to Sonya, Christina, Stefan, Howie, Arun and all other cell culturists who taught me everything about keeping the cells alive and they died anyway.

Thanks to everyone at MIT past and present for all your useful and not so useful suggestions. Thanks for putting up with my whining and I promise to tell you all where everything is located before I leave. Thanks to Debbie, Lila, Diane, Bernie, Mark, Jon and Sunil for putting up with me during this stressful time in my life and despite dire threats of bodily harm kept nagging me about my thesis. Well, it's done. Are you happy now?!

Thanks (I think) to Carol who started me on this odyssey toward a Ph.D. Hurry up and finish yours!

Many thanks to my family who didn't understand why I wanted to go to graduate school, but supported me anyway.

Last, but not least, many many thanks to Desi for just being there. You're a pain in the behind sometimes but I still love ya.

Table of Contents

List of Figures

List of Tables

CHAPTER I: INTRODUCTION

1.1 Statement of the Problem

When tendon is injured with a significant loss of tissue or when a large wound gap is formed, surgical reapposition of the uninjured tendon ends is generally not feasible. If the wound is left untreated either tissue with inferior mechanical properties fills the defect site or, in the worst case, the ends of the tendon are not bridged with any tissue.

1.2 Clinical Significance

Clinically, Achilles tendon injuries can be classified into four groups with increasing severity of the injury:

I Partial to full rupture of the Achilles tendon,

II a Gap (0.5 - 1 cm) between the tendon ends,

b Gap (> 1 cm),

III Gap with complications, such as:

a. necrosis of tendon in a chronic situation

b. problems such as additional trauma to surrounding tissue,

c. open wound with possibility of infection, and trauma to surrounding tissue, and

IV Absence of tendon.

The work in this thesis is primarily targeted for clinical situations in which the severity of tendon injury is of class **IIb** and higher, in which surgical apposition of tendon ends is not possible. In clinical situations of class IIb and higher, the use of a graft material, either synthetic or biological in origin, is needed to bridge the gap between the tissue ends. This prosthesis could a) provide a resorbable scaffold in which cells could migrate, proliferate and produce repair tissue that would reconnect the tendon ends [23, 68].or b) serve as a prosthesis to provide a permanent link between to the tendon ends, thus restoring the mechanical integrity of the tissue [105]. Without a prosthesis to bridge the gap between the tendon ends, the tendon ends will not reconnect.

Though the majority of patients with Achilles tendon injury return to their pre-injury level of activity [108], there are several potential complications in Achilles tendon healing. It should be noted, the majority of patients that were able to return to pre-injury activity levels were patients with a less severe injury than those injuries to be addressed in this thesis (tendon injuries of class I or class IIa) [108]. Although there appear to be few clinical statistics on return to activity level of patients with tendon injuries of class IIb and above, it is reasonable to assume that the percentage of patients returning to pre-injury activity levels decreases with severity of the injury.

Complications due to inadequate repair of the tendon can include: tendon ends that do not reconnect or the tissue that bridges the gap is so inferior to the original tissue in mechanical properties as to compromise the function of the tendon. This can lead to either 1) reduced flexibility of the ankle joint or 2) instability of the ankle joint. Since, Achilles tendon is connected to the calcaneous bone (ankle bone) and is one of the tendons responsible for the stability of the ankle joint, the extent of Achilles tendon movement and mechanical integrity of the tendon influences the stability of the ankle joint. Reduced flexibility of the ankle joint can be due to adhesion of the healing tissue to surrounding tissues. This adhesion reduces the movement of the tendon. Reduced flexibility of the ankle joint can also be due to reparative tissue that is contracted, placing the ankle joint in an overly extended position. There is an "optimal" length-tension relationship for the muscle-tendon-bone complex [91]. When this relationship is violated, for example when the tendon is "too short", there is increased tension (referred to as over-tensioning) on the complex which can lead to reduced flexibility. Instability of the ankle joint can be due to either a lack of sufficient tissue bridging the gap or healing tissue with under-tensioning which allows for over extension/ flexion of the ankle joints which leads to instability of the ankle joint. In all cases, the patient's quality of life, particularly if the patient enjoys an active lifestyle, can be compromised.

1.3 Animal models for the study of healing of tendon injuries

Most animal models that are used to study the spontaneous healing of tendon injuries involve either partial or full transection of the tendon. Transection results in a spontaneous retraction of the tendon ends and a gap is produced. There have been very few if any studies that investigated the ability of tendon to bridge a large wound gap (i.e., larger than that formed by retraction of the cut ends). Moreover, most models are not capable of studying the intrinsic capability of the tendon to bridge a large defect because the wound site in current models are in contact with the environment surrounding the tendon. An exception is a model developed by Gonzalez [57] in the 1940s in which a polyethylene tube was placed around the lesion site of a flexor tendon in a dog. However, the surgical wound was not a gap. In Gonzalez's model the tendon was transected but the tendon ends were surgically reapposed before the tubing was placed around the wound area. There was, in effect, no gap between the tendon ends.

1.4 Current treatment for large tendon wound gaps

Current clinical treatment of large tendon wounds in which surgical reapposition of the tendon ends is not feasible involve use of a replacement tendon. Tendon grafts are of either biological [56, 68, 69, 126] or synthetic [23, 54, 62, 63, 105] origins. These prostheses are, in general, designed to mimic the mechanical properties of the tendon thereby allowing for earlier remobilization of the patient. Most prostheses are generally comprised of close-packed aligned fibers, either resorbable[23, 56, 68, 126] or permanent [54, 62, 63, 105].

Results from the use of these prostheses have been mixed. At one extreme, Kato *et al* [68] found a very favorable healing response of the tendon to a collagen-based fiber tow. Tissue that infiltrated and replaced the collagen tow had many morphological and biochemical similarities to normal tendon. In contrast, Amis *et al* [2] comparing carbon and polyester based tows, found an adverse response to the carbon implant.

1.5 Rationale for using porous analogs of extracellular matrix

The rationale for our use of analogs of extracellular matrix (AECM) to facilitate healing of tendon is based, in part, on the success in implementing such analogs for the regeneration of dermis in animals [129, 130, 132] and human subjects [11, 83, 117] and the reconnection of axons across large gaps in transected peripheral nerves in rats [16, 129]. Moreover, there is an indication that such an approach has also been successful in the regeneration of the knee meniscus [119]. Left untreated, defects of the size treated in these tissues do not heal by regeneration.

1.6 Scope of present research

The effect of an AECM on early tendon healing in a novel animal model was investigated. This AECM was a porous graft copolymer of collagen-chondroitin 6-sulfate (CG). Although the chemistry of the CG copolymer used in this study was similar to CG copolymer grafts used in dermal [123, 130, 132-134, 136] and sciatic nerve [15, 76, 129, 137] studies, CG copolymer implants of a size and configuration required for treating tendon lesions had not been previously fabricated. A protocol for the manufacturing and characterization of AECM implants for tendon treatment was developed.

A new animal model for tendon healing was developed in order to evaluate the CG implants. Criteria for selection of this model included: 1) isolation of lesion site from factors external to the injured tendon and 2) accommodation of the porous CG matrices. That the primary interest of the study was the influence of the CG matrices on the intrinsic capability of the tendon to bridge a wound gap, is why an approach was taken to minimize the effect of external influences. Previous animal models used to study Achilles tendon healing did not satisfy the criterion of isolating the lesion site from external influences.

The criteria for the animal model led to the design of an implant consisting of a CG matrix within a silicone rubber tube. The tendon ends were inserted into the ends of the

tubing. The tube formed a barrier between the lesion site and the external environment. This was the first study of tendon gap healing in a tubular construct.

In this thesis, focus was placed on the early stages of tendon healing, .i.e., the first 12 weeks after injury. Time periods of evaluation were chosen to correspond to the various phases of spontaneous tendon healing as reviewed in section 2.3. Time periods were chosen to coincide with the inflammation phase, the repair phase, and the beginnings of the remodeling phase in an animal model of spontaneous healing [8, 32, 99, 107].

As a first approach, the effect of the CG matrices' pore channel diameter on the extent of tendon healing was chosen for investigation. The extent of dermal [133-135] and sciatic nerve [15, 129, 137] regeneration was found to be a strong function of pore channel diameter of the collagen-GAG AECM.

Techniques were developed to analyze the tissue resulting from the healing process. Quantitative evaluation of the extent of healing was based primarily on the morphological appearances of the cellular and matrix components. Histomorphometric techniques were used to determine the percentage of selected types of tissue present in the lesion site at sacrifice. Immunohistological techniques and transmission electron microscopy techniques were also utilized to evaluate the cellular and matrix contents in the reparative tissue.

Lastly, preliminary studies were undertaken to determine the feasibility of tenocyte cell seeding of the CG matrices. Although seeding of chondrocytes and keratinocytes onto CG matrices of similar chemistry have been documented, seeding of tenocytes (tendon fibroblasts) have not been previously attempted.

CHAPTER II: BACKGROUND

2.1 Review of normal tendon anatomy and function

Anatomy. Tendon is a specialized dense connective tissue that links bone to muscle and allows for the transmission of muscle contraction forces to the bone. Achilles tendon links the triceps surae muscle, the grouping of the gastrocnemius, the soleus and the plantaris muscle, to the calcaneous bone. Tendon consists of three parts: the muscle attachment, the substance of the tendon itself, and the bone attachment (Figure 2.1).

Composition. Morphologically, tendon is composed of highly aligned collagen fibers sparsely interspersed with spindle-shaped cells (fibroblasts) aligned in rows along the direction of the collagen fibers, as seen in a longitudinally derived tissue section (Figure 2.2). When

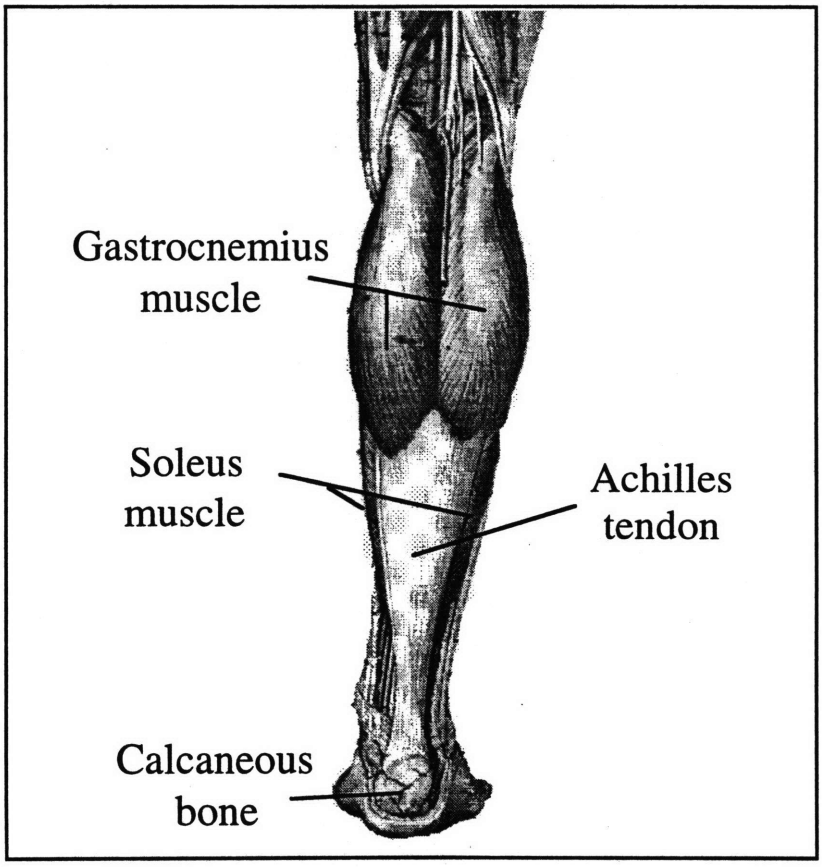

Figure 2.1. Posterior view of lower extremity in a human. The Achilles tendon connects the soleus and gastrocnemius muscles to the calcaneous bone.

viewed transversely, the cells appear as star-shaped figures among bundles of collagen.

Matrix. The major constituent of tendon is Type I collagen (approximately 86-90% dry weight), with the rest of the constituents comprised of Type III collagen, elastin, proteoglycans and glycosaminoglycans. The collagenous component of tendon is arranged in a hierarchical microstructure. The primary structure of collagen is the sequence of amino acids that make up the collagen chain. The collagen chain possess a high concentration of glycine (33%), proline (15%), and hydroxyproline (15%). The secondary structure relates to the left-hand arrangement of each primary chain and the tertiary structure describes the right-handed triple helical configuration formed from hydrogen and covalent bonding of three collagen chains into a "tropocollagen" molecule (Figure 2.3). For Type I collagen, two of the three chains are identical, called 1(I), and one is slightly different in primary structure, referred to as 2(I).

The quaternary structure encompasses several sublevels. Adjacent collagen molecules (tropocollagens) are arranged in a quarter stagger such that oppositely charged segments are aligned. Five collagen molecules in the staggered configuration form a microfibril. Collagen bundles are arranged in closely packed parallel bundles, oriented in a distinct longitudinal pattern to form ordered units of subfibrils, fibrils, and fascicles. At the fibril unit, a characteristic 64 nm periodic banding is seen by transmission electron microscopy (Figure 2.4).

Adult tendons in many species have a bimodal distribution of collagen fibril diameters [31, 65, 93, 95]. Collagen fibrils in adult human tendon have mean diameters of 60 and 175 nm [31]. Ultrastructural comparison [65] of collagen fibril diameters in various ages of rabbit tendon found that with aging, collagen fibril diameters increased. Collagen fibrils in newborn rabbit tendons were uniform in size and ranged between 18 to 55 nm in diameter with an average diameter of 37 nm; while the collagen fibrils of mature rabbit tendon ranged between 18 to 166 nm with the two most frequently encountered populations of fibril diameters measuring 55 and 92 nm.

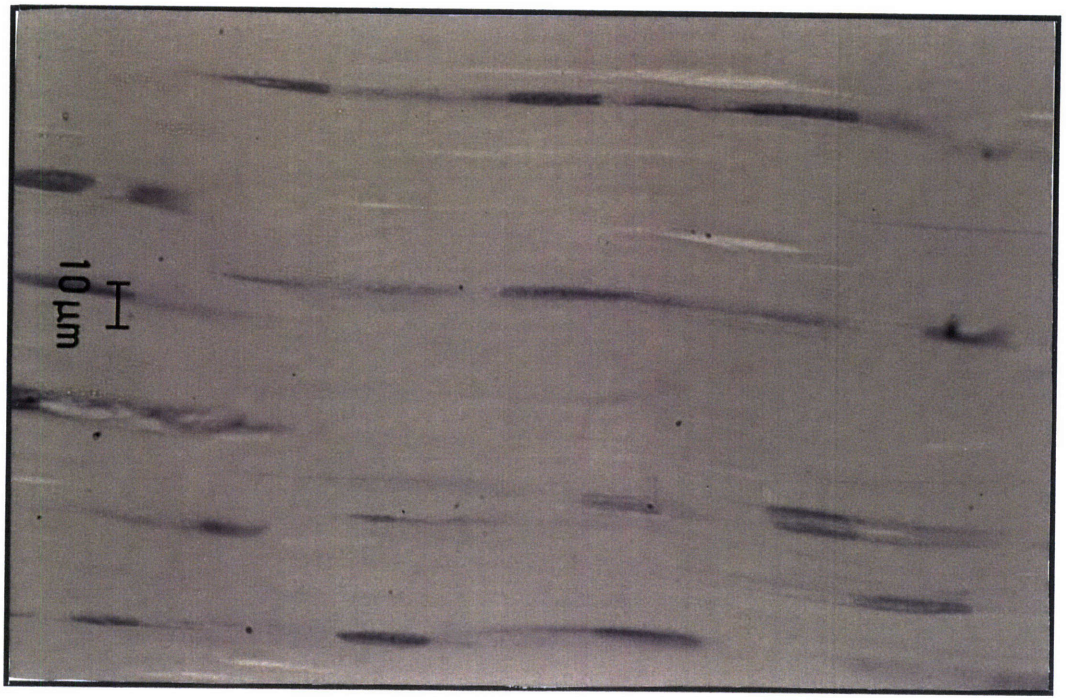

Figure 2.2. Photomicrograph of longitudinal section of normal rabbit Achilles tendon showing the spindle-shaped fibroblasts. Hematoxylin and eosin stain. Bar: 10 µm.

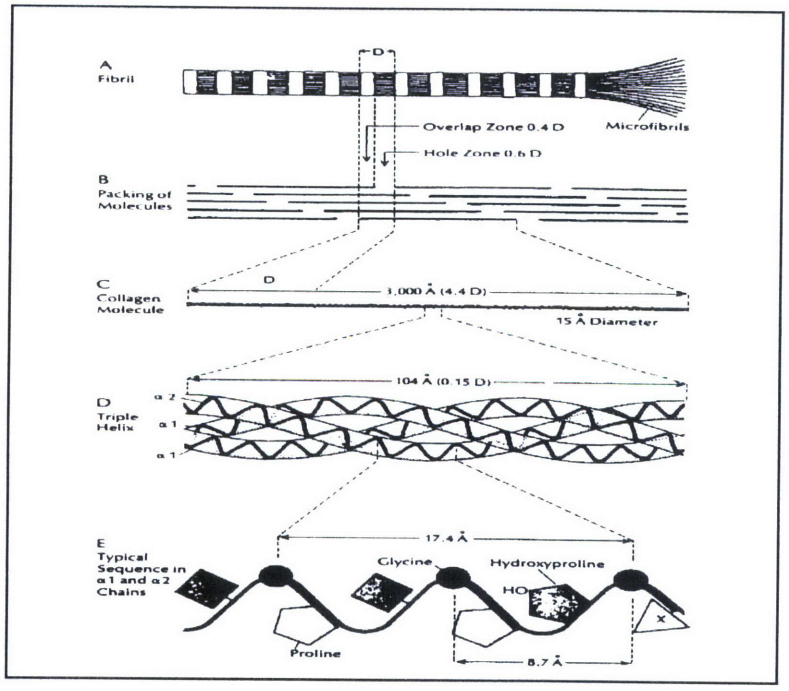

Figure 2.3. Schematic representation of the hierarchical structure of collagen to form a microfibril.

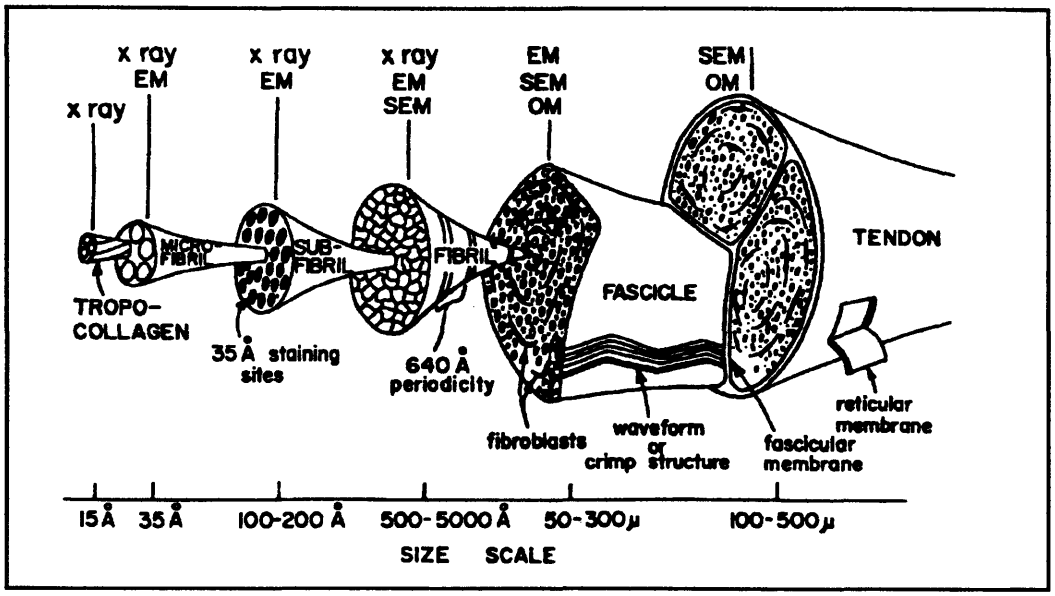

Figure 2.4. Schematic representation of the hierarchical architecture of tendon. (Modified from Kastekic *et al* (1978) [67].

A collection of fibrils bundled together form a fascicle. Fascicles are bound together by loose connective tissue that allows the fascicles to slide past one another. This loose connective tissue region, called the interfascicular membrane or endotenon, also supports the nervous tissue, blood vessels and lymphatics.

Tendons have a crimped, waveform appearance when seen under polarized light microscope (Figure 2.5a). Crimp has been observed at the level of the optical microscope. Diamant *et al* [22, 27] has shown that the crimp is a planar zigzag pattern which unfolds during initial loading of collagen. The periodicity of the alternating light and dark bands of crimped fibers can be used to determine the crimp angle, crimp length and crimp wavelength. [27, 68]. The crimp is frequently assumed to be a planar zig-zag, although other investigators have also modeled crimp as a sinusoidal waveform [20]. With these assumptions, the crimp wavelength (ℓ_c) and crimp length (ℓ) can be determined directly under polarized light using a calibrated eyepiece. The crimp angle (θ) is calculated as the inverse cosine of the crimp period divided by twice the length of the crimp. Figure 2.5b illustrates the calculation of crimp parameters from a polarized light image of normal tendon.

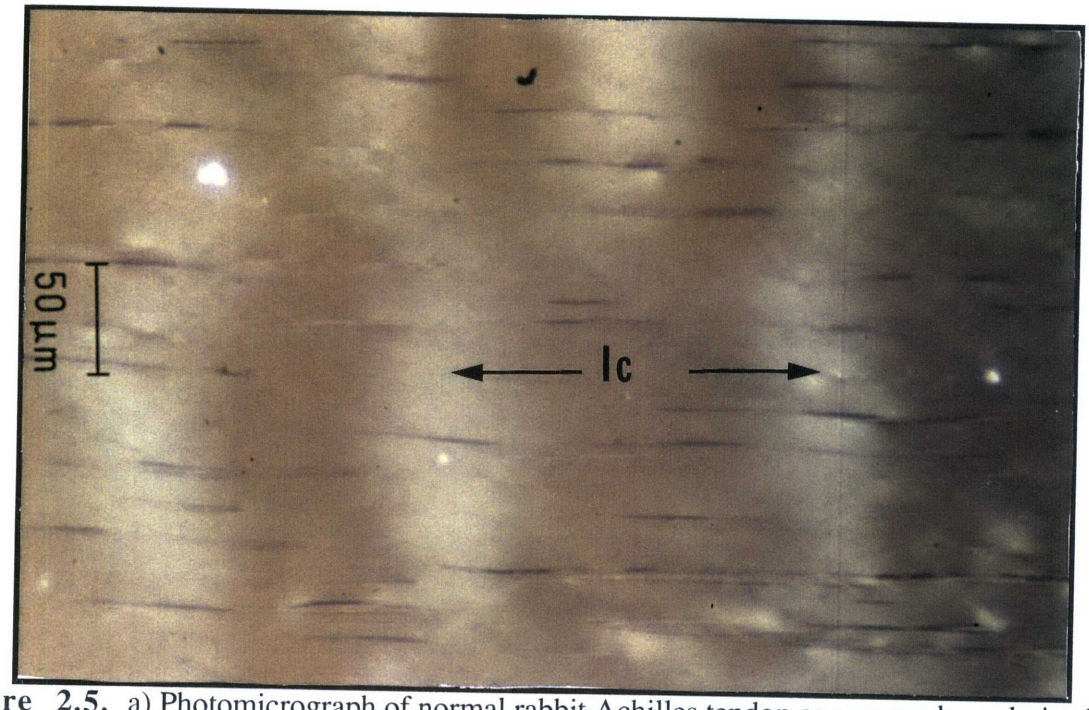

Figure 2.5. a) Photomicrograph of normal rabbit Achilles tendon as seen under polarized light showing the crimp in the collagen fibers of the tendon. The alternating light and dark bands represent the collagen fibers folding into a planar pattern. Bar : 50 µm.

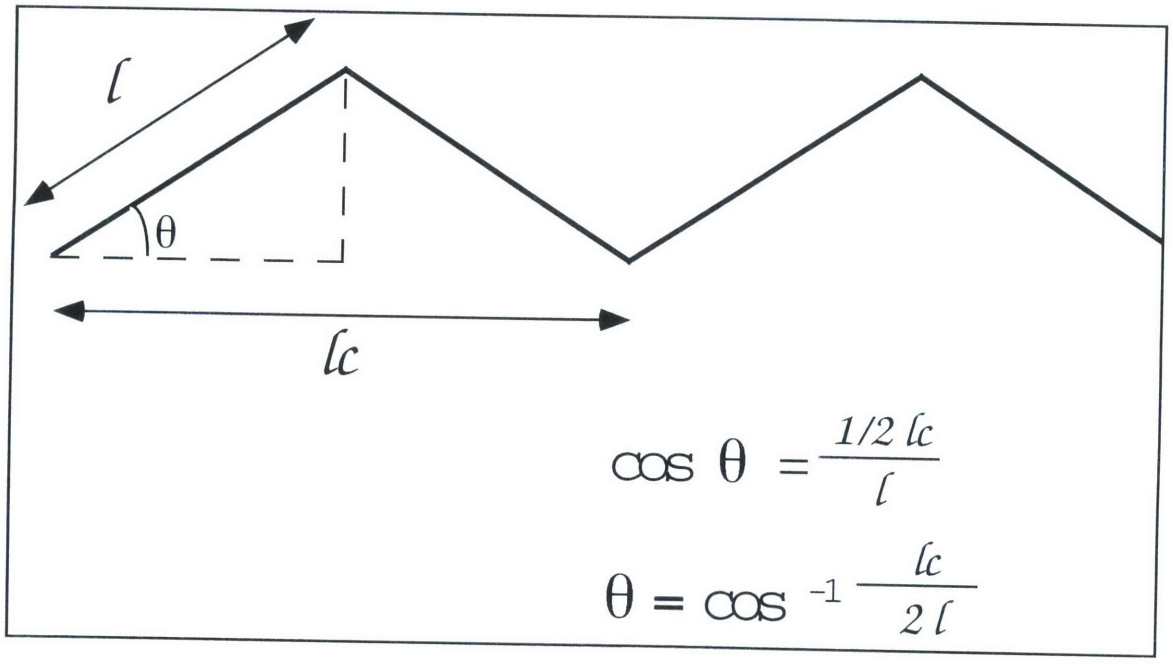

Figure 2.5. b) Diagram illustrating the calculation of crimp parameter. Crimp period (lc) and crimp length (l) are determined directed from the polarized light image. Crimp angle (θ) is calculated from the crimp wavelength and crimp length. Nomenclature adopted from Kato *et al* [68].

Tendons that generally move in a straight direction, such as Achilles tendon, have a loose areolar connective tissue, the paratenon, which is continuous with the tendon (Figure 2.6). The paratenon stretches several centimeters and recoils without tearing or disrupting tendon blood supply. An interlacing mesh work of thin collagen fibrils, elastic fibers and glycosaminoglycans gives the paratenon this elasticity and extensibility. On the other hand, tendons which bend sharply, such as the flexor tendons of the hand, are enclosed by a tendon sheath (Figure 2.6). The sheath helps to direct the path of tendon movement by acting like a pulley and allows low friction movement between tendon and the adjacent bones and joints. The sliding of these tendons through the sheath is assisted by the presence of synovial fluid between the outer wall of the tendon and the inner wall of the tendon sheath.

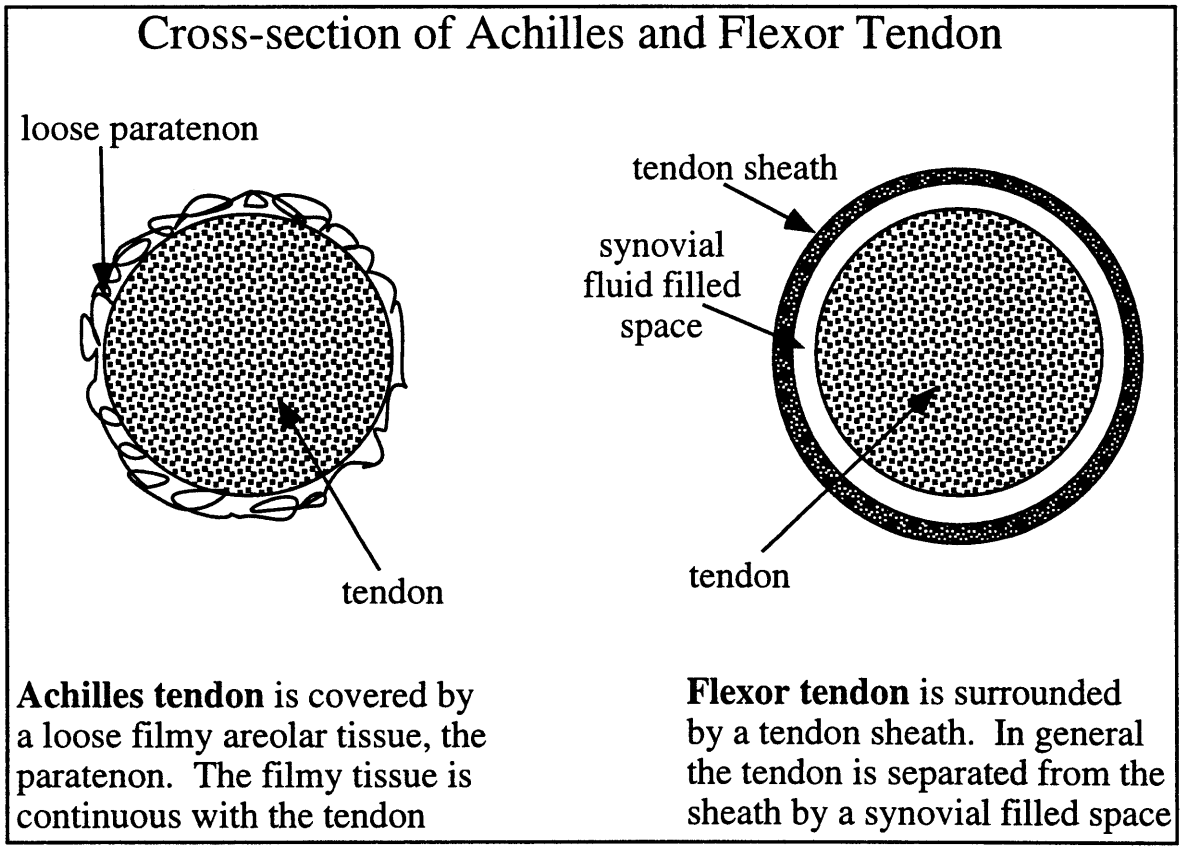

Figure 2.6. Schematic of the type of covering surrounding Achilles tendon and flexor tendon. Achilles tendon is surrounded by a loose areolar tissue, paratenon, while the flexor tendon has a tendon sheath. The tendon sheath is separated from the tendon by a synovial filled space.

Cells. Fibroblasts (also called tenocytes) form the predominant cell type in tendon. Endothelial cells and nerve processes form only a small part of the of the cell population. Ippolito *et al* [64] has shown that there is a subpopulation of myofibroblast-like cells present in normal tissue. These myofibroblast-like cells are speculated to be involved in a contractile activity [4, 50, 58, 64, 83, 114] This subpopulation of cells has been speculated to be involved in either the "tensioning" of the tendon and/or in the modulation contraction-relaxation of the muscle-tendon complex [64].

Blood supply and innervation. Tendons receive their blood supply from vessels in the perimysium, the periosteal insertion, and from the surrounding tissue via vessels in the paratenon or mesotenon. In the Achilles tendon and other tendons which are surrounded by a paratenon, vessels enter from many points on the periphery and anastomose with a longitudinal system of capillaries. Blood flow is low, averaging between 0.5 to 1.5 ml per 100 grams of tissue per minute [9, 61] and concentrated mainly on the circumferential surface of the tendon with decreasing blood supply in the interior of the tendon unit. For these reasons, tendon is considered to be a tissue of low vascularity.

Tendon has a complex set of sensory nerve receptors on its surface and throughout the tendon proper. Nerve endings function as pain receptors, vasomotor efferents, and mechanoreceptors. Mechanoreceptors sense joint position, muscle tension, and loads applied to the tendon. The stretch or deformation of a tendon can trigger a reflex muscle contraction or an adjustment in muscle tension. This reflex muscle contraction may play a role in stabilizing and protecting joints from potentially injurious movements.

Mechanical Properties. The main function of a tendon is to transmit tensile forces during muscle contraction. Because its collagen fiber structure is highly aligned in the direction of the tensile force and because collagen is one of the strongest fibrous protein in the body, tendon has one of the highest tensile strengths of any of the soft connective tissues in the body.

The stress-strain curve begins with a region call the "toe region" in which the tendon deforms easily without much tensile force (Figure 2.7). This is due to the "uncrimping" of the

crimp structure and the alignment of collagen fibers in the direction of applied stress. The toe region is followed by a linear region in which the slope of the region is referred to as the elastic stiffness, or Young's modulus, of the tendon. At large strains, plastic deformation of the tendon occurs and leads to eventual failure of the tendon. The ultimate tensile strength, the maximum stress level obtained, of tendons varies greatly from 5 to 7 MPa for mouse rat tail tendon [127, 128] to over 100 MPa for human tendon [12]. The ultimate strains, stain at which failure occurs, ranges from 9% to 35% for Achilles tendon.[12]. Achilles tendon is strained between 10 to 12% during normal activities such as walking [12, 127]. Mechanical properties measurements vary greatly with the age of donor, location, species, donor history, and testing procedures.

The mechanical properties of tendon have been specutlated and modeled as a function of the morphology and hierachical structure of the collagen fibers [20, 27, 41, 44, 93, 95] Although there have been many studies investigating the relationship between morphology and structure of collagen fibers in physiological tendon, few studies have investigated the relationship between morphology and return of mechanical properties in healing tendon [26, 41, 44] Frank *et al* [41] have investigated the possible presence of a correlation between collagen fibril diameter in healing medial collateral ligaments in a rabbit with the mechanical properties of these healing ligaments.

2.2 Tendon injury

Tendon injury occurs as a result of direct trauma, such as laceration or contusion, or indirect trauma such as tensile overload. Direct trauma frequently occurs from accidents involving sharp instruments. Although direct trauma of tendons can occur in any tendon, this is most prevalent in the tendons of the hand. Often, direct trauma of the tendon involves more than just a tendon injury; there can be accompanying nerve, soft tissue and bone damage. The complexity of the injury site complicates treatment.

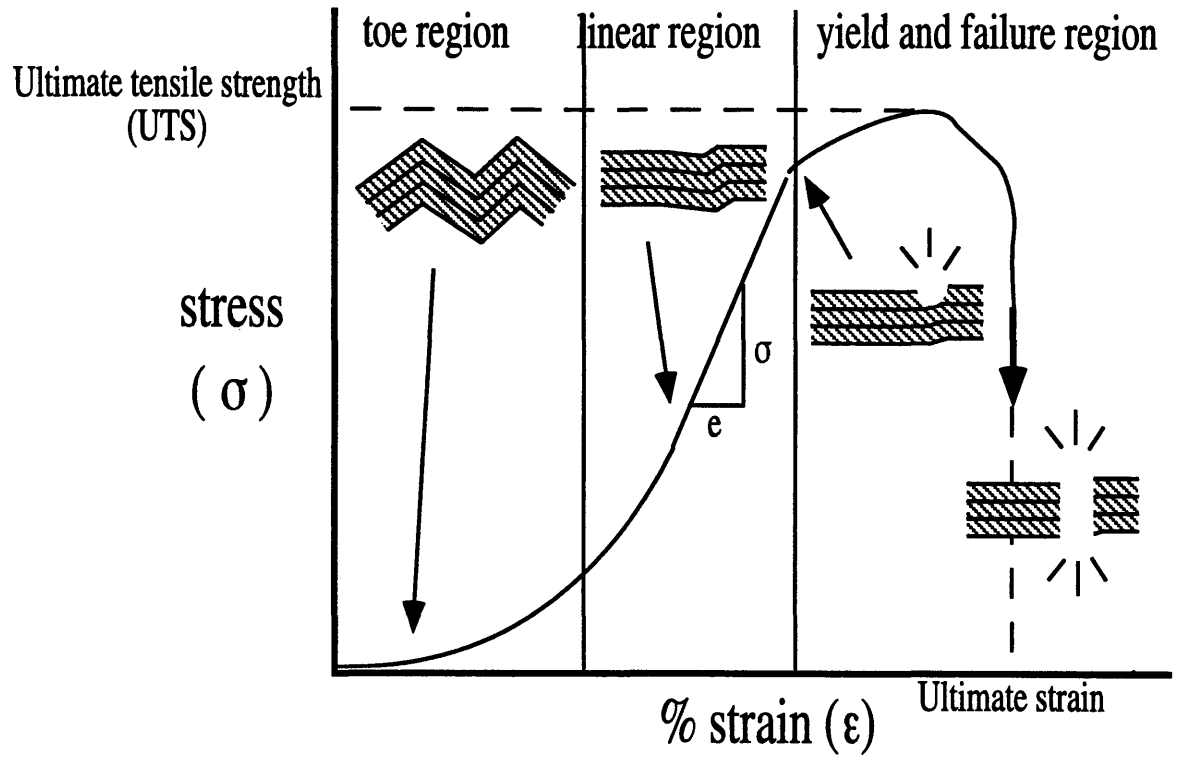

Figure 2.7. Schematic of stress-strain curve for tendon. The toe region represents the uncrimping and alignment of the collagen matrix in the direction of stress. The linear region represents the response of collagen matrix to further elongation. The curve appears linear throughout this region. The beginning of the yield and failure region is the start of matrix failure. Once maximum stress is reached, total failure in rapid.

The extent of tendon healing depends on many factors such as the anatomical location, vascularity, skeletal maturity as well as the magnitude of the mechanical forces applied. In general, failure of a muscle-tendon-bone complex occurs at the weakest link, which in most cases is the junction of the muscle-tendon complex. Indirect trauma to the tendon, itself, usually requires the presence of pre-existing pathology during mechanical overload. The classical case involves a middle-aged, typically male "weekend athlete" engaged in strenuous activities such as basketball or volleyball. The Achilles tendon rupture is often abrupt and accompanied by a popping sensation. Frequently the patient has no prior history of Achilles tendon injury or discomfort. In patients who had no prior history of Achilles tendon discomfort, there were reports of the presence of degenerative tendon tissue [19, 103, 108]

present prior to tendon rupture. Microscopic studies of Achilles tendons that have spontaneously ruptured have shown tendon tissue distant from the site of rupture to have undergone a degenerative process. There is generally fragmentation and fraying of collagen bundles and edema of the tendon [19] and a reduction of cell popluation. In some cases, there appears to be a transformation from tenocytes to chondrocyte cells with an accompanying increase in the concentration of matrix mucopolysaccharides [103] .

2.3 Spontaneous healing of tendon

Spontaneous healing of tendon has been studied extensively in both Achilles tendon and flexor tendons of the hand. Tendon healing involves the formation of scar, which is different morphologically, biochemically, and biomechanically from physiological tissue. With time, scar tissue assumes some of the characteristics of tendon; however, complete regeneration does not appear to occur. Although both Achilles and flexor tendons respond to injury by forming scar tissue, scarring in the flexor tendon appears to have a more detrimental effect on the function of the tissue. Flexor tendons need the ability to glide within their sheath to function properly and formation of adhesion sites to the sheath during tendon healing interferes with this gliding function.

Healing of a tendon covered with a paratenon (Achilles tendon). The response of Achilles tendon's response to injury follows a sequence similar to that found in other connective tissues such as ligament and skin. This sequence is generally considered to consist of four overlapping phases: injury, inflammation, repair, and remodeling.

Following tendon injury by full transection, there is a spontaneous retraction of the cut tendon ends. This retraction has also been reported to occur in a full-transection rabbit animal model for the medial collateral ligament. In the medial collateral ligament, the retraction of the cut ligament ends produced a gap as large as 2-4 mm [40]. In the Achilles tendon of both a rat and rabbit animal model, the gap formed by the retraction of ends, with the joints held in

neutral position, was observed to be approximately 9-12 mm [8]. Additional retraction of the ends can occur with movement of calcaneous and knee joints.

The response of Achilles tendon to injury has been reviewed in several articles [1, 9, 77, 127] Below is a summary of the response of tendon to a lesion produced by a full transection of tendon as reported by several authors [1, 8, 9, 32, 33, 77, 127].

Injury to the tendon triggers a cascade of events. Immediately after injury, the collagenous matrix is disrupted and tendon and blood cells die [32, 36, 37]. A hemorrhagic exudate fills the lesion site and within minutes, a fibrin clot forms and seals the wound [8]. The clot appears to contains inflammatory products (fibrin, platelets, red cells, and nuclear and matrix debris) [8, 99]. This clot has little tensile strength. These events occur within the first few hours after tendon injury.

The inflammatory stage generally starts within hours of injury and can take from 3 to 10 days to complete. This stage is associated with "clean-up" of the lesion site. Polymorphonuclear neutrophils and lymphocytes, acute inflammatory cells, invade and populate the wound site as early as hours after tendon injury. Monocytes and macrophages appear soon after the appearance of the polymorphonuclear neutrophils and lymphcytes.

The period of dramatic fibroblast migration and proliferation and matrix synthesis, the repair phase, start as early as 10 days and can take up 2 to 5 weeks to complete [8, 57]. Undifferentiated and disorganized fibroblasts containing well-developed endoplasmic reticulum from the wound edge and paratenon begin to proliferate and migrate into the wound site along the fibrin mesh of the clot. Simultaneously, endothelial cells of surrounding vessels enlarge and proliferate forming capillary buds that follow the migrating fibroblasts. Together the fibroblasts, macrophages and capillaries form the granulation tissue in the wound site [32]. This early stage of the repair phase is characterized by increased cellularity. Fibroblasts that have migrated to the wound site continue to proliferate. The fibrin clot is replaced by a collagen bridge. The collagen initially deposited in the wound site is predominantly collagen type III collagen. The collagen fibers are smaller in diameter than the collagen type I to be

deposited in the next stage of healing and are referred to as reticular fibers because of the network-like pattern of their deposition; the collagen type III fibers do not aggregate in a preferential direction the collagen type I fibers. Both collagen production and fibroblast proliferation peak during this phase (characterized as loosely organized fibrous tissue), and subsequently decrease over the next several months [37].

The remodeling phase, which can begin as early as 3 weeks and last for over 1 to 2 years, is marked by a reduction in the production of type III collagen and reorganization of the type I collagen fibers [37, 84, 99]. During the remodeling stage, the matrix fibers reorient themselves along the long direction of the tendon. This direction coincides with the direction of tensile stress in the tendon [37, 84, 99]. Figure 2.8 depicts, schematically, the re-orientation of the matrix fibers during the remodeling stage. The remodeling stage is also marked by a decrease in the number of fibroblasts present in the tissue.and a decrease in the overall volume of the scar tissue. The tensile strength of the tendon increases through this period of remodeling even though the total volume is decreasing. This increase has been explained by the reorganization of the collagen fibers, which has been observed to occur during the same period. However, Frank *et al* [37, 38, 42, 43, 84, 99] have shown that the tensile strength of healing ligament did not appear to return to normal levels even after a year. These data, appropriate to the case of the ligament, can probably be extended to the case of the tendon.

In short, the response of mature Achilles tendon to a injury involving a full transection of the tendon, results in reparative fibrous tissue that lacks the structure of normal tendon. A comparison of normal Achilles tendon and this fibrous "scar" tissue is detailed in section 2.4. There is a process of remodeling of the matrix fibers oriented in random directions to matrix fibers oriented in the longitudinal direction of the tendon, as well as a decrease in the fibroblast cell density , and an approach of the composition to normal biochemical levels. However, tendon scar does not appear to have regenerated to mature adult Achilles tendon [8, 99].

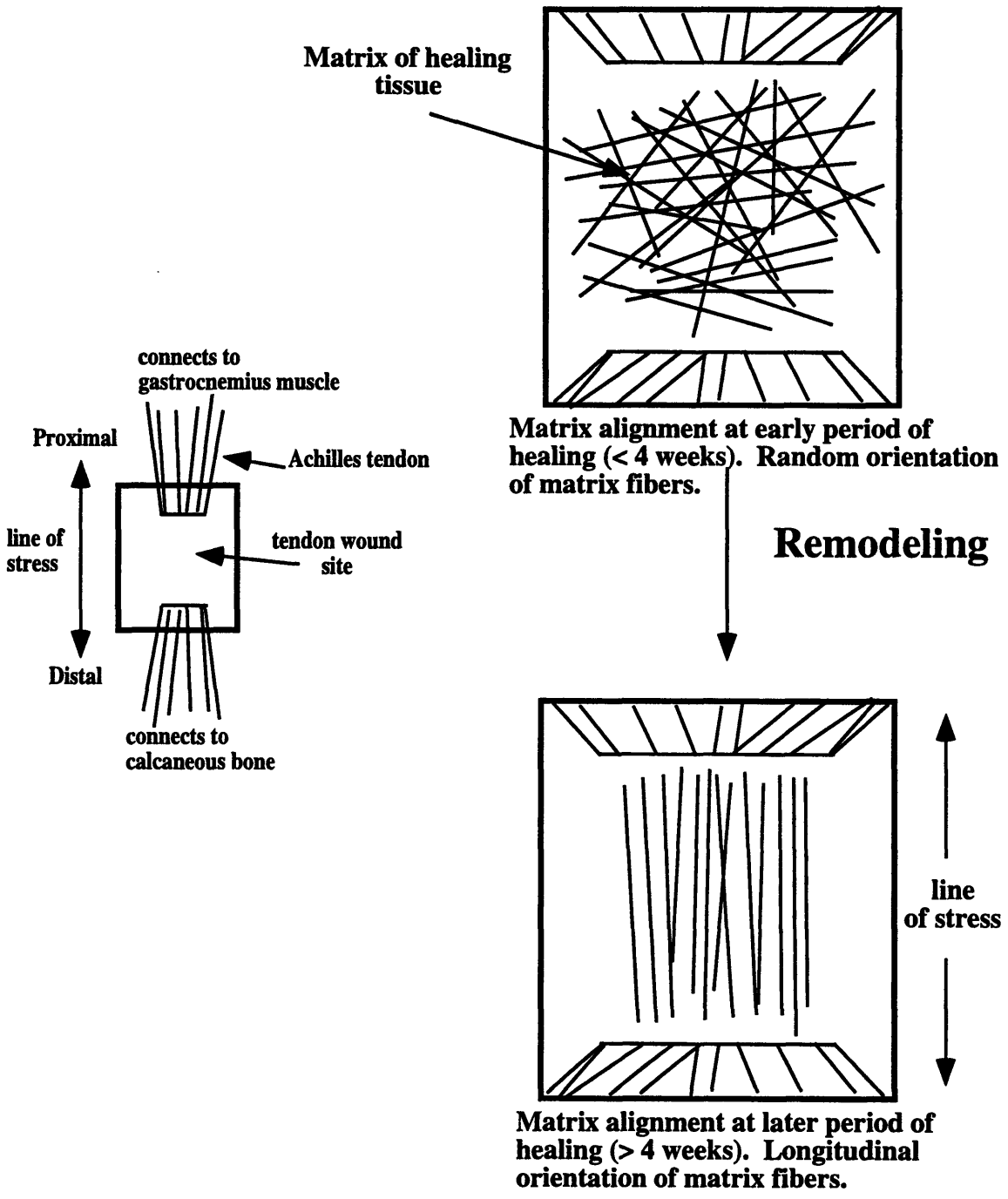

Figure 2.8. Schematic of a Achilles tendon wound site (**left figure**). An enlargement of the wound site at an early time period of healing in which the matrix fibers are oriented randomly (**upper right figure**). The same wound site at a later time period of healing (remodeling stage) in which the matrix fibers are aligned in the longitudinally direction of the original tendon. This longitudinal direction is also the same direction of the stress experienced by the tendon. (**lower right figure**).Based on structural data reported in Flynn (1965) and McGaw (1986) [37, 84].

Source of collagen producing cells. There is controversy surrounding the identity and location of the cells responsible for collagen synthesis during tendon repair, particularly flexor tendon repair. On one side of the controversy is the concept that tendon has the necessary cells to produce collagenous tissue [51, 78, 81], while on the other side, there is the belief that the source of collagen-producing cells is outside of the tendon (i.e., an extrinsic source such as the surrounding tissues or from the tendon sheath) [101, 102]. Others believe that both intrinsic and extrinsic sources of collagen-producing cells contribute to the healing process [80, 106].

In vitro studies [78, 79, 81] have shown that in response to tendon injury, cells within the tendon had the ability migrated and proliferate into the wound site. In these studies, by six weeks, the injury site appeared to be filled with collagen. *In vivo* data appears to parallel tthe in vitro studies. Matthews and Richards [53, 82] showed that cells within the rabbit flexor tendon particpated in the wound healing process when the synovial sheath was both not violated and the tendon was mobilized with early controlled passive motion. However, if the tendon sheath was compromised and the tendon was immobilized, cells from external sources (e.g., tendon sheath, blood vessels, and other neighboring tissue) migrated and proliferated into the wound site. Tendon repair, in that case, involved the participation of all surrounding tissue in the healing of the entire wound.

2.4 Normal tendon versus "scar"

Regeneration of healing tissue results in a tissue that is indistinguishable from the original tissue i.e. the new tissue is morphologically, ultrastructurally, biochemically, biomechanically, and functionally indistinguishable from the original tissue. Repair, in the classical use of the term, results in a fibrocollageneous tissue that is distinguishable from the original tissue, and generally referred to as "scar". Many studies have claimed regeneration of tendon [68, 99], but close examination of the studies shows that the tissue in question may appear to fulfill the criteria of regeneration in one area but not in another. In the field of tendon healing, regeneration and repair have, in general, not been clearly distinguished in the

literature. There is accordingly, a lack of consensus on the degree of functional recovery which can be considered acceptable to restore function.

There are many similiarities between normal adult Achilles tendon and tissue formed in a tendon wound site (Table 2.1). Both tissue tend to have highly aligned matrix fibers and a relatively low density of fibroblast cells present in the tissue. Morphologically, differences between these two tissue appear to be the crimp pattern and the average fibril diameter and distribution of the tissue. One year post-injury, Kato *et al* [68] found the crimp length of the healing tendon in their animal model, was smaller than that of normal tendon. Collagen fibril diameters were also significantly smaller than that of normal tendon [65, 99]. Biomechanically, mechanical properties of tissue formed in a tendon wound site appears to be 40-60% of normal tendon levels [8, 90].

2.5 Techniques for treatment of tendon injuries

Several studies investigated different techniques to facilitate the healing of tendon. Studies have ranged from investigation of the effect of suture technique [72, 124] to investigation of the effect of mechanical loading [8, 34, 40, 53, 62, 86, 89, 120]. on tendon healing. In the cases in which the tendon is absent or the wound site is too large to allow for reapposition of the ends , a tendon replacement is necessary. Several studies have focused on the use of biological replacements [3, 85, 121]., permanent replacements [2, 54, 63, 87, 105, 110]., or bioresorbable replacements[23, 56, 68, 69, 110] (Table 2.2). In this section, I will briefly review some of the current techniques being explored for facilitating tendon healing.

Surgical apposition of tendon ends. Considerable attention has been directed toward methods of suturing tendon lacerations and the effects of continuous passive motion on healing of this tissue. Several techniques of suturing have been proposed to increase the immediate strength of the repair, and to facilitate subsequent healing [72, 124]. Most modern techniques of suturing are variation of a technique devised by Kessler [70]. The challenge in obtaining a

Normal Tendon versus "Scar"

Criteria for comparison	Parameter measured	Normal	"scar"	Post-operative time of "scar" measurement	Reference
Morphological					
cells	density of cells	1.6 cells / mm^2	2.4 to12 cells/mm^2	1 year	Kato (1991)
	alignment/shape of cells	"spindle-shaped"	"aligned, thin"		
matrix	alignment of fibers	highly aligned	random to highly aligned	1 year	
	crimp*	crimp angle: 28°± 5° crimp length: 65 ± 10 μm	crimp angle: 25 to 35 ° crimp length: 8 to 12 μm	1 year	Kato (1991)
Ultrastructural					
cells	presence of myofibroblasts	yes	yes (staining more intense than control)	30 weeks	Ippolito (1980) Postacchinni (1978)
matrix	collagen fibril diameter	range:180 to 1600nm distribution: bimodal	range: 200 to 400nm distribution: unimodal	30 weeks	Ippolito (1980) Postacchinni (1978)
Biochemical					
	total collagen	86.8% dry wt	NR		
	collagen type I	> 95%	NR		
	collagen type III	< 5%	NR		
	GAG content	2.75 mg hexosamine/g dry wt	NR		
Biomechanical*					
	ultimate tensile strength	36.7 ± 9.4 MPa	40-60% of normal††	1 year	Kato (1991) Buck (1953)
	elastic modulus	184 ± 45 MPa			Kato (1991) Buck (1953)

* parameters defined in section 2.1

†† values for animal models such as rat model

NR: no values reported for healing Achilles tendon

Table 2.1. Comparison of normal Achilles tendon and healing Achilles tendon ("scar").

Tendon and Ligament Substitutes

Material	Advantages	Disadvantages	References
Autografts	Physiological structure Initial strength	Additional morbidity of graft Limited availabilility	
Allografts (fixed in glutaraldehyde)	Physiological structure Initial strength	Limited availability Reactivity (glutaraldehyde leaching) Possible immunogenicity	
Xenograft (fixed in glutaraldehyde)	Physiological structure Initial strength	Immunogenicity Reactivity (glutaraldehyde leaching)	Tauro (1991); McMaster (1976); Ellingsworth (1986)
Dacron	Versatility of weaves and shape Low toxicity Initial strength	Limited ingrowth of new tissue	Jaeger (1987); Park (1985)
PTFE*	Versatility of shape, structure Low toxicity Initial strength	Limited ingrowth of new tissue	Bolton (1985); Dunlap (1990)
Carbon fiber	Ingrowth potential Initial strength	Limited ingrowth fixation strength Reactivity of fibers	Gleason (1984)
Woven nylon	Biocompatibility Initial strength Low toxicity	Limited ingrowth fixation	Rueger (1986); Shieh (1990)
PGA† fibers	Biocompatibility Initial strength Bioresorption	Slight reactivity to degradation products	Howard (1985)
Collagen fibers	Biocompatibility Initial strength Bioresorption	Fibrous encapsulation if degradation rate of prosthesis not controlled	Kato (1991)

* Expanded polytetrafluoroethylene (Gore-Tex)
† Polyglycolic acid.

Table 2.2. Tendon and ligament substitutes. List of materials investigated for use in tendon and ligament substitues.
(Modified from Amadio PC, et al: Tendon and Ligament. In Cohen IK, et al (eds): Wound Healing, 1992. pp 384-395.)

suture repair of a tendon injury increases significantly the greater the segmental loss of tissue. Suturing techniques alone are not adequate for the treatment of tendon injuries with a large defect area resulting from segmental loss of tendon tissue.

Mechanical Loading during Tendon Healing. There have been many studies investigating the effect of post-operative mobilization on the healing of tendon injuries [8, 34, 40, 53, 62, 86, 89, 120]. The majority of studies investigated the mobiliation of healing flexor tendon. There is added concern of tendon scar tissue attaching surrounding tissue during healing which limits the gliding ability of the tendon. Limitation in gliding of Achilles tendon is generally not as large a concern.

Prostheses to Replace Tendons. *Tendon Grafts.* The performance of soft tissue autografts, allografts and xenografts used in treating tendon injuries have been evaluted in both human [10, 74, 109, 122] and animal [3, 85, 121]. Questions relate to the source of the donor graft, antigenicity of grafts, methods of harvesting and preserving grafts for surgery, methods of attachment to the residual tendon fragments, and proper tensioning. These grafts are generally used in situations where there is a desire to have immediate postoperative mobilization. Kato *et al* [68] used an autogenous tendon graft as a control in their study found that although the autogeneous tendon graft "had been completely filled with neotendon that was characterized by crimped, aligned collagen fibers", the neotendon was not identical to normal Achilles tendon. The "neotendon's" mechanical properties were approximately 60% of normal at 1 year and the histological morphology of the "neotendon" was not identical to normal, particularly, the crimp length was only 20% of normal at 1 year.

Permanent tendon prostheses. The search for a prosthesis to replace tendons and ligaments has been prompted by the desire to obtain immediate load bearing capability. Most of the efforts have focused on the replacement of ligaments, due to the greater number of overall ligament injuries that occur annually. Of the 33,000 tendon and ligament injuries that occur annually, two thirds were ligament injuries [115]. Prostheses fabricated from

polytetrafluorethylene, polypropylene, and carbon fibers have been investigated in animal and human trials [2, 54, 63, 87, 105, 110]. Problems generally relate to the insertion of the device into bone, proper tensioning, and issues related to the abrasion of the prosthesis against bone at sites at which the prosthesis exits a tunnel through bone. While encouraging results have been reported in the short term [54, 105, 110 Park, 1985 #149] , questions about the long-term performance of these devices have limited their use [75].

Bioresorbable tendon implants. Types of bioresorbable prosthesis currently being investigated to facilitate tendon healing include: collagen fibers tows [56, 68, 69] , resorbable fibers tows of dimethyltrimethylene carbonate - trimethylene carbonate copolymer [110], and a composite artificial tendon of poly (2-hydroxyethylmethacrylate)/ poly (caprolactone) blend hydrogel matrix and poly (lactic acid) fibers [23].

Kato and associates [56, 68, 69] have reported the use of a carbodiimide-crosslinked and a glutaraldehyde-crosslinked collagen-fiber prosthesis for the Achilles tendon of rabbits. They found that the healing response of the tendon was affected by the rate of implant degradation. The slower degrading implant (glutaraldehyde-crosslinked) was surrounded by a "capsule of collagenous connective tissue" at twenty weeks and both capsule and implant were still present at one year. Repair tissue infiltrated into the glutaraldehyde-crosslinked implant but the tissue was "not as developed" (was not as aligned and was not crimped) as the carbodiimide-crosslinked implant. The carbodiimide-crosslinked implant was resorbed by 10 weeks and was replaced with "neotendon". This "neotendon" was characterized by "aligned, crimped collagen fiber bundles" as early as at 20 weeks. However, it should be noted that Kato's study also stated that the neotendon produced was "similar, but not identical, to normal tendon", one year after implantation of the prosthesis.

2.6 Animal models used to investigate healing of tendon

Animal models are developed to study the *in vivo* response of a particular tissue subjected to various conditions. Table 2.3 summarizes some of the types of animals models

have been used to study Achilles and flexor tendon healing. The animal models listed for flexor tendon healing were limited to studies that claimed to have differentiated between intrinsic and extrinsic healing (as defined in section 2.3).

Animals models developed to investigate tendon healing involved a lesion produced either by a simple transverse incision or an excision of the tendon tissue. Models have ranged from simple transections of the tendon to excision of the whole tendon. Animal species used to study tendon healing have included the rat, sheep, rabbit, dog and chicken.

Various immobilization techniques have been employed in the animal model. Techniques include placing a plaster cast on the operated leg [62, 85] or removal of the sciatic nerve[8]. However, in many cases, since a desire to obtain immediate load bearing is an important consideration to many clinicians and patients, immobilization in many of the animal models was not utilized.

None of the tendon animal models, including those used to study intrinsic and extrinsic healing, appeared to be capable of studying tendon healing in isolation from effects due to the presence of other tissues adjacent to the injury (e.g., overlying dermal tissue, tendon sheath, neighboring blood vessels). Although these models may have accurately portrayed the clinical situation, as a model system in which to study the effects of particular test devices on the healing capability of tendon, itself (i.e. the intrinsic healing response), these models did not appear to conclusively differentiate between healing response due to the test implants and the response due to external influences. A better animal model may be one that could physically isolate the lesion site from the external environment. This would allow for a controlled, isolated environment in which to test the response of the tendon to (almost) solely the input devices. An introduction of external factors could, in the future, be introduced by choosing an appropriate lesion barrier that would allow for selected factors to move into and out of the lesion site.

Animal Models for Study of Tendon Healing

	Animal	Lesion (size of lesion)	Immobilization method (time)	Reference
Achilles tendon	rabbit	transection	None ? (45 days)	Postacchinni (1978) Davis (1991)
		excision of proximal third excision of 1.5 cm excision of 2.0 cm midsection excision of 3 cm	None None long plaster cast (6 weeks) None	Aragona (1981); Shieh (1990) Tauro (1991) McMaster (1976) Kato (1991)
	sheep	excision of (2.5 to 4 cm)	plaster (6 weeks) none	Howard (1985) Rueger (1986)
	rat	transection	? (7 days) or removal of sciatic nerve or removal of tibia and fibula external fixation knee & ankle (12 days)	Buck (1953) Murrell (1994)
Flexor tendon	dog	transection (sheath & tendon)	shoulder -spica cast or controlled passive motion	Gelberman (1983)
	chicken	transection (sheath & tendon) 50% of tissue removed	none ? (throughout post-op)	Garner (1989) Joyce (1992)

Table 2.3. The various types of animal models used to investigate tendon healing. Under immobilization method, "?" means that the author indicated that immobilization did occur but did not state the method of immobilization.

2.7 Structural and functional techniques for evaluation of tendon healing

Evaluation techniques utilized to study tendon healing can be classified into: structural and functional techniques. Structural techniques have included those at the morphological, ultrastructural and biochemical level. "Functional" techniques have included biomechanical testing and gait analysis. Table 2.4 summarizes the types of evaluation techniques employed in tendon healing and the parameters that were evaluated. Below are descriptions of the aforementioned techniques.

Structural Techniques. Structural evaluation of healing tendon, particularly morphological/ histological evaluation, is the oldest and most widely used technique to evaluate the extent of tendon healing. Knowledge of histological and morphological parameters, whether qualitative or quantitative, provides investigators with information to allow them to extrapolate the progression and extent of healing. Morphological evaluation is primarily histology-based (i.e. hematoxylin and eosin, trichrome staining), although new techniques in immunohistochemistry are being developed and adapted for tendon studies. Ultrastructural evaluation allows observation at the cellular and subcellular level. Since to a certain extent, the morphology/ function of the cells and matrix at the ultrastructural level is a determinant of ultimate "gross" tissue properties and morphologies, ultrastructural evaluation is an important tool. Biochemical analysis provides quantitative information about the chemical composition of the tissue.

Morphological evaluation. Historically, the extent of tendon healing was evaluated qualitatively by comparing histological sections of repair tissue to normal tendon [8, 52, 53, 68, 71, 99, 116]. This subjective method of evaluation provides useful information on the qualitative histomorphology of the cellular and matrix components in the tissue. The major drawback of a qualitative evaluation is it subjectiveness. One investigator's criteria are not necessarily another's. This leads to a technique that lacks objectivity and reproducibility.

Histomorphometry, the term used to describe the variety of methods for measuring morphological features in histological images, is steadily being adapted for use, particularly in

the field of histopathology [59]. The field of tendon healing still relies primarily on qualitative, descriptive terms for microscopic structures. The combination of interpretative qualitative assessment backed by specific quantitative methods could lead to better evaluation of the extent of tendon healing. In the past 20-25 years, new techniques have been developed or adopted from other fields to quantitatively evaluate the morphology of tendon tissue. These include measurement of the extent of matrix alignment with small angle x-ray analysis, image analysis of matrix alignment under a scanning electron microscope, determination of the percentage of fibers that are aligned relative to a predetermined axis when viewed under a light microscope.

Ultrastructural evaluation. Ultrastructural evaluation of healing tendon tissue provides information on the substructure of the cells and the structure of the matrix, such as collagen fibril diameter. Knowledge of the structure and substructure of the cellular components provides information on the functional state of the cells, such as the metabolic state of the cells (appearance of the rough endoplasmic reticulum, Golgi apparatus, etc.). Since tendon is composed primarily of collagen fibrils which provide the structural integrity of the tissue, knowledge of the collagen fibril diameter and distribution could in principle be extrapolated to predict the mechanical properties of the tissue [41, 93], especially when a quantitative model is used [20] .

Biochemical evaluation.. Biochemical assays are useful tools to evaluate the extent of healing because it allows for a direct quantitative comparison of particular biochemical components found in tissue. Biochemical assays are presently used to quantify the total amount of collagen present, the collagen type, the extent of collagen crosslinking, the amount of GAG's, and the DNA concentration. A drawback, is that these assays are destructive techniques. This is particularly a drawback in situations in which there is not a relatively large mass of tissue available to provide test material for evaluation by other techniques.

Types of Evaluation Techniques

	Parameter to be evaluated	Technique employed	Advantages	Disadvantages	Reference
Structural Gross Morphological	reconnection, volume of repair tissue, general appearance	gross observation	quantitative size measurements	generally, a qualitative approach	
	cell density	light microscopy	cell count possible	generally, qualitative	Kato (1991)
	cell shape	light microscopy		use of descriptive criteria such as "spindle-like"	
	types of cells present	histological or immunohistological stain	localization of cellular products	generally, qualitative	
	matrix alignment	small angle x-ray scattering (SAXS)	quantitative; simple	specialized equipment	Brodsky (1994)*; Sacks (1992)*
		scanning electron microscopy; measurement of % fibril off predetermined axes	quantitative	time consuming even with computerization	Frank (1991)*
		light microscopy; estimation of % fibrils off predetermined axis	fast, simple	time consuming	
	crimp appearance/ measurement	polarized light microscopy; correlation of interference pattern with crimp parameters	simple measurement		Kato (1991); Goodship (1985)
	types of matrix component present	histological or immunohistological stains	localization of matrix products	generally qualitative	

Table 2.4. Summary of techniques currently used to evaluate tendon healing.

	Parameter to be evaluated	Technique employed	Advantages	Disadvantages	Reference
Ultrastructural	collagen fibril diameter/ distribution	transmission electron microscopy (TEM); fibril measurement of micrographs (semi-automated, manual)	quantitative	time consuming	Postacchini (1977,1978)
	types cells present	observation under TEM		in general qualitative	Enwemeka (1991)
Biochemical	water content GAG content total collagen content collagen typing DNA content	biochemical assays	quantitative	tissue destroyed in process (disadvantage if mass of tissue small)	Williams (1980) Ippolito (1980)
Functional Biomechanical	stress-strain curve ultimate tensile strength (UTS) elastic modulus (E) ultimate strain	mechanical tensile testing under simple tension	quantitative; established techniques	scarifice of animal; entire tissue dedicated for testing therefore no other evaluation techniques can be performed on tissue	Takai (1991); Rueger (1986); Davis (1992)
Functional walking analysis	measurement of paw prints of walking rat	correlation of paw prints measurements to function of tendon	sacrifice of animals not necessary for measurement	technique appears best suited for rat/rodent model only	Murrell (1994)

* Technique applied to "aligned" tissue but not specifically tendon

Table 2.4. (cont.) Summary of techniques currently used to evaluate tendon healing.

Functional Techniques. Because functional techniques developed for clinical evaluation generally involve either the active participation of the patient or verbal feedback by the patient, different "functional" techniques have been utilized for evaluation in animal models. Biomechanical testing, although not a functional test in the strict sense, is the most widely used "functional" technique in the field. In recent years, investigators have adopted a functional walking test originally used to evaluate sciatic nerve function to evaluate tendon healing in vivo [7, 89, 90].

Biomechanical evaluation. Biomechanical testing in vitro provides a measure of the mechanical properties of the tissue in vitro but these properties do not necessarily give a true indication of tendon functionality in vivo. It should be noted that in theory, morphology can predict mechanical properties but a set of mechanical properties can not necessarily predict one particular morphology, but rather a set of potential morphologies. Mechanical properties are good comparative measures of different treatment groups, not necessarily a predictor of morphology. Current mechanical testing include measurement of stress-strain curves at constant strain rates, ultimate tensile strength (UTS), ultimate elongation, and elastic modulus at a specified strain.

Functional walking test. A walking test originally developed to evaluate the functional state of sciatic nerve damage in rats [24] was adopted by investigators to evaluate the extent of Achilles tendon healing [7, 90]. Measurements of paw prints recorded from a rat walking down a narrow track included: the plantar length, toe spreading, and distance between intermediary toes. Murrell and associates [89] claimed that these measurements "provided sensitive and reliable indicators of Achilles tendon function". The major advantage of this method is that, unlike biomechanical evaluation, the animal does not need to be sacrificed in order to provide the measurements. This allows for temporal studies utilizing fewer animals.

2.8 Previous studies of tissue regeneration using collagen-GAG copolymers

Several investigations have reported the use of collagen-based materials for the regeneration of tissues. Analogs of the extracellular matrix have been used to facilitate the regeneration of tissue in three cases, (a) the dermis in fully excised skin wounds in the guinea pig [129, 132] and in the human [11, 60, 83], (b) the rat sciatic nerve across a gap of 15 mm, [16, 137] and (c) the knee meniscus of the greyhound following 80% transection [118, 119]. The effects were strongly tissue-specific, in that different ECM analogs were found to be necessary in each case. These results, especially those obtained with the standardized rat sciatic nerve lesion, in which a cylindrical ECM analog with longitudinally aligned pore channels was fabricated, strongly suggest the value of studying tendon healing in the presence of an appropriately modified ECM analog.

Previous studies in animal models of skin loss and peripheral nerve loss have shown that the rate and completeness of tissue regeneration depend critically on the pore diameter and degradation rate of the ECM analog used [15, 129, 132, 135, 137]. For example, regeneration of the dermis in guinea pigs occurs when the average pore diameter of the ECM analog was in the range 20-125 μm [130-132, 136]. Other studies showed that regeneration of sciatic nerve in rats required an average pore diameter less of than 10 μm for optimal recovery of function [15, 16]. These results suggest that the optimal pore diameter for an ECM analog which induces regeneration is a tissue-specific property. If so, design of devices for treatment of tendon could also require optimization of pore diameter in order to achieve recovery of function fastest and nearest to physiological levels. This research is directed towards identification of the effect of pore size of such devices on the healing of tendon.

CHAPTER III: PROCESSING OF CG MATRICES

3.1 Introduction

It has been shown that the properties of the tissue formed in response to Achilles tendon injury are different from the original tendon [8, 32, 99, 127]. Previous studies have investigated the implantation of prostheses of either synthetic or biological origin into Achilles tendon lesion sites [23, 54, 56, 62, 63, 105, 126]. These prostheses were generally close-packed aligned fiber tows, both of resorbable and non-resorbable material designed primarily to mimic the mechanical properties of the tendon [23, 54, 56, 62, 63, 105, 126] . There are no studies to date on the in vivo response of tendon healing to porous resorbable sponge-like prostheses.

Analogs of extracellular matrix (AECM) comprising of porous resorbable collagen-glycosaminoglycan (CG) copolymers have been used to facilitate the regeneration of tissue in three cases: (a) the dermis in fully excised skin wounds in the guinea pig [129-134], and in the human [11, 60, 88, 117] (b) the rat sciatic nerve across a gap of 15 mm [129, 131, 137] and 10 mm [15, 129, 132] and (c) the knee meniscus of the greyhound following 80% transection [118, 119]. The effects were strongly tissue-specific, in that different AECMs were found to be necessary in each case. These results suggest the value of studying tendon healing response in the presence of an appropriately modified analog of extracellular matrix. Previous work has shown that the healing kinetics of both dermis [123, 129-132] and sciatic nerve [16, 21, 129, 132] are a function of the collagen-glycosaminoglycan matrix characteristics, such as the average pore size and the degradation rate of the matrix.

The porous collagen-glycosaminoglycan copolymer matrices are produced via a multi-step process involving; 1) the production of a suspension of collagen-glycosaminoglycan coprecipitates in 0.05M acetic acid, 2) the freezing of the suspension to form ice dendrites, 3) the sublimation of the ice dendrites to leave behind a porous foam composed of a collagen-glycosaminoglycan graft copolymer [21, 133, 134], and 4) the dehydrothermal treatment of the

foam to form crosslinks between the collagen and the glycosaminoglycan [134]. The second and third steps in this process are commonly grouped together and referred to as the process of freeze-drying, or also referred to as lyophilization [55]. In this method of freeze-drying, the pore size, pore morphology, and pore distribution of the matrix are determined by the process of ice dendrite formation.

Collagen-glycosaminoglycans copolymer matrices have been produced in different geometric configurations (Figure 3.1). CG matrices used to study dermal healing are fabricated as a sheet approximately 2 mm in thickness with pore diameters ranging from 5 μm to over 300 μm [123]. The CG matrices used to study sciatic nerve healing are fabricated inside a silicone tube as a cylinder, 1.5 mm in diameter [76] with pore diameters ranging from 5 μm to over 200 μm. Figure 3.2 shows a schematic of the CG matrix graft used in this work to investigate Achilles tendon response to these grafts and a list some of the variables of the structure of the matrix.

AECM devices used in the study of peripheral nerve regeneration possess the same general shape as that in the study of Achilles tendon healing but with considerably smaller dimensions. The diameter of nerve AECM is 1.5 mm [76] compared to the tendon AECM of 3.8 mm. Although Loree [76] had investigated the effect of manufacturing conditions, degree of undercooling and velocity of immersion into the coolant bath, on the pore size and pore channel orientation for the nerve AECM, his study was duplicated for the larger tendon AECM in this work in order to account for the over 2x increase in diameter.

This chapter addresses the effects of two manufacturing parameters on the pore size, orientation and uniformity of 3.8 mm diameter CG cylinders. The parameters, temperature of the coolant bath and the velocity with which the CG suspension is immersed into the bath, have already been investigated for smaller diameter (1.5 mm) cylinders used for nerve regeneration [76].

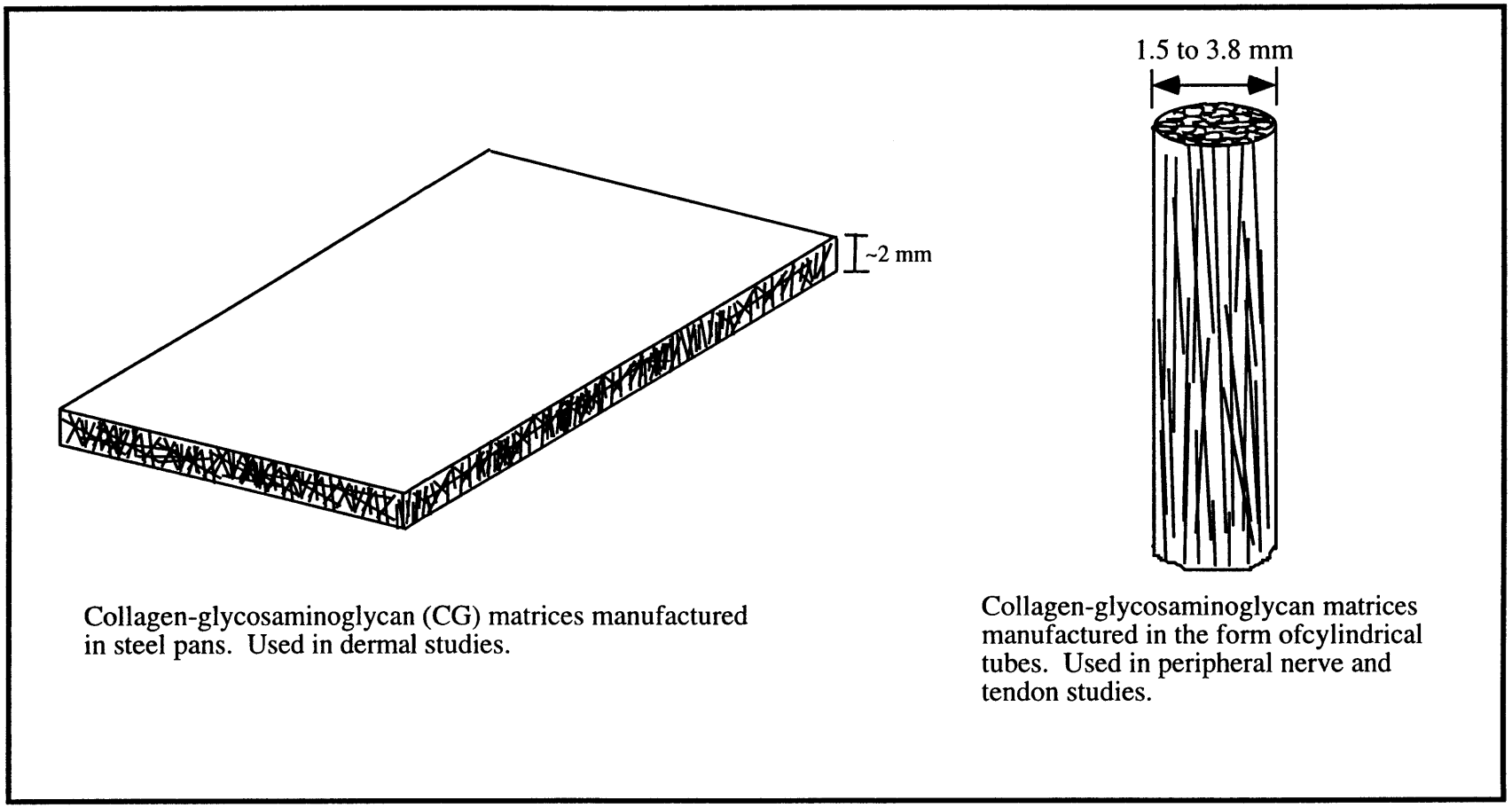

Figure 3.1. Schematic of the different geometric configurations of collagen-glycosaminoglycan (CG) matrices.

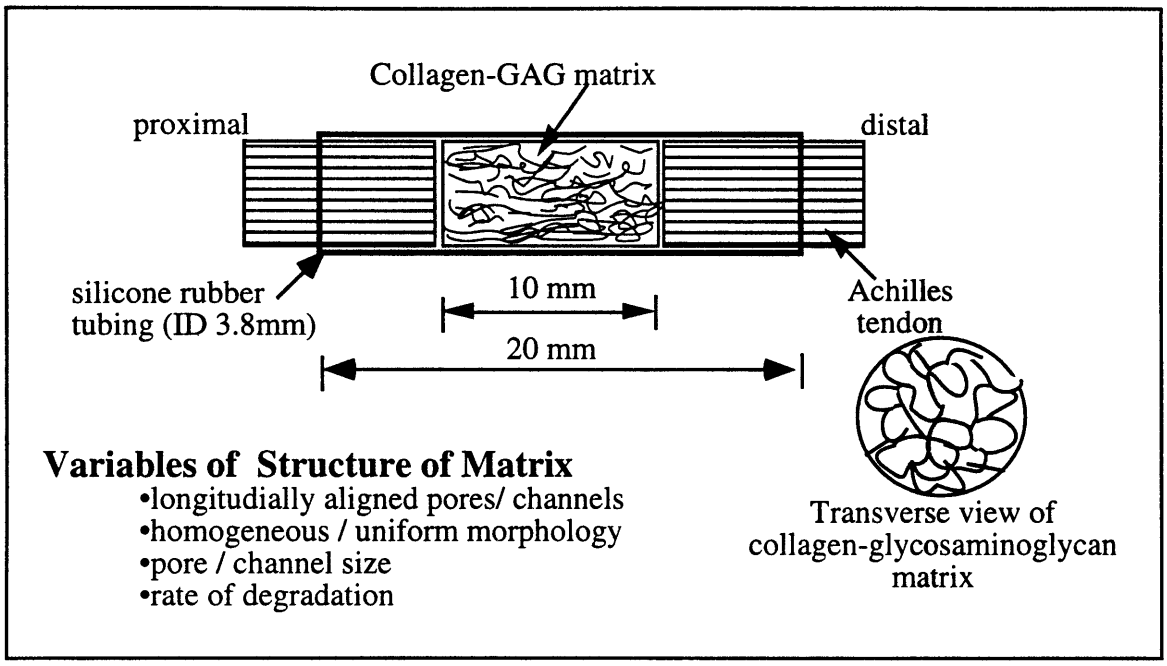

Figure 3.2. Schematic of a collagen-GAG matrix encased in a silicone rubber tube used in the study of tendon healing.

The study in this chapter had a two-fold purpose: 1) to map pore size diameters and morphology as a function of processing parameters at the larger cylinder size, which was used as a guide in the choice of matrices used to study tendon healing in the presence of matrices of different pore sizes (Chapter 4) and 2) to compare the results obtained in Loree's work at the smaller implant diameter with the results obtained in this study using the larger implant diameter.

3.2 Theory of processing of collagen-glycosaminoglycan matrices

The pore diameter, distribution and morphology of the collagen-glycosaminoglycan matrices are determined by the process of ice dendrite formation. A brief description of this process will be presented below along with a review of the process of freeze-drying, and a summary of the heat transfer model for the solidification of the CG suspension developed by Loree [76] . A more extensive overview of theory of CG individual process steps in the matrix manufacturing can be found in Loree's Master thesis [76].

3.2.1. Dendritic solidification

The process of solidification involves the solidification of water to form ice dendrites. Solidification of water begins with the formation of an ice nucleus followed by crystal growth. Crystal growth is dependent on the supply of water molecules in the liquid phase to the growing crystals and the removal of the latent heat of freezing. In the process for manufacturing collagen-glycosaminoglycan matrices for tendon studies, latent heat is removed by conduction through the ice that has already formed. The freezing rate of the water is directly related to the magnitude of the temperature gradient through the ice [25].

Control of the size of the ice dendrites formed in the collagen-glycosaminoglycan suspension has been studied by Irving [66], Chen [18], and Loree [76]. The temperature at which the collagen-glycosaminoglycan suspension is frozen appears to influence the pore channel diameter. Irving found that for CG matrices produced in a steel pan, the mean pore diameter decreased with decreasing temperature in a roughly linear fashion [66]. CG matrices produced in Irving's work were thin (2 mm thickness) sheets of matrices.

The CG matrices used in this thesis were similar in shape to those used in the study of peripheral nerve healing. Processing of these matrices involved the lowering of an enclosed tube of CG suspension into a freezing bath (see section 3.3 for full description of processing procedure). Loree [76] showed that the pore size and pore morphology of these cylindrical shaped matrices were influenced by both the temperature of freezing and the velocity at which the suspension is lowered into the freezing bath.

3.2.2. Freeze-drying theory

The process of freeze-drying (lyophilization) involves the sublimation of ice dendrites. Sublimation is the phase transformation from a solid phase to a gaseous phase. Figure 3.3 depicts the phase diagram of water. Considering only the liquid component of the collagen-glycosaminoglycan suspension (i.e., 0.05M acetic acid), the water (acetic acid) is at a liquid state at room temperature and atmospheric pressure (760 torr) [point A]. Decreasing the

temperature (at constant pressure) below 0°C freezes the water; producing a solid state [point B]. The pressure (at constant temperature) is decreased to below the triple point [point C]. The solid phase is transformed to a gaseous phase by raising the temperature (at constant pressure) [point D]. Since sublimation is a diffusion driven process, the reticular structure of the solute (collagen-glycosaminoglycan) component is not disrupted by the sublimation process. Once the sublimation process is complete, the matrix is brought back to room temperature and atmospheric pressure. What was once an ice dendrite is an empty pore in the collagen-glycosaminoglycan matrix.

3.2.3. Heat transfer theory of collagen-glycosaminoglycan solidification

A simple model to predict the dimensions of pore structures produced under various conditions of freezing bath temperature and velocity of immersion into the freezing bath was

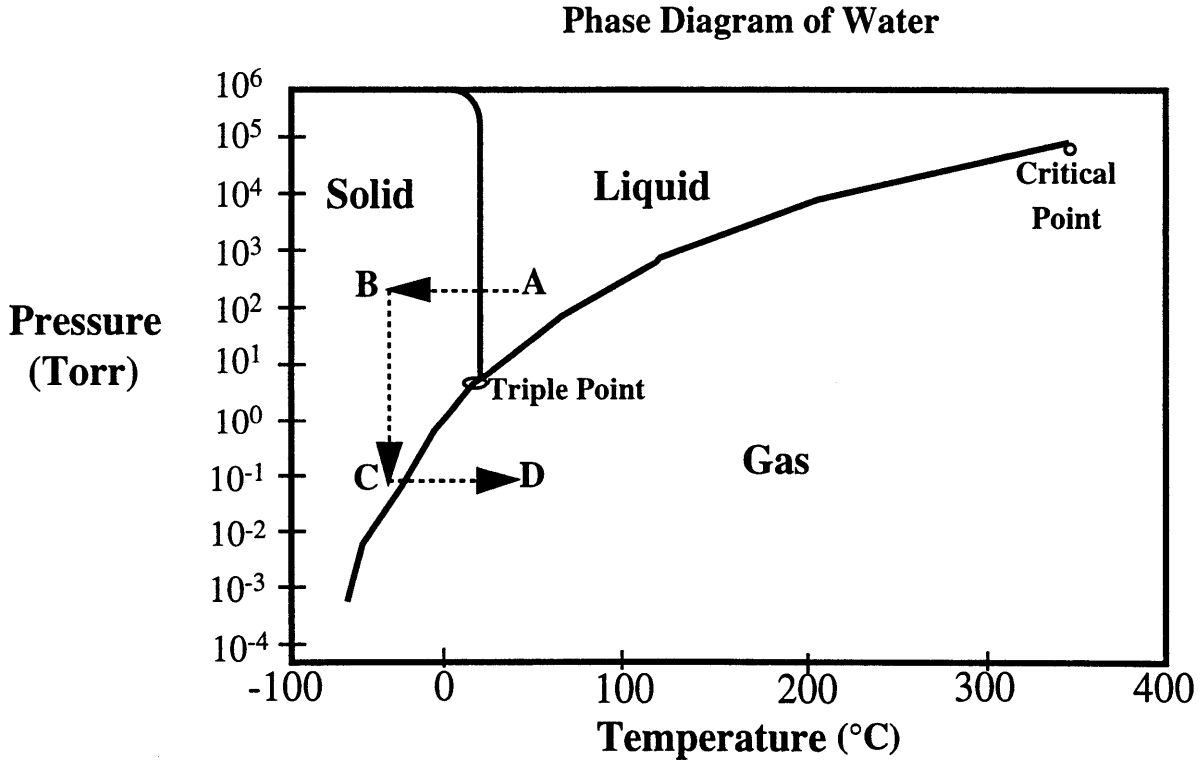

Figure 3.3. Phase diagram of water. The process of freezing-drying is outlined as following: phase transformation from liquid phase to solid phase (point A to point B); decrease of pressure (point B to point C); phase transformation from solid phase to gaseous phase (point C to point D)

developed by Loree [76]. A summary of Loree's theory along with the prediction of pore structure under various conditions will be presented below. A complete description of Loree's theory can be found in his Master's thesis [76] .

Loree's theory for the solidification of the collagen-glycosaminoglycan suspension describes the effect of the temperature of the freezing bath and velocity of immersion of the collagen-GAG suspension into the freezing bath on the pore structure of the CG matrix. Loree's model predicts that at a slow rate of freezing (small ΔT, slow V), the pore channel orientation is strongly axial. At a fast rate of freezing (large ΔT, fast V), the pore channel orientation is strongly radial. A dimensionless ratio, Mi, called the Mikic number was derived as a function of the velocity of immersion and temperature of freezing. The Mikic number, defined as the ratio between the radial freezing time and the convective time reduces to the following equation:

$$Mi = \frac{t_r}{t_c} = Const \frac{LV}{\Delta T^*}$$

where:

t_r = *radial freezing time*

t_c = *convective time*

L = *distance below bath surface at which suspension freezes at midline of cylinder*

V = *the velocity of immersion*

$\Delta T^* = T_{freeze} - T_{water}$

T_{freeze} = *freezing temperature*

T_{water} = *temperature at inside wall of jacket*

Const = function of material and heat transfer properties of solid, liquid and jacket.

Under slow freezing conditions, L is small and Mi is low (less than one). At fast freezing conditions, L is large and Mi is high (greater that one). Loree's prediction of pore orientation is summarized in Figure 3.4. For $Mi \ll 1$, the pore orientation is predicted to be strongly axial; conversely, for $Mi \gg 1$, the pore orientation is predicted to be strongly radial.

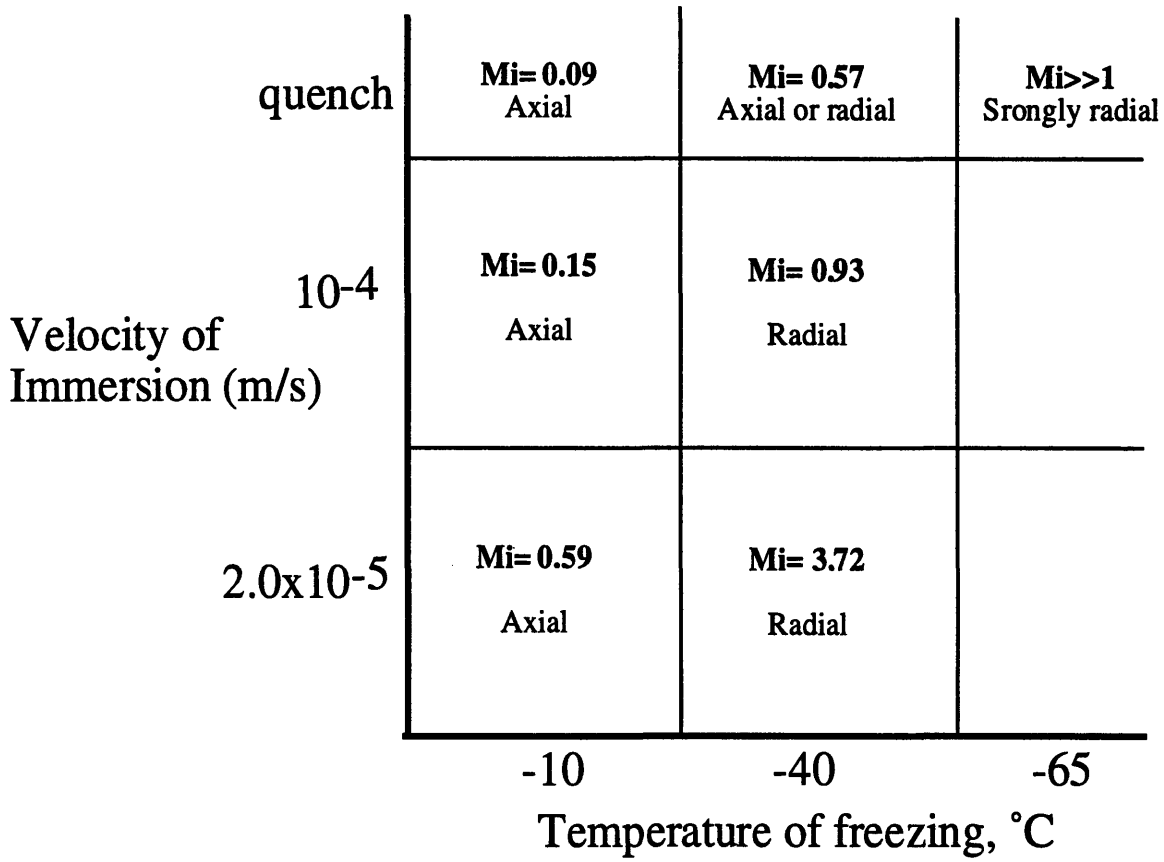

Figure 3.4. Prediction of Orientation for typical values of temperature of the freezing bath, T and velocity of immersion, V from Loree's theory for the solidification of CG suspension. (Modified from H. Loree (1988). In Loree (1988), the degree of undercooling, ΔT, is used in place of temperature of freezing. The degree of undercooling is defined as the difference between the freezing temperature of the collagen-GAG suspension and the freezing bath temperature. The degree of undercooling is approximately the temperature of the freezing bath in this case.)

3.3 Materials and Methods

3.3.1. Manufacturing of collagen-glycosaminoglycan tendon grafts

Protocols for the fabrication of collagen-glycosaminoglycan (CG) copolymers used in the study of Achilles tendon healing are adaptations and modifications of protocols for the fabrication of CG matrices used in dermal [123] and sciatic nerve [76] healing studies. Preparation of tendon grafts involves five primary steps: 1) the preparation of a suspension of collagen-glycosaminoglycan coprecipitates in 0.05 M acetic acid, 2) the filling of the

suspension into a silicone rubber tube, 3) the axial immersion of the suspension-filled silicone tube into a cooling bath to form oriented ice dendrites in the CG suspension, 4) the sublimation of the ice dendrites, producing a porous CG foam, and 5) the dehydrothermal treatment of the matrices to remove residual water and to crosslink the matrices.

Collagen–GAG slurry production. The collagen–glycosaminoglycan (CG) copolymers were prepared from type I collagen which had been precipitated from acid dispersion by chondroitin 6-sulfate. Type I insoluble collagen was prepared at the United States Department of Agriculture (USDA) in Philadelphia, PA, using the method of Komanowsky [73]. Collagen, in the form of a lyophilized slurry, was stored at the MIT Fibers and Polymers Laboratory at -20°C until use, at which time the collagen was further ground in a Wiley mill with a 20 mesh screen (Thomas-Wiley model 3383-L10, Arthur H. Thomas Co., Philadelphia, PA) to produce a uniform size distribution.

The collagen slurry was prepared by blending 1.65 g collagen in 600 ml 0.05 M acetic acid in a jacket-cooled blender (Eberbach Waring restaurant model blender, Ann Arbor, MI) at 4°C for 1 hour at high speed (approximately 23,000 rpm). After an hour of blending, 120 ml of a 0.11% (w/v) solution of chondroitin 6-sulfate (derived from shark cartilage, product no. C-4383, Sigma Chemical, St. Louis, MO) in 0.05 M acetic acid was added dropwise to the blending collagen solution over a 15 minute period via a peristaltic pump. The collagen–chondroitin 6-sulfate coprecipitate solution was blended for an additional 15 minutes after the addition of chondroitin 6-sulfate.

The slurry was transferred to a swinging cup centrifuge (IEC CRU-5000, International Equipment Co., Needham, MA) and centrifuged at 4°C for 1 hour at a velocity of 2200 rpm. After centrifugation, 420 ml of supernatant was decanted and discarded. The 300 ml of concentrated CG slurry was re-blended at low speed (approximately 14,000 rpm) in the above mentioned blender for 15 minutes at 4°C.

The CG slurry was then degassed by pulling a vacuum on a 6 L sidearm flask containing the 300 ml of slurry for approximately 5 to 15 minutes. The slurry was either used

immediately or stored at 4°C until use. Slurry stored for more than 1 month was reblended at low speed at 4°C for 15 minutes and degassed before use.

Solidification of collagen-glycosaminoglycan suspension The collagen-glycosaminoglycan coprecipitate suspension was injected with a 10cc luer lock syringe (Becton Dickinson & Co., Rutherford, NJ) into a silicone rubber tube (I.D.= 3.8 mm, O.D.= 4.8 mm, Cole Parmer, Niles, Il) approximately 14 cm long. The suspension was contained within the silicone rubber tube by clamping both ends of the silicone rubber tube with pinchcocks. Figure 3.6 is a schematic of the suspension-filled silicone tube. A PVC jacket (I.D. 4.8 mm, O.D. = 8 mm, Cole Parmer, Niles, Il), 10 cm in length, was placed around the outside of the silicone rubber tube to provide insulation to the side of silicone rubber tubing filled with CG suspension (Figure 3.5).

The CG suspension was lowered axially into the cooling bath. Figure 3.6 is a schematic of the freezing bath machine. The CG suspension-filled tube is attached to a plastic gear drive chain and the tube was lowered at a constant velocity into the freezing bath. The velocity of immersion was controlled by a 1/30 RPM timing motor (Cramer model 117P, Cramer Division of Conrac Co., Old Saybrook, CT) with various interchangable sprocket gears mounted to the timing motor (Berg model GG33S14-12, GGS14-30, and GGS14-64, Winfred M. Berg, Inc, East Rockaway, NY). The velocity of immersion was varied from $2x10^{-5}$ m/s to $10x10^{-5}$ m/s.

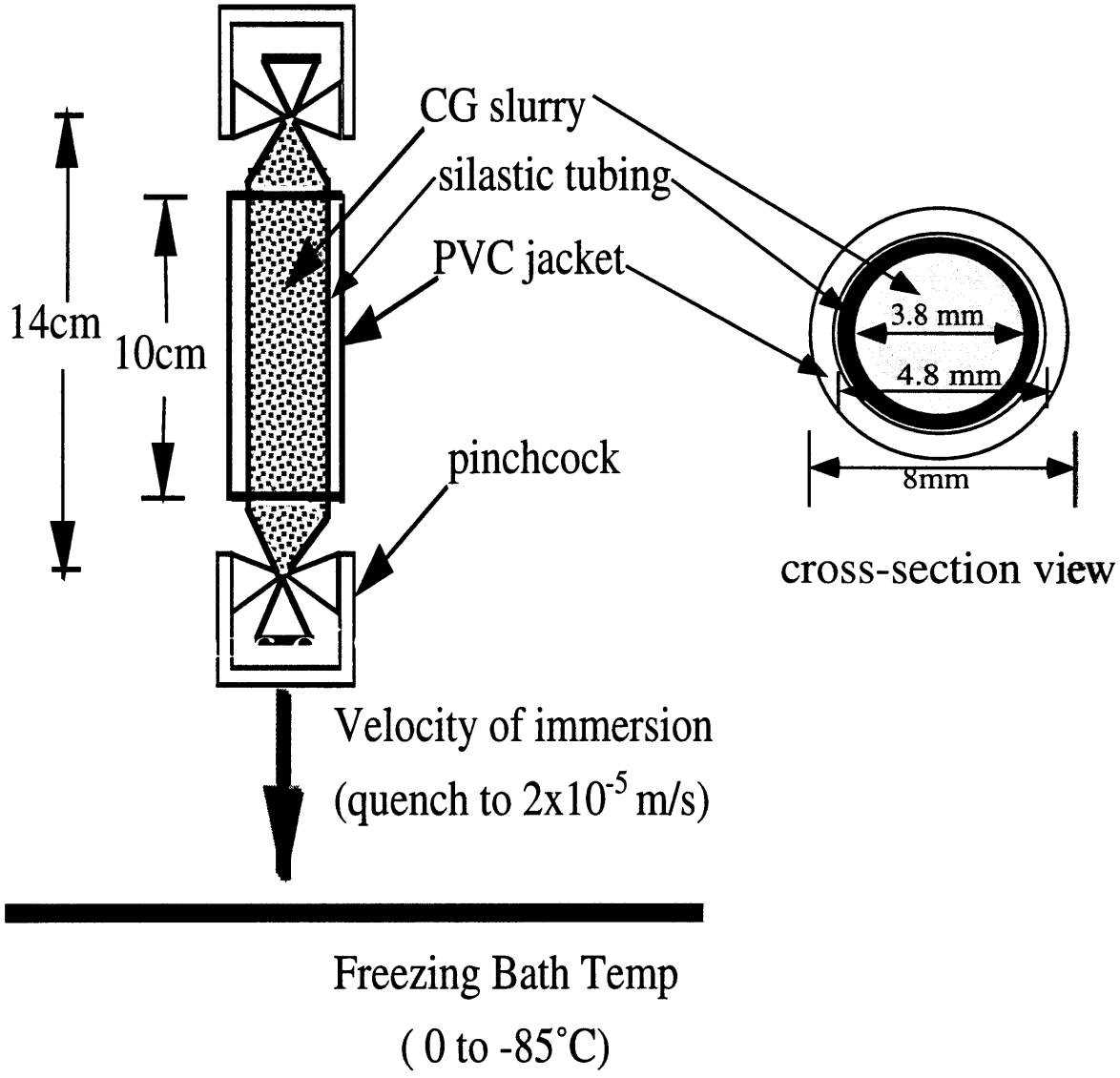

Figure 3.5. Schematic of solidification of CG suspension set-up.

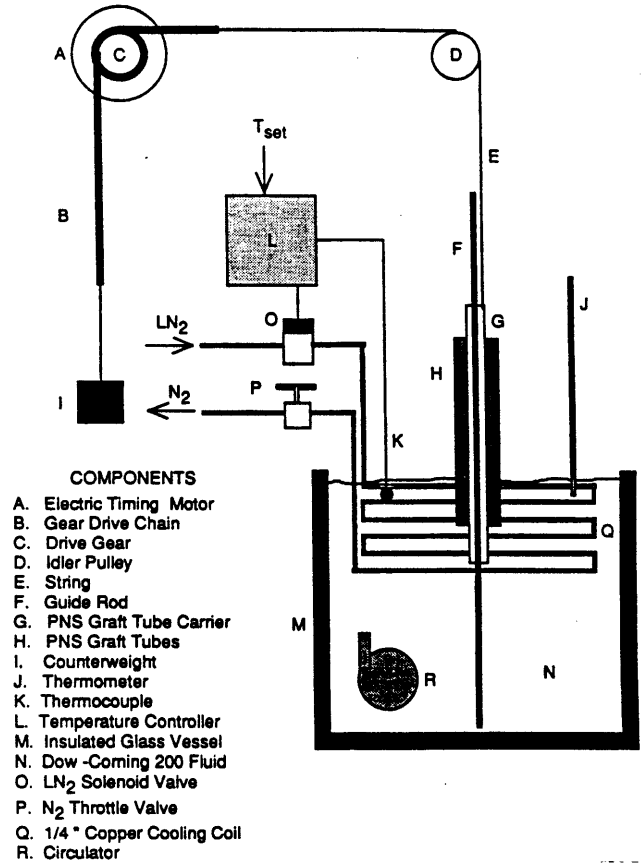

Figure 3.6. Schematic of the freezing bath set-up. (From H. Loree (1988)) Note: PNS was a term used in Loree's Master thesis to denote the PVC-jacketed silicone tube filled with collagen-GAG suspension.

The temperature of the freezing bath was varied from -10°C to -40°C. The lowest recommended temperature that the freezing bath can achieve before the heat transfer fluid (Dow Corning Heat Transfer Fluid 200, Dow Corning Corp, Midland, MI) becomes too viscous is -85°C. Once the suspension-filled tube was fully immersed in the coolant bath, the tube stayed submerged in the bath for an additional 30 to 60 minutes to insure complete solidification of the suspension. The tube was sectioned into five equal lengths. The two end sections were discarded. The remaining three sections were used for CG characterization. The frozen suspensions were either transferred directly to the FTS freeze-dryer (Triophilizer model, FTS Systems, Albany, NY) or stored at -20°C until ready to freeze-dry.

Freeze-drying and storage. Prior to transfer of the frozen collagen-glycosaminoglycan sections to the freeze-dryer, the freeze-dryer chamber was cooled to -30°C. The frozen CG

sections were placed sitting on its side on the surface a stainless-steel tray (Figure 3.7), cooled to -20°C in a freezer. The tray was transferred to the freezedryer and allowed to equilibrate for at least thirty minutes before the vacuum pressure was decreased. The frozen CG suspension was vacuum-dried at 100 mtorr for 12 to 24 hours with the chamber temperature maintained at 0°C. At the end of the sublimation step, the temperature of the chamber was raised to 22°C and the matrices dried for an additional 45 to 90 minutes. The matrices were removed from the freeze-dryer and placed in foil packets. The packets, were transferred to a vacuum oven (Fisher Isotemp vacuum oven, Fisher Scientific, Medford, MA) for dehydrothermal treatment (DHT) for 24 hours at 105°C and 30 mmHg pressure. Crosslinking of the CG matrices was achieved through the formation of interchain peptide bonds using drastic dehydration [134].

The matrices were stored at room temperature in a desiccator jar. A schematic summarizing the steps used in the manufacturing, from beginning (raw material) to end (storage) is presented in Figure 3.8.

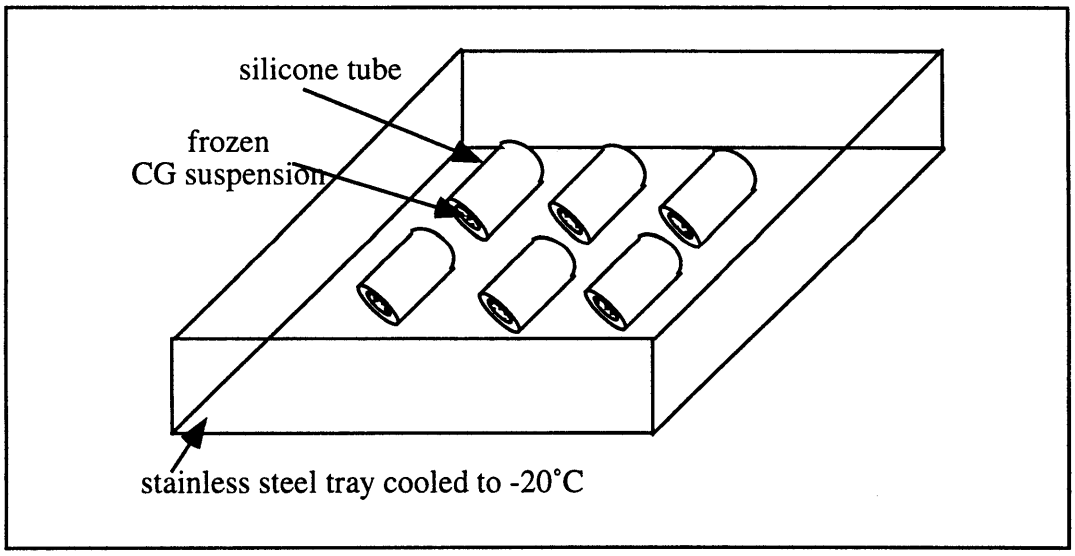

Figure 3.7. Schematic of sections of silicone tubes filled with frozen collagen-glycosaminoglycan suspension on pre-cooled stainless steel tray prior to placement into freezedryer.

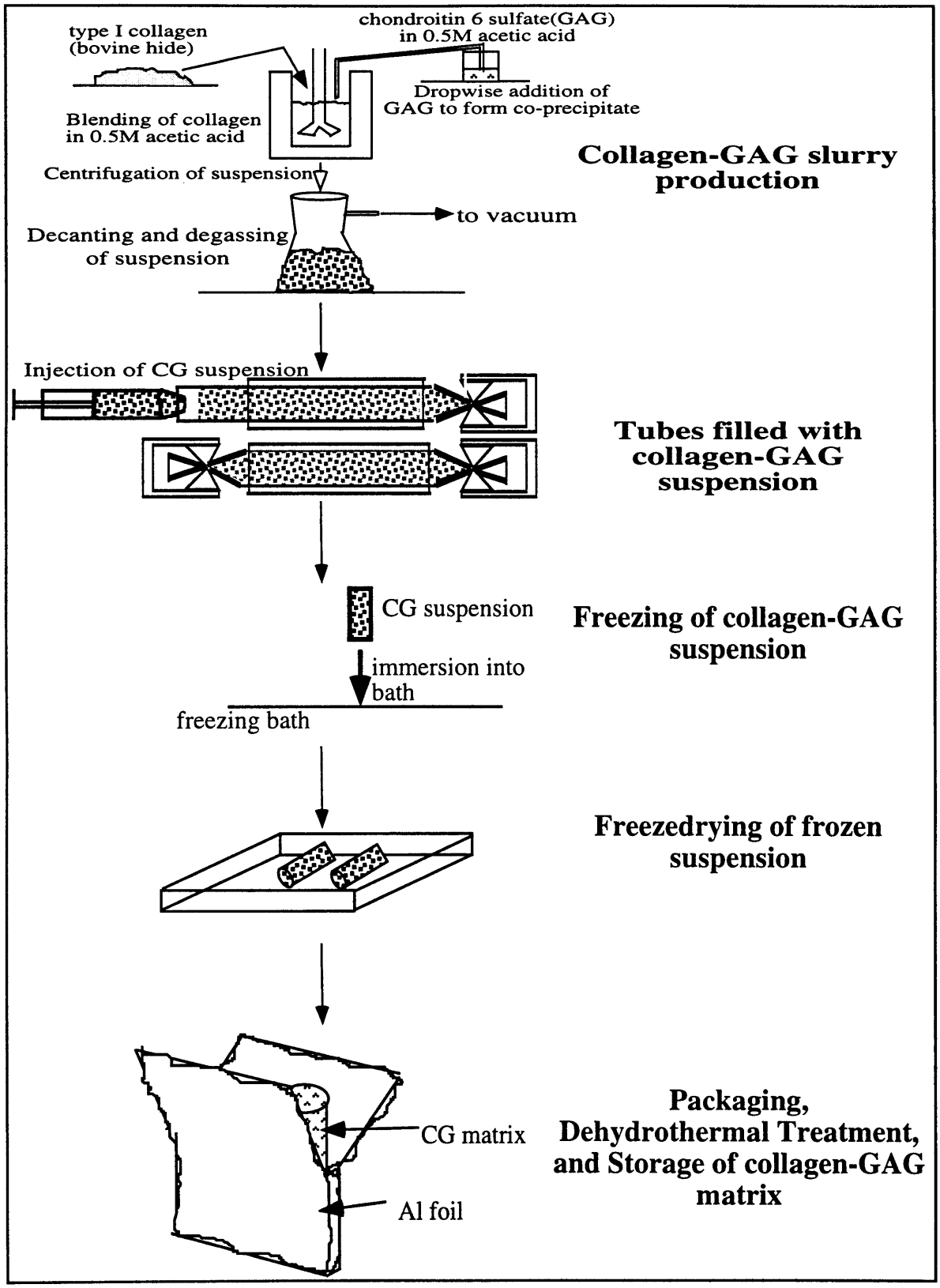

Figure 3.8. Schematic of collagen-GAG matrix manufacturing steps from beginning (raw material) to end (packaging and storage)

Summary of manufacturing conditions studied. The effects of two manufacturing parameters on the pore size, pore orientation, and pore morphology were investigated. Matrices were produced at three velocities of immersion, $2X10^{-5}$ m/s, $5X10^{-5}$ m/s, and $10X10^{-5}$ m/s, and at coolant bath temperatures of -10°C, -25°C, and -40°C. At least eight specimens were made for each combination of temperature and velocity of immersion. A grid summarizing the manufacturing parameters studied is presented in Figure 3.9.

3.3.2. Collagen-GAG characterization

Digitization and pore size analysis. Analysis of the percent porosity, pore size distribution, and orientation of pore channels was performed using an automated stereological

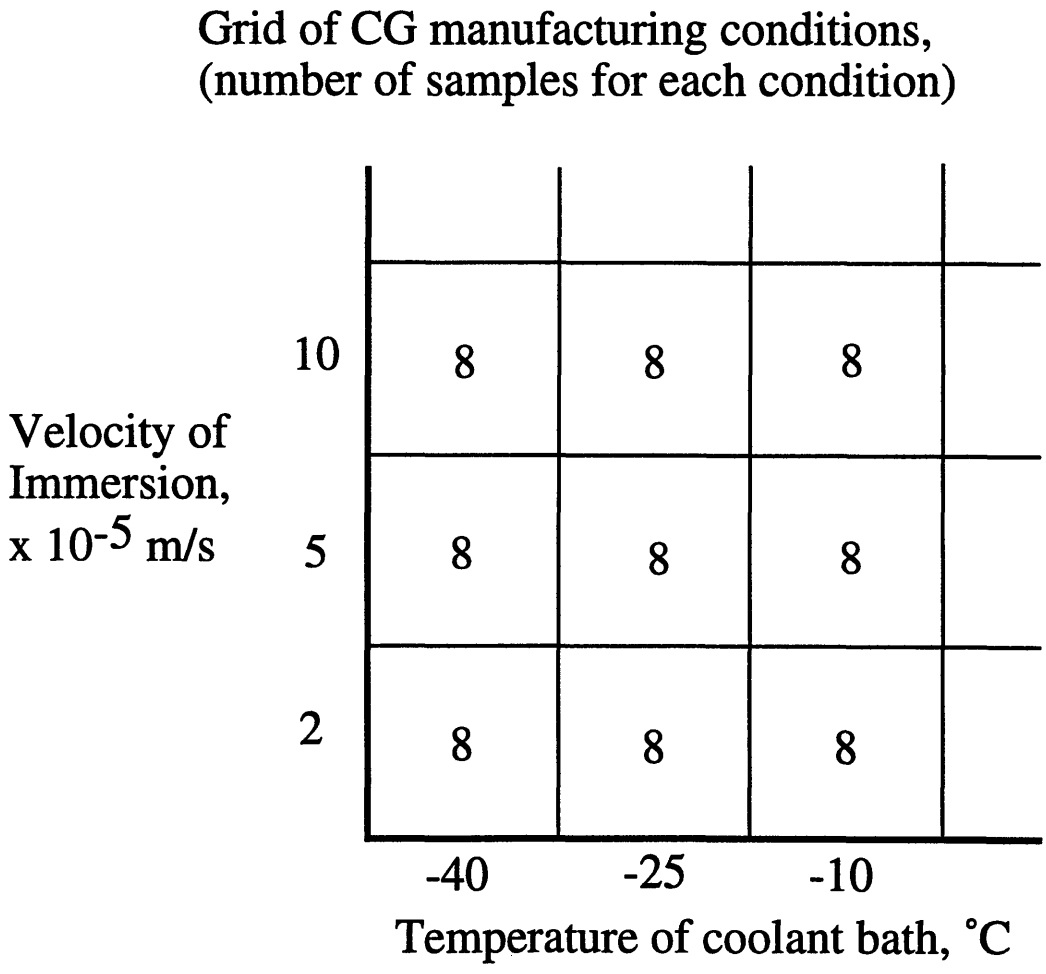

Figure 3.9. Grid of manufacturing conditions investigated.

system. Samples of the collagen-GAG copolymers were embedded in glycolmethacrylate plastic (JB-4, Polysciences Inc., Warrington, PA). Collagen-glycosaminoglycan copolymers were immersed in 10% neutral buffered formalin for 2-4 hours, followed by serial dehydration in graded ethanol (70%, 80%, 95%, 95%, 100%, 100%, 100%) for 15 minutes in each solution. The collagen-GAG copolymers were then infiltrated with the catalyzed-buffer of solution A of the JB-4 embedding kit overnight at 4°C, according to manufacturer's recommendation [96]. Matrices were polymerized in a solution of fresh catalyzed buffer of solution A with added initiators. Three micron-thin sections were microtomed (model 1512, Leitz Wetzlar, Easton, MA), floated onto a water bath (Tissue float bath, Lo Boy, Lab-line, obtained through Fisher Chemical, Pittsburgh, PA), collected onto clean glass slides (Superfrost Plus, cat#48311-703, VWR, Boston, MA) and allowed to dry overnight. The sections were made transverse to the long axis of the matrix cylinder.

Slides were stained with 2.5% acidified aniline blue stain (2.5 gm aniline blue (w.s.), 100 ml distilled water, and 2.0 ml glacial acetic acid) to highlight the collagen substance of the material. The staining protocol is as following: tissue sections on glass slides are immersed in the 2.5 % aniline blue stain for 2-4 minutes, rinsed in 95% ethanol, rinsed to a 100% ethanol solution, then air dried, mounted (Cytoseal 60, low viscosity, Stephen Scientifics, Riverdale, NJ) and coverslipped.

Light microscopic images of these sections were digitized using a video camera (Hamamatsu CCD Camera C2400-60, obtained through Photonic Systems, Bridgewater, NJ) mounted on an Olympus Vanox AH-2 microscope. A video interface board and custom software allowed for analysis of the images on a Macintosh IIx computer. The image analysis software, DIGIT (developed by Ed Cheal formerly of Brigham and Women's Hospital Orthopedic Research Laboratory) [17], was used to compute the average pore size, percent porosity, and pore channel aspect ratio and pore size distribution. In order to determine these parameters, the image analysis program used the method of directed secants. A short description of the computer algorithm is included below. In this algorithm, a region of the

image of the CG matrix (typically 0.3 to 0.5 mm^2) was scanned with an array of equidistant parallel test lines. The number of intersections of the collagen-GAG material with the lines was determined for a particular scan-line orientation. The array of parallel test lines was subsequently rotated and the procedure (to count intersections of these lines with the collagen substance) was repeated. The image analysis software performed mathematical rotation of the digitized images at 15° increments through 180° for the test line scans. This procedure yielded a mean path line of the pores in the collagen substance. A polar plot of these data yielded a circle for isotropic structures and an ellipse for partially oriented architectures. The degree and direction of collagen orientation (i.e., pore channel orientation) was computed by solving the eigenvalue-eigenvector numerical representation of this ellipse. A schematic of the algorithm is presented in Figure 3.10.

ESEM. Micrographs of the CG matrices were obtained by environmental scanning electron microscope (ESEM, Electroscan, Waltham, MA). The major advantage of utilizing the ESEM rather than the more conventional scanning electron microscope (SEM) was that artifacts in sample preparation were minimized. Samples used in the SEM need to be inherently conductive, as in a metal, or they need to be coated with a conductive material, such as a gold coating. Since the collagen-GAG copolymers were not inherently conductive, they needed to be coated with a conductive metal, a procedure which can alter the structure of the matrix To be viewed under the ESEM, a conductive coating was not need on the collagen-GAG copolymers.

Sample preparation of CG matrices for viewing under the ESEM involved cutting sections of the CG matrices with a sharp razor blade and mounting the sections onto ESEM studs with conductive tape. Sections transverse to the long axis of cylindrical matrices were mounted. ESEM samples were stored in desiccator jars until use. A qualitative assessment of the pore morphology of the matrices was made from the micrographs obtained.

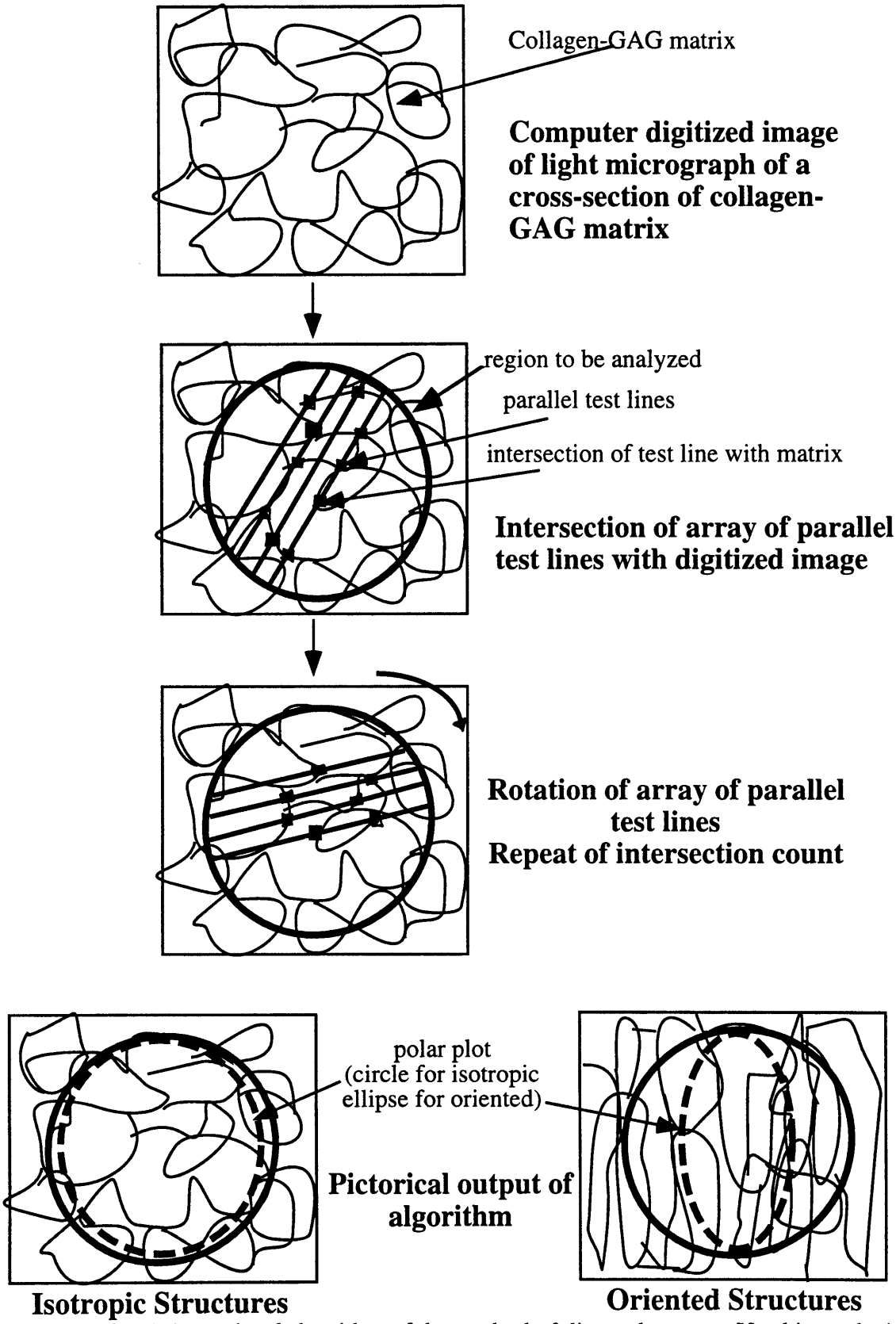

Figure 3.10. Schematic of algorithm of the method of directed secants. Used in analysis of collagen-GAG matrix pore characteristics

3.4 Results

3.4.1. Average Pore Size

The temperature of the freezing bath and velocity with which the suspension was immersed into the bath affected the average pore size of the CG matrix. The average pore size decreased with decreasing temperature of the coolant bath for the three velocities investigated (Figure 3.11). The effect of the temperature of the coolant bath on the average pore size was more pronounced at a high velocity of immersion ($10x10^{-5}$ m/s) than at a low velocity ($2x10^{-5}$ m/s). For a velocity of immersion of $10x10^{-5}$ m/s, the pore size ranged from 20 μm to 120 μm for coolant temperatures of -40°C to -10°C, respectively. A velocity that was one-fifth this magnitude ($2x10^{-5}$ m/s), yielded average pore sizes that varied from about 80 μm to 100 μm, for the same coolant temperature range.

The velocity of immersion had a more pronounced effect on the pore size at a low freezing temperature than at a high freezing temperature (Figure 3.12). At a coolant temperature of -40°C, the pore size ranged from 20 to 80 μm, whereas at a freezing

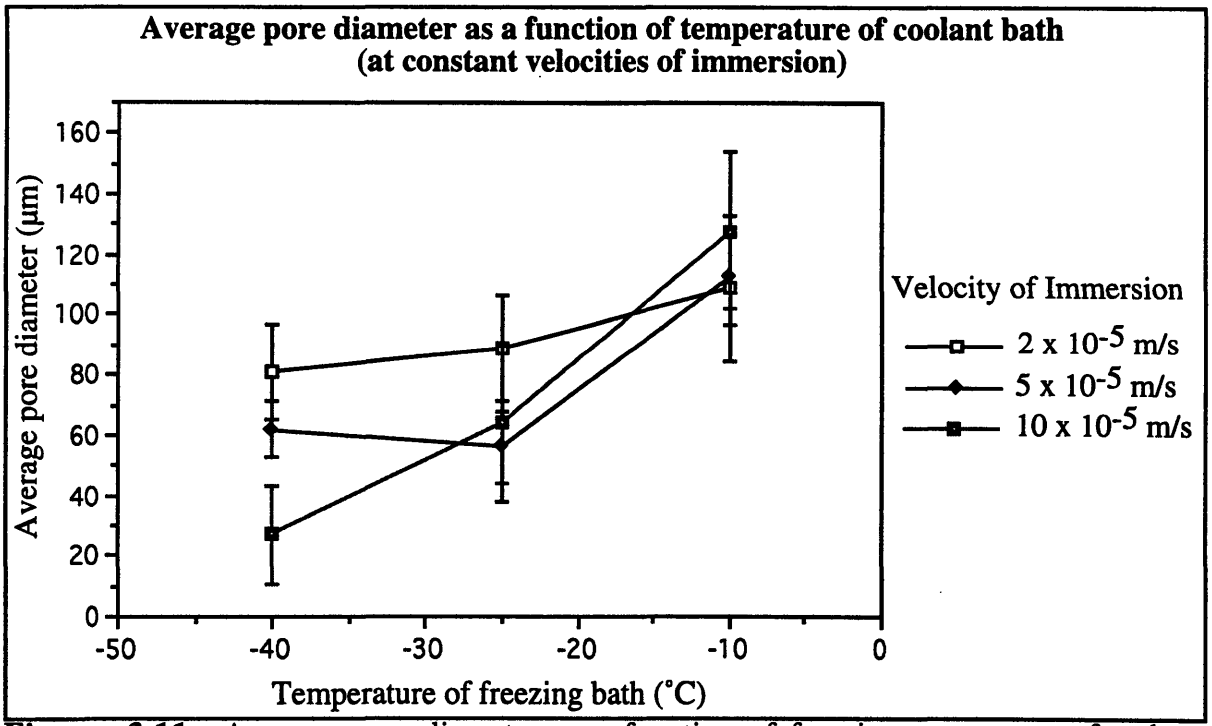

Figure 3.11. Average pore diameter as a function of freezing temperature for three velocities of immersion The bars indicate standard deviations. The CG suspension was injected into a silicone tube, clamped at both ends, and immersed into a coolant bath.

temperature of -10°C, the pore size averaged around 115 μm with no statistically significant difference among the three velocities. Figure 3.13 shows ESEM micrographs of different pore channel diameters.

3.4.2. Percent Porosity and Aspect Ratio

The temperature of the coolant bath and velocity of immersion had little effect on the percent porosity of the matrices; the pore volume fraction of all of the matrices, at all combinations of velocity of immersion and coolant bath temperature, ranged between 0.90 and 0.94. However, the pore channel aspect ratio, orientation, and distribution were markedly affected by the velocity with which the CG suspension was immersed into the coolant bath (Figure 3.14). At high temperatures and rapid rates of immersion, the pore channels became radially elongated with respect to the center of the matrix. In contrast, at low temperatures and slow rates of lowering the CG suspension into the bath, the matrices had an equiaxed pore structure.

Under certain conditions, the pore morphology of the CG matrices was heterogeneous in appearance in that there was both radially elongated pores and axially aligned pores were present in the matrix. In general, axially aligned pores were present in the inner central portion of the cylindrically shaped matrices as seen in a transverse section of the matrix. There pores were also generally smaller in size than the pores on the periphery of the cylindrical matrix. Pores with a radially elongated appearance were present predominantly at the outer diameter of the cylindrical matrix. Non-uniformity of pore shape and size resulted from conditions of low freezing bath temperature and fast velocity of immersion. Figure 3.15 shows ESEM micrographs of two representative pore morphologies: a radially elongated pore channel and an example of a uniform, axially aligned pore morphology.

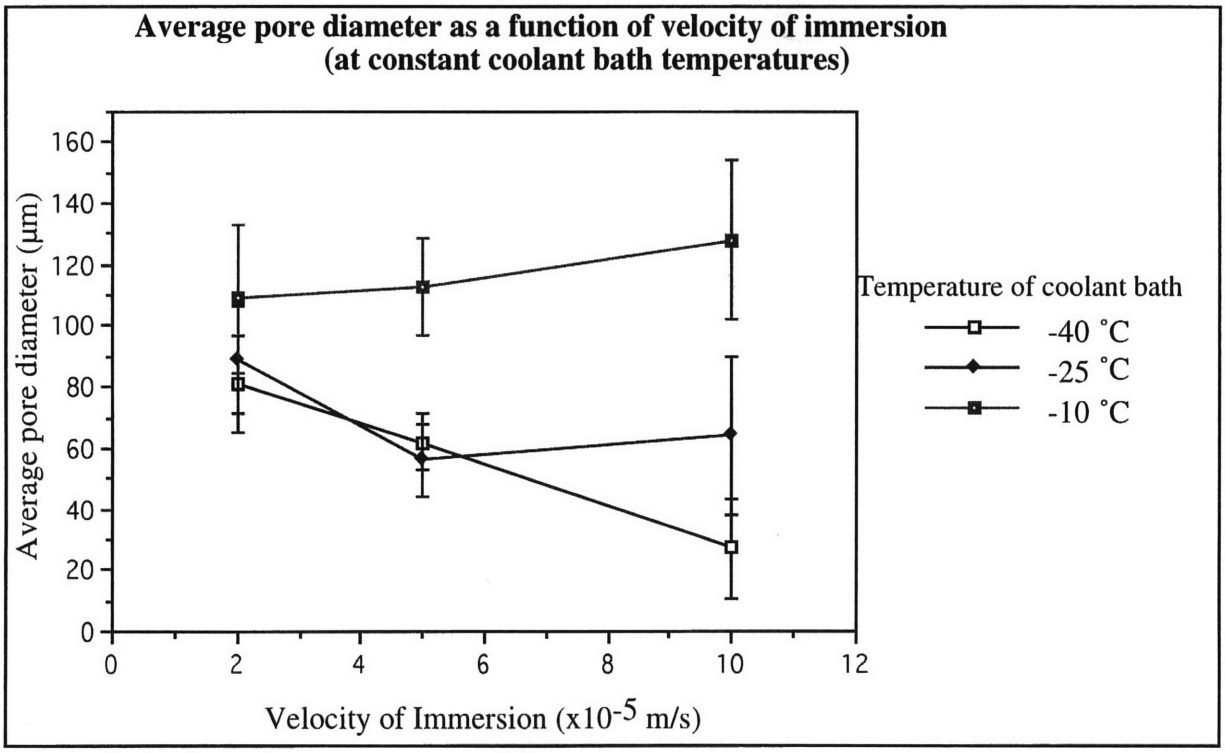

Figure 3.12 Average pore diameter as a function of velocity of immersion into freezing bath for three freezing bath temperatures. The bars indicate standard deviations. The CG suspension was injected into a silicone tube, clamped at both ends, and immersed into a freezing bath.

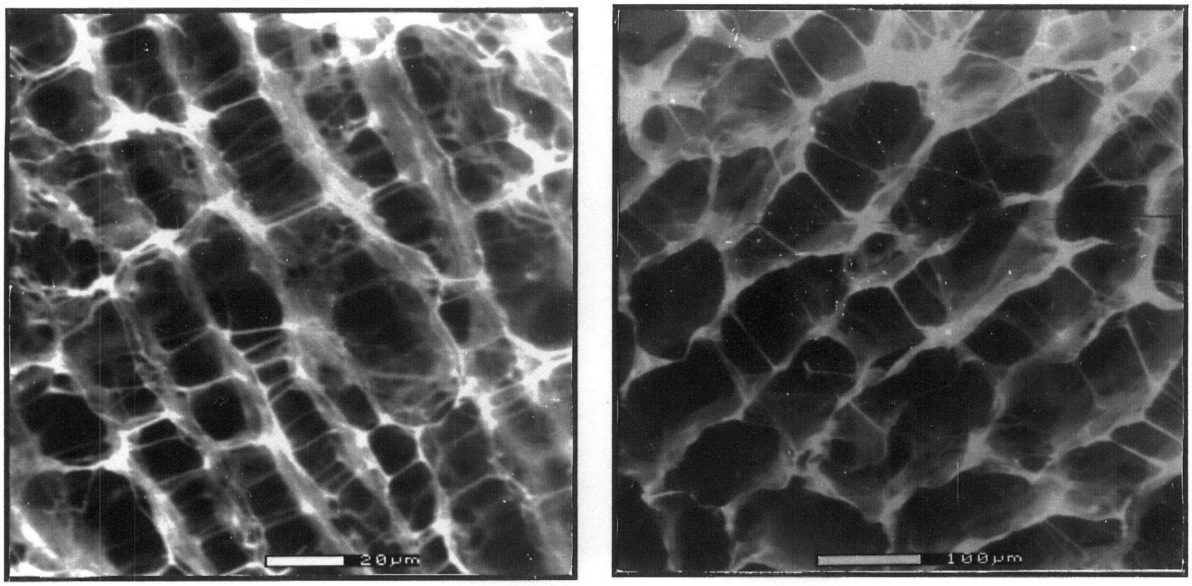

Figure 3.13 ESEM micrographs of a CG matrix with pore channel diameters; pore channels with an average diameter of 27 μm (**left**) and pore channels with an average diameter of 80 μm pore channels (**right**). The micrographs are at different magnification. Left scale bar: 20 μm. Right scale bar: 100 μm.

Velocity of immersion, $x10^{-5}$ m/s	-40 °C	-25 °C	-10 °C
10	Homogeneous Isotropic 27 ± 16 μm	Heterogeneous Elongated outer;isotropic center 64 ± 26 μm	Homogeneous Radially elongated pores 128 ± 26 μm
5	Homogeneous Isotropic 62± 9 μm	Heterogeneous Isotropic and elongated pores 56 ± 20μm	Heterogeneous Radially elongated outer with smaller pores in center 113 ± 16 μm
2	Homogeneous Isotropic 81 ± 16 μm	Homogeneous Isotropic 89 ± 18 μm	Homogeneous Isotropic 109 ± 24 μm

Temperature of freezing bath, °C

Figure 3.14 Pore morphology, distribution, and orientation resulting from various combinations of velocity of immersion and coolant bath temperature. Average pore diameter (± standard deviation).

3.4.3. Effect of Cylinder Diameter on Pore Characteristics of the Matrix

Table 3.1 compares the average pore sizes of cylindrical CG matrices with diameters of 1.5 mm and 3.8 mm. The large standard deviations preclude definitive conclusions about the effect of cylinder diameter on the average pore size for the selected processing conditions. From the limited data, it appears that at the scale of a few millimeter, cylinder diameter is not a primary factor affecting average pore size. However, the lower coefficients of variation for the larger diameter specimens appear to indicate that there is a narrower pore size distribution. Qualitatively, there appeared to be similar relationships between the selected processing parameters and pore orientation for the CG cylinders with diameters of 1.5 and 3.8 mm.

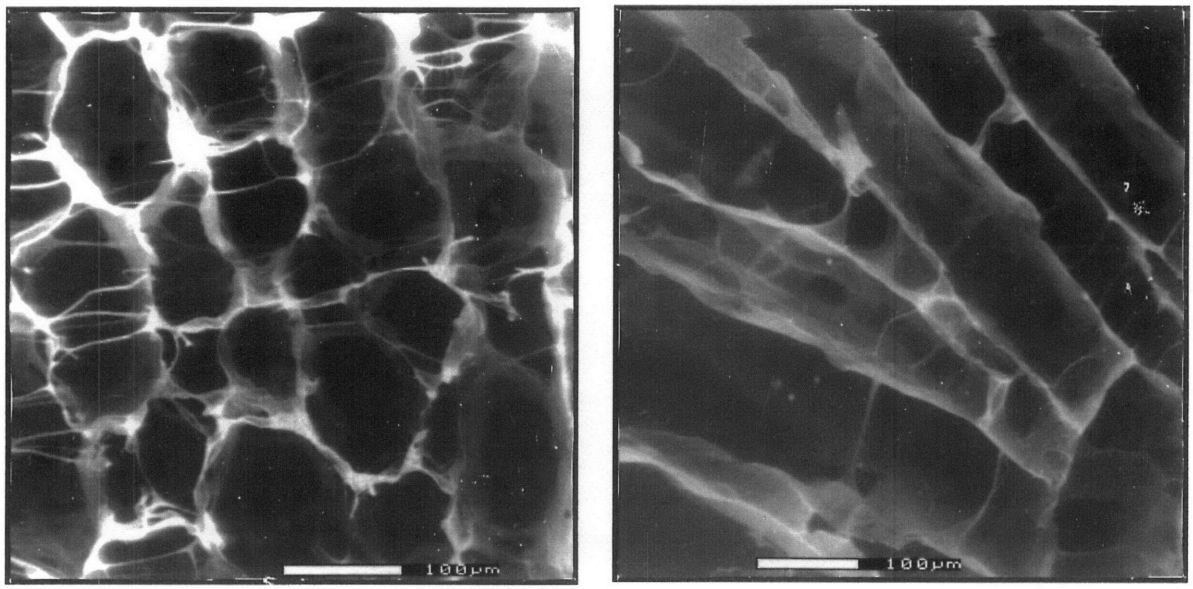

Figure 3.15 ESEM micrographs of a representative radially elongated morphology (left) and a uniform equiaxed morphology (right). The scale bar represents 100 µm.

Conditions	Cylinder Diameter 3.8 mm	Cylinder Diameter 1.5 mm*
T= -40 °C , $\upsilon = 10 \times 10^{-5}$ m/s	27 ± 16 µm	27 ± 16 µm
T= -40 °C , $\upsilon = 2 \times 10^{-5}$ m/s	81 ± 16 µm	70 ± 50 µm
T= -10 °C , $\upsilon = 10 \times 10^{-5}$ m/s	128 ± 26 µm	75 ± 54 µm
T= -10 °C , $\upsilon = 2 \times 10^{-5}$ m/s	109 ± 24 µm	71 ± 51 µm

Table 3.1. Comparison of average pore diameter (± standard deviation) for AECM diameters of 3.8 mm and 1.5 mm. *Data from H. Loree (1988).

3.4 Discussion

3.4.1. Scaling-up size of collagen-glycosaminoglycan matrix

Studies on the pore characteristics of collagen-glycosaminoglycan matrices used as analogs of extracellular matrices (AECM) for sciatic nerve injuries were for matrices cylindrical

in shape with a diameter of 1.5 mm [76]. In this study, the diameter of the cylindrically-shaped CG matrices were increased to 3.8 mm, a factor increase of 2.5. This increase in CG matrix size was need to accommodate for the larger diameter of the Achilles tendon. The pore size, orientation and morphology of the larger diameter matrices did not appear to differ significantly from the smaller diameter matrices for comparable freeze-drying conditions. The mechanism by which ice dendrites form in the CG suspension appears to be scale independent over the diameter range 1-4 mm.

In this study, the results that the pore sizes of the CG matrices decreased with decreasing temperature of the freezing bath is consistent with classical ice nucleation theory associating the degree of undercooling with critical nucleus size (pore size of the matrix) [98]. This result is also consistent with results obtained by Loree [76] for the cylindrically shaped CG matrices and by Irving [66] for pan cast CG matrices. The formation of ice nuclei appears independent of the surface area of the freezing front and is a localized phenomenon.

The results of the effect of the velocity of immersion on the pore structure for the 3.8 mm diameter matrices are consistent with the results obtained by Loree[76] for the 1.5 mm diameter matrices. The rate at which the CG suspension is lowered into the bath changes the freezing front direction and thus changes the direction along which the ice dendrites grow. This determines the pore channel morphology. The faster the CG suspension is immersed into the bath, the more likely the dominant heat transfer vector will be radially directed outward because the radial direction is the more favorable for the heat flux. This causes the ice dendrites to form from the outer surface toward the center of the tube.

The heterogeneity of the pore shapes found under certain processing conditions was reported in Loree's thesis [76] . Smaller sized axially aligned, isotropically-shaped pore channels were found at the central midline of the cylindrically-shaped CG matrix with larger sized radially elongated pore channels at the periphery of the cylinder. The smaller sized pores in the central portion of the matrices are probably due to the migration of collagen-glycosaminoglycan precipitates toward the midline of the cylinder during radial dendritic

growth of the ice. Since the rate at which the radial freezing front and the axial freezing front move through the CG suspension determines the orientation of the pore channels, the degree of heterogeneity of the pores may be a function of the tube diameter. The larger the tube diameter, the greater the distance that the radial pores must travel to reach the midline of the tube. This increase in time increases the probability that the axial freezing front will interfere with the radial front. This would lead to two types of pore shapes present. This effect would be more pronounced at the faster rates of immersion, since at the slow rates of immersion there is generally only the axial freezing front present. However, in theory, if the rate of immersion was such that there was only a radial freezing front, then the matrix pore shapes would be uniformly radially elongated.

3.4.2. Choice of processing conditions to produce the desired pore morphology

In this study, the combination of the two processing conditions, temperature of freezing bath and velocity of immersion of the CG suspension into the freezing bath produced a wide variety of pore size and pore orientation (Figure 3.13). Pore sizes varied from 20 to 150 μm and the pore channel shape varied from axially aligned to radially elongated.

More than one set of manufacturing conditions appear to be capable of producing a desired pore size. Two sets of processing conditions appear to be capable of producing an average pore diameter of 60 μm. One possible combination of manufacturing conditions is a freezing bath temperature of -25°C and a velocity of immersion of $5x10^{-5}$ m/s. The other possible combination is a freezing bath temperature of -40°C and a velocity of immersion of $5x10^{-5}$ m/s. In some cases, the choice of manufacturing conditions may be arbitrary; the resulting CG matrix will have nearly indistinguishable pore size and morphology. However in other cases, different sets of manufacturing conditions are capable of achieving the same average pore size but the pore morphology may differ. In the above example, although both produced an average pore size around 60 μm, the former condition (T= -40°C, v= $5x10^{-5}$ m/s) produced a matrix with an axially aligned pore channels (as seen in a transverse cross section);

while the latter condition (T= -25°C, v= $5x10^{-5}$ m/s) produced a matrix that had axially aligned pore channels in the central portion of the cylinder and radially elongated pores at the outer edges of the cylinder.

In choosing processing conditions to produce a particular pore size, uniformity of pore morphology should be factored into the decision. A map of not only pore size, but also pore morphology as a function of manufacturing conditions, such as that shown in Figure 3.11, would appear to be useful in choosing the proper processing conditions for a particular CG matrix pore structure.

3.5 Conclusion

The coolant bath temperature and immersion velocity can be selected to fabricate AECMs with average pore sizes ranging from 20 to 150 μm. These two variables also affect the morphology of the matrices. CG cylinders can be produced with both uniform axially aligned pores and with radially elongated pore channels, depending on the combination of the coolant bath temperature and velocity of immersion. In general, the faster the velocity of immersion and the higher the coolant temperature, the more radially elongated the pores. The slower the immersion the more homogeneous and isotropic the pore structure. There is a trend toward smaller pore size with lower temperature, independent of the velocity of immersion. The smallest pore sizes are obtained with low temperatures and high rate of immersion. For diameters of 1.5 and 3.8 mm, the size of the tube in which the CG suspension is prepared does not have a significant effect on pore size.

CHAPTER IV: EVALUATION OF TENDON HEALING IN A NOVEL ANIMAL MODEL

4.1 Introduction

When tendon is injured such that there is a significant loss of tissue and a large wound gap is formed, surgical reapposition of the uninjured tendon ends is generally not feasible. If the wound is left untreated either inferior tissue fills the defect site or in the worst case, the ends of the tendon are not bridged with any tissue. Previous studies have investigated the use of prostheses of either synthetic or biological origin into Achilles tendon lesion sites [23, 54, 56, 62, 63, 105, 126] to treat these types of injuries. These prostheses were generally close-packed aligned fiber tows, both of resorbable and non-resorbable materials designed primarily to mimic the mechanical properties of the tendon [23, 54, 56, 62, 63, 105, 126] .

It has been shown that the properties of the tissue formed in response to Achilles tendon injury are different from the original tendon in both untreated [8, 32, 99, 127] and treated (i.e., devises are implanted into the wound site) [23, 56, 62, 68] cases. Although many investigators have shown that the tissue formed in response to Achilles tendon injury had many features similar to normal tendon, there were still other features, such as the crimp pattern and collagen fibril diameters, that were not similar to normal tendon [68, 99].

Analogs of extracellular matrix (AECM) have been used in the studies of regeneration of dermis in animals[129, 130, 132] and human subjects [11, 83, 117] and in the study of reconnection of axons cells across large gaps in transected peripheral nerves in rats[16, 129]. It has been found that the pore channel diameters of these AECMs effect the kinetics of healing associated with these tissues [133-135]

In this study, a novel rabbit animal model that isolates a tendon defect site from surrounding tissue during healing was developed. This model entubulated the tendon wound site. This model allows for the evaluation of the healing response of the tendon to analogs of extracellular matrix (AECM) absent the influences of the external environment. Using this

model, the effects of a porous collagen-glycosaminoglycan (GAG) copolymer matrix of different pore diameter channels on the early healing (up to 12 weeks) of Achilles tendon were evaluated histologically, immunohistochemically, and ultrastructurally.

4.2 Materials and Methods

4.2.1. Animal model

An animal model to study the healing of a gap wound in Achilles tendon of an adult rabbit was developed. An important component of the animal model was the physical isolation of the lesion site (gap) from the external environment. This isolation allowed for a controlled isolated environment in which to test the response of the tendon stumps to devices implanted into the wound site.

Confirmation of animal age Skeletally mature, male New Zealand white rabbits weighing 3.0-3.5 kg were used for the animal model. The maturity of the animal was confirmed by x-ray examination of "suspicious" rabbits along with a random sampling of rabbits at the time of surgery. The right knee was radiographed for the fusion of the epiphysis to the femur bone. This fusion is an indication of the skeletal maturity of the animal.

Implantation procedure The following describes the surgical procedure and animal model. The animal was placed on its side for the entire surgical exposure. A generous area around the right hock and stifle joints were shaved and cleaned with Betadine solution. Under general anesthesia and aseptic condition, the right Achilles tendon was opened using a straight longitudinal incision approximately 4 cm in length. The incision was made from the level of the distal third of tibia to the level of the calcaneus to expose the entire length of tendon which spans from the musculotendinous junction to the plantaris fascia of the calcaneus (Figure 4.1a). The skin and soft tissues were dissected and retracted. The whole length of the achillis tendon and of the plantaris tendon was measured. The midpoint of the Achilles tendon and the point one-third from the distal end of the plantaris tendon were identified and marked with a surgical pen.

The Achilles and plantaris tendons are retracted posteriorly to expose the anterior area of the Achilles tendon, and the intermuscular septum was cut to expose the anterior portion. The tendons of the peroneus long, brevis and tertius were exposed, when the surrounding tissue were released while protecting the lateral saphenous artery and vein throughout (Figure 4.1b). The tendons were cut and a portion of each tendon was dissected away.

The right leg was kept positioned such that the knee is in approximately 120 degrees in flexion and the hock joint was in approximately 45 degrees in extension. The plantaris tendon was cut, at its previously identified position, by a 5 millimeter "Z" cut technique. The Achilles tendon was transected at its middle part. The tendons immediately retracted about 8-10 mm. The wound area was kept covered and moist with a wet saline soaked gauze while the knee immobilization procedure was performed.

The right knee joint line was identified and two stab wound incision were made, one 2 cm below the joint line at the lateral tibia and the other 1 cm above the lateral distal condylar edge. The 2 mm and 1.5 mm threaded Kirshnecher pins were drilled through the lateral and medial cortex and out the opposite skin of the tibia and femur bones, respectively. These pins permit placement of the external fixation bars with special clamps such that the knee was placed in 120 degrees flexion.

The silicone tubing was placed in the gap of the tendon by three stitches of modified Kessler repair technique with 3-0 Prolene suture. Maintaining the hock joint at 45 degree extension, the tendon stumps were inserted into the tubing so as to produce an 10 millimeter gap between the stumps. The configuration was held into place by 3 modified Kessler type stitches. Each stitch loops the suture from the distal tendon stump to the proximal tendon stump and back to the distal via running the suture along the outside section of tubing that spans the gap (Figure 4.1c). Thus, an 10 mm gap was maintained in the tubing between the both ends of stumps while allowing any mechanical stresses imparted to the system to be taken up by the sutures. The two "Z" surfaces of the tendon of plantaris were separated away, then the

touched parts were sutured under minimum tension condition with 4-0 Prolene suture (Figure 4.1d).

The wound was flushed with sterile saline. All bleeding points were clamped and cauterized. The subcutaneous was closed with 4-0 Vicryl sutures. The lateral X-ray was taken directly after the surgery. The animal was allowed to recover from anesthesia before being returned to its cage. Figure 4.2 provides an overview of the surgical procedure.

Animal care The general care of the animals were in accordance with Harvard Medical Area Animal Care Committee protocol. The animals were allowed food and water *ad libitum* and had unrestricted cage activity. The animals were monitored daily for general appearance and loosening of external fixation device. External fixation devices were tightened as needed or removed completely if deemed hazardous to the animal's welfare. Removal of external fixation devices occurred no later than 12 days with 10 days being the average. After a thorough cleaning with Betadine solution of the external fixation pin areas, the device is removed while the animal is under general anesthesia. Animals are restricted to cage activity until time of sacrifice.

4.2.2. Collagen-glycosaminoglycan (CG) implants

Processing of CG matrices Collagen-glycosaminoglycan copolymer matrices consists of type I bovine hide collagen precipitated from acid dispersion (5.5 mg/ml in 0.05 M acetic acid) by chondroitin-6-sulfate (derived from shark cartilage). The suspended coprecipitate suspension was injected into a silicone elastomer tube (3.8 mm in diameter) and immersed into a coolant bath. The aqueous portion of the suspension was frozen in the coolant bath then transferred to a freeze-drying apparatus. The resulting ice crystals were sublimated under reduced vacuum (100-200 mtorr) to produce the porous collagen-glycosaminoglycan matrices.

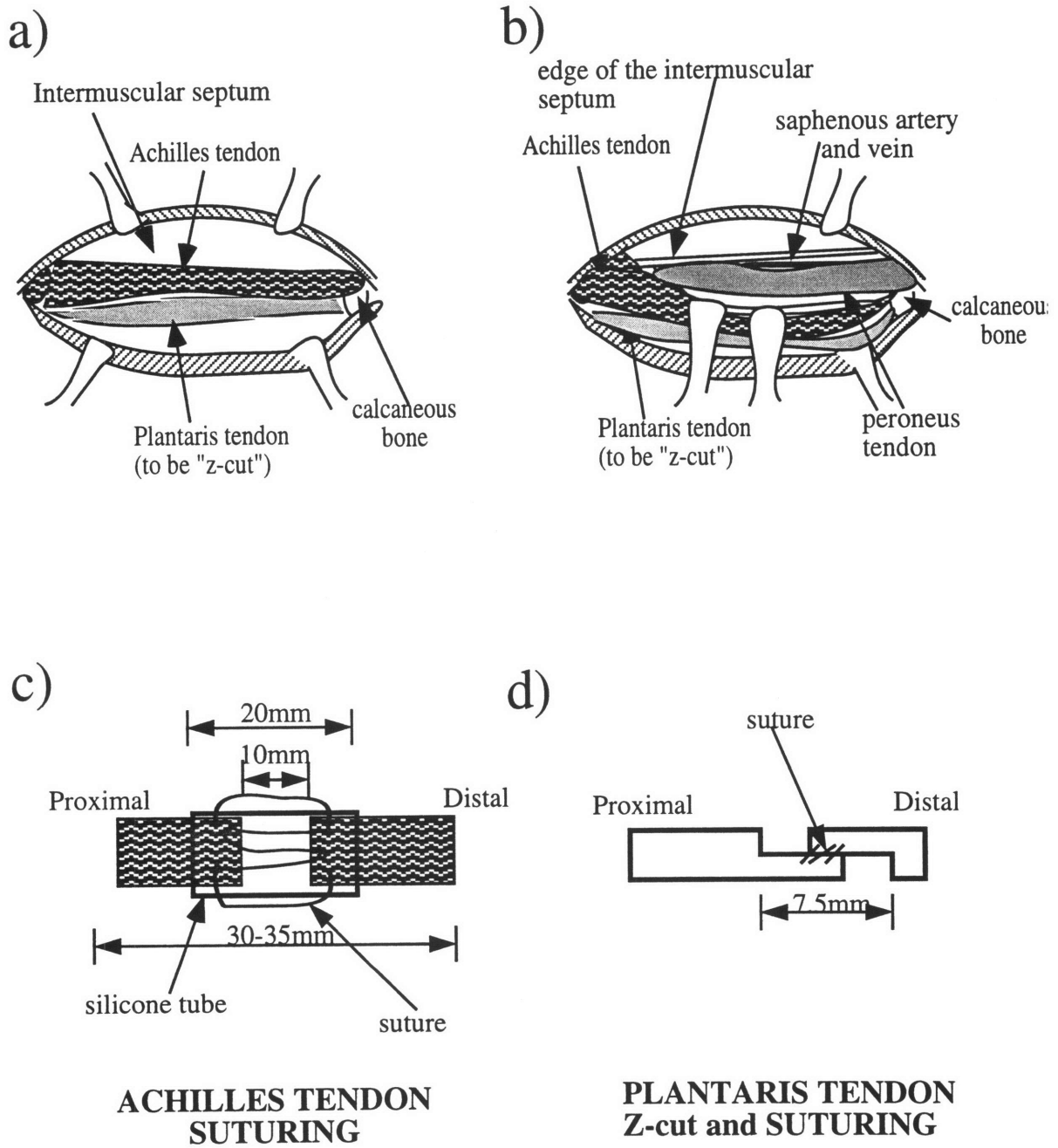

Figure 4.1. Schematic of surgical procedure. a) Exposure of Achilles tendon and the plantaris tendon. b) Exposure of peroneus long tendon behind the intermuscular septum. c) Configuration of Achilles tendon stumps within the silicone tube and suture placement to hold the configuration. d) Suturing configuration on the plantaris tendon with a "z-cut".

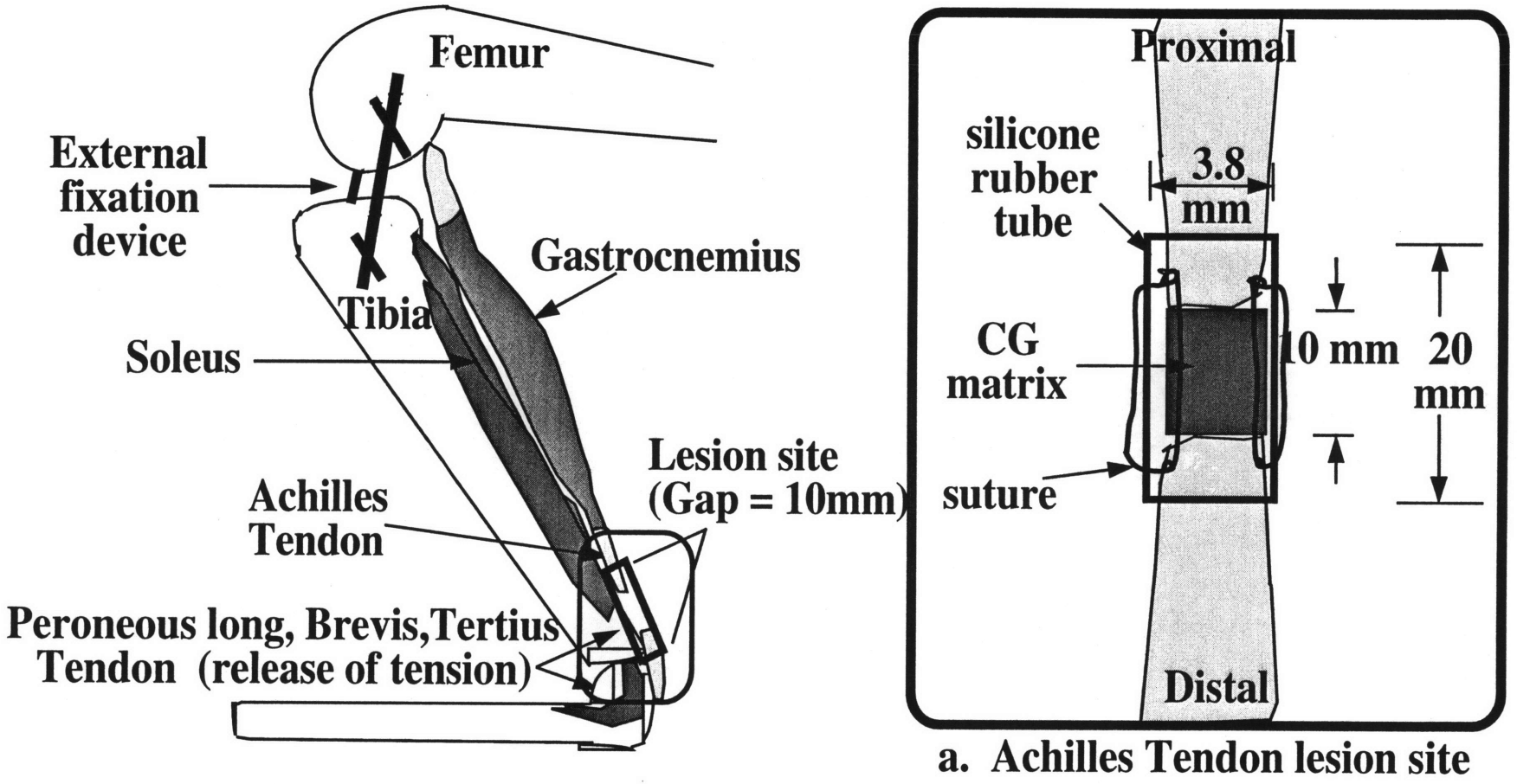

Figure 4.2. Schematic of animal model.

The matrices were then exposed to a dehydrothermal treatment at a temperature of 105°C and a pressure of 30 mmHg in a vacuum oven for 24 hours. The sterile matrices were stored in a desiccator jar at room temperature until ready for use. A full description of the matrix manufacturing procedure is described in Chapter 3.

The matrices used in the in vitro studies were manufactured to have axially aligned pore channels with average pore sizes of 25 μm, 60 μm and 120 μm. The manufacturing conditions to produce the pore sizes are summarized in Table 4.1.

Average pore size	Temperature of coolant bath, T	Velocity of immersion, υ
25 μm	-65 °C	$5x10^{-5}$ m/s
60 μm	-40 °C	$2x10^{-5}$ m/s
120 μm	-10 °C	$5x10^{-5}$ m/s

Table 4.1. Table of manufacturing conditions to produce collagen-glycosaminoglycan matrices of average pore sizes 25 μm, 60 μm , and 120 μm.

Preparation of implants Preparation of the collagen-GAG matrices for surgery included the following steps: 1) CG matrices were removed from their silicone and PVC jacket and trimmed to 10-12 mm. 2) The CG matrices were dehydrated to phosphate buffered saline solution (PBS) starting with 100% ethanol to 70% ethanol to 5 changes of PBS for an hour each. If the surgery was to be performed within 2 days of this process, the grafts were stored in PBS solution at 4°C; otherwise for long term storage, the hydrated grafts were stored in 70% isopropanol at 4°C until use. 3) Prior to storage, the CG grafts were re-ensheathed in 20 mm long silicone rubber tubing. All the above steps were performed under sterile conditions in a laminar flow hood with sterile materials and instruments following a protocol developed in this laboratory proven to produce sterile implants. Figure 4.3 is a schematic of this preparation process.

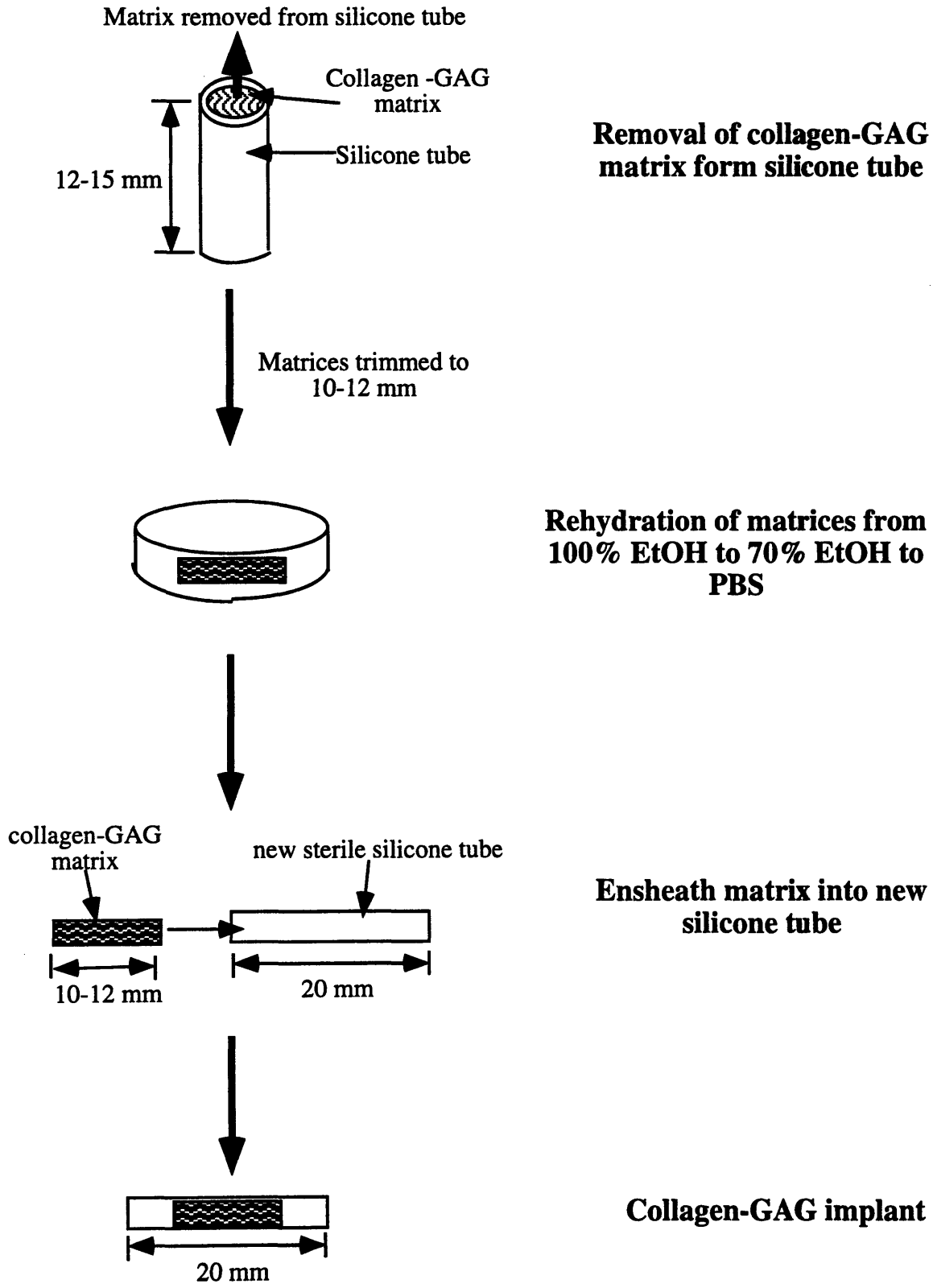

Figure 4.3. Schematic of implant preparation process.

4.2.3. Experimental plan

Table 4.2 summarized the experimental test grid of this project. Three different pore channel diameters were chosen to be studied: small pore channels (average pore channel diameter of 25 μm), medium pore channels (average pore channel diameter of 60 μm), and large pore channels (average pore channel diameter of > 120 μm). Empty silicone tubes served as controls. Four time frames of study were chosen: 3 weeks, 6 weeks, and 12 weeks. In addition, the control, empty silicone tube was investigated at 10 days. These times were chosen to correspond to the 4 early phases of tendon healing. Four animals were allocated to each condition to allow for 3 specimens should an animal die prematurely.

	10 days	3 weeks	6 weeks	12 weeks
CONTROL (empty)	4	4	4	4
AECM # 1 (> 120 μm)	0	4	4	0
AECM # 2 (60 μm)	0	4	4	4
AECM # 3 (25 μm)	0	4	4	0

Table 4.2. Chart of experimental test grid. The number in each grid denotes the number of animals per experimental condition.

4.2.4. Tissue sampling, fixation and sectioning

Animals were sacrificed either by lethal injection with sodium pentobarbital at a dosage advised by a veterinarian. The lesion site was exposed and the entire right Achilles tendon was removed. The contralateral tendon was also removed. The tissues were fixed overnight in 10% neutral buffered formaldehyde (pH 7.4) (see Appendices). The samples were washed in phosphate buffered solution (pH 7.4) for 5 minutes prior to gross examination of the tissue. Tissue surrounding the outside of the tube was dissected away to expose the silicone tube. The silicone tube was split in half lengthwise to expose the contents within the tube. Tissue was

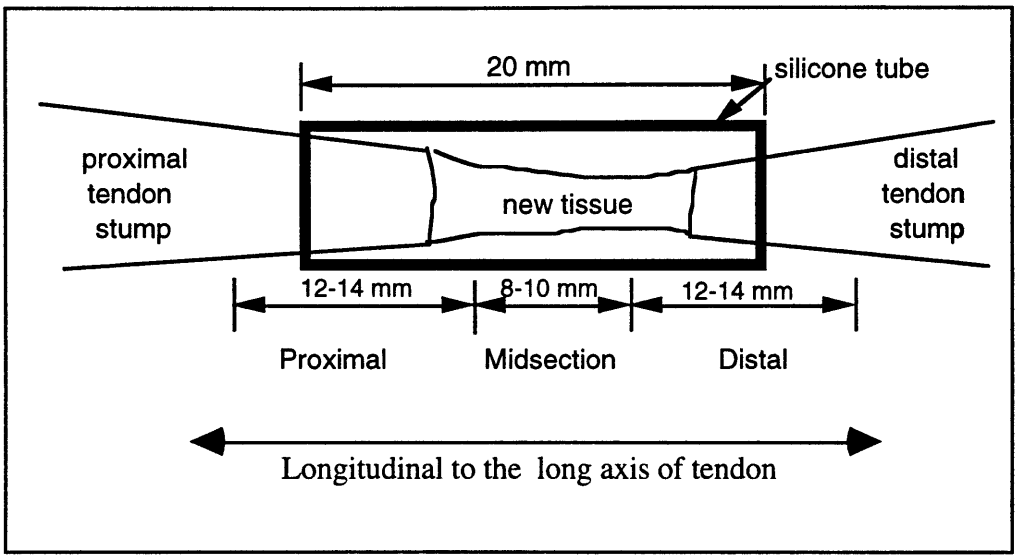

Figure 4.4. Tissue for collagen fibril diameter distribution study to come from remaining paraffin-embedded tissue in "midsection" tissue blocks.

sectioned into three parts: proximal tissue which included tissue of the proximal tendon stump, midsection tissue which was composed of "new tissue", and distal tissue which included tissue of the distal stump (Figure 4.4). The contralateral tendon was similarly sectioned. The tissues were processed and embedded in paraffin with the following protocol:

Tissue embedding and sectioning.

Paraffin embedding and sectioning protocol. Samples were dehydrated through graded alcohol (50%, 70%, 80%, 95%, 95%, 100%, 100%, 100% ethanol) using a Tissue-Tek automatic processor (Tissue-tek VIP, Miles Laboratory, a division of Ames Scientific, Mishawaka, IN) to three changes of histoclear (S/P Brand Americlear histology clearing solvent, cat# C4200-1, Baxter Scientific, Deerfield, IL) for 30 minutes in each solution. The samples were infiltrated in three changes of the melted paraffin for 30 minutes in each change prior to embedding in fresh paraffin. Tissue were embedded longitudinal to the long axis of the tendon (Figure 4.4).

Six micron-thin sections were microtomed (model 1512, Leitz Wetzlar, Easton, MA), floated onto a water bath (Tissue float bath, Lo Boy, Lab-line, obtained through Fisher

Chemical, Pittsburgh , PA) heated to 46°C, collected onto clean glass slides (Superfrost Plus, cat# 48311-703), VWR, Boston, MA), and allowed to dry overnight at 45°C. Sections were cut such that the longitudinal cross-section of the tissue was shown.

Epon embedding protocol. Epon embedded samples were needed for electron microscopy. Because tissue in the midsection of the implant tubes (see figure 4.4) were of primary interest for electron microscopy evaluation (the tissue in the center of wound site primarily consisted of all newly synthesized tissue and not tissue from the original Achilles tendon stump) and because of the small volume of midsectional tissue available, midsectional tissue previously embedded in paraffin for histological use was reprocessed for electron microscopy evaluation.

Reprocessing of paraffin embedded tissue samples consisted of dewaxing of the desired region of the tissue block in xylene for at least two hours with 3 fresh changes of solution. After dewaxing, the tissue was trimmed of unnecessary tissue with a sharp scalpel to the desired size, approximately 1x1 mm^2 blocks, and rehydrated through graded alcohol to two changes of PBS solution. The samples were post-fixed in 1% osmium tetroxide in PBS for 1.5 hours, dehydrated through graded alcohol to two changes of acetone before infiltration with Poly/Bed 812 solution (Polysciences Inc., Warrington, PA), mixed according to manufacturer's recommended mixture ratio. The infiltration schedule consisted of 2:1 acetone: Poly/Bed, 1:1 acetone: Poly/Bed, 1:2 acetone: Poly/Bed, 100% Poly/Bed, 100% Poly/Bed over a 2-3 days time period, followed by embedding of the infiltrated samples, in their desired orientation in flat embedding molds. Samples were polymerized at 60°C for 24-48 hours.

4.2.5. Gross Evaluation

Prior to allocation and sectioning of the tissue for paraffin embedding, the intact tissue was evaluated grossly. A visual record of the tissue was obtained and the gross dimensions of tissue was recorded.

4.2.6. Histology

4.2.6.1. Routine histology

Routine histology consisted of histological staining of the paraffin-embedded tissue sections for general cellular components and collagen matrix.

Hematoxylin and Eosin (H&E) stain Paraffin embedded sections were rehydrated to distilled water by 2 washes in xylene for 5 minutes, followed by serial rehydration (100%, 100%, 95%, 80%, 70% ethanol) for 1 minute in each solution, and distilled water for 5 minutes. Rehydrated tissue sections were stained for 15 minutes in Harris' hematoxylin solution (cat# HHS-128, Sigma Co., St. Louis, MO) and rinsed in distilled water, followed by 10 dips in acid-alcohol solution (1 ml HCl in 100 ml 70% ethanol). The hematoxylin was blued by 1 minute immersion in weak ammonia solution (2-4 drops ammonium hydroxide per 500 ml distilled water), followed by thorough rinsing in distilled water. The slides were counterstained with Eosin (0.1% Eosin Y in 70% ethanol with 0.5% glacial acetic acid) for 30 seconds and rinsed under running water. The slides were dehydrated through graded ethanol solutions, cleared in 2 changes of xylene prior to mounting (Cytoseal 60, low viscosity, Stephan Scientifics, Riverdale, NJ) and glass coverslipping.

Masson's tri-chrome stain Paraffin embedded sections were rehydrated to distilled water by 2 washes in xylene for 5 minutes, followed by serial rehydration (100%, 100%, 95%, 80%, 70% ethanol) for 1 minute in each solution, and distilled water for 5 minutes. Rehydrated tissue sections were stained for 10 minutes in Weigert's iron hematoxylin (equal parts 1% hematoxylin in 95% ethanol and an aqueous solution of 1.2% ferric chloride and 1% concentrated hydrochloric acid), followed by 10 minutes under running water. The slides are then stained in Biebrich scarlet solution for 2 minutes, rinsed in distilled water, and mordanted in a 2.5% phosphomolybdic–2.5% phosphotungstic acid solution for ten minutes before staining in an acidified aniline blue solution (aqueous solution of 2.5% aniline blue and 2% glacial acetic acid) for 10 minutes. Excess aniline blue solution was removed by rinsing in a 1% glacial acetic acid solution before thorough rinsing in distilled water. The slides were

dehydrated through graded ethanol solutions, cleared in 2 changes of xylene prior to mounting and glass coverslipping.

4.2.6.2. Immunohistochemistry

Type I collagen Paraffin embedded sections were rehydrated to tris-buffered saline solution (TBS, cat# T6664, Sigma Co., St. Louis, MO) by 2 washes in xylene for 5 minutes, followed by serial rehydration (100%, 100%, 95%, 80%, 70% ethanol) for 1 minute in each solution, and TBS for 5 minutes. Sections were digested in a 0.1% trypsin solution (cat# T8128, Sigma Co., St. Louis, MO) for 1 hour; followed by 2 washes in TBS for 3 minutes. The sections were blocked with a 20% nonimmune donkey serum (cat# D9663, Sigma Co., St. Louis, MO). Sections were incubated in primary antibody (goat anti-type I collagen, 1: 50, cat# 1310-01, Southern Biotechnology Associates, Inc, Birmingham, AL) for overnight; secondary antibody (donkey anti-goat IgG, 1:20, cat# G7767, Sigma Co., St. Louis, MO) for 60 minutes; then PAP complex (goat peroxidase-anti peroxidase, 1:200, cat# P1901, Sigma Co., St. Louis, MO) for 60 minutes. Sections were washed twice in TBS after exposure to the primary, secondary, and complex. The stain was developed by incubation with the AEC substrate solution (4 ml distilled water, 2 drops acetate buffer, 2 drops AEC chromogen, and 1 drop 3% hydrogen peroxide, from Sigma kit cat# IMMH-2, Sigma Co., St. Louis, MO) for 15-20 minutes. Sections were rinsed in distilled water for 3 minutes; counterstained with Gill's hematoxylin (cat# GHS-3-16, Sigma Co., St. Louis, MO) for 1 minute; and rinsed under tap water for 3 minutes. Sections were dried and mounted with Aqua-poly/mount (cat# 18606, Polysciences, Inc., Warrington, PA) and coverslipped.

Type III collagen Paraffin embedded sections were rehydrated to tris buffered saline solution (TBS, cat# T6664, Sigma Co., St. Louis, MO) by 2 washes in xylene for 5 minutes, followed by serial rehydration (100%, 100%, 95%, 80%, 70% ethanol) for 1 minute in each solution, and TBS for 5 minutes. Sections were digested in a 0.1% trypsin solution (cat# T8128, Sigma Co., St. Louis, MO) for 1 hour; followed by 2 washes in TBS for 3 minutes.

The sections were blocked with a 20% nonimmune donkey serum (cat# D9663, Sigma Co., St. Louis, MO). Sections were incubated in primary antibody (goat anti-type III collagen, 1: 50, cat# 1330-03, Southern Biotechnology Associates, Inc, Birmingham, AL) for overnight; secondary antibody (donkey anti-goat IgG, 1: 20, cat# G7767, Sigma Co., St. Louis, MO) for 60 minutes; then PAP complex (goat peroxidase-anti peroxidase, 1: 200, cat# P1901, Sigma Co., St. Louis, MO) for 60 minutes. Sections were washed twice in TBS after exposure to the primary, secondary, and complex. The stain was developed by incubation with the AEC substrate solution (4 ml distilled water, 2 drops acetate buffer, 2 drops AEC chromogen, and 1 drop 3% hydrogen peroxide, from Sigma kit cat# IMMH-2, Sigma Co., St. Louis, MO) for 15-20 minutes. Sections were rinsed in distilled water for 3 minutes; counterstained with Gill's hematoxylin (cat# GHS-3-16, Sigma Co., St. Louis, MO) for 1 minute; and rinsed under tap water for 3 minutes. Sections were dried and mounted with Aqua-poly/mount (cat# 18606, Polysciences, Inc., Warrington, PA) and coverslipped.

Alpha-smooth muscle actin The immunostaining of the tissue sections used a prediluted alpha smooth muscle actin kit (cat# IMMH-2, Sigma Co., St. Louis, MO). Alpha smooth muscle actin antibody stain is used to detect the presence of myofibroblasts. Modifications to the suggested protocol [111] included in the kit were made. A brief description of the staining protocol was as following:

Paraffin embedded sections were rehydrated to phosphate buffered saline solution (PBS, cat# P3813, Sigma Co., St. Louis, MO) by 2 washes in xylene for 5 minutes, followed by serial rehydration (100%, 100%, 95%, 80%, 70% ethanol) for 1 minute in each solution, and PBS for 5 minutes. Sections were digested in a 0.1% trypsin solution (cat# T8128, Sigma Co., St. Louis, MO) for 1 hour; followed by 2 washes in PBS for 3 minutes. The sections were treated to an endogenous peroxide quench in 3% H_2O_2 for 5 minutes; followed by 2 washes in PBS for 3 minutes. The sections were blocked with a 20% nonimmune goat serum (cat# G9023, Sigma Co., St. Louis, MO). Sections were incubated in primary antibody (mouse monoclonal IgG specific for smooth muscle actin) for 1 hour; secondary antibody

(biotinylated goat anti-mouse IgG) for 20 minutes; then avidin-peroxidase conjugate for 20 minutes. Sections were washed twice in PBS after exposure to primary, secondary, and conjugate. The stain was developed by incubation with the AEC substrate solution (4 ml distilled water, 2 drops acetate buffer, 2 drops AEC chromogen, and 1 drop 3% hydrogen peroxide) for 15 minutes. Sections were rinsed in distilled water for 3 minutes; counterstained with Gill's hematoxylin (cat# GHS-3-16, Sigma Co., St. Louis, MO) for 1 minute; and rinsed under tap water for 3 minutes. Sections were dried and mounted with Aqua-poly/mount (cat# 18606, Polysciences, Inc., Warrington, PA) and coverslipped.

4.2.7. Histomorphometry

A classification scheme was developed to evaluate tissue sections stained with H&E and Masson's trichrome. The classification scheme was based on cellular and matrix morphology. A brief description of the classification system is described below. A table of the classification system along with the cellular and matrix criteria is shown in Table 4.3.

Cellular morphology Cellular morphology was determined by staining with hematoxylin and eosin stain. Cells were classified based on the density of cells within a given area and the aspect ratio of the cells. Aspect ratio was defined as the ratio of the length of the cell to the width of the cell. Class I tissue, granulation tissue was composed of primarily rounded (low aspect ratio) cells (Figure 4.5). These cells included some acute inflammatory cell types, macrophages, and undifferentiated cells. There were very few visible matrix elements present. With the increase in class number (i.e., from class II to IV), there was a decrease in the density of cells and an increasingly elongated (high aspect ratio) shape (Figure 4.6, Figure 4.7, and Figure 4.8). The direction of elongation usually was related to the directional orientation of the matrix and was generally in the long direction of the tendon. Class V tissue, normal adult tendon had a low density of cells (< 2% of the viewing area) and cells with a very high aspect ratio that has been referred to as spindle-shaped in the literature (Figure 4.9).

Matrix morphology Matrix morphology was assessed by staining with Masson's trichrome stain. Matrix was classified based on the degree of alignment of the tissue in the long direction of the tendon and the presence and characteristic of a crimp pattern as seen under polarized light. Crimp characteristics included the wavelength of the crimp, the thickness of the bundle of fibers that possessed the crimp pattern (Figure 4.8), and the coherence length (the length over which the fiber bundles exhibited the crimp pattern). The crimp wavelength and fiber bundle thickness were measured from the alternating light and dark bands which represent the collagen fibers folding into a planar pattern, as seen under polarized light. The coherence length was not measured because of the difficulty in assessing its boundaries. Class I tissue, granulation tissue had very few visible matrix elements present (Figure 4.5). Class II tissue, loose fibrous tissue, had randomly oriented loosely packed collagen fibers and no visible crimp pattern (Figure 4.6). With increasing class number, class III and class IV, there was a increase in the packing density of the matrix, i.e. "dense fibrous tissue" and an alignment of the matrix fibers in the long direction of the tendon. Class III and class IV tissue (Figure 4.7 and Figure 4.8) was differentiated based on the appearance of crimp in class IV tissue. Class IV and normal adult tendon, class V tissue, was differentiated based on the characteristic of the crimp pattern. Class IV tissue had on average small bundles of fibers (bundle thickness between 10-100 μm) with a small crimp wavelength (10-50 μm). On the other hand, normal adult tendon (Class V) had on average fiber bundles (> 500 μm thick) with crimp wavelength between 100-120 μm (Figure 4.9).

Tissue samples were evaluated using a light microscope (Olympus Vanox AH-2, Olympus America Inc., Lake Success, NY) fitted with a calibrated eyepiece reticule. All samples were viewed at an objective lens of 10x, which corresponded to a square viewing area of 0.36 mm^2.

Class	Cells (Based on H&E stain)		Matrix Fibers (Based on Masson's trichrome stain)		
	Arealpercentage (% of viewing area)	Aspect ratio (L/W)	Alignment (% along tendon long axis ± 5° off the axis)	Crimped Fiber	
				Wavelength	Thickness
Granulation	> 80%	1 to 2	n/a	n/a	n/a
II	20 to 10%	2 to 10	0 to 50%	n/a	n/a
III	10 to 5%	10 to 15	50 to 90%	n/a	n/a
IV	< 5%	15 to 20	> 90%	10-50 μm	10-100 μm
Tendon	< 2%	> 20	> 95%	100-120 μm	> 500 μm

* Aspect ratio (length of cell / width of cell)

Table 4.3. Classification of tissue. Criteria based on cellular and matrix morphology; class I, granulation tissue composed of primarily cells, class II, loose fibrous tissue, classes III and IV, dense fibrous tissue, and class V, normal adult tendon. (n/a: not applicable)

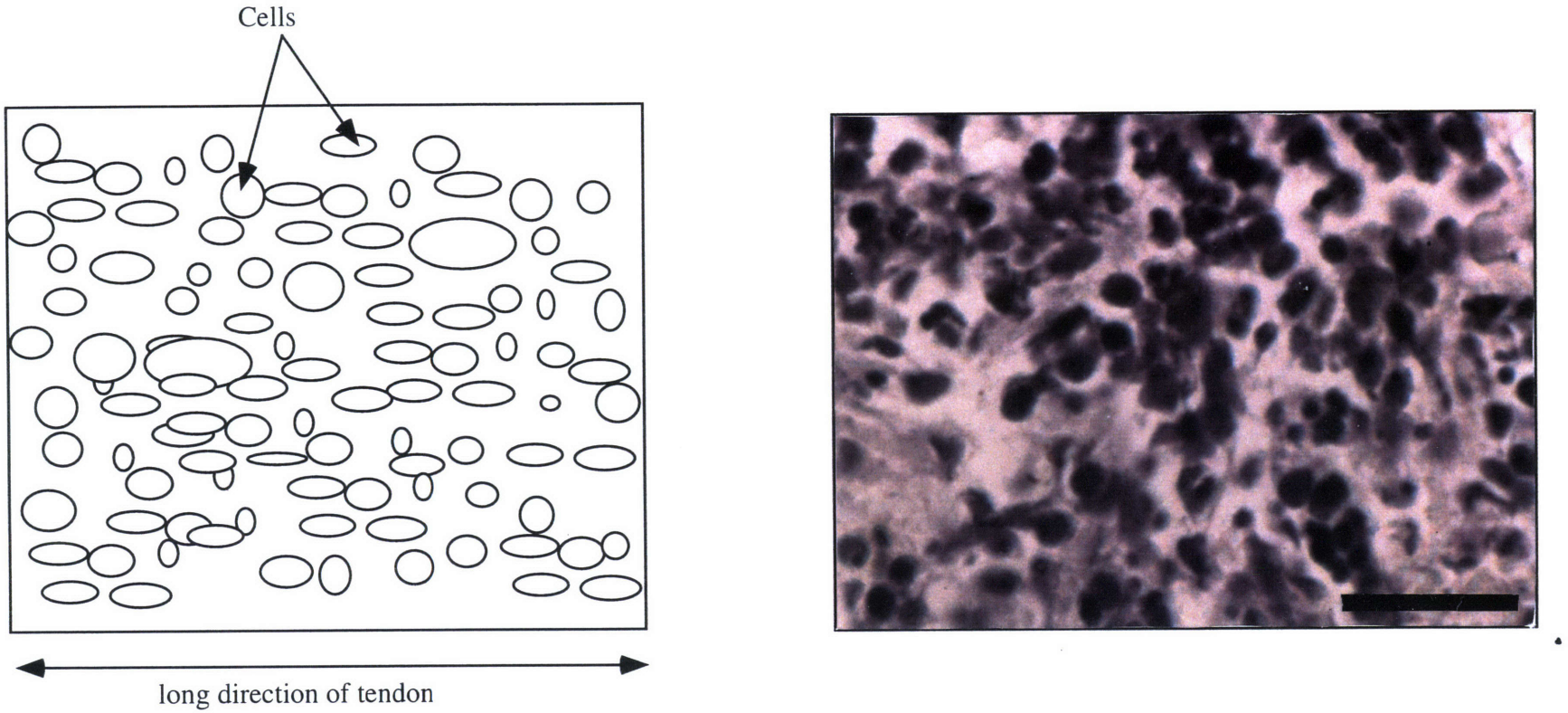

Figure 4.5. Class I tissue, granulation tissue. Class I tissue is composed of primarily cellular products with few visible matrix products. A schematic (**left**) depicts the abundance of cellular products with a primarily rounded appearance. A light micrograph (**right**) shows a tissue section which was classified as a class I tissue. (H&E, scale bar equals 50 μm)

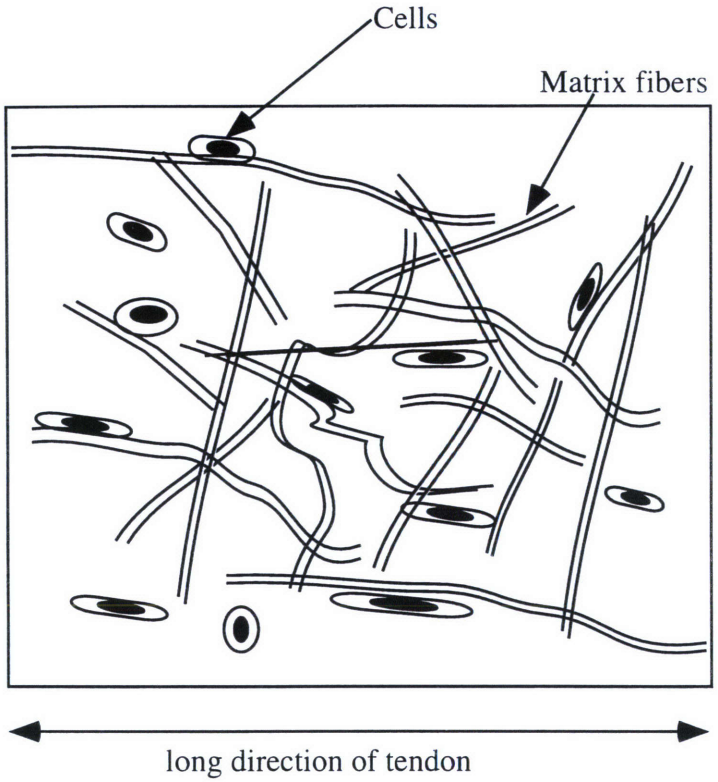

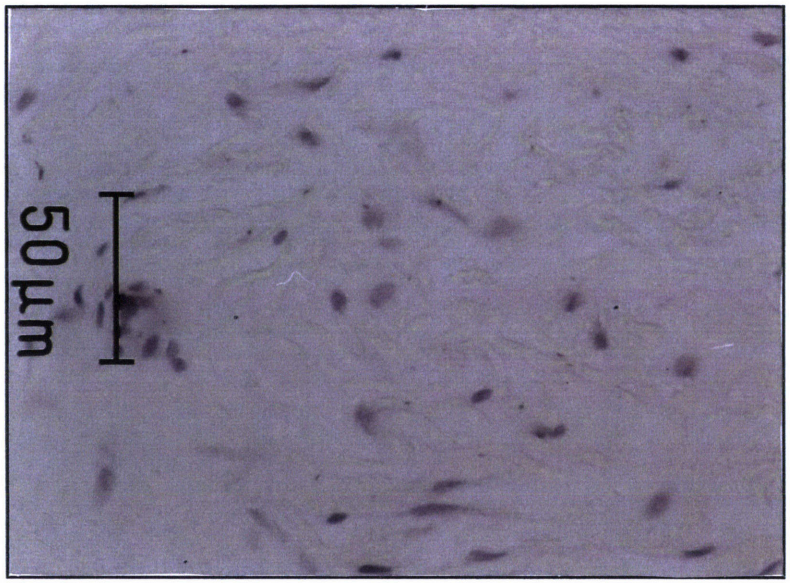

Figure 4.6. Class II tissue, loose fibrous tissue. Class II tissue is composed of loose randomly oriented fibrous matrix with rounded to slightly elongated cells. A schematic (**left**) depicts fibroblast cells within a randomly oriented matrix of fibers. Light micrograph (**right**) shows a tissue section which was classified as a primarily class II tissue. (H&E, scale bar equals 50 µm)

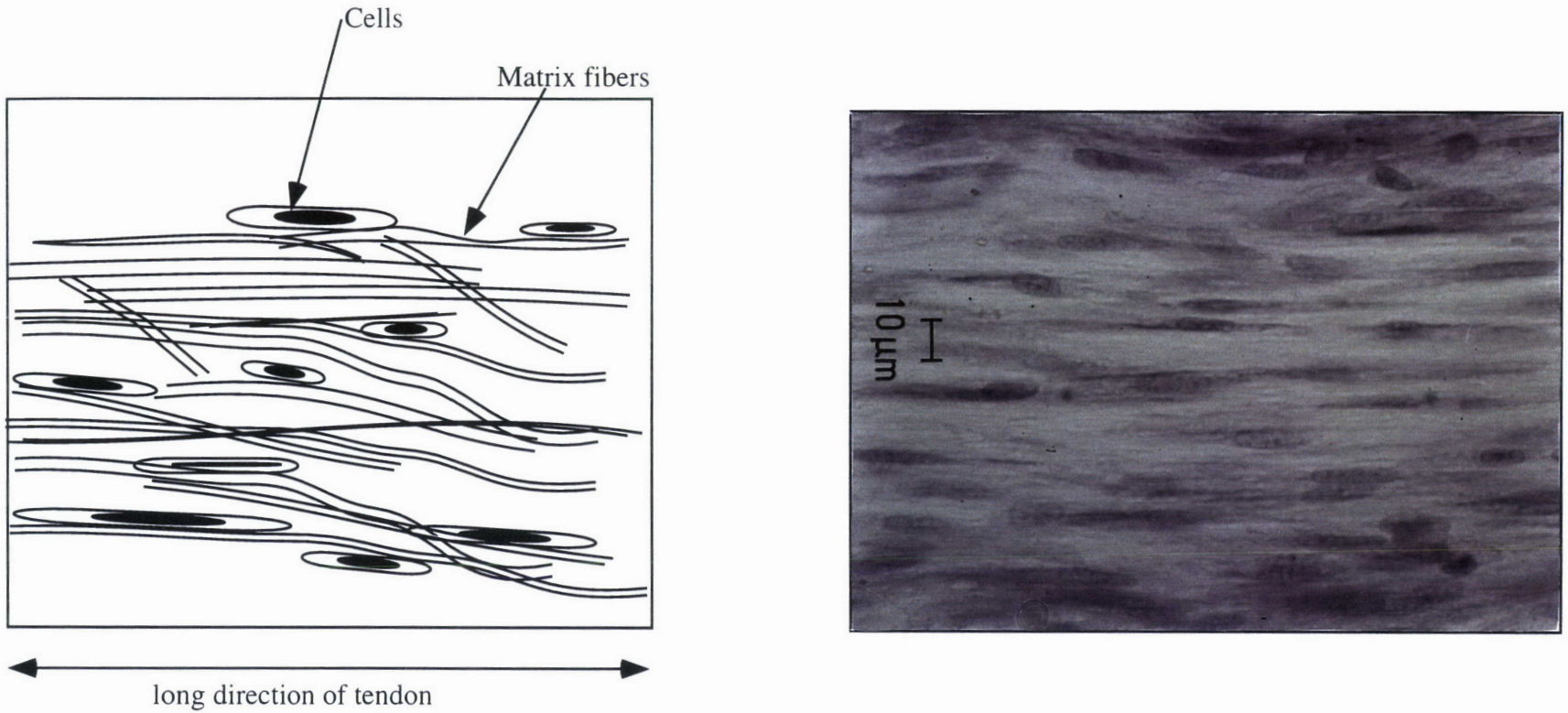

Figure 4.7. Class III tissue, dense fibrous tissue. Class III tissue is composed of dense oriented fibrous matrix, oriented in the long direction of the tendon with highly elongated cells. A schematic (**left**) depicts fibroblast cells within a highly oriented matrix of fibers. Light micrograph (**right**) shows a tissue section which was classified as a primarily class III tissue. (H&E, scale bar equals 10 µm)

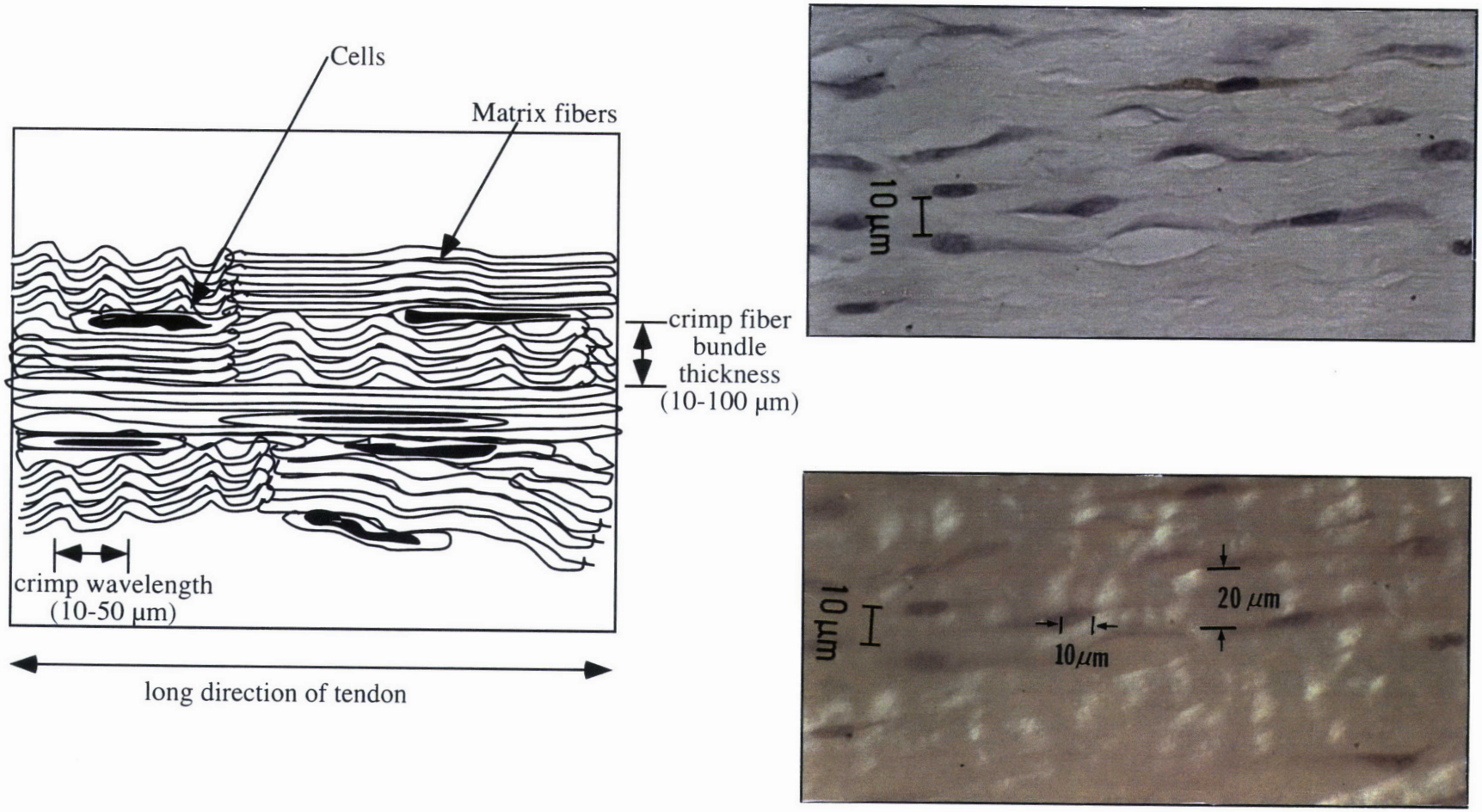

Figure 4.8. Class IV tissue, crimped dense fibrous tissue. Class IV tissue is composed of dense oriented fibrous matrix, oriented in the long direction of the tendon with highly elongated cells. Class IV tissue differed from Class III tissue in the frequent presence of a crimp pattern when seen under polarized light. A schematic (**left**) depicts fibroblast cells within a highly oriented matrix of fibers. Light micrograph (**top right**) shows a tissue section which was classified as a primarily class IV tissue. Polarized light micrograph (**bottom right**) shows the crimp pattern of a typical class IV tissue. (H&E, scale bar equals 10 μm)

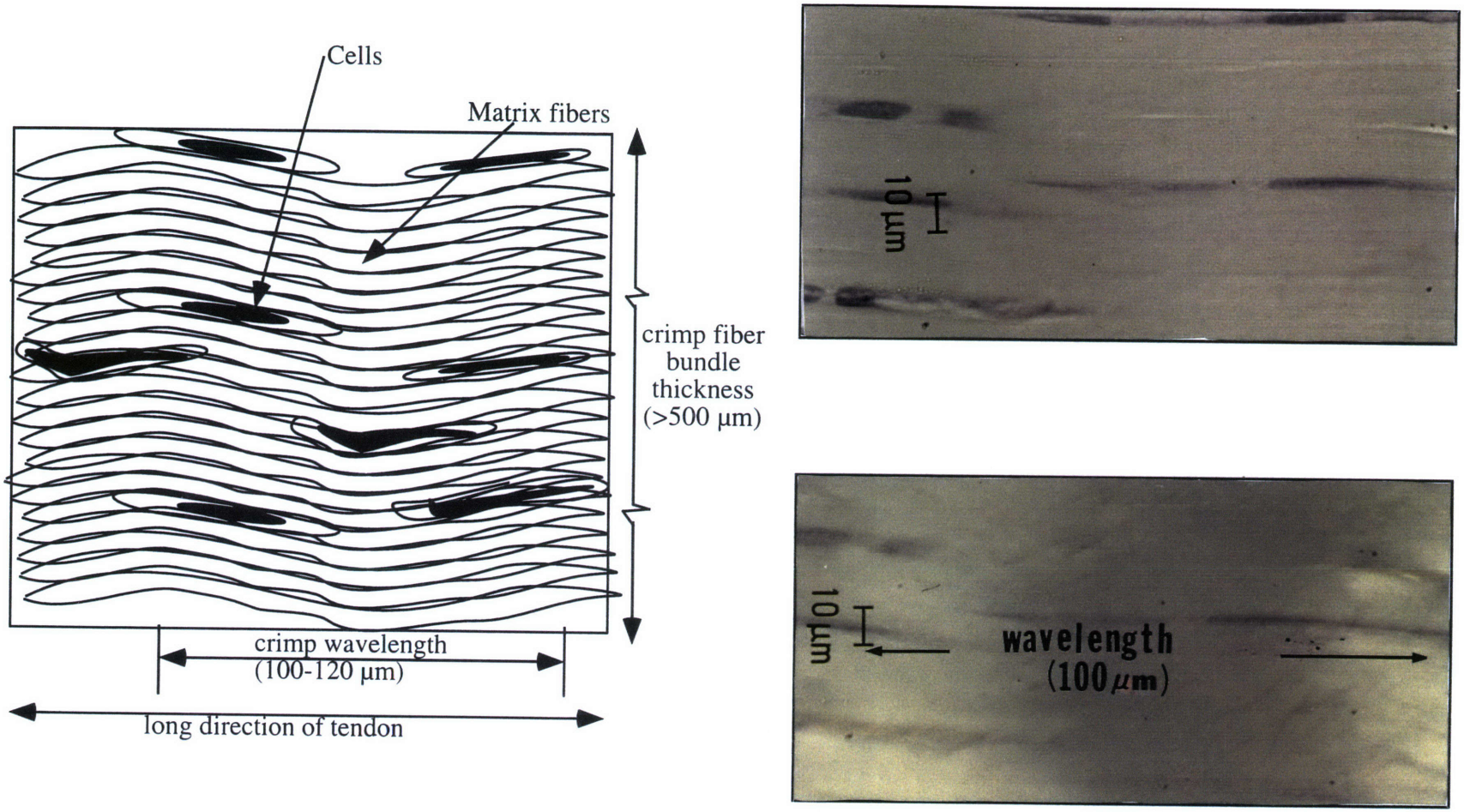

Figure 4.9. Class V tissue, dense fibrous tissue. Class V tissue is composed of densehighly aligned fibrous matrix, oriented in the long direction of the tendon with highly elongated cells. Class V tissue also a well-developed and highly regular crimp pattern when seen under polarized light. A schematic (**left**) depicts fibroblast cells within a highly oriented matrix of fibers that have a crimp pattern. Light micrograph (**top right**) shows a tissue section which was classified as a primarily class V tissue. Polarized light micrograph (**bottom right**) shows the crimp pattern of a typical class V tissue. (H&E, scale bar equals 10 μm, magnification 130x)

4.2.8. Transmission Electron Microscopy (TEM)

Epon embedded samples were cut with a diamond knife (Dupont Instruments, Wilmington, DE) on a Reichert Ultracut S ultramicrotome, and mounted on 200 mesh uncoated copper grids (Polysciences Inc., Warrington, PA). Tissue sections were approximately 100 nm thick. The sections were stained with a 2% aqueous uranyl acetate solution for 10 minutes, rinsed in 3 changes of distilled water, blotted dry and then stained with Reynold's lead citrate (formulation can be found in Appendix A) for 3-10 minutes, rinsed in 3 changes of distilled water and blotted dry.

Stained grids were examined on a JEOL 1200 CX electron microscope operating at 80 kV. Longitudinal and cross-sections of the healing tissue were evaluated for primarily for collagen fibril orientation and evidence of myofibroblast-type cells.

Cross-sections of the healing tissue, relative to the long axis of the tendon, were used to quantify collagen fibril diameter and distribution. Micrographs of fibril cross-sections were taken at a magnifications of 12,000- 40,000X in random regions of the specimen. A minimum of five micrographs were taken for each sample with a maximum of 10 micrographs being collected. Regions containing cell processes, resin fractures an cutting artefacts were avoided as much as possible.

Negatives (3.25" x 4") of each micrograph were processed into black and white photographs (8" x 10"). The negatives were enlarged to encompass the maximum area of the negative to fill the 8" x 10" space. It should be noted that each photograph contained a calibrated scale marker. High contrast of the images were sought in order to facilitate subsequent binary imaging of the micrograph for image analysis.

Photographic images of a minimum of five regions per sample were digitally scanned with a color flatbed scanner (AGFA StudioScan IIsi) into a Macintosh IIsi computer via Adobe Photoshop LE. Scanner settings were set to capture the image at 200 ppi, enlarged to a 100% scale. Because of large files sizes required to capture the images, the size of the images were

reduced further in size to approximately 8" x 10" images in Photoshop. Each file size was limited in size not to exceed 3.3 MB of space, while still allowing for a pixel resolution of at least 100 pixels per inch.

Computer image files were transferred to a Power Macintosh 6100, where the subsequent image analysis of the computer files were performed. A public domain image analysis program, NIH Image (version 1.55, written by Wayne Rasband at the U.S. National Institutes of Health and available from the Internet by anonymous ftp from zippy.nimh.nih.gov) was used to quantify the collagen fibril diameters. The image analysis program involved an interactive process of discriminating the collagen fibrils from the background and from each other, followed by an automated measurement of the fibril areas and elliptical major and minor axis lengths. Because minor axis length measurement (i.e., minimum fibril diameter) was less sensitive to the obliquity of section cuts, minimum fibril diameter was the primary parameter compared. Two thousand collagen fibrils were counted per each specimen, with on average 400 collagen fibrils counted per computer image file.

Data collected from NIH Image was transferred to Microsoft Excel (ver.4.0, Microsoft Corp.), a spreadsheet program capable of simple statistical analysis. A histogram of the 2000 collagen fiber diameter per specimen was produced. Fibril diameters were classified into 20 groups ranging from 0-500 nm (25 nm per group).

4.3 Results

4.3.1. Animal model evaluation

A total of fifty two animals were used in the study. Nine animals were lost on the operating table due to anesthesia and replaced in the study. Loosening of the external fixation did occur to some extent in all the animals but daily monitoring of the animals ensured that the fixation devices were retightened within a day. No fixation device was removed prematurely. All devices were removed by 10 days or at most 14 days postoperatively. Two animals were

sacrificed prematurely due to complications unrelated to the surgical procedure and were discarded from the study.

Gross examination of the excised tissue at time of sacrificed showed that two animals had "pull-out". Pull out was defined as the pulling out of either the distal and/or proximal tendon stump from the silicone tube. This was a major problem with earlier version of the animal model. These earlier versions did not incorporate the release of additional tendons located around the hock joint. This extra procedure of protecting the lesion site from mechanical loading appeared effective in preventing pull-out of the tendon stumps from the silicone tube.

4.3.2. Gross morphology

4.3.2.1. Qualitative evaluation

The outside of the silicone tubes were covered by a tissue mass (Figure 4.10). The appearance of this outer tissue changed as a function of time. At 10 days and three weeks, the tissue covering the silicone tube was thick (thickness averaged 2-3 mm) and opaque in appearance. By 6 weeks the mass of tissue was not as great (1-2 mm), but was still opaque though not as rough in appearance as the 10 days and 3 weeks specimens . At 12 weeks, the tissue covering the silicone tube had become thinner (1 mm) and partially transparent . In most cases, the outline of the silicone tube could be seen through this tissue. In general, this tissue covering the outer surface of the silicone tube did not adhere to the tubing and could be easily dissected away from the tube. The surface of the tissue in contact with the silicone tube was very smooth in appearance.

Within the silicone tube, there appeared to be a cable of tissue spanning the wound gap for all specimens, except for the specimens that had "pull-out" of the tendon stump (section 4.3.1). The cable of tissue decreased in volume as a function of time (Figure 4.10 and Figure 4.11). Generally, a tissue mass filled the entire defect area at 10 days for empty tubes and 3 weeks for collagen-GAG filled tubes. This tissue mass was in most cases bloody in

appearance. At the time period increased the diameter of the tissue mass decreased. In addition, the tissue mass changed from a bloody appearance to opaque in color to almost translucent in appearance by 12 weeks. The tissue that spanned the lesion site appeared to be attach at the radial center of the tendon stumps (Figure 4.12).

4.3.2.2. Volume of tissue

The volume of new tissue found in the lesion site decreased with time for all groups (Figure 4.13). By 12 weeks, tissue in the empty tube and tube filled with CG matrix with 60 μm pores had decreased from a 100 % of the defect site filled to about 3 % and 16 % of the defect site filled, respectively.

At twelve weeks, there was a statistically significant difference ($p < .005$, Student t-test) between the volume of tissue found in the empty tubes (n=3) and in the tubes filled with 60 μm pore channel CG matrices (n=3) (Figure 4.14). There was also a statistically significant difference between these groups at 3 weeks ($p< 0.01$, n=5 for empty, n=3 for CG-filled). However, there was no statistically significant difference between the groups at 6 weeks. There was no meaningful difference in the volume of tissue filling the defect site among the 3 different pore diameters at 3 weeks and 6 weeks.

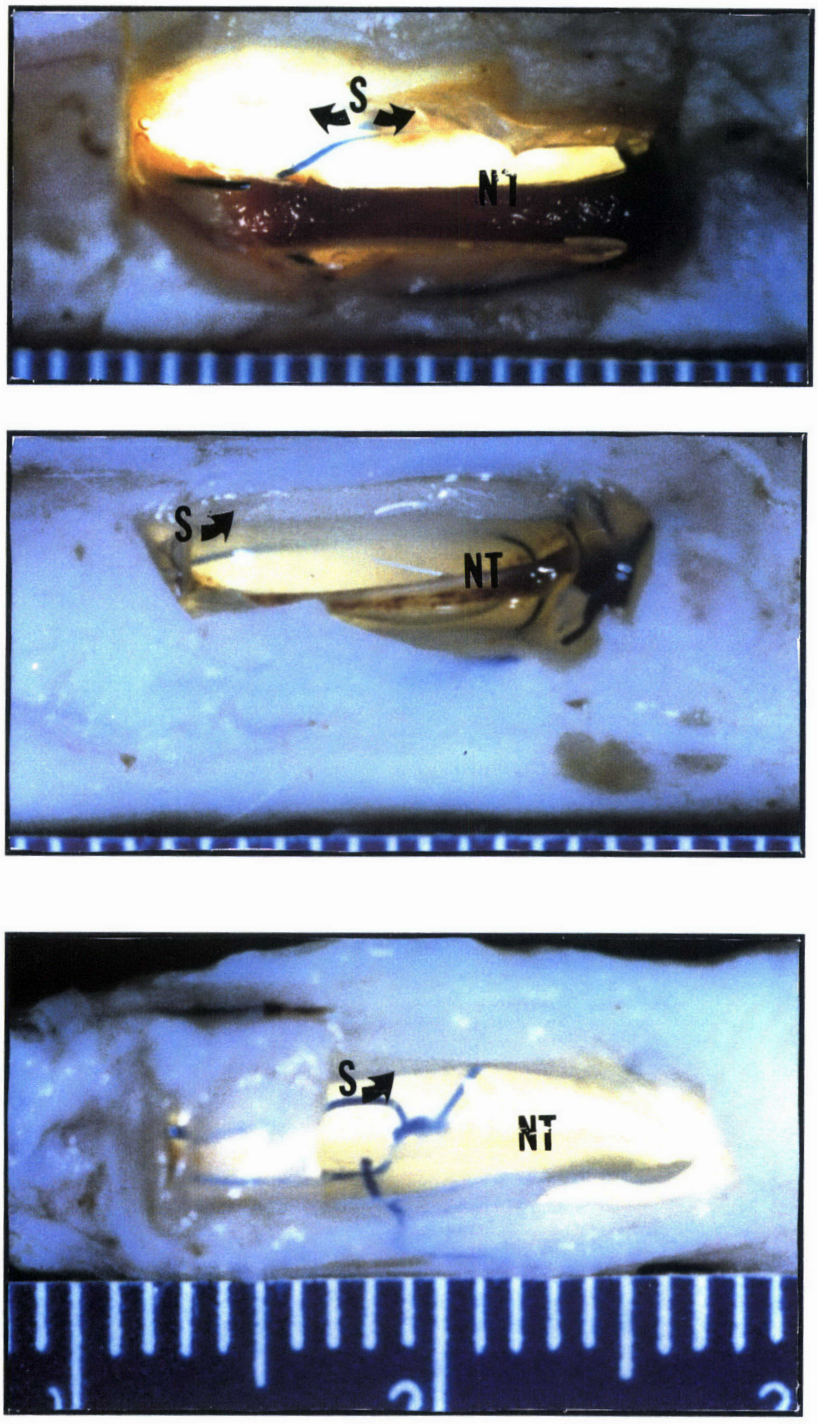

Figure 4.10. Gross morphology of tissue spanning empty tube samples at 3 weeks (**top**), 6 weeks (**middle**) and 12 weeks (**bottom**). The volume of the new tissue (NT) decreases as a function of time. Scale of each division: 1mm. S: silicone tube. NT: new tissue.

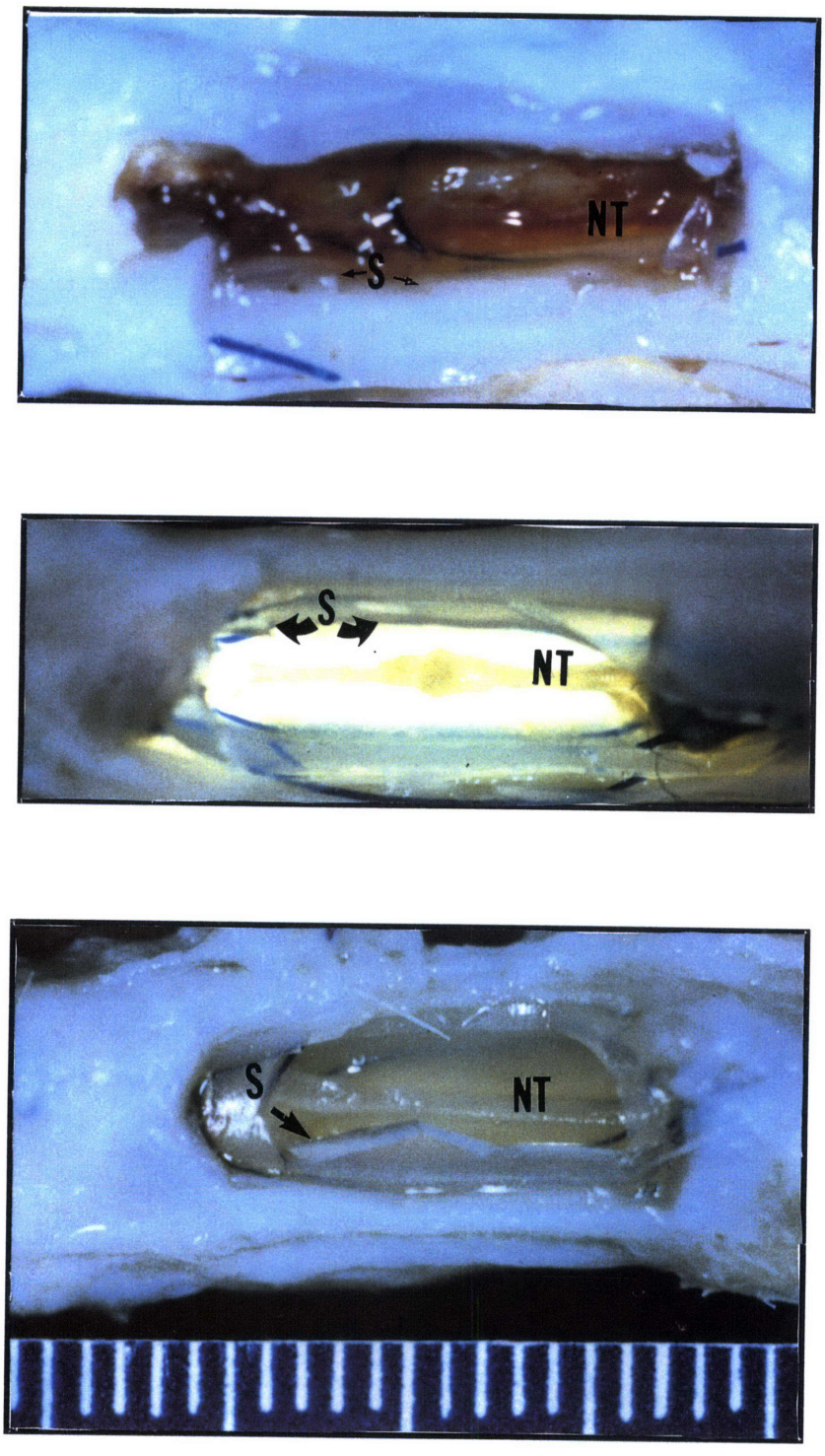

Figure 4.11. Gross morphology of tissue spanning collagen-GAG filled tubes samples at 3 weeks (**top**), 6 weeks (**middle**) and 12 weeks (**bottom**). The collagen-GAG matrices had average pore diameter of 60 μm. The volume of the new tissue (NT) decreases as a function of time. Scale of each division: 1mm. S: silicone tube. NT: new tissue.

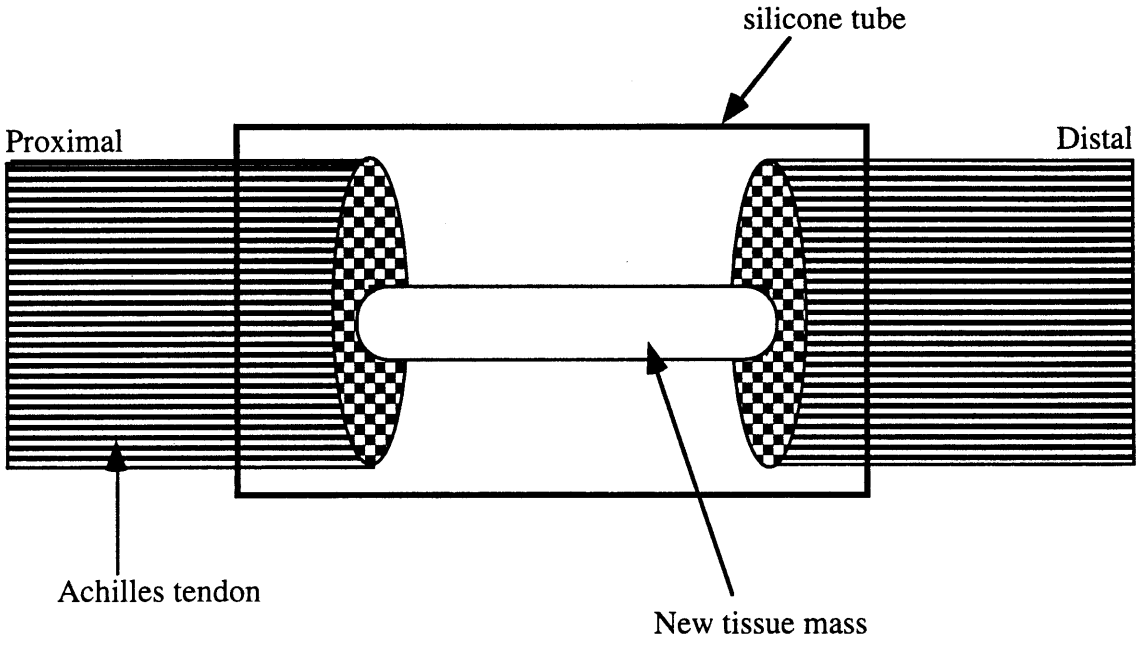

Figure 4.12. Schematic of the location of tissue mass spanning lesion site for a typical 12 week sample. The tissue connects the center of the proximal and distal tendon stumps.

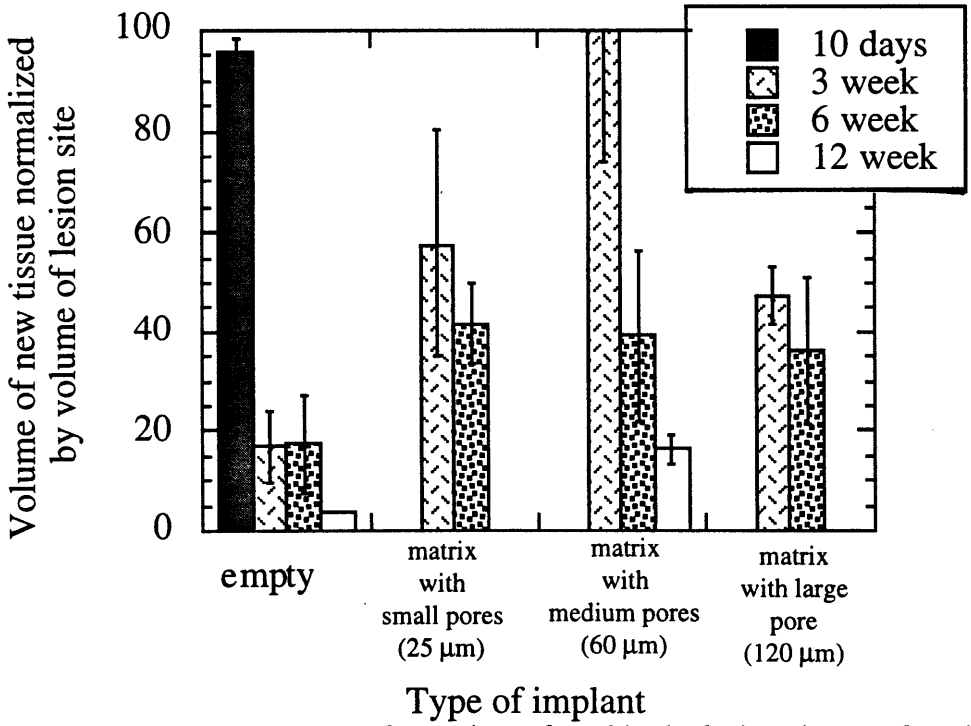

Figure 4.13. The mean volume of new tissue found in the lesion site as a function of the implant group at the time periods of evaluations. The bars represent standard errors of the mean.

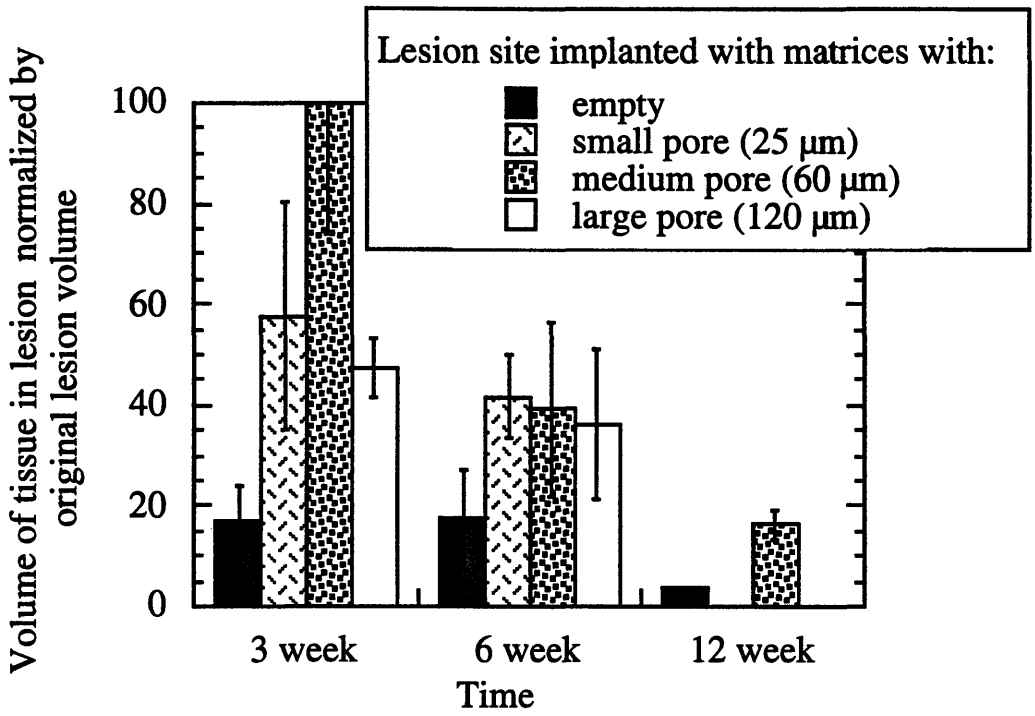

Figure 4.14. The mean volume of new tissue found in the lesion site as a function of time for all implant groups. The bars represent standard errors of the mean.

4.3.3. Histology Evaluation

4.3.3.1. Qualitative cellular evaluation

The cellular make-up of the healing tissue was determined using sections stained with hematoxylin and eosin (H&E). At 10 days, tissue recovered from the empty tubes was primarily cellular. These cells were mainly inflammatory cells (lymphocytes, macrophages , monocytes) and red blood cells. Fibroblasts could not be found in the tissue. By 3 weeks, there was a dramatic decrease in the number of cells present. Inflammatory cells were still present but fibroblast-like cells were also readily identifiable. The fibroblast cells were rounded and with a large nuclei. At six weeks, the predominant cells were fibroblasts. The fibroblast cells had become less rounded and more elongated. The overall direction of the elongation was random, ranging from perpendicular to the tendon stump to parallel to the long axis of the tendon. The nuclei of the cells appear to be decreasing and the spacing between cells appeared to be have increased compared to the 3 week samples. At twelve weeks, the

majority of cells had become highly elongated with a further decrease in the nuclei size. The cells along with the matrix fibers appeared to be aligned in the long direction of the tendon. The overall number of cells also appeared to have diminished from 6 weeks.

At 3 weeks, cells predominated in tissue in CG matrix-filled tubes. The cells were primarily inflammatory cells and blood products. The cells were dispersed throughout the CG matrix. Fibroblast-like cells were not readily identifiable in these 3 weeks samples. At 6 weeks, significant inflammatory response was still present but less that at 3 weeks. The majority of the inflammatory cells appeared to be in the same regions as the CG matrices. Along the edges of the tissue, there appeared to be fibroblasts. The fibroblast cells appeared rounded to slightly elongated with relatively large nuclei. By 12 weeks, the inflammatory response appeared to have diminished significantly. Fibroblasts appeared to be the predominant cell present. The fibroblasts ranged from slightly elongated to highly elongated with diminished cell nuclei. In general cells toward the edges appeared to be more highly elongated and aligned in the long direction of the tendon, with the cells toward the center of the tissue slightly less elongated and not necessarily aligned in the long direction of the tendon.

4.3.3.2. Qualitative matrix evaluation

Tissue sections stained with Masson's tri-chrome were evaluated for presence and orientation of collagen matrix. At 10 days, tissue in empty tubes did not appear to have much matrix content. The tissue samples were primarily cellular. By 3 weeks, there appeared to be primarily loose fibrous tissue with regions of densely packed tissue. This loose fibrous tissue appeared to be randomly oriented (i.e., no preferential fiber direction) but the denser-packed fibers appeared to be aligning in the long direction of the tendon. The denser-packed fibers appear to be localized at the outer regions of the tissue while the central portion of the tendon had loose randomly oriented fibers. At 6 weeks, the central portion of the tissue appeared to contain more areas of the aligned matrix fibers, although there were still regions that were not

as highly aligned. At 12 weeks, on average, all the tissue samples appeared to have highly aligned matrix fibers. The fibers were all aligned in the long direction of the tendon.

Tissue recovered from CG-filled tubes appear to be composed of primarily cellular material and loose fibrous matrix with localized regions of aligned dense fibrous matrix fibers at 3 weeks. There was, in general, more cellular material present in the CG-filled tube than the empty tubes. Those regions that were dense aligned matrix fibers were located toward the edges of the tissue. At 6 weeks, the new tissue in the CG-filled tubes had more fibrous tissue although there was still a good amount of cellular material present. In general, the matrix fibers were aligned more in the long direction of the tendon. Also the central portion of the tissue that did not appear have aligned matrix fibers at 3 weeks, appeared to have isolated regions with aligned matrix fibers. At 12 weeks, on average, the tissue in tubes filled with CG matrix of 60 μm pore diameters was a mixture of primarily aligned matrix fibers and not as highly aligned fibers. The majority of the 12 weeks CG-filled tubes had tissue with aligned matrix, but one of the three samples had randomly aligned matrix fibers.

4.3.3.3. Presence of crimp

Tissue sections stained with hematoxylin and eosin (H&E) were viewed under polarized light microscope for the presence and or absence of a crimp pattern. At 10 days and 3 weeks, no tissues recovered from empty and CG-filled tube appeared to have any crimp pattern. At six weeks, none of the tissue recovered from CG-filled tubes had crimp, but one of the empty tube specimens (out of n=5) had small regions with a crimp pattern. These regions were confined to the outer edges of the tissue sample. By 12 weeks, tissue found in empty tubes had more regions with crimp pattern . On average, the crimp wavelength was 12.2 ± 3.0 μm (average ± SEM) and the fiber bundle thickness was 30.2 ± 11.0 μm. Normal tendon on average, had a crimp wavelength of 110 ± 20 μm and fiber bundle thickness of 1.2 ± 0.4 mm. The fiber bundle thickness is the thickness of the bundle of collagen fibers that undulates

together to form the crimp pattern (see figure 4.8). Tissue in tubes filled with collagen-GAG matrices with pore diameters of 60 μm did not have a crimp pattern associated with it.

4.3.3.4. In vivo degradation of CG matrices

Implanted collagen-GAG matrices were still present at 3 weeks postoperative for all pore sizes. There did not appear to be resorption of the matrices at this time period. By six weeks, CG matrices still appeared present in the wound site although some resorption of the matrices was evident. At twelve weeks there was no evidence of CG matrix present. Total resorption of the matrices occurred between 6 and 12 weeks.

4.3.3.5. Histomorphometry

Random sections within each tissue specimen were evaluated using criteria discussed in section 4.2.10. Following are the results of the quantification of the results presented qualitatively in the previous sections.

Healing of tendon in empty tubes Figure 4.15 is a bar graph representation of classification of tissue recovered from the lesion site as a function of time for the empty tubes. Granulation tissue, 92±2% (average ± SEM, n=4) of the defect volume, predominated at the early period of healing (10 days) but dramatically decreased with time to practically zero (2.1±1.4 %, n=3) of the defect volume by 3 weeks (Figure 4.16). From 3 to 6 weeks, there appeared to be an equal percentage of loose fibrous tissue (class II) and dense fibrous tissue (class III). At 12 weeks, dense fibrous tissue predominated, with approximately one-half of that tissue composed of class IV type tissue (i.e., with a crimp pattern). However, there did not appear to be normal adult tendon (i.e., class V) present.

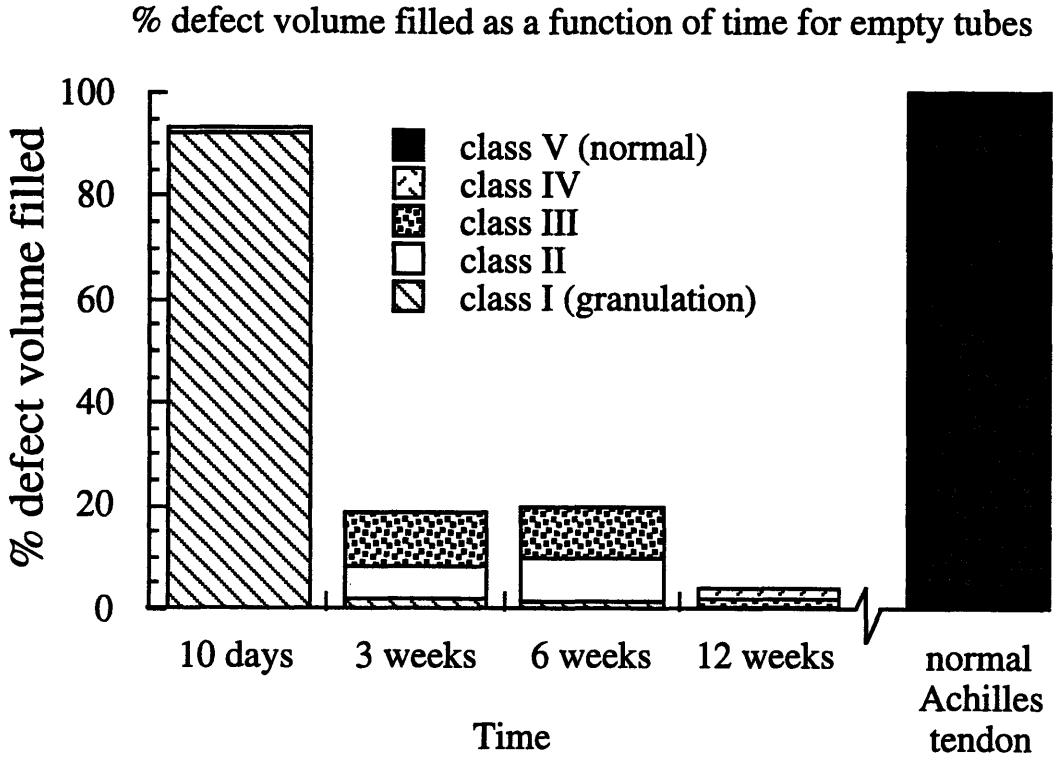

Figure 4.15. Percentage of each class filling defect site as a function of time for the empty control tubes. Criteria for classification based on cellular and matrix morphology: class I, granulation tissue (cellular-based); class II, loose fibrous tissue; classes III and IV, dense fibrous tissue; and class V, normal adult tendon. See section 4.2.10 for detailed description. Normal Achilles tendon, i.e. uninjured case, shown for comparison.

Comparison of healing in empty tubes and tubes filled with CG matrix of medium pore size (60 μm) Figure 4.16 is a bar graph representation of the classification of tissue recovered from the lesion site as a function of time for the empty tubes and the CG (60 μm pore diameter)-filled tubes. In all cases, the CG-filled tubes displayed a greater amount of tissue in the defect. Also, significantly more granulation tissue was found to be present in the CG-filled tubes at 3 and 6 weeks (Figure 4.16 and 4.17). At 3 weeks, 66 ± 26% (n=4) of the defect volume was filled with granulation tissue in the CG-filled tubes compared to 2±1 % (n=3) in the empty tube. There was a slower rate of decrease in the amount of granulation tissue in the CG-filled tubes compared to the empty tube.

The amount of dense fibrous tissue (class III and class IV combined) was overall greater in the empty tubes at 3 weeks and 6 weeks (Figure 4.18). At 12 weeks, however, there

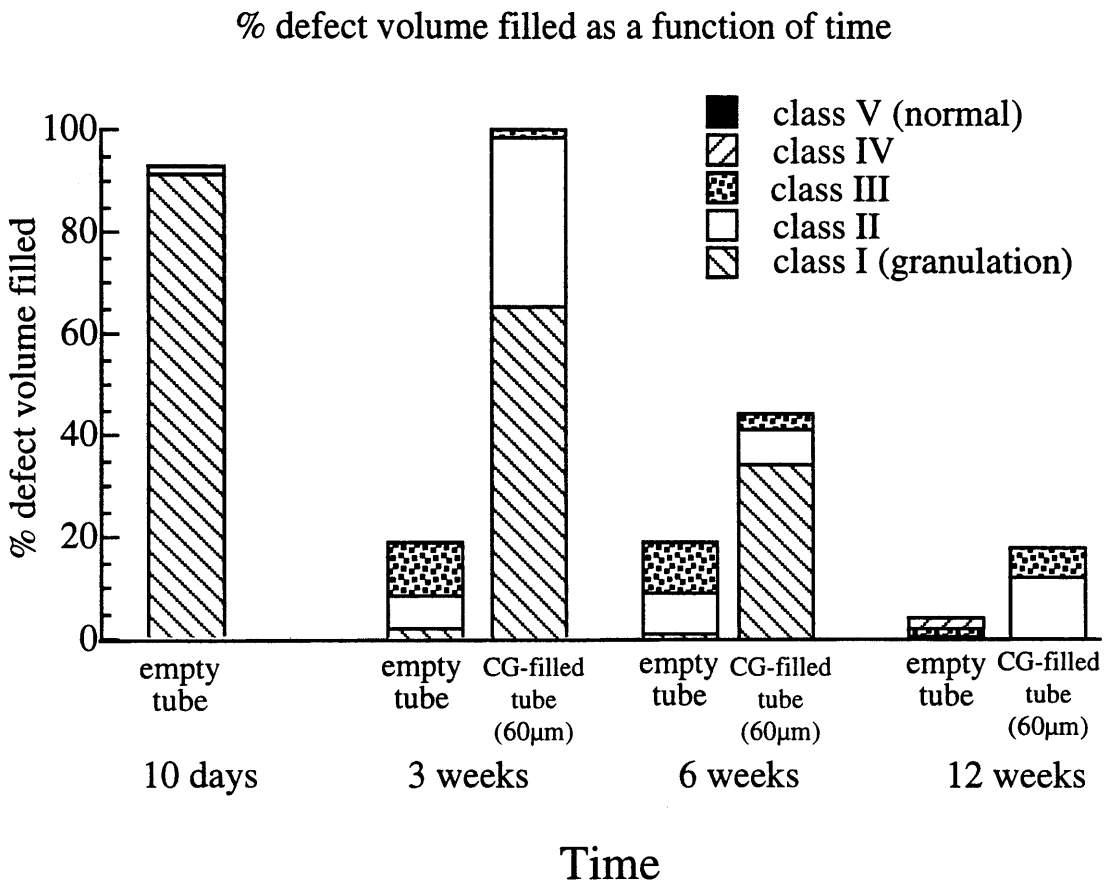

Figure 4.16. Percentage of each class filling defect site as a function of time for the empty tubes and tubes filled with 60 μm pore diameter CG matrix. Criteria for classification based on cellular and matrix morphology: class I, granulation tissue (cellular-based); class II, loose fibrous tissue; classes III and IV, dense fibrous tissue; and class V, normal adult tendon. See section 4.2.10 for detailed description. Normal Achilles tendon, i.e. uninjured case, shown for comparison.

was more dense fibrous tissue (class III and IV) in the CG-filled tube (albeit not statistically significant). Comparing the amount of class III tissue in the empty tube and CG-filled tube, showed a trend in favor of the matrix-implanted defect but no significant difference. The amount of dense fibrous tissue in the defect site appeared to peak between 3 to 6 weeks and decrease thereafter for the empty tube, while the amount of this tissue appeared to be increasing between the period of 3 to 12 weeks for the CG-filled tubes.

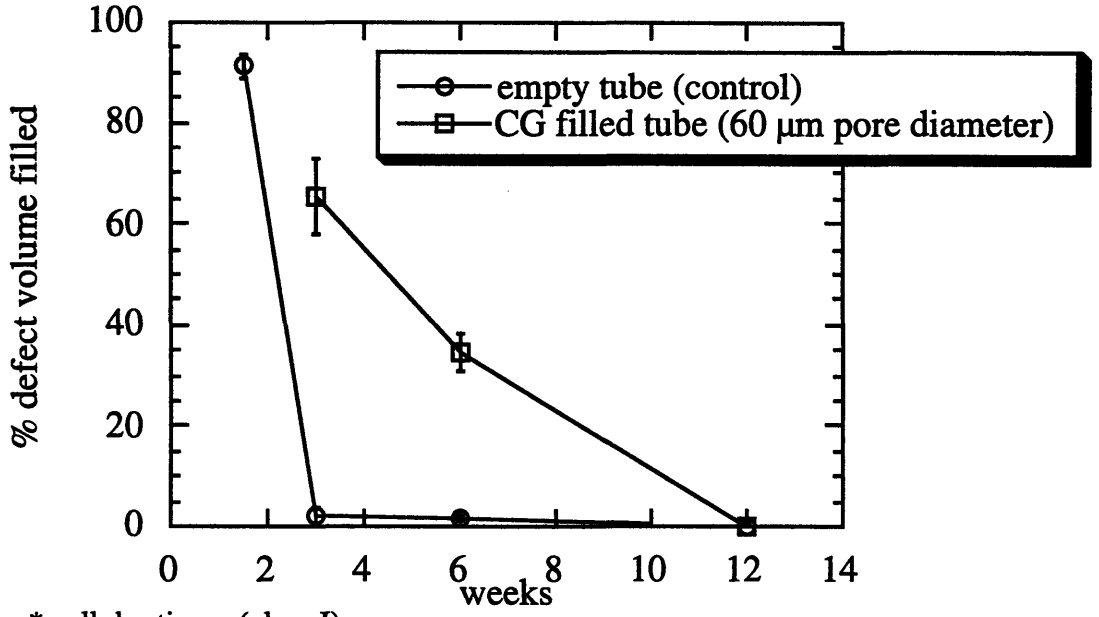

* cellular tissue (class I)

Figure 4.17. The percentage of the defect volume filled with granulation tissue (class I) as a function of time for empty tubes and CG-filled (60 μm pore diameter) tubes. There is a rapid decrease in the percentage of granulation tissue in the empty to while the decrease was gradual in the CG-filled tubes. See section 4.2.10 for detailed description of classes.

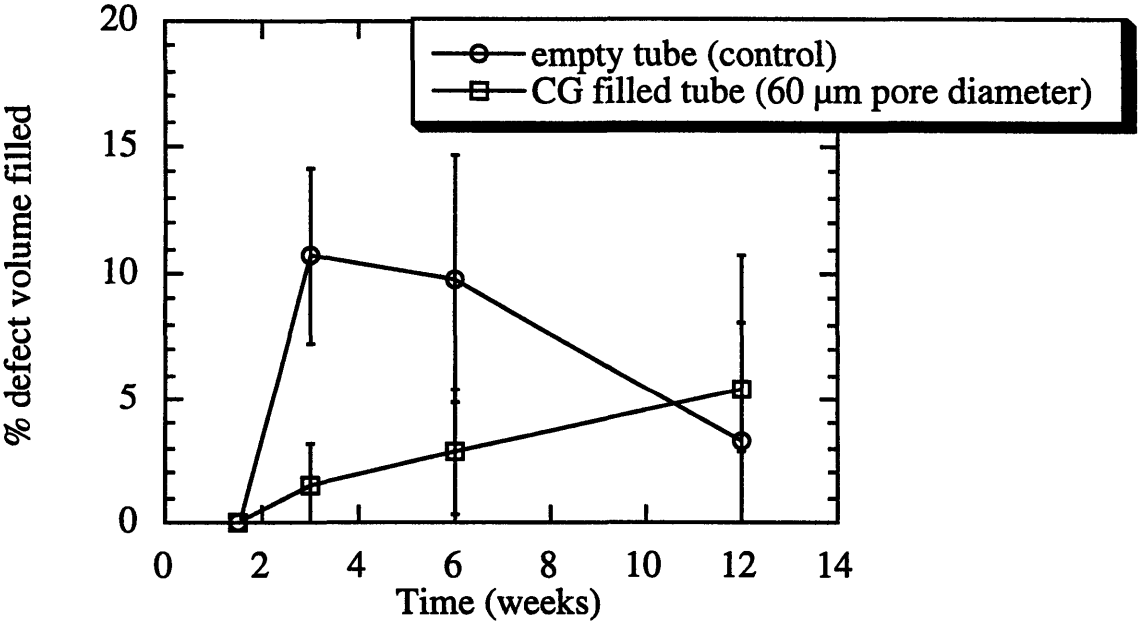

* dense fibrous tissue (class III and class IV combined)

Figure 4.18. The percentage of the defect volume filled with dense fibrous tissue (class III and class IV tissue combined) as a function of time for empty tubes and CG-filled (60 μm pore diameter) tubes. The amount of dense fibrous tissue appeared to peak between 3 to 6 weeks in the empty tubes. There appeared to be a linear increase in amount of dense fibrous tissue in the CG-filled tubes between 3 to 12 weeks. See section 4.2.10 for detailed description of classes.

Effect of CG pore diameter on tendon healing. There appeared to be a trend that matrices with the large pore diameters (120 μm diameter) had the least amount of granulation type tissue (type I) (Figure 4.19) and the most amount of dense fibrous tissue (classes III and IV combined) (Figure 4.20) at 3 and 6 weeks. These finding were however, in general, not statistically significant due to high variability between specimens.

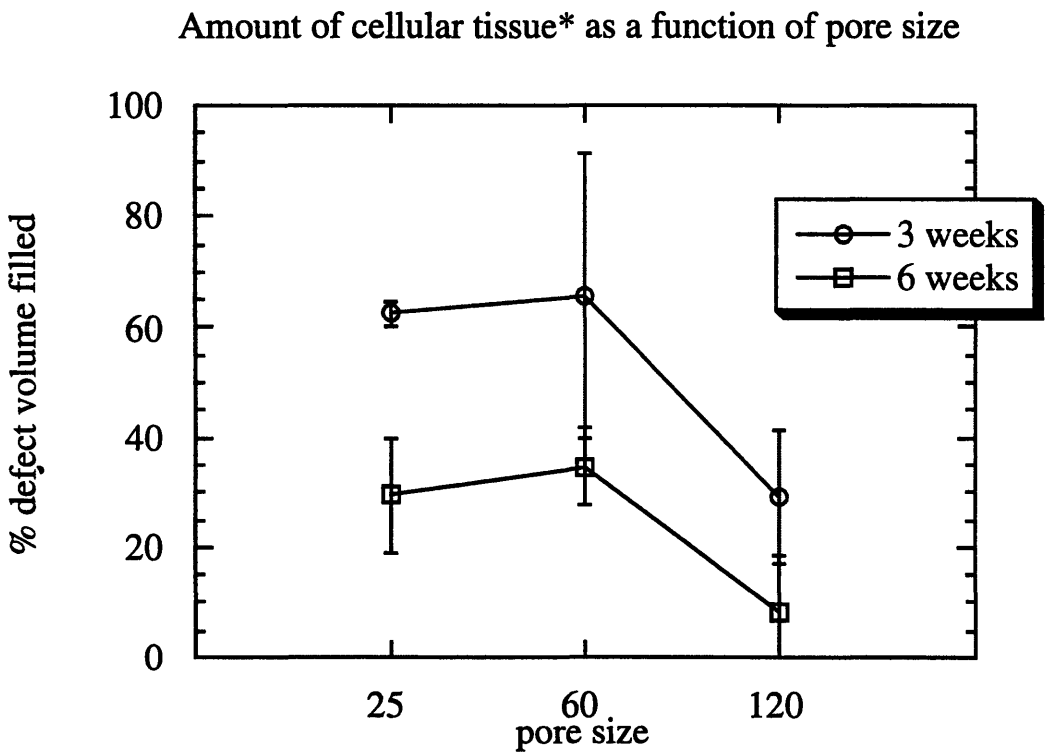

* cellular tissue (class I)

Figure 4.19. The percentage of the defect volume filled with granulation tissue (class I) as a function of collagen-GAG matrix pore size. There was a trend that the matrices with large pore size (120 μm) had the least amount of granulation tissue at both 3 and 6 weeks. ANOVA showed no statistical difference between pore sizes ($p > 0.$) See section 4.2.10 for detailed description of classes.

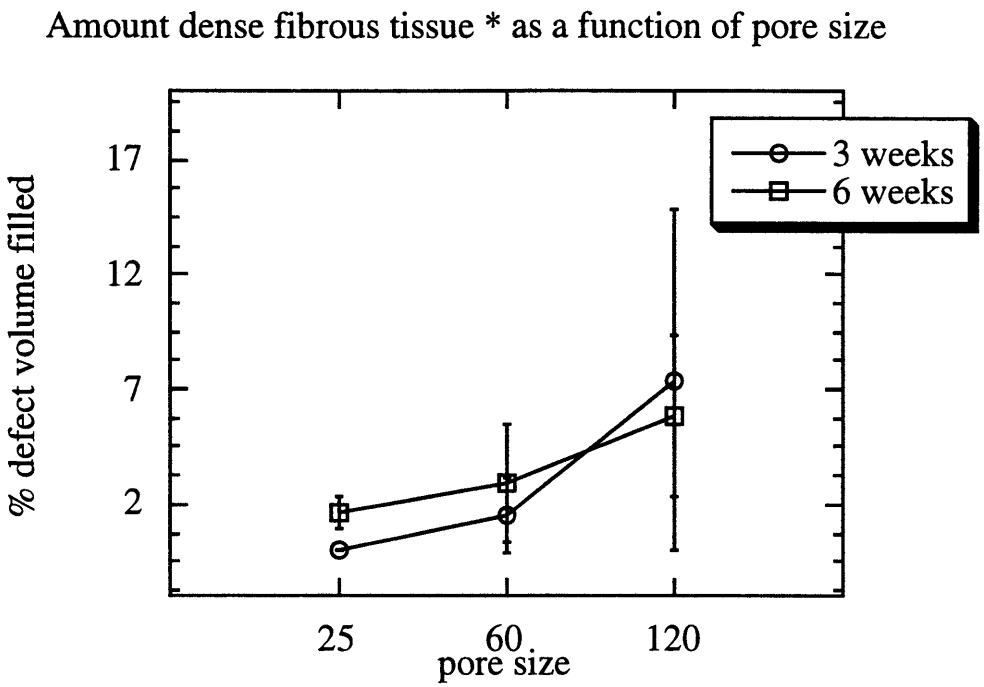

* dense fibrous tissue (class III and class IV combined)

Figure 4.20. The percentage of the defect volume filled with dense fibrous tissue (class III and class IV tissue combined) as a function of collagen-GAG matrix pore size. There was a trend that the matrices with the large pore size (120 μm) had the greatest amount of granulation tissue at both 3 and 6 weeks. See section 4.2.10 for detailed description of classes.

4.3.4. Immunohistochemistry

4.3.4.1. Collagen staining

In general, normal tendon stained positive for both type I and type III collagen. Normal tendon appeared to stain slightly more intensely for type I than for type III (Figure 4.21). In general, because there was a wide range of staining results for each implant group within a given time, correlations between presence of positive staining and time period could not be made. Figure 4.22 shows light micrographs of tissue stained for collagen type I and collagen type III. Both sets of tissue samples were tissue from empty tubes recovered at 12 weeks, but from different animals. The top sample stained positive for type I but very faintly and localized at the center for type III. While, the bottom sample stained for type I but very positive for type III. Generalization on which type of collagen predominates at a particular time

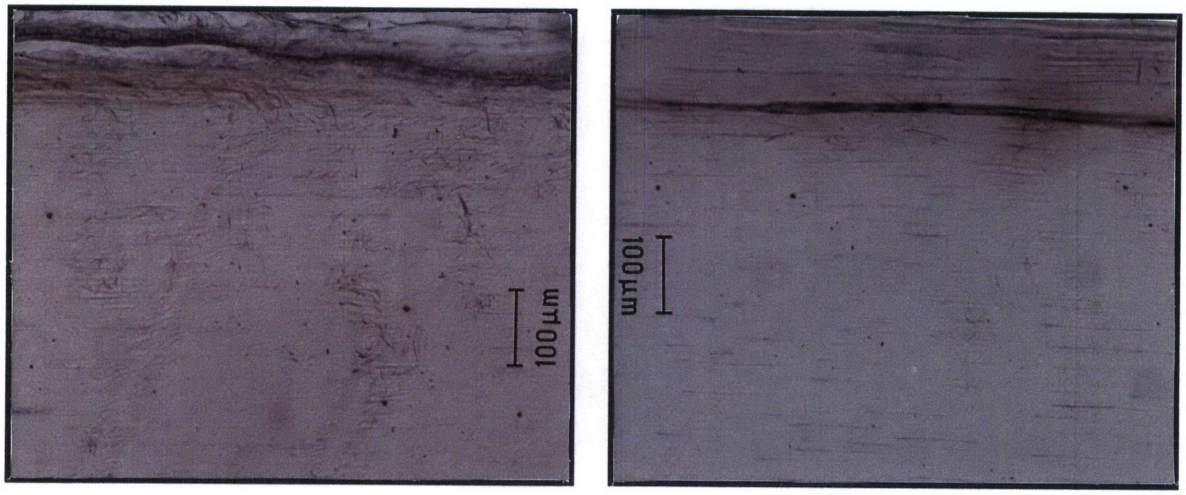

Figure 4.21 Light micrograph of normal tendon stained for collagen type I (**left**) and collagen type III (**right**). Scale bar: 100 µm.

period did not appear possible; however, the staining appeared complementary (i.e., when there was intense staining for collagen type I, there is generally, fainter staining of collagen type III, and conversely).

4.3.4.2. Alpha-smooth muscle actin staining

Normal adult tendon stained positive for alpha-smooth muscle actin (Figure 4.23). The majority of staining was localized at the interface between the tendon and paratenon sheath, although staining of a subset of tendon cells were seen within the tendon. Blood vessels also stained positive for the alpha-smooth actin stain.

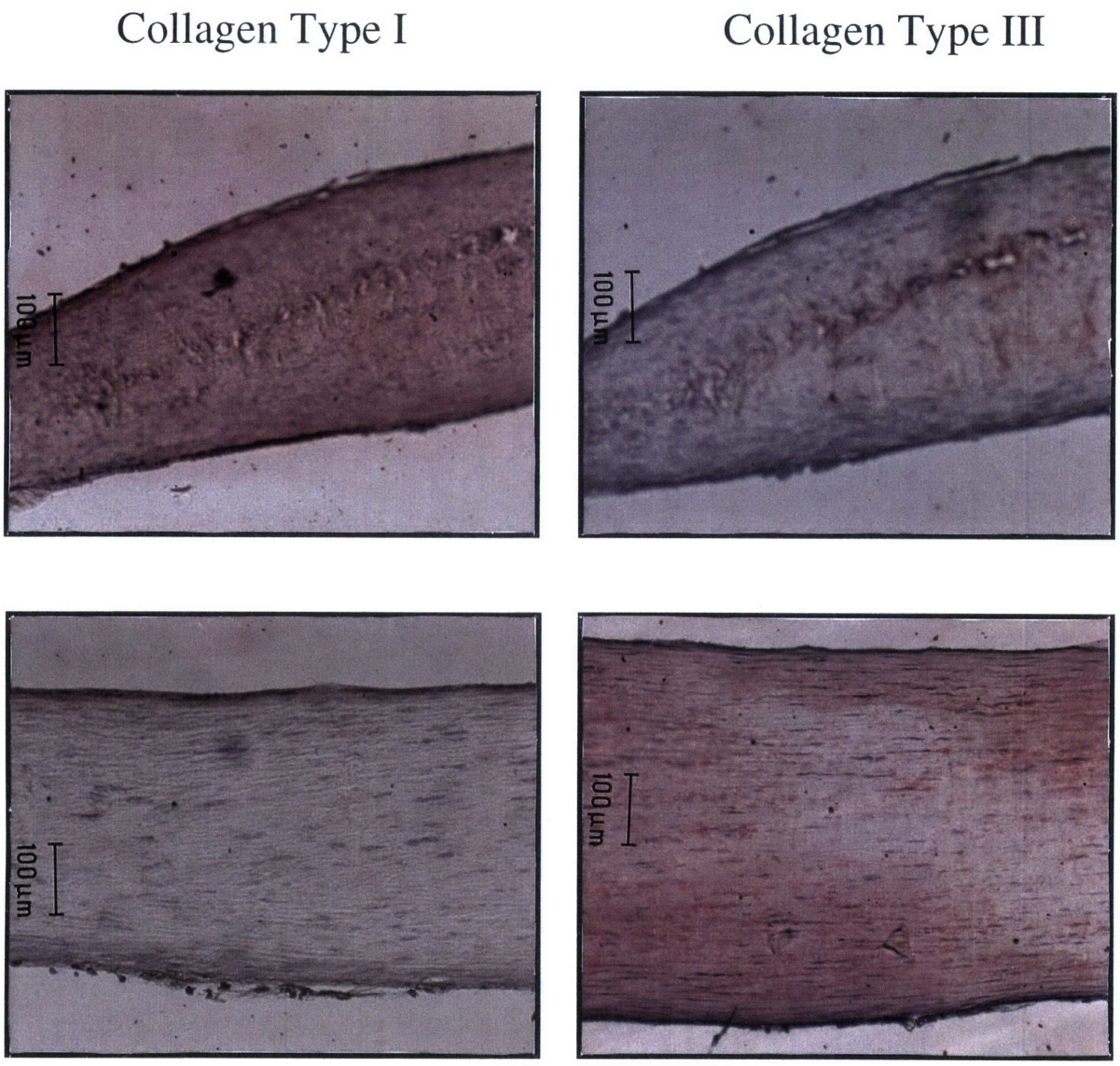

Figure 4.22. Light micrograph of tissue recovered from two different samples from empty tubes at 12 weeks (top and bottom), each stained for collagen type I (**left**) and collagen type III (**right**). Scale bar: 100 µm.

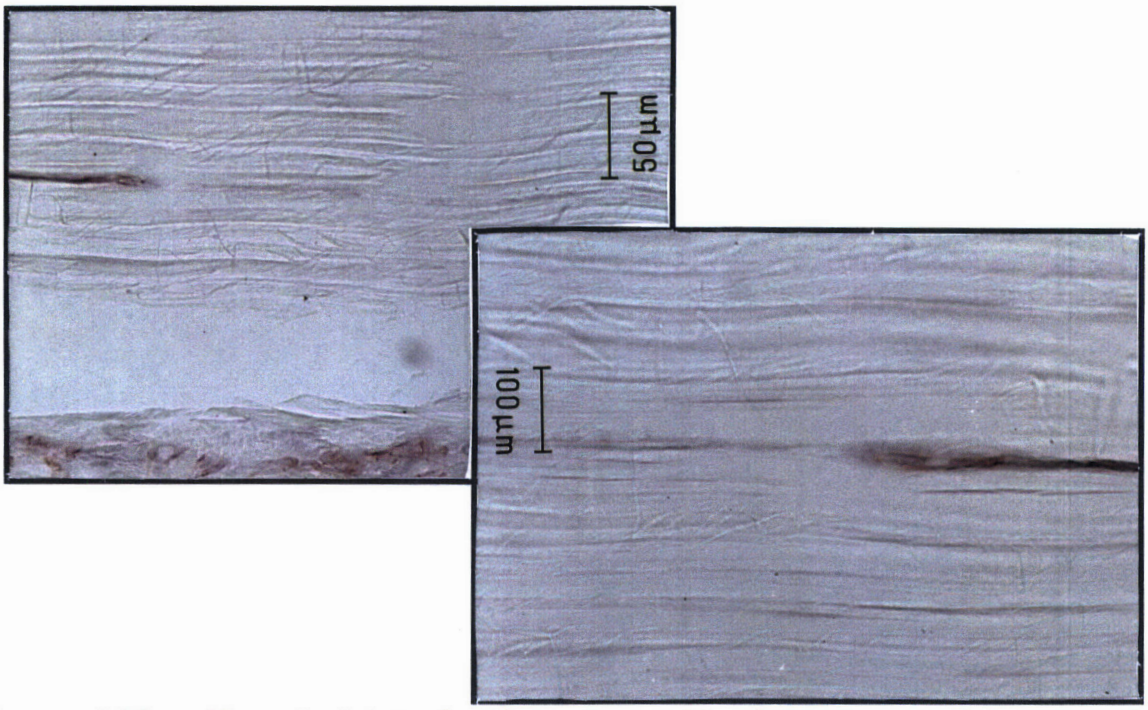

Figure 4.23. Normal adult tendon that stains positive for alpha-smooth muscle actin. Generally few tendon cells stain positive. Low magnification (**left**). Scale bar: 50 µm. High magnification (**right**). Scale bar: 100 µm.

All tissue samples recovered from empty control tubes, except for 10 day tissue, stained positive for alpha-smooth muscle actin. Three week and six week tissue samples appear to stain with equal intensity. Cells throughout the tissue stained positive for alpha-smooth muscle actin with greater intensity of staining for cells located at the interface along the silicone tube. The intensity of staining and the extent of staining appeared to slightly decrease by 12 weeks compared to 6 week samples, although it was still more intense than normal tendon (Figure 4.24). Fewer cells appeared to stain positive at 12 weeks and the staining appeared to be localized along the interface of the tissue and silicone tube.

The majority of tissue recovered from collagen-GAG matrix-filled tubes at three weeks did not stain positive for alpha-smooth actin. Of these three-weeks tissue samples that did stain positive for alpha-actin the stain appeared localized at the edges of the tissue sample (along the interface with the silicone tube) (Figure 4.25). In these samples the positive staining was in areas in which the matrix fibers were bundled and aligned in the long direction of tendon. At

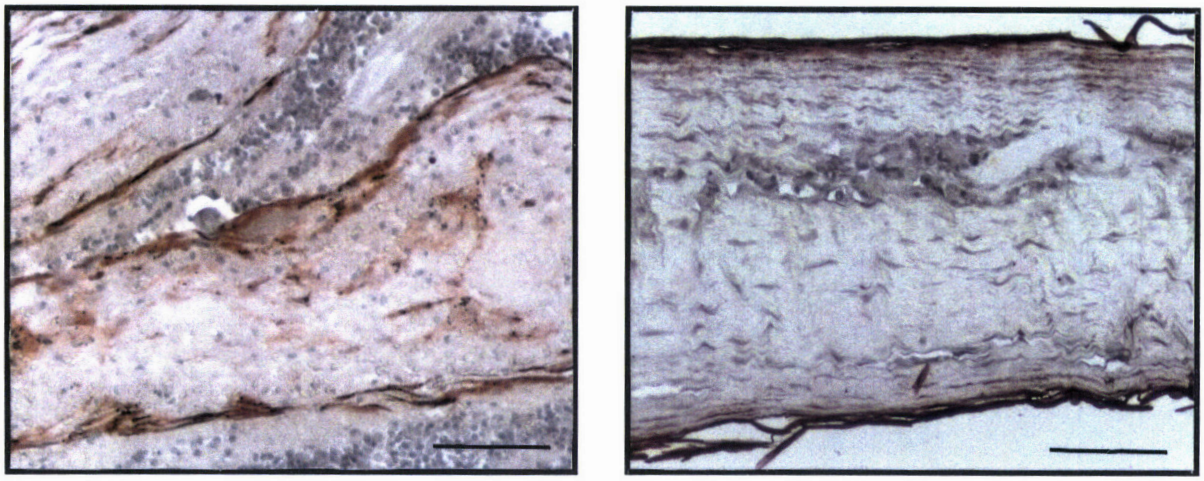

Figure 4.24. Tissue recovered empty tubes that stain positive for alpha-smooth muscle actin. Staining intensity appeared to slightly decrease from 6 weeks (**left**) to 12 weeks (**right**). Scale bar: 100 μm.

six weeks, cells in the tissue recovered from tubes filled with CG matrices with large pore sizes (<120 μm) and medium pore diameter (60 μm) stained positive for alpha-smooth muscle actin. The staining was again most intense toward silicone tube interface of the tissue samples. At 12 weeks, the cells in the tissue in CG matrices of medium pore diameters also stained positive. The intensity and extent of staining appeared slightly greater for the 12-week CG filled tubes than the 12-week empty tubes.

4.3.5. Ultrastructural evaluation

4.3.5.1 Collagen fibril diameter distribution

None of the healing 12-week specimens, whether empty or CG filled, were observed to have collagen fibrils larger that 75 nm. There appeared to be a uniform distribution of small collagen fibril diameter for the healing samples as opposed to the normal adult Achilles tendon samples that had collagen fibrils ranging in size from 10 nm to over 400 nm. The collagen fibrils in the both the empty and CG-filled specimens appeared to be banded. Figure 4.26 shows the histogram of collagen fibrils for tissue samples at twelve weeks, both with a

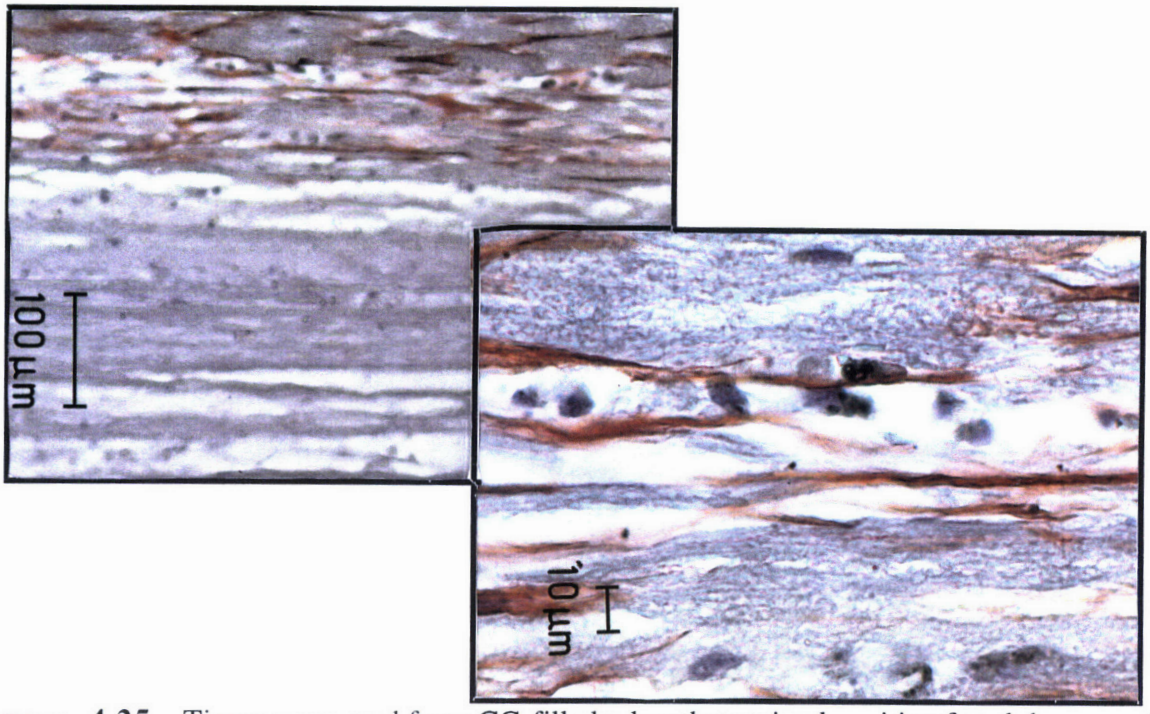

Figure 4.25. Tissue recovered from CG-filled tubes that stained positive for alpha-smooth muscle actin. Staining localized toward the edges of the sample (**left**, lower magnification). Scale bar: 100 µm Higher magnification (**right**). Scale bar: 10 µm.

collagen-GAG matrix (medium pore size – average pore channel diameter of 60 µm) inserted into the lesion site and an empty lesion site. A histogram of collagen fibrils for normal Achilles tendon is also shown for comparison. Micrographs of representative collagen fibrils for normal tendon and new tissue at 12 weeks in an empty tube are shown in Figure 4.27.

The average collagen fibril diameter for the tissue in the empty tube at 12 weeks was 28.0 ± 4.0 nm (average ± SEM, n= 2) while the tissue in 12 weeks, CG–filled tubes (60 µm pore diameters) was 39.3 ± 9.67 (average ± SEM, n=2). In comparison, the average collagen fibril diameter for the normal adult tendons was 145.0 ± 74.5 nm (n=3). Analysis by ANOVA showed no statistical significance between the average fibril diameters of the tissue in the empty and CG-filled tubes.

4.3.5.2. Ultrastructural morphology of cells

Myofibroblast-like cells along with fibroblast cells were visible under TEM. Although there were myofibroblasts cells present, as evidenced by the ultrastructural presence of bundles of actin interspersed with dense bodies and pinocytotic vesicles, in tissue recovered from 12 weeks–empty tube samples, the myofibroblasts appeared to be dying (Figure 4.28). The cellular membrane of the cells was missing in some locations and the bundles of actin appear to be depolymerizing at some sites. In contrast, micrographs of tissue recovered for 6 week–empty tube samples showed evidence of normal myofibroblasts. The cellular membrane was still intact and there was no evidence of actin de-polymerization.

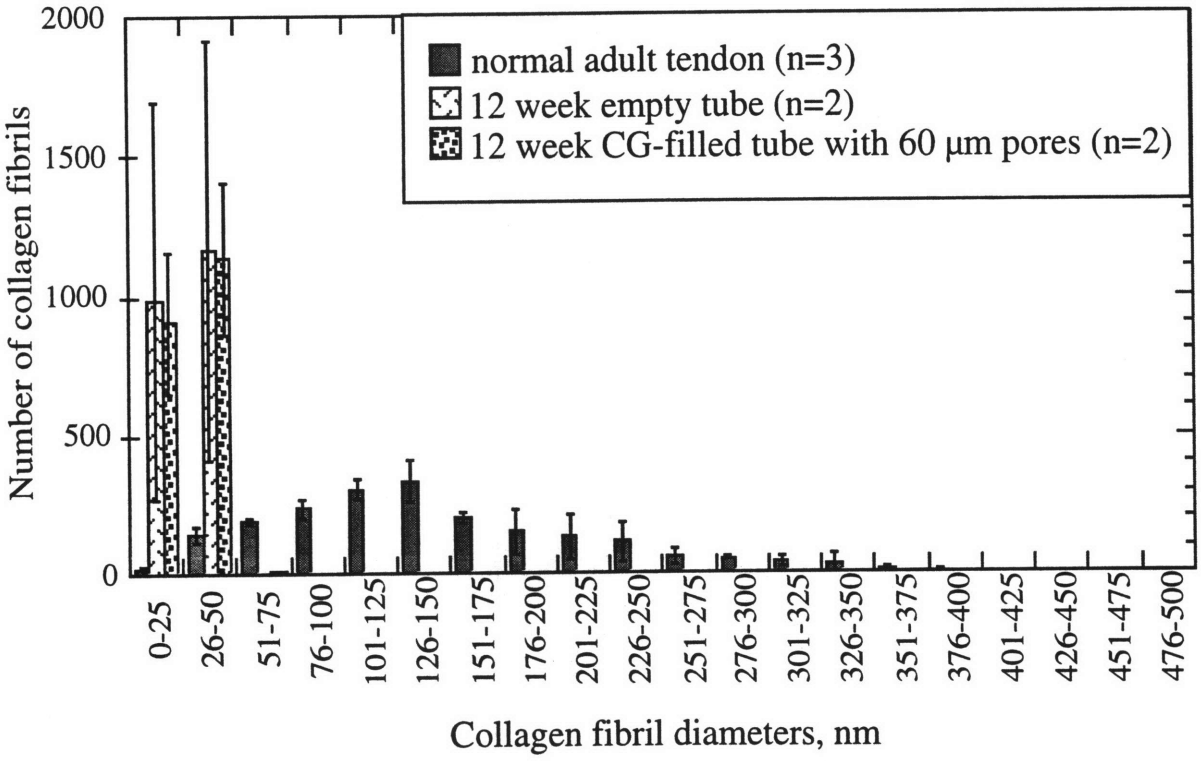

Figure 4.26. Histogram of collagen fibrils for repair tendon tissue at 12 weeks in both empty and filled lesion sites. Histogram of collagen fibrils for normal adult tendon added for comparison. There do not appear to be collagen fibrils larger than 50 nm for any of the repair tendon tissue of either condition. 2000 collagen fibrils were counted per specimen. Bar represent standard errors of the mean.

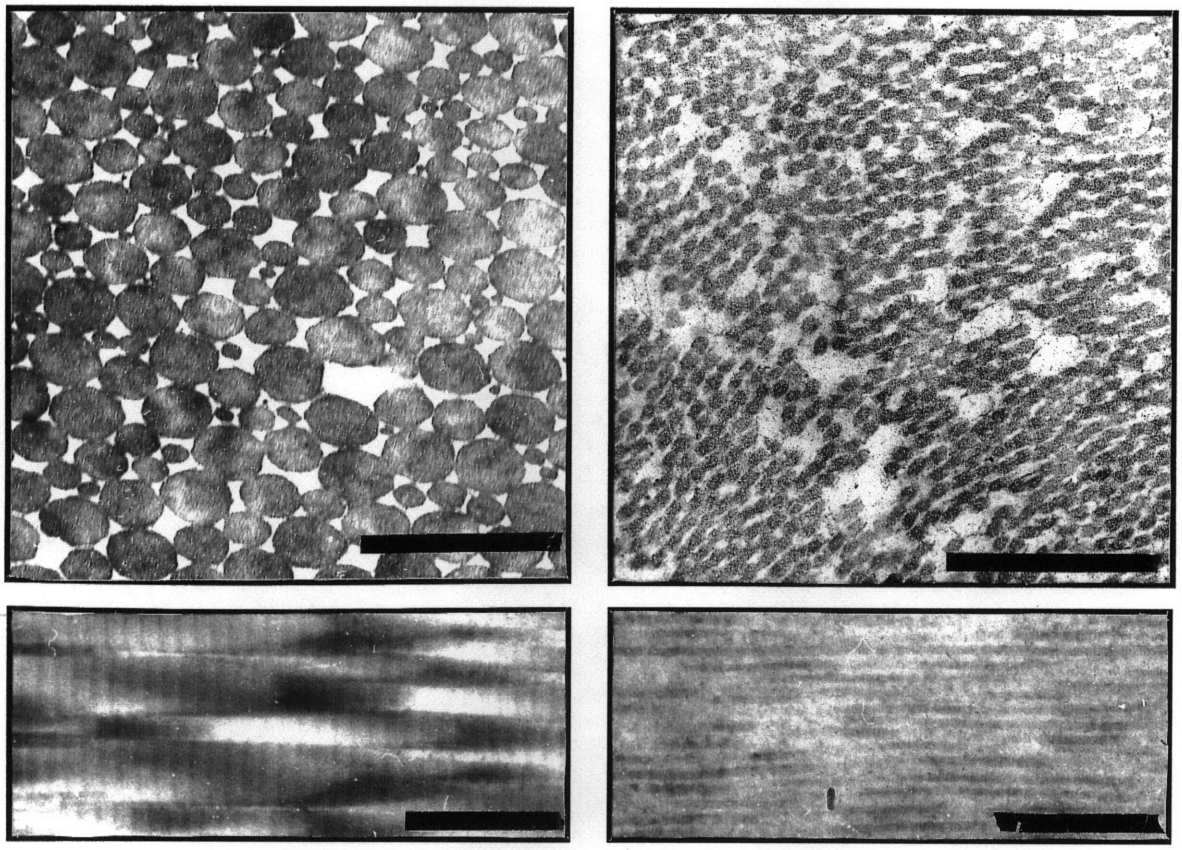

Figure 4.27. TEM micrographs of normal Achilles tendon (**left**) and new tendon tissue at 12 weeks in an empty tube (**right**) . Notice the difference in size of collagen fibrils. Transverse cross-section (**top**) and longitudinal cross-sections (**bottom**). Banding can be seen in the longitudinal cross-section. Scale bar : 500 nm.

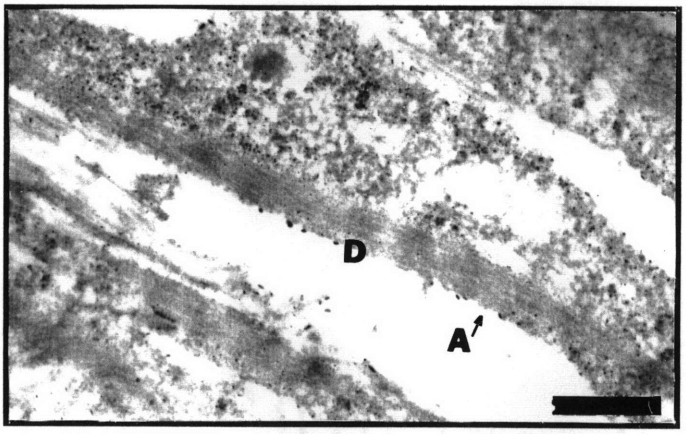

Figure 4.28. TEM micrographs of myofibroblasts from a 12 week empty tube sample. Aligned actin filaments (**A**) and dense bodies (**D**), features found in myofibroblasts, can be seen within the cell. Scale bar: 200nm.

4.4 Discussion

4.4.1. Animal model

This study is the first investigation of the healing of an entubulated tendon gap. The model was novel: a tendon lesion gap (10-12 mm) was isolated both biologically and mechanically from the external environment provided by other tissues and organs. Biological isolation was achieved by placing a silicone tube around the lesion gap which was impermeable to cells and soluble regulators. Mechanical isolation was achieved by immobilizing both the knee and hock (calcaneous bone) joint of the operated leg, using an external device and removing tendons around the joint, respectively.

In the 1950's, Gonzalez [57] had developed an animal model in which the tendon (in this case, flexor tendon) lesion site was also biologically isolated by using a polyethylene tube to surround the lesion site. However, in Gonzalez's model, the lesion site was not a "gap" lesion; instead, following transection, the two stumps were surgically reapposed before the tubing was placed around the wound site so that there was no gap visible between the tendon ends. The author was primarily interested in preventing the adhesion of healing tendon to surrounding tissue.

Biological isolation. In the model used in this study, a wound gap of 10-12 mm was biologically isolated from the external environment by placing an impermeable silicone tube around the lesion site. The value of this model consisted in enabling the study of the intrinsic ability of tendon to bridge a wound gap in the absence of external biological influences (such as cells migration and regulator diffusion into the lesion site from external tissue sources). At sacrifice, gross examination of the silicone tubing showed that there was a large mass of tissue that adhered to the outside of the silicone tube. It can be argued that if the tube was not present, this tissue could have been incorporated into the wound site and a differentiation of the tissue produced by the tendon and the tissue produced by external factors would not be possible.

Kato and associates [56, 68, 126] studied tendon healing in the presence of resorbable collagen-based grafts. They used an animal model that did not biologically isolate the healing lesion site from the external environment. The tissue described to be present in the lesion site in Kato's animal model appeared to be morphologically similar to tissue found in the empty tube at 12 weeks in this study. Both in Kato's study and in this study, dense highly aligned tissue with a crimp pattern was observed. The characteristics of this crimp pattern were similar in both studies. The major difference between the response of tendon to injury in these two animal models was the amount of tissue found in the defect site. The amount of tissue produced in Kato's study was much greater than that of tissue found in this study. Although not explicitly stated, it appeared that tissue filled the entire defect site in Kato's study at all time periods of investigation (up to 52 weeks); while, tissue in this study decreased in volume to less than 5% of the defect site by 12 weeks in empty tubes. This difference in tissue volume is speculated to be due to the biological isolation of the lesion site in this study. The reduction of cells and soluble regulators to the wound site due to the impermeability of the silicone tube may have affected the volume of tissue produced.

The choice of tube material may be a factor in the extent of tendon healing observed. A study by Chamberlain [14] on the effect of tube material in an entubulated peripheral nerve gap animal model demonstrated that the permeability of tube material appeared to affect the volume of nerve tissue found in the lesion site. The volume of nerve tissue in the silicone tubes was small to non-existent while the volume of tissue in porous collagen tubes was significantly greater and in many cases filled the defect volume. It is speculated that if the material of the tube was changed in this study to a more permeable material, the volume of tissue in the lesion site would increase.

Mechanical isolation. The reduction of mechanical loading to the lesion site was not an easy accomplishment. Due to the large dependence of rabbits on the use of the gastrocnemius-Achilles tendon-hock joint complex to move (i.e., hop), the isolation of the Achilles tendon site from mechanical loading was quite involved. Pullout of the tendon ends from the silicone tube

was frequent in the earlier versions of the animal model. In the current animal model, reduction of mechanical loading, was achieved by 1) immobilization of the knee joint by an external fixation device and 2) reduction of mobility of the hock joint by removing tendons around the hock joint.

It was necessary to immobilize the knee joint because the gastrocnemius muscle is attached to the femur bone (Figure 4.2) and movement of the knee joint causes movement of the proximal portion of the Achilles tendon stump. The hock joint needed to be immobilized because the distal portion of the Achilles tendon is connected to the hock (calcaneous) bone and movement of the distal tendon stump is controlled by the movement of the hock joint. The additional procedure of removing the tendons around the hock joint, has the disadvantage of 1) not being clinically representative and 2) introducing an additional complication to the wound area.

A simpler animal model that did not involve as complicated an immobilization procedure the one used in this model would have been preferable. This could be achieved by using an animal that 1) did not depend solely on its hind legs to move about (as the rabbit does) and 2) a hind limb that is easily immobilized. Dogs, goats and sheep would fulfill this requirement. The use of larger animals could not be justified at the start of this study because of the novelty of the study and of the need to perform many experiments to form a reasonable database of results (61 rabbits were used in this study).

A drawback to our model is the inability to monitor the time period and extent of return of mechanical loading to the lesion site. Retraction of both the proximal and distal tendon stump from the lesion site is possible. Proximal tendon stump movement during the 10 days of knee immobilization can be due to the loosening of the external fixation device. This loosening, although checked daily, could have allowed the rabbit opportunity to move its knee joint which in turn would allow the proximal tendon stump to retract away from the lesion site. Distal tendon stump movement can occur due to the healing of the removed tendons. Reconnection of the tendons around the hock joint would return mobility to the hock joint. The

uncertainty in the time period and extent of return of loading to the lesion site precludes definitive correlations between the mechanical loading and the extent of tendon healing.

The uncertainty in the time period and extent of return of mechanical loading to the lesion site is a concern because mechanical loading has been speculated to be important in the healing of tendons and ligaments [40, 41, 44, 89, 94, 127, 128]. Tissue spanning the wound site reconnect the proximal tendon stump to the distal tendon stump. Movement of the knee or hock joint causes tensile forces to be transmitted through the tendon. These tensile forces have been shown to align the matrix fibers in the long direction of the tendon (see Figure 2.8).

This model does not simulate closely the current clinical condition for Achilles tendon healing. In particular, the lesion site is generally not biologically isolated from the external environment. However, this model does appear to be a system in which the study of different implants could be evaluated in a controlled environment. This model allows for the introduction of selected biological factors via a change in the tube material (for example, using a particular collagen tube with a given porosity may allow for soluble factors but not cells to enter the wound site) into the wound site. Also, the effects of mechanical loading of the defect site can be studied by varying the immobilization time of the animal's knee joint. It appears that the model provides the investigator with substantial control over biological and mechanical variables which might affect the outcome of the experimental healing process.

4.4.2. Healing response of tendon in an empty tube

Alignment of matrix fibers. A cable of tissue was seen to span the wound gap in empty tubes at all time periods. The volume of this tissue appeared to decrease with time and the reduction in volume appeared to correspond to the remodeling and "densification" of the matrix material. The volume of tissue decreased from filling over 90% of the lesion site at 10 days to less than 5% of the lesion at 12 weeks. At 3, 6 and 12 weeks, the majority of tissue found in the empty tube was of dense matrix material. About half of the matrix fibers in the tissue were

highly aligned (in the long direction of the tendon) at 6 weeks. All the tissue appeared aligned by 12 weeks.

The densification of the tissue from a loose network of fine fibrin fibers within a cellular mass (10 days) to the highly aligned, densely-packed collagen fiber (12 weeks) has been observed by other investigators [8, 32, 36, 37, 68, 84, 99, 127]. The alignment of fibers has been speculated to be due to a mechanical loading of the tendon which coincides with the long direction of the tendon [84]. Based on this speculation, if the time period of immobilization was increased, the tissue formed in response to tendon injury would not be as highly aligned as tissue formed in response to tendon injury in a model that was not immobilized or immobilized for a shorter period. Although, the loading of the wound site was diminished by the use of external fixation for the first ten days in this study, the animal was not immobilized thereafter and mechanical loading could be acting on the new tissue that spanned the lesion site. The alignment of the matrix fibers would be in the long direction of the tendon. This model did not allow for the measurement of in vivo mechanical strains in the wound area, therefore confirmation of this speculation could not be done.

Return of crimp and mechanical properties of tissue. At 12 weeks, a proportion of the tissue formed in the empty tubes was found to have a crimp pattern. The crimp pattern was significantly smaller for normal tendon with respect to the wavelength and thickness of fiber bundles associated with the crimp. Similar results have been reported by Kato and associates [56, 68, 126]. In Kato's study, the response of tendon healing in the presence of resorbable collagen-based grafts was investigated. The tissue in Kato's tendon lesion site was described to have crimp characteristics (crimp lengths on the order of 10 μm) on the same order as that of tissue in the empty tube at 12 weeks described in this study (12 ± 3 μm (mean ± SEM)). In Kato's study, it was also observed that this crimp pattern was present from 3 weeks to 52 weeks with minimal change in the crimp characteristics.

Crimp has been shown to play an important role in the mechanical properties of the tendon [20, 22, 27]. The toe region of a stress-strain curve is dependent on the crimp

characteristic. Because of the decrease in wavelength of the tissue found in the empty tube at 12 weeks compared to normal tendon, it is speculated that the tissue would have greater ultimate strain. Comninou and Yannas [20] modeled the stress-strain behavior of connective tissue based on the crimp characteristics of the collagen fibers. This model predicts that the stress-strain curve for the tissue from the empty tube at 12 weeks would be displaced to the region of higher strains relative to the stress-strain curve for normal tendon.

Ultrastructural evaluation of the fibril diameters of the tissue in the empty tube is consistent with results obtained by other investigators who studied tendon healing [32, 36, 99, 126]. The average fibril diameter of the new tissue, 28.0 ± 4.0 nm (mean ± SEM) was significantly smaller than normal adult rabbit tendon (145.0 nm) but was comparable to fibril diameters of newborn rabbit tendon (37.0 nm) [65]. Many investigators [39, 41, 44, 93, 95] have modeled the mechanical properties (such as ultimate tensile strength) of tendon and ligament based on the collagen fibril diameters of these tissues. These models predict that the larger the collagen fibril diameter, the greater the ultimate tensile strength.

Models of mechanical properties of connective tissue based on the crimp characteristics and collagen fibril diameters predict that the tissue in the empty tube at 12 weeks would be mechanically and functionally inferior to normal adult rabbit tendon. Observations of the capability of the rabbit to hop was not evaluated, but it is reasonable to assume based on the above prediction, that the rabbit did not return to pre-injury activity level.

Speculation on the mechanism of crimp formation. It has been speculated that myofibroblasts play a role in tissue contraction and in recovery of ligament "tension" [35, 64, 100]. Myofibroblasts are a subset of fibroblast cells that have been implicated in the contraction of wound during the healing process [112-114, 123]. The presence of cells that stained positive for alpha-smooth muscle actin was consistent with results obtained by Faryniarz *et al* [35] and Ippolito *et al* [64, 100]. Positive staining for alpha-smooth muscle actin was observed as early as 7 days in Ippolito's study and between the period of 6 to 12 weeks in Faryniarz's study of ligament healing. In this study, positive staining was observed

at 3, 6 and 12 weeks. Cells in the regions of aligned matrix fibers appeared to stain positive for alpha-smooth muscle actin.

It is possible that the myofibroblasts have contracted the matrix fibers so that the matrix fibers have buckled; causing an crimp pattern to develop. Although the alpha-smooth muscle actin stain did not appear to differentiate a difference between regions of tissue that possessed crimp and regions that did not possess crimp, this hypothesis should be further explored. It is speculated that regions with a higher concentration of myofibroblasts may exerted greater forces on the surrounding matrix fibers therefore buckling the matrix fibers to a greater extent.

Another possible hypothesis is that alternating compressive and tensile forces are acting upon the healing tissue. Under physiological conditions, the gastrocnemius muscle is able to contract and release tension. This causes a lengthening and contraction of the Achilles tendon. It is possible that this alternating contraction and tension causes the healing tendon to develop a crimp pattern to accommodate the alternating mechanical forces.

Questions that need to be addressed include: why do only selected areas of tissue in the empty tube at 12 weeks appear to have a crimp pattern? Also what is the correlation of the magnitude of forces or frequency of contraction/tension to the crimp characteristics? It is speculated that the greater the frequency of contraction/tension, the smaller the crimp wavelength. Monitoring of the *in vivo* mechanical forces acting on the healing tissue and a method of applying known magnitude of tension and compression is needed to test this hypothesis.

4.4.3. Effect of collagen-GAG matrices on kinetics of healing

Effect of CG matrix on the volume of repair tissue. The volume of this tissue from tubes filled with each of the three collagen-GAG matrices was greater than the tissue in the empty tubes at all time periods. At 3 and 6 weeks, part of the volume of tissue was probably due to the presence of undegraded CG matrices, but by 12 weeks the CG matrices were not observed. At 12 weeks, the defect was filled new tissue. The larger volume of tissue

observed in the lesion gaps which were implanted with the CG matrix could be due to the fact that the tissue was not as highly densified and aligned as the tissue in the empty tubes. A high proportion of tissue consisted of " loose randomly aligned matrix fibers" (class II) at 12 weeks. It is conceivable that the tissue had not fully densified by 12 weeks and that, given a longer period of time, the volume of tissue in the CG matrix could be comparable to the volume of tissue in the empty tube. This suggestion is supported by the observation that the percent defect volume which was filled with dense fibrous tissue in the CG-filled defect sites increased continuously throughout the period of observation and had not shown evidence of reaching a plateau by the end of the experimental period of 12 weeks.

Effect of CG matrix on transition between granulation tissue and dense connective tissue. The presence of the CG matrix in the tube appeared to alter the kinetics of healing observed in the empty tubes. The sharpness of the transition from being a cell-based material (granulation tissue, class I) to a matrix-based material (classes II, III, IV and V) appeared to be altered by the presence of the matrix. It was observed that there was a rapid transition between the cell-based to matrix-based tissue filling the originally empty tube between 10 days and 3 weeks; however, this transition appeared slower for the tissue in the tube filled with CG matrix with the pore diameter of 60 μm (Figure 4.17). In the empty tube, a significant portion of the defect site was filled with granulation tissue at 10 days (>90%), but by 3 weeks, there was less than 3% of the defect site filled with granulation tissue. In the CG-filled tube, granulation tissue was observed to fill 60% and 40% of the lesion site at 3 weeks and 6 weeks, respectively. Less than 3% of the lesion site was filled with granulation tissue at 12 weeks in the CG-filled tubes. The presence of the CG matrices appeared to coincided with the presence of granulation tissue in the lesion site (CG matrices appeared to have degraded by 12 weeks). It is possible that the presence of the CG matrix may have prolonged the synthesis of granulation tissue.

If the CG matrix was tailored to degrade at a faster rate, it is possible that there would be less granulation tissue present in the lesion site at a later period of evaluation and the

transition from granulation tissue to matrix-based tissue would have mimicked the kinetics of the empty tube case. Conversely, if the CG matrix was tailored to degrade at a slower rate, it is possible the transition from granulation tissue to matrix-based tissue would be slower than that seen in this study. Although the *in vivo* degradation rate of the matrices was not studied, there did not appear to be, in general, a noticeable difference between the amount of CG matrix present in the 3-week and 6-week samples. The amount of non-degraded CG matrix and the amount of granulation tissue cannot be definitively correlated. The degradation rate of CG matrices has also been found to effect the kinetics of dermal regeneration [136]. Matrices that degraded faster than a limiting value were found to be less effective at inhibiting the contraction of dermal wounds than matrices that degraded slowly.

Effect of CG matrix pore size. In addition, the pore size of the CG matrix appeared to affect the transition from being a cell-based material to a matrix-based tissue. The larger pore sizes had the least amount of granulation tissue and the most amount of dense fibrous tissue present at 3 and 6 weeks (see Figure 4.19 and Figure 4.20). This alteration in kinetics could be a function of the surface area of the collagen-GAG fibers. The surface area of the collagen-GAG matrix decreased with increasing pore size (empty tubes are considered to have zero surface area). An increase in specific surface of CG matrices (decrease in pore diameter) coincided with the greatest difference between filled and empty sites. Exposure of cells or regulators to the surface of the collagen-GAG could have triggered a response from the injured tendon.

It is speculated that the effect of pore diameter on tendon healing may be similar to that of the effect of pore diameter on dermal healing. The pore diameter of the CG matrices has been shown to affect the regeneration of both peripheral nerve and dermis [15, 16, 129, 132, 136]. Matrices with 5-10 μm pore diameters were found to be optimal for nerve regeneration while matrices with pore diameters between 20 and 125 μm were found to be optimal for dermal regeneration. The mechanism of tendon healing is speculated to more closely resemble that of dermal healing than that of nerve healing. In nerve, the mechanism of regeneration

appears to involve the elongation and reconnection of axons through a wound site. In dermal and tendon, the mechanism of healing appears to involve the migration and proliferation of a large number of cells into the wound site. There would appear to be a range of pore size that would alter the kinetics of tendon healing to the same extent. Below this range, the pore channels may be too small for cells to migrate into the wound site. Without cells, tissue would not be formed in the lesion site. Above this range, the pore channels may be too large that the cells do not "sense" the presence of the CG matrix surface area. This range of pore size did not appear to be revealed in this set of experiments. It is possible that a larger range of pore channels diameters need to be tested to differentiate the possible presence of an optimal pore channel diameter range for tendon healing.

Effect of CG matrix on alignment of matrix fibers. The presence of the CG matrices may have also affected the ability of the matrix fibers in the tissue to align. In regions where the CG matrix was still present, there did not appear to be newly synthesized matrix fibers that were aligned. Highly aligned tissue (class III and above) was generally located along the interface of the tissue and the silicone tube. These areas did not appear to have a significant amount of CG matrix present due to either preferential degradation of the CG matrices in those areas or the possible shrinkage of the CG matrices away from the silicone tube.

One possible explanation for the smaller proportion aligned matrix fibers in lesion sites implanted with CG matrices is that the prolongation of the granulation tissue formation phase delayed the formation of matrix fibers which in turn delayed the densification and alignment of the fibrous tissue. Regions of CG matrix appeared to coincide with regions of with a high percentage of granulation tissue. In these regions, the energy of the healing tendon may have been channeled into producing granulation tissue in response to the presence of the CG matrix. If the hypothesis is that fibrous tissue can not form until the signals to produce granulation tissue has decreased to a particular level (i.e., the amount of granulation tissue is sufficiently low), then in these CG-regions there is a delay in the start of the matrix production and subsequently a lag in the alignment and densification of the matrix fibers.

Another possible hypothesis is that mechanical loading has returned to the lesion site and the tension exerted by the tendon ends are responsible for the alignment of the newly synthesized matrix fibers. It is possible that the CG matrix may be shielding the newly synthesized tissue from the tensile forces, thus impeding alignment of the tissue.

A third hypothesis is that myofibroblast cells may be involved in the process of matrix fiber alignment. The positive staining for alpha-smooth muscle actin (myofibroblasts) appears to coincide with the alignment of newly synthesized matrix fibers. Positive staining appeared primarily in areas in which the fibers were bundled and aligned in a particular direction. There did not appear to be substantial positive staining of cells in the regions with CG matrix present.

Speculations on why regeneration was not achieved. Implantation of a CG matrix did not result in the regeneration of a tendon-like tissue, by twelve weeks post-implantation. By this period, such matrices resulted in more regenerative tissue in lesions of dermis and peripheral nerve. It is possible that over a longer period, the CG matrix could have facilitated regeneration of tendon. However, clinically, a prolonged healing period could pose additional concerns to the patient and in general is not desired.

The experience in dermis served in part, as the basis for the justification of implantation of this matrix for treating defects in tendon. Important differences between tendon and dermis are the avascular nature of the midsection of tendon compared to the highly vascular character of dermis, and the relatively low density of tendon cells compared to the numerous fibroblasts in dermis. Moreover, the lesion site of the tendon animal model was isolated from surrounding tissue which may have further limited the number of fibroblast-like cells migrating to the lesion site. These considerations led to the preliminary work investigating the seeding of matrices in vitro with tendon cells prior to implantation into the animal model.

It is speculated that the addition of exogenous tendon cells to the lesion site would result in a larger volume of tissue filling the lesion site. The kinetic of tendon healing is speculated to be different for lesion sites filled with cell-seeded matrices and non cell-seeded matrices. It is possible that quality of healing tissue in sites implanted with cell-seeded matrices

would be higher than sites implanted with non cell-seeded matrices (i.e., tissue in the cell-seeded matrices site would be similar in characteristic to normal tendon). Studies by Orgill [92] , in which fibroblasts-seeded CG matrices are implanted in a dermal wound healing model, demonstrated that the kinetics of dermal wound contraction was different than that of sites implanted with CG matrix only; wound contraction was arrested and the degree of final wound contraction was significantly lower in the wound sites implanted with cell-seeded matrices. These cell-seeded matrices appeared to have induced morphogenesis of skin.

4.4.4. Class IV tissue: Is it scar?

By twelve weeks, tissue in the empty tube appeared to be dense highly aligned collagen fibers with aggregates of collagen fibers that display a crimp pattern when viewed under polarized light (class IV tissue). A question that arises is "Is this an end-stage scar tissue?". Investigations by Kato and associates [56, 68, 126] on the response of tendon healing in the presence of resorbable collagen-based tendon grafts in an animal model that did not isolate the lesion site from the external environment showed that tissue produced in the lesion site was comparable to tissue classified as class IV. Class IV-type tissue appeared as early as 3 weeks in Kato's study and persisted up to 52 weeks, the end point of investigation. The fact that the tissue in Kato's study did not appear to remodel significantly by 52 weeks and is similar to tissue found in the empty tube at 12 weeks in this study that was classified as class IV tissue, leads one to believe that this class IV tissue may be an end-stage "scar" tissue.

If the class IV tissue were to be considered scar-like then the results indicate that the presence of the CG matrix appeared to alter the kinetics of tendon healing so that "scar" tissue had not formed by 12 weeks.

4.5 Conclusions

Use of the novel animal model allowed observation of healing events in a 10-mm gap in Achilles tendon. The results showed that the tendon stumps induced synthesis of a tissue cable

inside the silicone tube in both the presence and absence of CG matrix. In empty tubes, the new tissue consisted of dense aggregates of crimped fibers with a wavelength and fiber bundle thickness that were both significantly shorter than those in normal tendon. Tubes filled with CG matrix contained a significantly greater volume of tissue at all time periods. At 3 and 6 weeks, the presence of the undegraded CG matrix may have contributed in part to the volume, but no residual CG matrix was observed at 12 weeks. Although, CG-filled tubes contained dense fibrous tissue by 12 weeks, the tissue had no crimp. The presence of the CG-matrix appears to alter the kinetics of tendon healing. Granulation tissue appears to persist longer in the lesion site of CG-filled matrices. The amount of dense fibrous tissue increased continuously during the period of study in defects filled with CG matrix; by contrast, the amount of dense fibrous tissue decreased after 6 weeks in originally empty lesions. The data support the suggestion that healing of tendon was significantly modified in the presence of CG matrices; the higher the specific surface area of the CG matrix (smaller pore size), the greater the amount of granulation tissue was observed in the lesion site at 3 and 6 weeks.

Although tissue was found to span the wound site, the volume of tissue present at 12 weeks in both empty and CG-filled did not fill the defect site adequately (less than 10% of the defect site was filled). The problem likely was due to an inadequate supply of tendon cells due to the relatively low density of tenocytes and the avascular nature of the tendon, particularly in the midsubstance region in which the lesion gap was produced. Isolating the gap to eliminate the influence of neighboring tissue, further reduced the supply of potential collagen producing cells to the lesion site. In addition, the isolation of the lesion site, reduced the exchange of soluble regulators to and from the lesion site, which could also be affecting the extent of tendon healing. The role of soluble regulators on tendon healing has not been elucidated. Possible solutions may include: introduction of exogenous cells or soluble regulators into the lesion site. Also, longer term studies are needed to determine if tendon crimp characteristics, important determinants of the mechanical performance, develop over a longer course of time and to determine if the tissue features change over a longer course of time.

CHAPTER V: CELL SEEDING OF CG MATRICES

5.1 Introduction

Scaffolds of synthetic [13, 125] or biological origins [30, 104] have been investigated as a device for transplanting cells to defect sites in the body. Porous collagen-glycosaminoglycan (CG) copolymer matrices have been investigated as transplantation devices for chondrocytes [104] and dermal fibroblasts [92, 136]. Using this approach, cells are harvested from donor tissue, isolated in vitro, seeded into a matrix, and implanted into the patient at a desired site. Transplantation of cells have an advantage over whole organ transplantation in that the population of harvested cells can be expanded in vitro by cell culture techniques thus sacrifice of a whole tissue organ is not necessary.

In vitro studies of synthetic polymer matrices [45, 46, 125] have shown that the physical and chemical characteristics of the matrices along with the method of cell seeding and culturing in the matrices affect the distribution and morphology of the seeded cells in these transplantation devices. Investigators [28, 29] have also studied the in vitro behavior of cells cultivated into porous 3-D collagen sponges containing different glycoproteins and glycosaminoglycans.

Implantation of unseeded matrices into an Achilles tendon animal model (Chapter 4) has shown that though a cable of tissue spanned the 10 mm wound gap, this cable of tissue was very small (< 1mm in diameter) in comparison to the defect size (3.8 mm in diameter). One possible investigational route is to study the effect of implanting cell seeded matrices into the animal model. It is hypothesized that the controlled implantation of exogenous tendon cells in an analog of extracellular matrix (AECM) in the lesion may facilitate regeneration. Prior to the animal study with the cell-seeded matrices, it was necesary to develop a protocol for reproduciby for isolating tendon cells and seeding them into porous CG matrices.

The purpose of this study was to investigate the effect of pore channel diameter of collagen-GAG copolymer matrices and methods of tendon cell seeding and implant culture on the distribution and density of tendon cells.

5.2 Materials and Methods

Cell seeding of the CG matrices involved the processing of CG matrices to be seeded, the recovery of tendon cells (tenocytes), the culturing of the tenocytes to produce a sufficient number of cells for seeding, the seeding of the cells into the matrices, and the characterization of the seeded matrices.

5.2.1. CG matrices for *in vitro* studies

Collagen-glycosaminoglycan copolymer matrices consisted of type I bovine hide collagen precipitated from acid dispersion (5.5 mg/ml in 0.05 M acetic acid) by chondroitin-6-sulfate (derived from shark cartilage). The suspended coprecipitate suspension was injected into a silicone elastomer tube and immersed into a coolant bath. The aqueous portion of the suspension was frozen in the coolant bath then transferred to a freeze-drying apparatus. The resulting ice crystals were sublimated under reduced vacuum (100-200 mtorr) to produce the porous collagen-glycosaminoglycan matrices. The matrices were then exposed to a dehydrothermal treatment at a temperature of 105°C and a pressure of 30 mmHg in a vacuum oven for 24 hours. The sterile matrices were stored in a desiccator jar at room temperature until ready for use. A full description of the matrix porcessing procedure is in Chapter 3.

The matrices used in the in vitro studies were manufactured to have axially aligned pore channels with average pore sizes of 25 μm, 60 μm and 120 μm. The processing conditions to produce the pore sizes are summarized in Table 5.1. The matrices used for this set of in vitro studies were larger in diameter (6.0 mm) than the matrices used in the in vivo studies in Chapter 4 (3.8 mm). Previous investigations of cell seeding of chondrocyte cells into collagen-glycosaminoglycan matrices of similar chemistry to the matrices used in this study showed a

Average pore size	Temperature of coolant bath, T	Velocity of immersion, υ
25 μm	-65 °C	$5x10^{-5}$ m/s
60 μm	-40 °C	$2x10^{-5}$ m/s
120 μm	-10 °C	$5x10^{-5}$ m/s

Table 5.1. Table of manufacturing conditions to produce collagen-glycosaminoglycan matrices of average pore sizes 25 μm, 60 μm , and 120 μm.

shrinkage of the matrices after cell seeding [104]. With the future intention of implanting the tenocyte seeded matrices into the animal model described in Chapter 4, CG matrices with a larger diameter were used in the in vitro studies to compensate for potential matrix shrinkage.

5.2.2. Tenocyte recovery from rabbit Achilles tendon

Tenocytes were recovered by enzymatic digestion of the Achilles and plantaris tendon of New Zealand white rabbits. The rabbits were euthanized by lethal injection of sodium pentobarbital following dosage recommendations of a veterinarian. Tendons from both legs were sterilely removed from the animal and placed in a sterile 50 ml polypropylene centrifuge tube filled with a 50:1 Dulbecco-phosphate buffered saline (D-PBS ,1x, liquid, cat no. 14190-09, Gibco BRL, Grand Island, NY) : penicillin-streptomycin solution (cat no. 15250-020, Gibco BRL, Grand Island, NY). The stock penicillin-streptomycin solution had concentrations of 5000 units/ml and 5000 μg/ml , respectively. The centrifuge tube was placed on ice (4°C) for transportation to the laboratory. Enzymatic digestion took place between 1-3 hours after harvest, but no later that 6 hours.

Collagenase digestion of the tendon consisted of separation of non-tendon tissue from the tendon tissue using sterile instruments in a laminar flow hood. The tendon was diced to approximately 1x1 mm pieces and placed in a 50 ml polypropylene centrifuge tube with 40 ml of 0.15% collagenase type I (Worthington Biochemical Corp., Freehold, NJ) in DMEM/F12 (1:1,1x, cat no. 11321, Gibco BRL, Grand Island, NY). The activity of the collagenase type I

was 183 U/μg. The tube was attached to a rotating apparatus (Labquake Shaker, cat no. 400-110, Laboratory and Research Instruments, Berkeley, CA) and placed in a 37°C incubator for 16 hours or until the majority of tissue was digested with small remnants of tissue still visible. Constant agitation of the collagenase-tissue solution was necessary to facilitate adequate digestion. The digested tendon was filtered through a 0.70 μm cell strainer (Falcon, Franklin Lake, NJ) into a sterile polypropylene centrifuge tube.

The filtered solution was centrifuged (IEC HN-SII centrifuge, IEC, Needham, MA) at 1500 rpm for 10 minutes at room temperature. The supernatant was decanted off and the pellet resuspended in 25 ml of D-PBS and recentrifuged with the above conditions. This process was repeated one more time.

The final pellet was resuspended in 5 ml of media. The medium was composed of 435 ml DMEM/F12, 10 ml penicillin -streptomycin, 5 ml Glutamine (200 mM, cat no. 25030-081, Gibco BRL, Grand Island, NY),and 50 ml Fetal calf serum (heat inactivated, cat no. A-1905-N, Hyclone Lab Inc., Logan, Utah). Heat inactivation of the fetal bovine serum was accomplished by heating the serum in a 56°C water bath for 30 minutes as recommended by the manufacturer.

The tendon cells were deposited into a 75 cm^2 culture flask and incubated at 37°C in a humidified 5-10% CO_2 environment (Napco CO_2 Incubator, model no. 6200, Fisher Scientific, Medford, MA).

5.2.3. Culturing of primary tenocytes

To allow for proper attachment of cells to tissue flask , the cells were left undisturbed for 2-3 days. Medium (same as described above) changes were every third day with daily viewing of cells to determine confluency of cells. Once confluency of the cells on the bottom of the culture flask had occurred, the cells were passed. Passage of cells consisted of replacement of the media with 5 ml of D-PBS for 20 seconds at room temperature. The D-PBS was then replaced with 2 ml of trypsin-EDTA solution (0.05% trypsin in 0.53 mM

EDTA·4Na, 1x, liquid, cat no. 25300-047, GibcoBRL, Grand Island, NY) for 4-5 minutes in a 37°C incubator, or until the monolayer of cells was detached from the flask. Eight milliliter of medium was added to the flask and the contents of the flask were transferred to a 50 ml centrifuge tube. An additional 5 ml of medium was used to rinse the culture flask and then added to the centrifuge tube. The tube was centrifuged for 10 minutes at 1500 rpm. The supernatant was decanted and the pellet was resuspended in 10 ml of medium. 50 µl of the suspension was saved to perform a cell count. Cell count and cell viability were quantified via trypan blue (cat# 15250-020, GibcoBRL, Grand Island, NY.) exclusion using a hemacytometer (double improved Neubauer Hausser, Reichart-Jung, obtained through VWR, Boston, MA) and an inverted phase-contrast light microscope (Nikon, Tokyo, Japan). The rest of the suspension was re-centrifuged with the above conditions. The final pellet was resuspended in 4 ml of medium. One milliliter of cell suspension was added to a 75 cm^2 culture flask. Sixteen millimeter of fresh medium was added to each flask and the flask was incubated at 37°C in a humidified 5-10% CO_2 environment.

5.2.4. Seeding of cultured tenocytes into CG matrices

Sterile collagen-GAG matrices (as described in 5.2.1) were removed from the silicone tubing and trimmed to 10-15 mm lengths. The matrices were split lengthwise in half. The dimensions of the matrices were on average 10 mm in length, 6 mm in width, and 3 mm in depth. Matrices were placed in 6-well culture plates (Falcon, Franklin Lake, NJ). The matrices were subjected to a prewetting and soaking step before cell seeding. The matrices were wetted with 70% ethanol for 15 minutes, followed by replacement of the alcohol with D-PBS for 15 minutes. The D-PBS solution was changed a minimum of three times and the matrices were soaked in the medium overnight at 37°C in a humidified 5-10% CO_2 environment before seeding. The medium was removed before cell seeding and matrices were transferred to new 12-wells tissue culture plates (Falcon, Franklin Lake, NJ). The wells were either coated with a thin film of sterile 2% agarose solution (Bio-rad standard low-m_r, cat no,

162-0100, Bio-rad, Richmond, CA) or left untreated. All of the above procedures were performed sterilely with sterile instruments in a laminar flow hood.

Secondary and tertiary passage cells used for seeding of the matrices. Preparation of the cultured cells for seeding was similar to the procedure for passage of the cells. Instead of the final resuspension into a culture flask, the final pellet was resuspended in medium to produce a suspension of 10^6 cells per 100 µl of media. The cell suspension was pipetted onto the cut side of the matrix. Three-fourth to one and one-half million cells were seeded onto each matrix. The seeded matrix was incubated at 37°C in 5-10% humidified CO_2 environment for an hour before 1.5 ml medium was added to each well. Tissue culture plates were either returned to the incubator and left unperturbed for the experimental time frame or the plate was attached to an agitator set (Labquake Shaker, cat no. T400-110, Laboratory and Research Instruments, Berkeley, CA) and agitated constantly for first 16-20 hours after seeding. Thereafter, the plate was left unperturbed for the duration of the experiment. Medium was changed every other day. Figure 5.1 is a schematic of the cell seeding protocol.

5.2.5. Experimental Grid

The methods of pore diameter and methods of cell seeding and culture were varied. Collagen-GAG matrices of three different pore channel diameters were investigated. Tissue culture plates were either left uncoated or were coated with a thin film of 2% agarose solution. The cell seeded matrices were either left unperturbed throughout the experimental time period or they were agitated the first 16 to 20 hours post-seeding and then after left unperturbed. Samples subjected to uncoated wells and no agitation were designated "controls". Cells-seeded matrices were evaluated either 1, 3, 7, and 14 days post-seeding. A summary of the experimental grid is shown in Table 5.2.

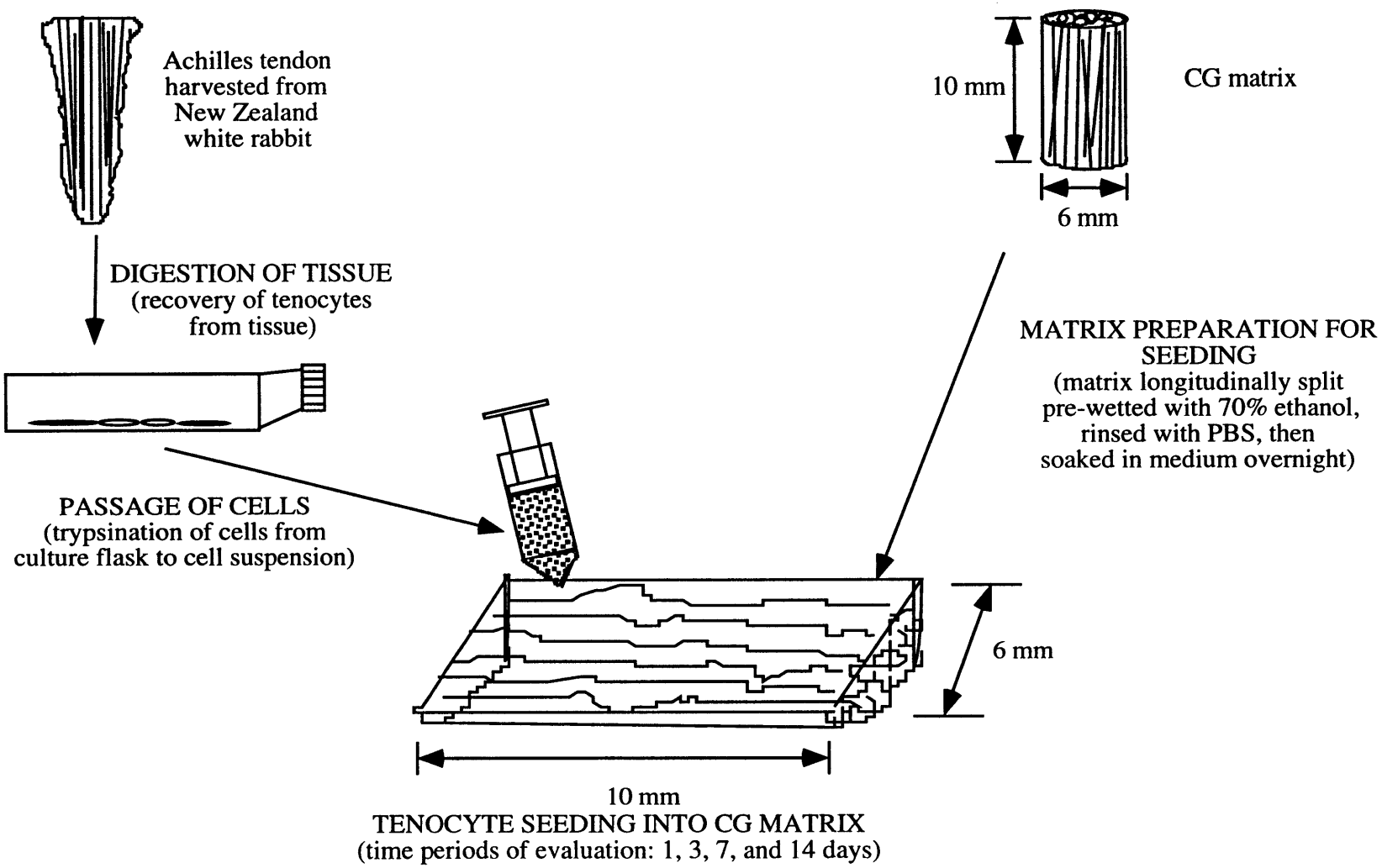

Figure 5.1. Schematic of cell seeding protocol. Tenocytes were recovered from Achilles tendon of New Zealand white rabbit. CG matrices were pre-wetted with alcohol, rinsed in phosphate buffered saline (PBS) and soaked in medium overnight before seeding.

Cell seeding experimental grid (Number of matrices)

Pore size	1 day				3 day			
	control*	w/agarose	w/agarose + agitation†	w/ agitation†	control*	w/agarose	w/agarose + agitation†	w/ agitation†
Small (25μm)	3	2	3	2	2	1	2	1
Medium (60 μm)	3	2	3	2	2	1	2	1
Large (120 μm)	3	2	3	2	2	1	2	1

Pore size	7 day				14 day			
	control*	w/agarose	w/agarose + agitation†	w/ agitation†	control*	w/agarose	w/agarose + agitation†	w/ agitation†
Small (25μm)	2	0	2	0	2	0	2	0
Medium (60 μm)	2	0	2	0	2	0	2	0
Large (120 μm)	2	0	2	0	2	0	2	0

* no agarose coating, no agitation
† agitation for first 16-20 hours

Table 5.2. Cell seeding experimental grid with the cell seeding conditions and the number of matrices per seeding condition.

5.2.6. Characterization of seeded matrices

Cell count. Measurements of the number of cells that did not attach to the matrices were performed on "1-day" samples. The medium was collected aseptically from each "1-day" matrix well and deposited into individual sterile 15 ml centrifuge tubes. The wells were rinsed with 1 ml of D-PBS for 20 seconds at room temperature. The D-PBS was then discarded and replaced with 1 ml of trypsin-EDTA solution for 6-8 minutes in a 37°C incubator, or until the monolayer of cells was detached from the well. In wells with the thin film of 2% agarose gel, the trypsin solution was left in the well for 10-12 minutes, or until the agarose layer detached

from the well surface. One milliliter of fresh medium was added to the tube to stop trysinization and the contents of the well were transferred to the 15 ml centrifuge tube. The tube was centrifuged for 10 minutes at 1500 rpm. The supernatant was decanted and the pellet was resuspended in 0.5 ml of medium. 50 µl of the suspension was pipetted into a microcentrifuge tube and mixed with 50 µl of 0.04% trypan blue stain (cat# 15250-020, GibcoBRL, Grand Island, NY). Trypan blue stains dead cells blue. Cell count and cell viability were quantified using a hemacytometer and an inverted phase-contrast light microscope.

Shrinkage measurements of Collagen-GAG matrices. Dimensions of the collagen-GAG matrices were measured. Length and width measurements of the pre-seeded matrix and the post-seeded matrix were taken. Matrix area, normalized by pre-seeded dimensions, was recorded.

Tissue sampling, fixation and sectioning. Cell seeding collagen-GAG matrices were fixed with a 2% cacodylate buffered gluteraldehyde solution (pH 7.4) for 6-16 hours at 4°C. The samples were rinsed three times in cacodylate buffered solution (pH 7.4) for 5 minutes prior to allocation of CG matrices into three different embedding mediums: glycolmethacrylate (GMA, JB-4, Polysciences Inc., Warrington, PA), paraffin (Paraplast Plus, Sherwood Medical Industries, obtained through Fisher Chemical, Pittsburgh, PA), and epon (Poly/Bed 812, Polysciences Inc., Warrington, PA). Figure 5.2 is a schematic of the sample allocation. Samples embedded in epon medium were allocated for a possible future transmission electron microscope study of cell–matrix interaction at an ultrastructural level and were not used in this study.

GMA embedding and sectioning protocol. Samples were dehydrated through graded ethanol (50% 70%, 80%, 95%, 95%, 100%, 100%, 100%) for 15 minutes in each solution. The samples were then infiltrated with the catalyzed-buffer of solution A of the JB-4 embedding kit overnight at 4°C, according to manufacturer's recommendation [96]. Matrices were polymerized in a solution of fresh catalyzed buffer of solution A with added initiators.

Three micron-thin sections were microtomed (model 1512, Leitz Wetzlar, Easton, MA), floated onto a water bath (Tissue float bath, Lo Boy, Lab-line, obtained through Fisher Chemical, Pittsburgh, PA), collected onto clean glass slides (Superfrost Plus, cat#48311-703, VWR, Boston, MA) and allowed to dry overnight. The sections were cut such that the cross-section of the matrices were shown.

Paraffin embedding and sectioning protocol . Samples were dehydrated through graded alcohol (50%, 70%, 80%, 95%, 95%, 100%, 100%, 100% ethanol) to two changes of xylene for 15 minutes in each solution. The samples were infiltrated in two changes of the melted paraffin for 30 minutes in each change prior to embedding in fresh paraffin.

Six micron-thin sections were microtomed, floated onto a water bath heated to 46°C, collected onto clean glass slides and allowed to dry overnight at 45°C. Sections were cut such that the cross-section of the matrices were shown.

Epon embedding protocol:. The samples were post-fixed in 1% osmium tetroxide in cacodylate buffer solution (pH 7.4) for 1.5 hours, dehydrated through graded alcohol to two changes of acetone before infiltration with Poly/Bed 812 solution, mixed according to manufacturer's recommended mixture ratio [97]. The infiltration schedule consisted of 2:1 acetone: Poly/Bed, 1:1 acetone: Poly/Bed, 1:2 acetone: Poly/Bed, 100% Poly/Bed, 100% Poly/Bed over a 2-3 days time period, followed by embedding of the infiltrated samples, in their desired orientation in flat embedding molds (Polysciences Inc., Warrington, PA). Samples were polymerized at 60°C for 24-48 hours.

General Histology. Cell seeded matrices embedded in GMA and sectioned onto glass slides were stained with hematoxylin and eosin (H&E). The cellular components stain a darkish purple to black color while the matrix components stain pink in color. The protocol for H&E staining was as following:

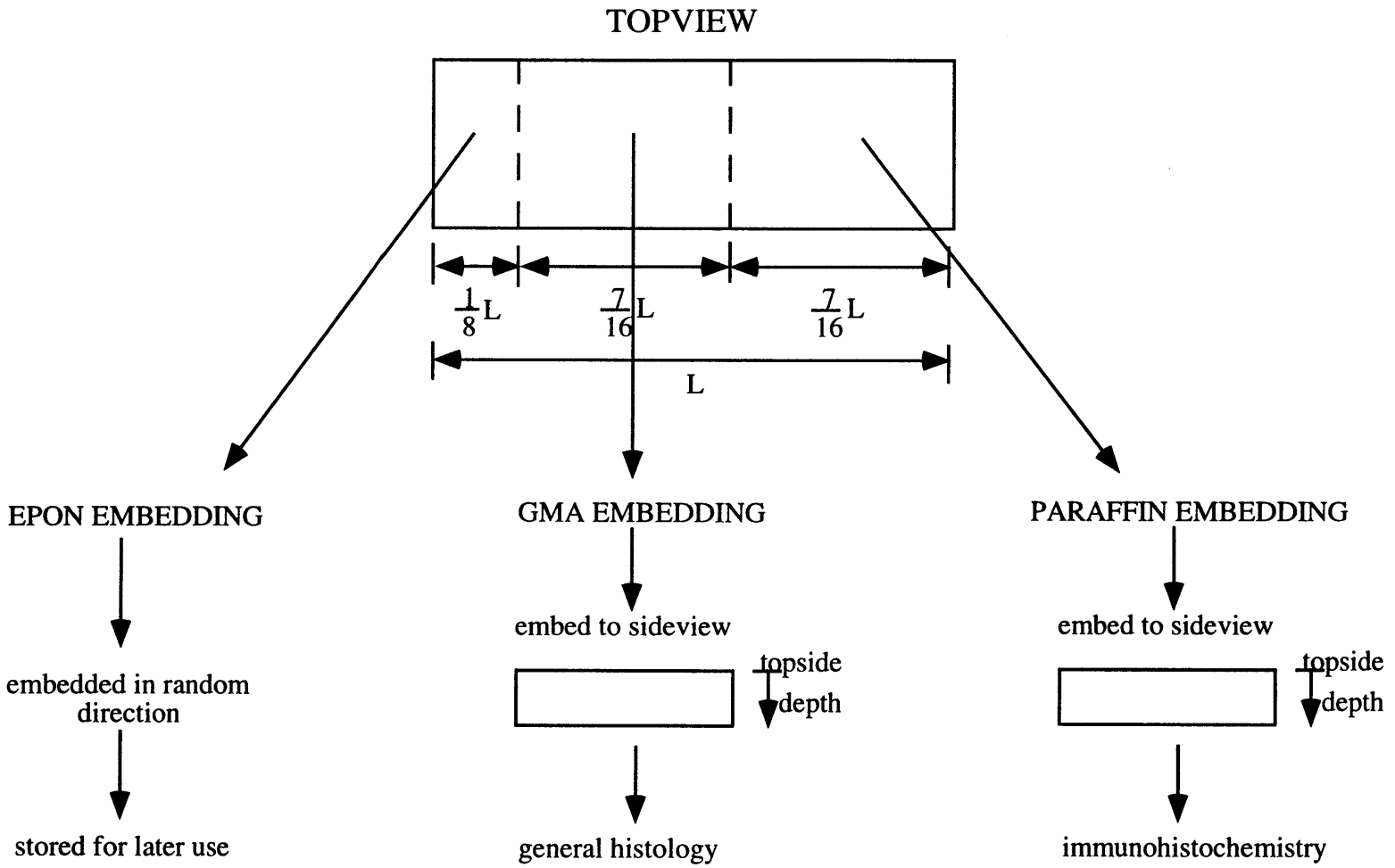

Figure 5.2. Schematic of allocation of cell seeded collagen-GAG matrix samples into different embedding mediums.

Rehydrated tissue sections were stained for 1.5 hours in Harris' hematoxylin solution (cat# HHS-128, Sigma Co., St. Louis, MO) and rinsed in distilled water, followed by 10 dips in acidified alcohol solution (1 ml HCl in 100 ml 70% ethanol). The hematoxylin was rinsed in distilled water, then blued by 1 minute immersion in weak ammonia solution (2-4 drops ammonium hydroxide per 500 ml distilled water), followed by thorough rinsing under slowly running water for 10 minutes. The slides were counterstained with aqueous eosin Y solution (cat# HT110-2-128, Sigma Co., St. Louis, MO) for 5 minutes. The slides were rinsed in water for 5 minutes, dried, mounted (Cytoseal 60, low viscosity, Stephan Scientifics, Riverdale, NJ) and coverslipped.

Quantification of cells attachment onto CG matrices. The density and distribution of the tendon cells attached to the CG matrices were evaluated. The degree of infiltration by tendon cells into the interior of the CG matrices was also measured using a light microscope fitted with a calibrated eyepiece reticule. Cell density was measured at different depths of the sponge, starting from the surface of the sponge to the midsection of the sponge (Figure 5.3). A minimun of five random sections within each depth level was measured.

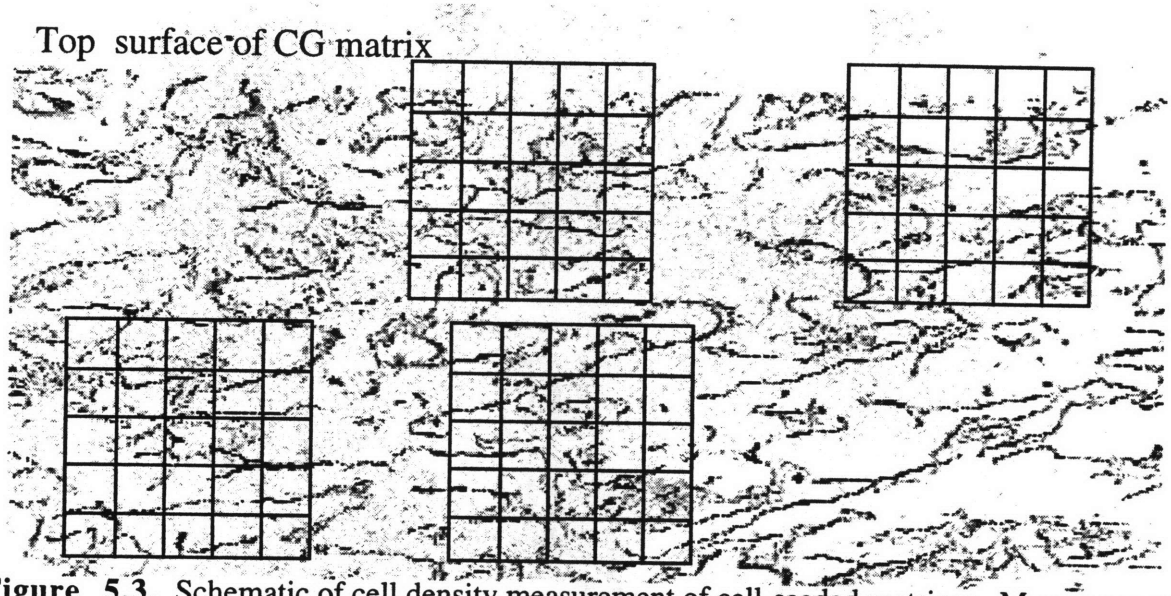

Figure 5.3. Schematic of cell density measurement of cell-seeded matrices. Measurements made at different depths of the matrix. A minimun of five sections measured per depth level.

Immunohistochemistry Cell seeded matrices embedded in paraffin and sectioned onto glass slides were stained with an alpha smooth muscle actin antibody stain. The immunostaining of the sections used a prediluted alpha smooth muscle actin kit (cat# IMMH-2, Sigma Co., St. Louis, MO). Alpha smooth muscle actin antibody stain is used to detect the presence of myofibroblasts. Modifications to the suggested protocol [111] included in the kit were made. A brief description of the staining protocol was as following:

Paraffin embedded sections were rehydrated to phosphate buffered saline solution (PBS, cat# P3813, Sigma Co., St. Louis, MO) by 2 washes in xylene for 5 minutes, followed by serial rehydration (100%, 100%, 95%, 80%, 70% ethanol) for 1 minute in each solution, and PBS for 5 minutes. Sections were digested in a 0.1% trypsin solution (cat# T8128, Sigma Co., St. Louis, MO) for 1 hour; followed by 2 washes in PBS for 3 minutes. Sections were treated to an endogenous peroxide quench in 3% H_2O_2 for 5 minutes; followed by 2 washes in PBS for 3 minutes. The sections were blocked with a 20% nonimmune goat serum (cat# G9023, Sigma Co., St. Louis, MO). Sections were incubated in primary antibody (mouse monoclonal IgG specific for smooth muscle actin) for 1 hour; secondary antibody (biotinylated goat anti-mouse IgG) for 20 minutes; then avidin-peroxidase conjugate for 20 minutes. Sections were washed twice in PBS for 3 minutes after exposure to primary, secondary, and conjugate. The stain was developed by incubation with the AEC substrate solution (4 ml distilled water, 2 drops acetate buffer, 2 drops AEC chromogen, and 1 drop 3% hydrogen peroxide) for 15 minutes. Sections were rinsed in distilled water for 3 minutes; counterstained with Gill's hematoxylin (cat# GHS-3-16, Sigma Co., St. Louis, MO) for 1 minute; and rinsed under tap water for 3 minutes. Sections were dried, mounted with Aqua-poly/mount (cat#18606, Polysciences, Inc., Warrington, PA), and coverslipped.

5.3 Results

5.3.1. General observations

Cells were present in all the matrices seeded. However, the number of cells and distribution of cells attached to the CG matrices varied from few cells uniformly distributed throughout the matrix (Figure 5.4) to cells concentrated on the surface of the matrix (Figure 5.5). In general, there did not appear to be a large number of cells attached to the matrices. Cells were either spread out along the surface of the collagen-GAG fiber (Figure 5.4) or clumped together (Figure 5.5). Resorption of the matrices within the fourteen days of implant culturing did not appear to occur.

Variability within the matrix appeared high. There were areas of high cell density and areas were there were little to no cells present. Matrix to matrix variability did not appear abnormally high . Variability between matrices was expected to occur and the seeded density and degree of infitration appeared within a reasonable range of variability.

5.3.2. Shrinkage measurements

Cell seeded matrices shrunk over time. By 14 days, the area of the matrices had reduced by over 50% for all pore sizes and cell seeding and culturing conditions (Figure 5.6). There was an overall reduction in dimensions and in some cases, a curling up of the edges of the matrices.

5.3.3. Efficiency of cell seeding

A layer of cells was observed on the bottom of the uncoated tissue culture wells when viewed under an inverted phase-contrast light microscope (Figure 5.7). The cells were spread out on the tissue culture plate. There did not appear to be a similiar layer of cells attached to the bottom of the wells coated with the 2% agarose solution. However, there appeared to be cells floating in the medium.

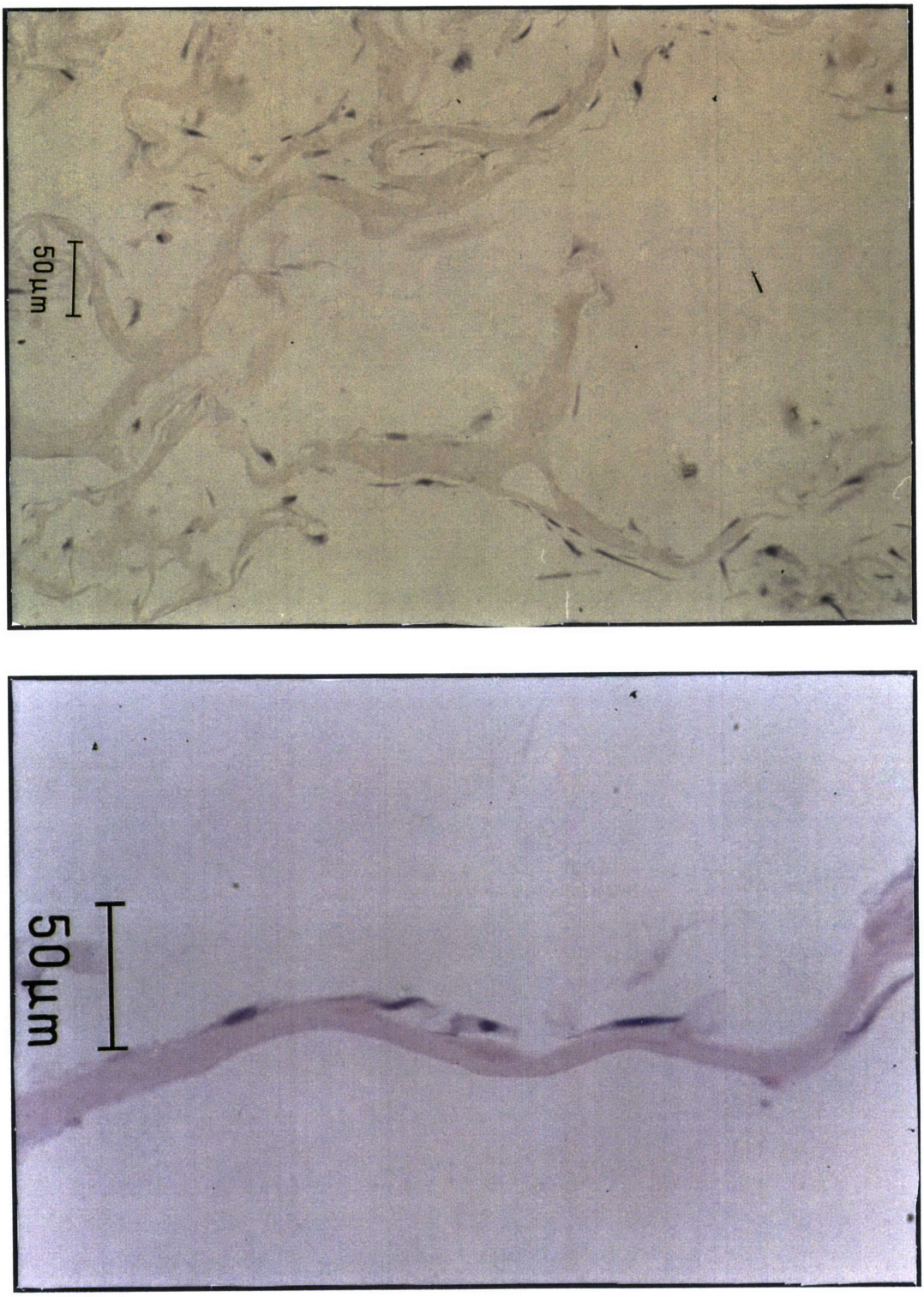

Figure 5.4. Uniform distribution of tendon cells within a collagen-GAG matrix. Cells are evenly distributed throughout the matrix and appear spreadout along the collagen-GAG fibers. Lower magnification **(left).** Higher magnification **(right)**. Scale bar 50 µm.

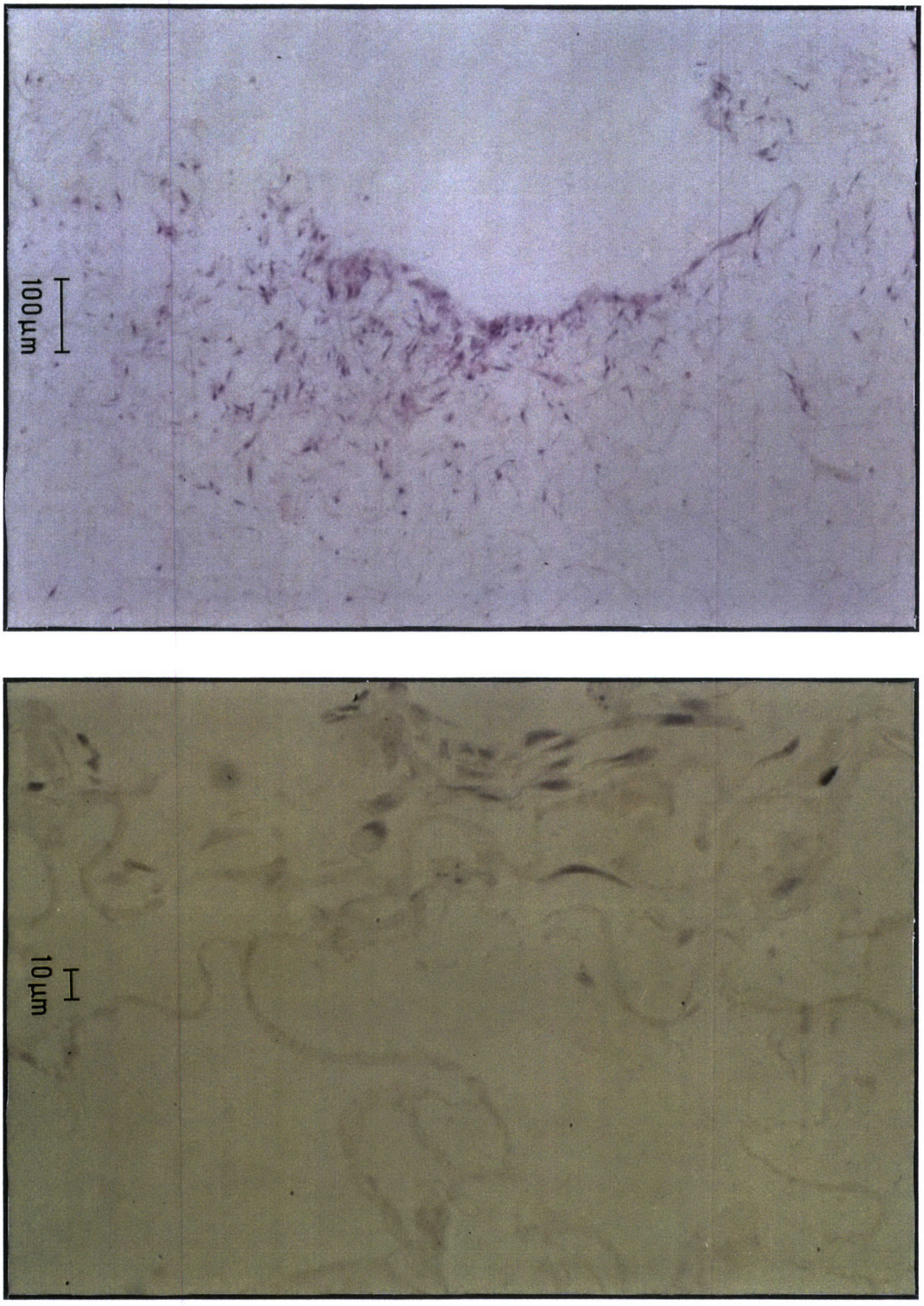

Figure 5.5. Uneven distribution of tendon cells within a collagen-GAG matrix. Higher concentration of cells at the surface of the matrix. Cells appear rounded and aggregated together. Lower magnification **(top).** Higher magnification (**bottom**). Scale bar 100 µm (low magnification) and 10 µm (high magnification).

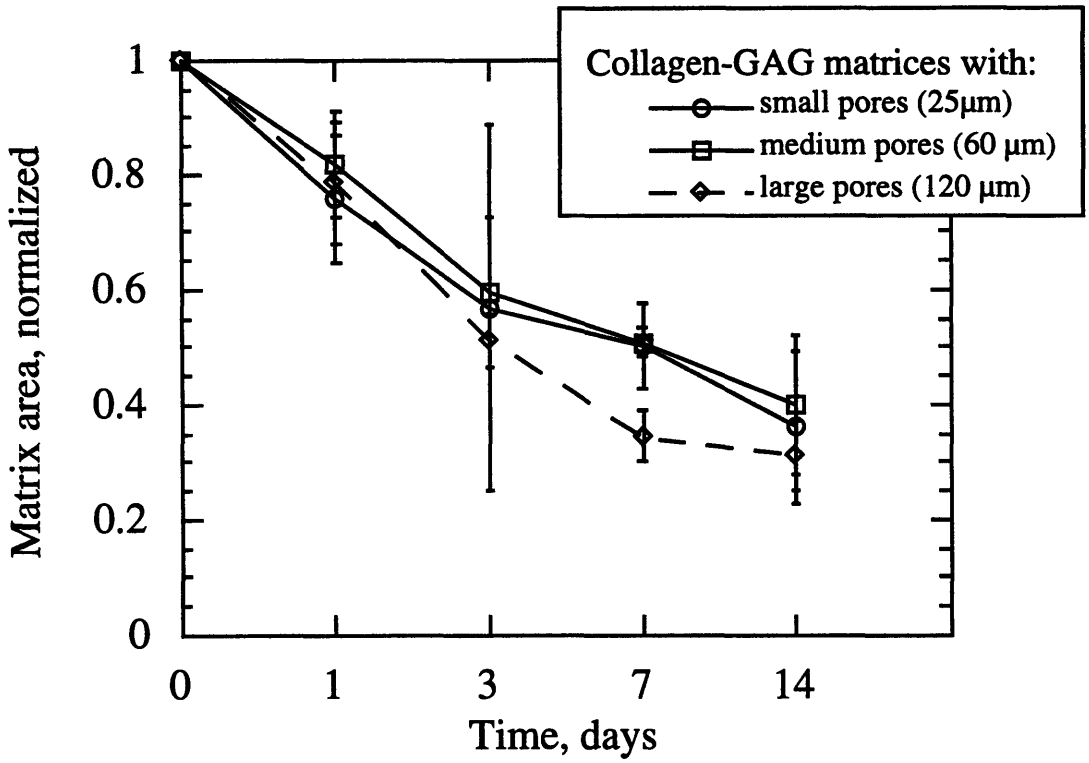

Figure 5.6. Shrinkage of cell-seeded collagen-GAG matrices as a function of implant incubation time for matrices in culture wells that were agarose-coated and agitated for the first 20 hours post-seeding. On average, there over a 50% reduction in matrix area by 14 days. Bars indicate standard error.

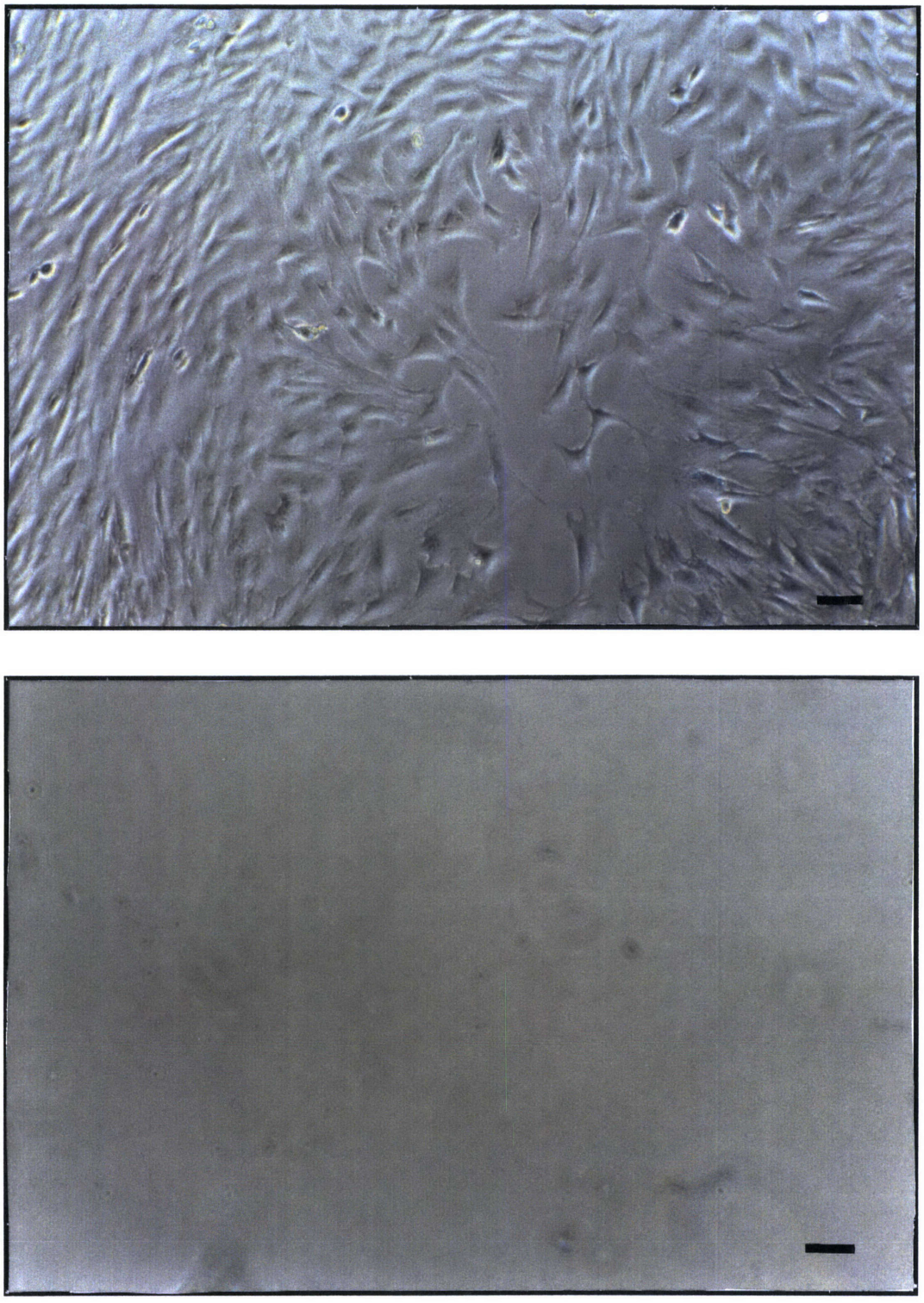

Figure 5.7 Light micrographs of culture wells uncoated (**top**) and coated with a thin layer of 2% agarose (**bottom**). Cells appear to sediment to the bottom of the uncoated wells and attach. No cells appear to attach to the agarose-coated wells. Scale bar: 10 μm.

A cell count of the medium and trysinized contents of the wells revealed that from 2% to 50% of the intial tendon cells seeded were not incorporated into the CG matrices after one day. The method of cell seeding and culture affected the number of cells recovered. There was a significant difference between the number cells recovered in the control (non-coated, non-agitated) wells and the three other seeding conditions (Figure 5.8). The control wells had on average more cells recovered than the coated, agitated wells. On average, cells recovered from wells that were agarose-coated but not agitated and cells recovered from wells that were agitated but not agarose-coated were not significantly different from the agitated, agarose-coated wells or from one another.

5.3.4. Degree of infiltration

Generally, there was a low degree of infitration into the matrices. On average, the thickness of the matrices were one millimeter, while the average depth of cellular infiltration

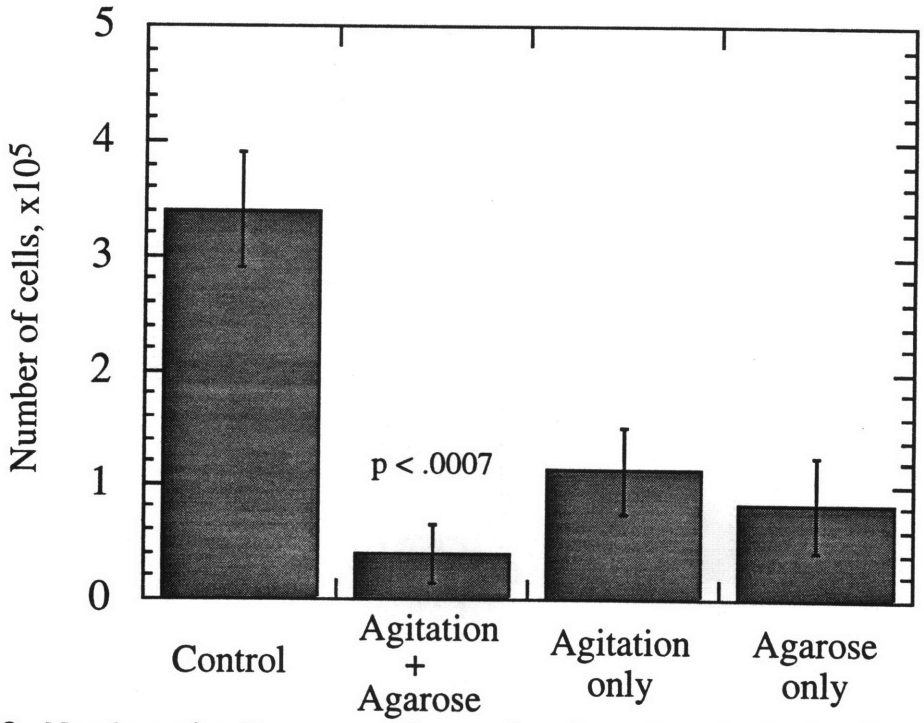

Figure 5.8. Number of cells recovered as a function of method of cell seeding and culturing. The bars indicate standard error. Significant difference between control and other three groups. Control conditions were no agarose coating and no agitation.

into the matrix was 0.35 mm. In many of the matrices, the interior of the matrix was devoid of cells (Figure 5.5). The majority of cells were near or on the surface of the cells. The degree of infitration appeared to be dependant on the pore diameter of the CG matrices rather than on the method of cell seeding and culturing (Figure 5.9). There was a significant difference ($p<0.01$) between the depth of cellular infiltration into matrices at one day for agarose-coated wells that were agitated. Average depth of infiltration into matrices with small pore diameters was 0.05 mm (± .01 mm, standard error), while the average depth of infiltration into matrices with large pore diameters was 0.43 mm (± .12 mm, standard error).

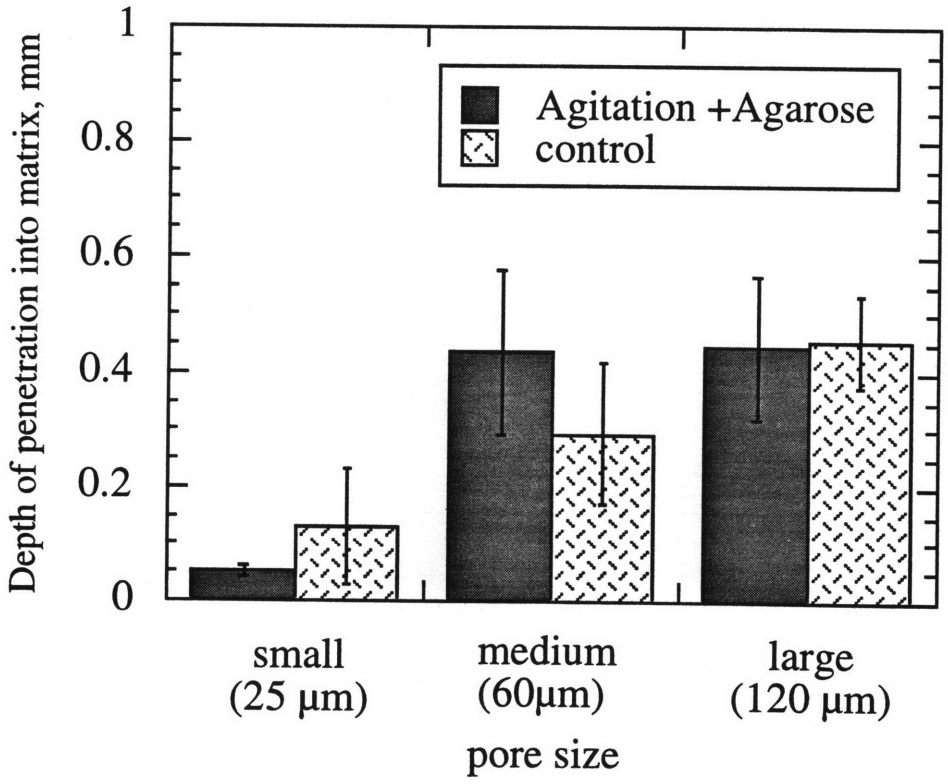

Figure 5.9. Depth of infitration of cells into CG matrices as a function of pore size and implant seeding and culturing at day one post-seeding. The bars indicate standard error. No significant difference in infiltration depth between the methods of implant seeding and culturing, however there is a significant difference ($p <0.01$) in infiltration depth between the different pore sizes.

5.3.5. Cell density

Cell density was greatest at the surface of the matrices in all cases. The cells appeared not to be able to infiltrate in great numbers into the matrix (Table 5.3). Cells were primarily concentrated on the surface of the matrices. There appeared to be a slightly greater density of cells present in the central portion of matrices that were in the matrices that were agitated and in agarose-coated culture wells. In general, the smaller the pore size, the smaller the density of cells present in the central portion of the matrix.

5.3.6. Immunohistochemistry

Tendon cells seeded into the collagen-GAG matrices appear to stain positive for alpha-smooth muscle actin. Cells on the surface of the CG matrix, both spread-out and aggregated, and in the interior of the matrix appear to stain appear to stain positive (Figure 5.10). There did not appear to be a correlation between time period, pore size of the matrix, or conditions of cell seeding/culturing and the presence of positively stained cells in the matrix.

	seeding condition	pore size	Surface of matrix		Middle of matrix	
			cell density (per mm^2)	± SEM	cell density (per mm^2)	±SEM
Day 1	Ag+ Ag	small (25 μm)	75.56	±49.49	5.93	± 3.92
		medium (60μm)	82.22	±23.76	30.37	±15.52
		large (120 μm)	107.41	±39.76	23.70	±12.13
	control	small (25 μm)	90.37	±77.42	12.59	±12.59
		medium (60μm)	54.07	±15.94	23.70	±3.22
		large (120 μm)	57.78	±20.16	18.52	±10.91
Day 14	Ag+ Ag	small (25 μm)	158.89	±41.11	16.67	±5.56
		medium (60μm)	84.44	±2.22	11.11	±6.67
		large (120 μm)	100.00	±33.33	64.44	±22.22
	control	small (25 μm)	33.33	±17.78	0.00	0.00
		medium (60μm)	55.56	±20	8.89	±4.44
		large (120 μm)	67.78	±7.78	23.33	±3.33

Table 5.3. Table of number of cells per square millimeter on the surface of the CG matrix and in the middle of the matrix as a function of matrix pore size and conditions of cell seeding and implant culture. Ag+Ag were agitated, agarose-coated wells. Controls were culture wells neither agitated nor coated.

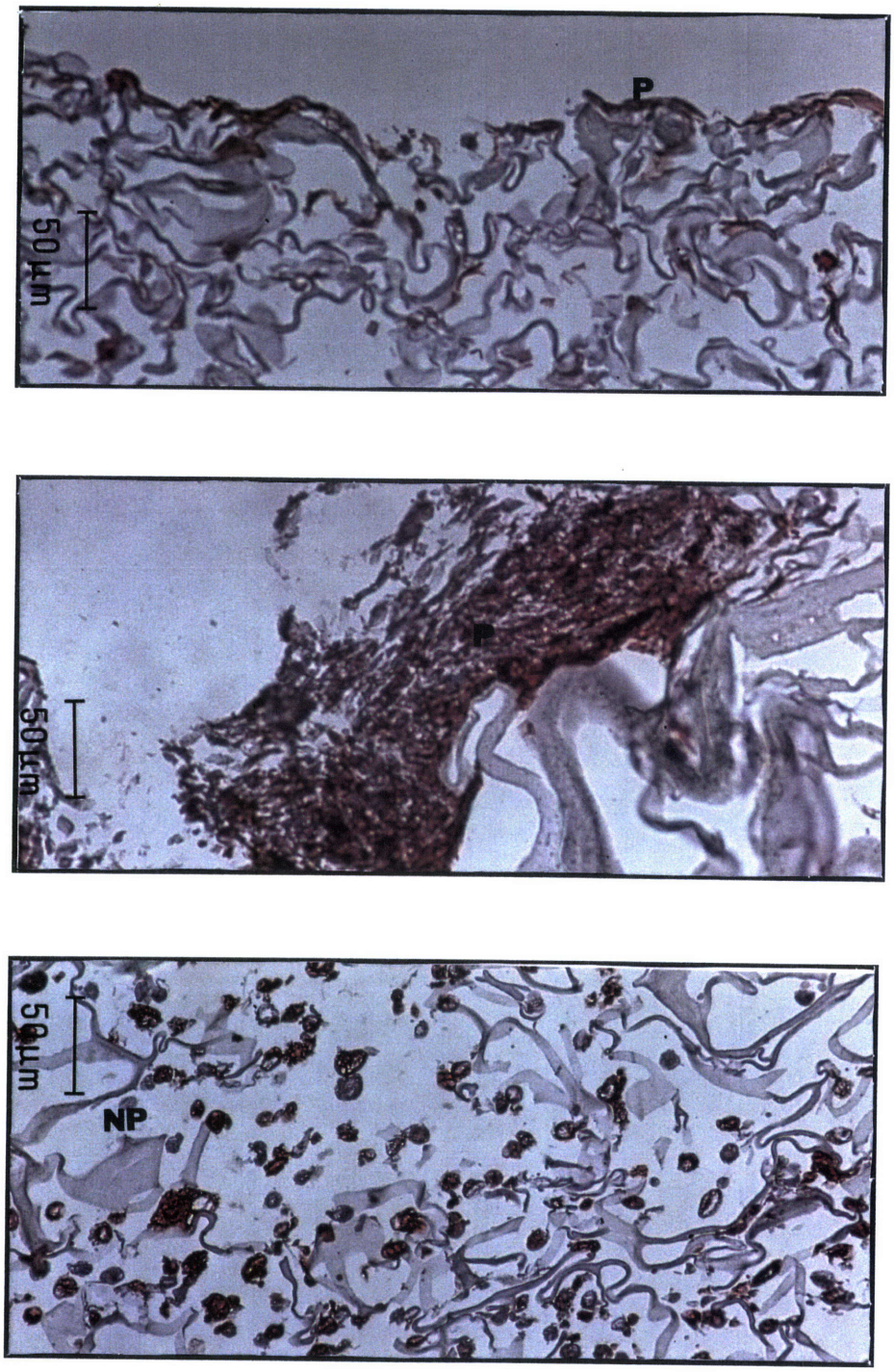

Figure 5.10. Light micrographs of collagen-GAG matrices stained for alpha-smooth muscle actin. Positive staining appeared in tendon cells that were spread-out on the surface of the CG matrix (**top**), aggregated into clumps on the surface (**middle**), and cells within the interior of the matrix (**bottom**). (**P**: positive stained cells. **NP**: non-positive stained cells). Scale bar: 50 µm.

5.4 Discussion

5.4.1. Shrinkage and shape change of matrices

Collagen-GAG matrices seeded with tendon cells were found to decrease in size with the increase in implant cultivation time (i.e., the longer the implant was cultured on the matrices, the greater the reduction in size. Between the period of 1 to 14 days, there appeared to be a linear correlation between time of cell culturing on matrices with reduction of size (Figure 5.6). Although the amount of shrinkage was not statistical different for the three different matrix pore sizes, there appeared to be a trend of the matrices with large pore sizes to contract at a slightly greater rate. This could be due to the larger void space (i.e. non-matrix area) in the larger pore size matrices. Collagen-GAG fibers should be able move into this available void space with little resistance from neighboring collagen-GAG fibers, thus the matrices should be able to contract readily. Matrices with small pore sizes do not have as much void space, therefore there is not as much area to fill with the moving fibers. Also, the collagen-GAG fibers are more restricted in their movement in the small pore size matrices (there is not enough elbow room, so to speak). Although Ramappa [104] did not quantify his results, similar observations of matrix contracture was seen in his studies of the seeding of chondrocyte into porous collagen-GAG matrices.

Studies of fibroblasts cultured onto collagen gels [5, 6] has demonstrated contraction of the collagen gels. It has been shown in these gels that the cultured cells were responsible for the contraction. These cells had a large bundles of actin filaments aligned in the direction of the contracture. Myofibroblasts are cells implicated in the contraction of wounds during the healing process [112-114, 123]. These contractile cells stain positive for alpha-smooth muscle actin. Tendon cells seeded CG matrices stained positive for this actin stain. It is speculated that the tendon cells transformed to myofibroblasts to contract the matrices. It is however, uncertain if all the tendon cells seeded into the CG matrices stained positive for alpha-smooth muscle actin. The staining procedure precludes definitive assessment of the percentage of cells

not stained by the actin, although there does appear to be some unstained cells in the CG matrix.

Contracture of collagen-GAG matrices were generally accompanied by a bowling (curling up of the edges of the matrix) of the matrix. This bowling caused a shape change in the matrices. The bowling effect has been previously observed [104, 123]. It is speculated that the cells on the surface of the CG matrix are responsible for the this bowling effect. These cells may contract the matrix to a greater extent than the cells in the interior of the matrix. It is speculated that the cells on the surface act in an cooperative manner to contract the surface of the matrix. Cells in the interior of the matrix are generally not in contact with one another. It is unsure if these cells participate in the contraction of the matrix.

5.4.2. Effect of pore size on cellular incorporation into matrices

Matrices with larger pore sizes allowed for the infiltration of cells into the interior of the matrices and produced, in general, matrices with evenly distributed cells throughout the devise. In general, matrices with small pore diameters (smaller than 25 μm) did not allow for the infiltration of the cells into the interior of the matrix and cells were aggregated on the surfaces of the matrix. It should be noted that cellular density for all the matrices tested was in general greatest at the surfaces of the matrices for all cases. That notwithstanding, there appeared to be a optimal matrix pore size for cellular incorporation into the matrices (Figure 5.9). Pore diameters less than 25 μm appear not to allow the cells to migrate into the interior of the matrix, while matrices with larger pore diameters (at least 60 μm) allowed the cells to migrate freely.

Although it would appears that matrices with larger pore sizes would be desirable for cell transplantation devices because of the greater the infiltration of cells and the uniform distribution of the cells throughout the matrix, there might be drawbacks to using too large of a pore diameter. For the matrices with pore sizes averaging 120 μm, the cells attached and spread out along the surface of collagen-GAG fibers. The surface area of collagen-GAG fibers are inversely proportional to the matrix pore size; therefore with the larger pore sizes, there is

less surface area for the cells to attach. In theory, the pore size of the matrix (i.e., collagen-GAG fiber surface area) limits the number of cells that are able to be incorporated into the matrix. It should be noted that there were regions on the surface of the matrix that had cells aggregated on top of one another such that there was not a correlation between surface area of matrix and cell number. However, aggregation of cells was not seen in the interior of the matrix.

5.4.3. Effect of agitation and agarose coating on cellular incorporation

The conditions of cell seeding and implant culturing appears to effect the extend and effectiveness of cellular incorporation into the collagen-GAG matrices. Seeded matrices that were seeded onto culture wells that were not coated with a thin layer of agarose and not agitated during the first 20 hours post-seeding (control matrices) appeared to have the most cells recovered from the contents culture well (minus the seeded matrix) at one day post-seeding (section 5.3.3). Assuming an inverse relationship between the number of cells recovered and the number of cells incorporated into the matrix, the control matrices should have the least amount of cells incorporated into the matrix, according to the cell count data. However, data on the cellular density and general observations did not show as obvious a difference between control matrices and matrices with the other cell seeding/culturing conditions as the cell count data would indicate. However, in general, there appeared to be more cells in the non-control matrices. A study in which the cells are labeled (such as radioactively) and seeded into the matrix may be a better quantitative study to determine the number of cells incorporated into the matrix.

The degree of cellular infiltration into the matrix did not appear to influenced by the seeding/culturing conditions. This result is contrary to the results obtained by Freed *et al* [46-48]. Freed showed that the culture conditions (i.e., agitation of polymers during seeding and culturing) in which chondrocytes were seeded into synthetic polymers influenced the cellular density and distribution within the polymer. However, the pore diameters used in Freed's

studies were on the order 200-250 μm [45, 46]. The pore diameter of the matrices in this study were between 25 to 120 μm. It is reasonable to conclude that agitation of the matrices would not have a large effect on the infiltration of cells into the matrix if the limiting factor to infiltration into the matrix was the pore diameter. Agitation of the culture wells would have little effect if the cells could not physically penetrate into the matrix due to the limited path size.

In general, matrices that were on agarose-coated wells and subjected to agitation had a higher cell density than the control matrices (Table 5.3). It was thought that by coating on the bottom of the cell culture well with a thin layer of agarose, cellular attachment to the bottom of the culture well would be inhibited. Agarose gels have been previously shown to inhibit cellular attachment [49]. Cells would not be able to attach to the bottom of the well plate. The cells would then be left to either attach themselves to the side of the well plate or stay in suspension in the medium. Agitation of the cell suspension and medium was thought to provide both nutritional diffusion and increased probability of the cells to come into contact with the CG matrix. Studies by Ramappa [104] on the seeding of chondrocytes into similar matrices showed that by as early as three hours, cells were attached to the matrix, therefore 20 hours of cell suspension agitation should provide enough time and opportunity for the cells to attach. However, Freed *et al* had shown that constant agitation during the entire time period of culturing may have a beneficial effect [46-48].

5.5 Conclusions

Tendon cells recovered from Achilles tendon can be sucessfully seeded into porous collagen-GAG matrices. The tendon cells appear to attach to the matrices and appeared alive throughout the time period of the study. Contraction of matrices that were seeded with cells occurred. The longer the cells were cultured on the matrices, the greater the extent of contraction. By 14 days, matrices had contracted to 50% of its original size. Preliminary studies reveal the presence of myofibroblasts, a type of contractile cell, as evidenced by the positive staining for alpha-smooth muscle actin.

The pore diameter of the matrices appear to affect the degree of infiltration of the cells into the matrices. Pore diameters of 25 μm appear to physically impede the infiltration of the cells into the matrix. Cells tended to agglomerate on the surface of these small pore diameter matrices. However, cellular density was greatest at the surface of the matrix for all matrices.

The conditions of cell seeding and culturing onto the implants appear to have a slight effect of the density of cells incorporated in the matrix. Coating culture well with agarose and the agitation of the culture wells may have a beneficial effect on the incorporation of cells into porous collagen-GAG matrices.

The finalization of a reliable, reproducible protocol for the seeding of tendon cells into a porous collagen-GAG matrix is not complete. This study is a first step in the development of this protocol; many other variables need to be investigated and optimized. Also, the number of samples per condition was extremely small (n=2-3) and these experiments needed to be reproduced to confirm the preliminary results of this study. This study looked at just two variables, the pore diameter of the CG matrix and the agitation and agarose-coating of culture wells in which these matrices were cultured in. The degree of cellular incorporation into the matrices appeared to be affected by these variables. Agitation of matrices with pore diameters of at least 60 μm placed in culture wells coated with agarose appear to produce matrices with good cellular incorporation, although the overall number of cells appears to be relatively small. For implantation of an animal model, the overall number of cells transplanted should be higher than the number of cells seen seeded onto matrices in this study. Refinements are still needed to increase the total number of cells in the matrices before these cell-seeded matrices are implanted in vivo.

CHAPTER VI: CONCLUSIONS AND RECOMMENDATIONS FOR FUTURE STUDIES

6.1 Summary of results

Tendon injuries resulting in a gap larger than one centimeter generally do not heal well if left untreated. In many cases, a tendon substitute is needed to bridge the gap. Analogs of extracellular matrix (AECM) have been used previously to study dermal and nerve regeneration. A study of the effects of a porous collagen-glycosaminoglycan (CG) copolymer matrix on tendon healing was conducted. In order to accomplish this study, 1) an animal model was needed in which to study the response of tendon to various implants, 2) CG matrices needed to be processed to the specifications of the animal model, and 3) techniques were needed to evaluate the extent of healing. A separate study on the feasibility of seeding matrices with tendon cells was also conducted with the future plan of implanting these matrices into the animal model.

A process was developed to prepare matrices of varying pore structure. By varying the processing parameters, temperature of the freezing bath and velocity of immersion into the freezing bath, tubular shaped matrices with controlled pore morphology and pore diameter could be processed. It was found that the pore diameter was highly dependent on the temperature of freezing. The pore morphology and pore channel orientation were dependent of the velocity of immersion into the freezing bath. Results also showed that pore diameter was independent of the overall size of the tubular implant. Small diameter implants (1.5 mm) [76], previously prepared for peripheral nerve regeneration, appeared to have the same range of pore channel diameters as large diameter implants (3.8 mm) at the same processing conditions. Manipulation of the processing parameters allowed the pore morphology and size to be tailored to specific applications. CG matrices with axially aligned pore channels and average pore channel diameters of 25, 60 and 120 μm were chosen to be studied in vivo.

A novel animal model was developed to study the effect of CG matrices on the early healing of Achilles tendon. The animal model consisted of a lesion site that was biologically and mechanically isolated from the external environment. This isolation of the lesion site allowed for the study of the intrinsic capability of the tendon to bridge a wound gap of 10 mm in the presence and absence of implants. Matrices of the three pore sizes mentioned above were implanted into the animal model for 10 days, 3 ,6, and 12 weeks.

As a result of the healing process, a tissue cable was observed to span the lesion gap in all the experimental groups. However, the volume of tissue decreased with increasing time. None of the repaired tissue, at any time period, displayed the appearance or response to handling of normal tendon. At 10 days, 90% of the defect site in the empty tubes was filled with tissue, but by 12 weeks, less than 5% of the lesion site was filled. The volume of tissue filling the empty-tubes was smaller than the tissue in the CG-filled tubes at all time periods. At 12 weeks, tissue in the CG-filled tubes filled on average 16% the defect site by volume.

Histologically, most of the material in the empty tubes was dense fibrous tissue after only 3 weeks. The tissue had spindle-shaped cells, consistent in appearance with fibroblasts, and highly aligned matrix fibers without a crimp pattern. In comparison, tissue in the CG-filled tube was composed primarily of cellular material, consistent with granulation tissue, at the same time period; the cellular material comprised of chronic inflammatory cells, active fibroblasts, endothelial cells, and undifferentiated cells. By 12 weeks, most of the tissue in the empty tube was of a dense fibrous nature that also had a crimp pattern when observed under a polarized light microscope; however, the crimp pattern differed significantly in wavelength from normal tendon.

Although the volume of healing tissue was greater in the CG-filled tubes, at 12 weeks, the tissue appeared more similar to that found in the empty tubes after 6 weeks. The CG-filled tubes contained dense fibrous tissue by twelve weeks, but unlike the tissue in the empty tube at 12 weeks, this tissue had no discernible crimp pattern.

Average collagen fibril diameter and diameter distribution profile for both the empty tube and CG-filled tube did not appear to differ significantly from one another but differed significantly from normal; no fibrils larger than 75 nm in diameter were observed in the 12-week samples.

The presence of the CG matrices appeared to alter the kinetics of tendon healing. Granulation tissue appeared to persist in the wound site longer in the CG-filled tubes than in the empty tubes. The smaller pore sizes tended to have more granulation tissue than the large pore sizes leading to the speculation that the surface area of the collagen-GAG fibers may play a role in altering the healing kinetics. There also appeared to be a general trend of increasing percentage of dense fibrous tissue with increasing pore diameter.

Results of preliminary studies on the feasibility of seeding and culturing cells in CG matrices demonstrated that tendon cells were able to attach to the walls of the CG matrices. This investigation revealed several parameters associated with the efficiency of cell seeding: pore diameter, agitation during seeding, and use of agarose-coated culture plates. Matrices of large pore diameter appeared to allow for the best infiltration of cells into the center of the matrix; the smaller pore diameter matrices appeared to impede the movement of the cells into the center of the matrix. Future studies on a more effective and reproducible method of incorporating cells into the matrices are needed. Additionally, the effect of the cell-seeded matrices should then be investigated in the animal model.

6.2 Evaluation and conclusions

6.2.1. Processing of CG matrices

The morphology the CG matrices can be controlled to a certain degree by varying the velocity of immersion into the freezing bath and the temperature of the freezing bath. Due to the nature of dendritic ice nucleation and growth; the absolute direction of dendritic growth can not be controlled although the overall direction can be controlled with the two aforementioned parameters. Since the dendritic ice formation determines the nature of the pore morphology,

total control of the pore channel direction is not possible. Pore channels do not go from one end of the cylinder to the other without deviation off the preferential axis. In general, this is not a large concern, but a method for processing CG matrices with better controlled pore channel morphology may be of benefit.

6.2.2 Animal model

Although this animal model does not necessarily mimic the current clinical situation for Achilles tendon healing (external influences are generally not precluded in the clinical situation), it does appear to be a model system to study the effect of different implants on tendon healing in a controlled environment.

The choice of tube material may be a factor in the extent of tendon healing observed. At sacrifice, there appeared to be a substantial amount of tissue on the outside of the silicone tube. If the tube was not present, tissue observed on the outside of the tube could have been incorporated into the wound site. Also, the isolation of the wound site from cells and soluble regulators from external sources could affect the volume of tissue produced. A study by Chamberlain [14] on the effect of tube material in an entubulated peripheral nerve gap animal model demonstrated that the permeability of tube material appeared to affect the volume of nerve tissue found in the lesion site. The volume of tissue in the silicone tubes was small to non-existent while the volume of tissue in porous collagen tubes was significantly greater and in all cases filled the defect volume.

The method used to reduce mechanical loading to the lesion site was not straight-forward. To prevent pull-out of the tendon ends from the silicone tube, 1) the knee joint of the operated leg was immobilized by using an external fixation device, and 2) tendons around the hock joint were removed to limit the amount of movement of the distal tendon stump. This additional procedure of removing the tendons around the hock joint has the disadvantage of 1) not being clinically representative and 2) introducing an additional complication to the wound area. A simpler animal model that did not involve as complicated an immobilization procedure

as the one employed in this model would have been an improvement. A possible solution is to use an animal that 1) did not depend solely on its hind legs to move about (as the rabbit does) and 2) a hind limb that is easily immobilized. Dogs, goats and sheep would fulfill this requirement.

6.2.3. Kinetics of tendon healing in an empty tube

The volume of this tissue appeared to decrease with time. The reduction in volume appeared to correspond to the remodeling and "densification" of the matrix material. The densification of the tissue from a loose network of fine fibrin fibers within a cellular mass (10 days) to the highly aligned, densely-packed collagen fiber (12 weeks) has been observed by other investigators [8, 32, 36, 37, 68, 84, 99, 127]. The alignment of fibers has been speculated to be due to mechanical loading of the tendon in the long direction of the tendon [84]. Based on this speculation, if the time period of immobilization was increased, the tissue formed in response to tendon injury would be less highly aligned than tissue formed in response to tendon injury in a model that was either not immobilized or a model that was immobilized for a shorter period. Although, the loading of the wound site was diminished by the use of external fixation for the first ten days in this current study, the animal was not immobilized thereafter and mechanical loading could be acting on the new tissue and causing the alignment of the matrix fibers in the long direction of the tendon. This model did not monitor the *in vivo* mechanical strains in the wound area, therefore confirmation of this speculation could not be performed.

At 12 weeks, a proportion of the tissue formed in the empty tubes was found to have a crimp pattern. The crimp pattern was significantly smaller than normal tendon with respect to the wavelength and thickness of fiber bundles associated with the crimp. In addition, average collagen fibril diameter of tissue formed in the empty tube at 12 weeks was significantly smaller than that of normal tendon.

Models of mechanical properties of tissues based on the crimp characteristics and on collagen fibril diameter predict that the tissue in the empty tube at 12 weeks would be mechanically and functionally inferior to normal adult rabbit tendon. Biomechanical testing of tissue in the lesion site is needed to confirm this prediction.

6.2.4. Effect of CG Matrix Parameters

The volume of tissue from tubes filled with each of the three collagen-GAG matrices was greater than the tissue in the empty tubes at all time periods. The larger volume of tissue observed in the lesion gaps which were implanted with the CG matrix could be due to the fact that the tissue was not as highly aligned as the tissue in the empty tubes.

The presence of the CG matrix in the tube appeared to alter the kinetics of healing which were observed in the empty tubes. The sharpness of transition from being a cell-based material (granulation tissue, class I) to a matrix-based (classes II, III, IV and V) appeared to be altered by the presence of the matrix. The presence of the CG matrices coincided with the presence of granulation tissue in the lesion site. It is possible that the presence of the CG matrix may induce synthesis of granulation tissue.

In addition, the pore size of the CG matrix appeared to affect this transition. The larger pore sizes had the least amount of granulation tissue and the most amount of dense fibrous tissue present at 3 and 6 weeks. It is speculated that there is an optimal range of pore sizes in which below this optimal range, the pore channels may be too small for cells to migrate into the wound site. Above this pore size range, the distance between CG matrix walls (large pore channels) may be too far apart that the migrating cells do not "sense" the presence of the CG matrix surface area. In this later case of large pore channels, the effect of the CG matrix approaches the effect of an empty tube. This range of "optimal" pore size did not appear to be revealed in this set of experiments. It is possible that a larger range of pore channels diameters need to be tested to differentiate the possible presence of an optimal pore channel diameter range for tendon healing.

The presence of the CG matrices may have also affected the ability of the matrix fibers to align. In regions where the CG matrix was still present, there did not appear to be newly synthesized matrix fibers that were aligned. Highly aligned tissue (class III and above) was generally located along the interface of the tissue and the silicone tube where there did not appear to be a significant amount of CG matrix present.

One possible explanation for the CG matrices' effect is that the prolongation of the granulation tissue formation phase (seen in CG-matrix filled tubes) delayed the formation of matrix fibers. In turn, this delayed the densification and alignment of the fibrous tissue. If the hypothesis is that fibrous tissue can not form until the signals to produce granulation tissue has decreased to a particular level (i.e., the amount of granulation tissue is sufficiently low), then in these CG-regions there is a delay in the start of matrix production and subsequently a lag in the alignment and densification of the matrix fibers. This would imply that the tissue in the CG-filled tubes would, given enough time, eventually remodel to highly dense aligned tissue.

Another possible hypothesis is that mechanical loading has returned to the lesion site and tension exerted by the tendon ends are responsible for the alignment of the newly synthesized matrix fibers. It is possible that the CG matrix may be shielding the newly synthesized tissue from tensile forces, thus impeding alignment of the tissue.

Implantation of a CG matrix did not result in the regeneration of a tendon-like tissue, by twelve weeks post-implantation. By this period, such matrices resulted in more regenerative tissue in lesions of dermis and peripheral nerve. It is possible that over a longer period, the CG matrix could have facilitated regeneration of tendon. However, clinically, a prolonged healing period could pose additional concerns to the patient and in general is not desired.

The experience in dermis served, in part, as the basis for the justification of implantation of this matrix for treating defects in tendon. Important differences between tendon and dermis are 1) the avascular nature of the midsection of tendon compared to the highly vascular character of dermis, and 2) the relatively low density of tendon cells compared to the numerous fibroblasts in dermis. Moreover, the lesion site of the tendon animal model was

isolated from surrounding tissue which may have further limited the number of fibroblast-like cells migrating into the lesion site.

It is speculated that the addition of exogenous tendon cells to the lesion site would result in a larger volume of tissue filling the lesion site. The kinetics of tendon healing are speculated to be different for lesion sites filled with cell-seeded matrices and non cell-seeded matrices. It is possible that the quality of healing tissue in sites implanted with cell-seeded matrices would be higher than that sites implanted with non cell-seeded matrices (i.e., tissue in the cell-seeded matrices site would be similar in characteristic to normal tendon).

6.3 Potential future studies

6.3.1. Animal model

Potential modifications and studies of the animal models include: development of a method to determine *in vivo* strain within the lesion site, investigation of the effect of mechanical loading on tendon healing, and investigation of the effect of varying the tube material on tendon healing.

The development of a method to determine *in vivo* strain would be helpful in correlating the effect of mechanical loading at the lesion site with the extent of tendon healing. Varying the time period of immobilization of the knee roughly correlates to varying the time period of mechanical unloading to the lesion site. However, the exact extent and time period of this mechanical unloading can not, at this time, be quantified in this animal model. It is speculated that the longer the time period of immobilization, besides potentially causing degeneration of the knee joint, the less highly aligned the healing tissue.

Investigations of tubes of controlled permeability to cells, proteins and small molecules could be conducted to determine the effect of these external biological influences to the volume and morphology of tissue produced in the wound site. The animal model allows for the introduction of selected external factors via a change in the tube material (for example, using a

particular collagen tube with a given porosity may allow for soluble factors but not cells to enter the wound site).

6.3.2. Kinetics of tendon healing

Long term studies are needed to confirm the hypothesis that the tissue in the empty tube at 12 weeks is end-stage scar tissue and will not remodel to tissue more closely resembling normal adult tendon. In this animal model, the majority of tendon healing activity appeared to occur between 10 days and 6 weeks in the empty tube and between 10 days and over 12 weeks in the CG-filled case. By 12 weeks, remodeling of the tissue in the empty tube appeared to have reached a plateau. In addition, results from Kato's study suggest that tissue in the empty tube at 12 weeks in this animal model, which, morphologically, resembled the tissue described in Kato's study at 52 weeks, will not develop to a great extent over a longer period of time.

Tissue found in tubes filled with CG matrix had not shown evidence of reaching a plateau by the end of the experimental period of 12 weeks; the percent defect volume which was filled with dense fibrous tissue in the CG-filled defect sites increased continuously throughout the period of observation. Longer term studies are needed to determine if the tissue in the CG-filled tubes will develop tissue with similar morphological features as that of tissue in the empty tube at 12 weeks (i.e., the development of a crimp pattern). Possible scenarios are 1) a crimp pattern does not develop at any later period of time, 2) a crimp pattern with characteristics similar to that of the crimp pattern in the tissue in the empty tubes at 12 weeks develops, 3) a crimp pattern with characteristics similar to that of normal tendon develops, or 4) a crimp pattern with characteristics dissimilar to latter two cases develops.

Time points of evaluation could include: 24 weeks and 52 weeks. By 24 weeks, the majority of tissue remodeling activity should have reached a plateau ("stable" tissue). By 52 weeks, a comparison of tissue from Kato's study can be evaluated with tissue from the animal model used in this study. Beyond one year, it is still possible that the CG matrix could have remodeled to tissue similar in characteristics to normal adult tendon. However, clinically, a

prolonged healing period could pose additional concerns to the patient and in general is not desired.

Mechanical testing should also be performed. Mechanical testing is the most commonly used "functional" evaluation of the extent of tendon healing. By quantifying the mechanical properties of healing tendon tissue, the "quality" of the healing tendon can be assessed. In addition, models that predict the mechanical properties of tissue based on morphological data can be correlated with the experimental data.

6.3.2. CG Matrix Parameters

The presence of the CG matrix appeared to alter the kinetics of tendon healing. Additional parameters of the CG matrix that can be tested are the effect of degradation rate, the effect of pore channel alignment, the effect of a larger range of pore size, and the effect of seeding exogenous tendon cells into the CG matrices.

It has been shown that degradation rate affects the regeneration of both peripheral nerve and dermis. Matrices with varying rates of degradation can be controlled by varying the time period of exposure of the CG matrices to chemical cross-linking agents. If the CG matrix was tailored to degrade at a faster rate, it is possible that there would be less granulation tissue present in the lesion site at a later period of evaluation and the transition from granulation tissue to matrix-based tissue would mimic the kinetics of the empty tube. Conversely, if the CG matrix was tailored to degrade at a slower rate, it is possible the transition from granulation tissue to matrix-based tissue would be slower than that seen in this study.

Overall pore channel orientation can be controlled by varying the processing parameters of CG manufacturing. A faster rate of immersion leads to radially oriented pore channels. It is speculated that pore channels oriented in the long direction of the tendon would lead to more highly aligned healing tendon tissue than pore channels that were oriented perpendicular to the long axis of tendon. It is possible that the pore channel walls physically impede the advancement of cells into the wound site .

Although the effect of pore channel was investigated in this study, the small number of pore sizes tested may not have been sufficient to determine if there is an optimal range of pore channel diameters. Pore channel diameters smaller than 20 μm and larger that 120 μm should be tested to fill out a larger range of pore sizes. It is hypothesized that pore diameters below a particular size may be too small for cells to migrate into the wound site and without cells migrating into the wound site, new tissue could not be synthesized to bridge the lesion site. Pore channel diameters above a particular range may be too large such that the cells are not able to "sense" the presence of the CG matrix surface area and the effect of the CG matrix approaches the effect of an empty tube.

Seeding the CG matrices with exogenous tendon cells is speculated to improve the quantity and possibly the quality of the healing tissue. Exogenous cells provide additional collagen-producing cells to the wound site at the time of implantation. It still remains to be seen if these cells will be viable and proliferate in the lesion site and to what extent. If the exogenous cells were to die soon after implantation, the benefit of additional cells is negated. Prior to implantation into the animal model, a reproducible protocol for seeding of exogenous tendon cells is needed.

Appendices

A1: Chemical formulation of fixation solutions

2.5% cacodylate buffered glutaraldehyde

Gluteraldehyde, 25% in water	10 ml
Cacodylate buffer, pH 7.4	100 ml

Cacodylate Buffer (pH 7.4)
Stock solution

Stock A (0.2 M Sodium cacodylate (mw 214)):
4.28 gms sodium cacodylate
100 ml distilled water

Stock B (0.2 M HCl (mw 36.46))
1.7 ml HCl
100 ml distilled water

Buffer (pH 7.4):

Stock A	25 ml
Stock B	1.4 ml
distilled water	73.6 ml

4% paraformaldehyde-.20% glutaraldehyde fixative solution

4% paraformaldehyde solution	99.2 ml
Glutaraldehyde, 25% in water	0.8 ml

4% paraformaldehyde* solution

Sodium phosphate, monobasic	4.0 gms
Sodium phosphate, dibasic	6.5 gms
Paraformaldehyde	40 gms

Dissolve both sodium phosphates in water to 1000 ml, heat to 60-70 °C (in fume hood), add 40 of paraformaldehyde powder, stir well, cool, and filter.
Keeps for several weeks. pH is 7.2-7.4

* Justification: Paraformaldehyde used as fixative for electron microscopy and often for enzyme histochemistry or immunohistochemistry.

A2: Histological Protocols

Hematoxylin and Eosin Stain for Paraffin-Embedded Tissue, modified

(Manual of Histological Staining: Methods of the Armed Forces Institute of Pathology, III Ed, 1968, pp.94-95)

FIXATION: Bouin's or 10% buffered neutral formalin

TECHNIQUE: paraffin embedded, sectioned at 5-10μm

SOLUTIONS:

Harris Hematoxylin Solution

(Sigma Co., HHS-128)

Eosin Y Solution, Aqueous

(Sigma Co., HT110-2-128)

Acid Alcohol

Alcohol, 70%	100.0 ml
Hydrochloric acid, concentrated	1.0 ml

Ammonia Water

Tap water	1000.0 ml
Ammonium hydroxide, 28%	2-3 ml

STAINING PROCEDURE:

1. Deparaffinize and hydrate to distilled water.

xylene	2 minutes	2X
100% EtOH	1 minute	2X
95% EtOH	1 minute	
80% EtOH	1 minute	
70% EtOH	1 minute	
tap water	10 minutes	

2. Stain with Harris Hematoxylin solution 2-3 minutes.
3. Rinse with distilled water for 5-10 seconds.
4. Acid alcohol for 1-2 dips.
5. Rinse with distilled water for 5-10 seconds.
6. Dip in ammonium hydroxide solution for 5-60 seconds, until blue.
7. Rinse with distilled water for 2 minutes.
8. Eosin dip for 3 seconds.

9. Dehydrate and clear .

70% EtOH	1 minute	
80% EtOH	1 minute	
95% EtOH	1 minute	
100% EtOH	1 minute	2X
xylene	2 minutes	2X

10. Mount with Permount or Histoclad.

A2: Histological Protocols

Masson's Tri-Chrome Stain for Paraffin-Embedded Tissue

(Manual of Histological Staining: Methods of the Armed Forces Institute of Pathology, III Ed, 1968, pp.94-95)

FIXATION: Bouin's or 10% buffered neutral formalin

TECHNIQUE: paraffin embedded, sectioned at 5-10μm

SOLUTIONS:

Bouin's Solution

(Sigma Co.)

Weigert's Iron Hematoxylin Solution

Solution A:	
Hematoxylin crystal	1.0 gm
Alcohol, 95%	100.0 ml
Solution B:	
Ferric Chloride, 29% aqueous	4.0 ml
distilled water	95.0 ml
HCl, conc.	1.0 ml

Mix equal part of solution A and solution B.

Biebrich Scarlet-Acid Fuchsin Solution

Biebrich scarlet, aqueous, 1%	90.0 ml
Acid fuchsin, aqueous, 1%	10.0 ml
Glacial acetic acid	1.0 ml

Phosphomolybdic-Phosphotungstic Acid Solution

Phosphomolybdic acid	5.0 gm
Phosphotungstic acid	5.0 gm
Distilled water	200.0 ml

Aniline Blue Solution

Aniline blue	2.5 gm
Glacial acetic acid	2.0 ml
Distilled water	100.0 ml

1% Glacial Acetic Acid Solution

Glacial acetic acid	1.0 ml
Distilled water	100.0 ml

STAINING PROCEDURE:

1. Deparaffinize and hydrate to distilled water.

xylene	2 minutes	2X
100% EtOH	1 minute	2X
95% EtOH	1 minute	
80% EtOH	1 minute	
70% EtOH	1 minute	
tap water	10 minutes	

2. Mordant in Bouin's solution for 1 hour at 56°C, or overnight at room temperature, if formalin fixed.
3. Cool and wash in running water until yellow color disappears.
4. Rinse in distilled water.
5. Weigert's iron hematoxylin solution for 10 minutes. Wash in running water 10 minutes.
6. Rinse in distilled water.
7. Biebrich scarlet-acid fuchsin solution for 2 minutes. Save solution.
8. Rinse in distilled water.
9. Phosphomolybdic-phosphotungstic acid for 10 to 15 minutes before aniline blue solution. Discard solution.
10. Aniline blue solution for 5 minutes. Save solution.
11. Rinse in distilled water.
12. Glacial acetic solution for 3 to 5 minutes. Discard solution.
13. Dehydrate and clear .

70% EtOH	1 minute	
80% EtOH	1 minute	
95% EtOH	1 minute	
100% EtOH	1 minute	2X
xylene	2 minutes	2X

14. Mount with Permount or Histoclad.

A2: Histological Protocols

Hematoxylin and Eosin Stain for GMA Embedded Tissue, modified

FIXATION: Bouin's or 10% neutral buffered formalin
TECHNIQUE: GMA embedding, 2-4 μm sections

SOLUTIONS:

Harris Hematoxylin Solution
(Sigma Co., HHS-128)

Eosin Y Solution, Aqueous
(Sigma Co., HT110-2-128)

Acid Alcohol

Alcohol, 70%	100.0 ml
Hydrochloric acid, concentrated	1.0 ml

Ammonia Water

Tap water	1000.0 ml
Ammonium hydroxide, 28%	2-3 ml

STAINING PROCEDURE:

1. Air dry slides overnight or dry on hot plate (60°C) for 30 minutes.
2. Stain with Harris Hematoxylin solution 90 minutes.
3. Rinse well with distilled water for 2 minutes.
4. Acid alcohol for 1-2 dips.
5. Rinse with distilled water for 30 seconds.
6. Dip in ammonium hydroxide solution for 5-60 seconds, until blue.
7. Rinse in slowly running water for 10 minutes.
8. Eosin dip for 5 minutes.
9. Air dry.
10. Mount with Permount or Histoclad.

A2: Histological Protocols

Masson's Tri-Chrome Stain for GMA-Embedded Tissue

FIXATION: Bouin's or 10% buffered neutral formalin
TECHNIQUE: paraffin embedded, sectioned at 3-5 μm

SOLUTIONS:

Weigert's Iron Hematoxylin Solution

Solution A:

Hematoxylin crystal	1.0 gm
Alcohol, 95%	100.0 ml

Solution B:

Ferric Chloride, 29% aqueous	4.0 ml
distilled water	95.0 ml
HCl, conc	1.0 ml

Mix equal part of solution A and solution B.

Biebrich Scarlet-Acid Fuchsin Solution

Biebrich scarlet, aqueous, 1%	90.0 ml
Acid fuchsin, aqueous, 1%	10.0 ml
Glacial acetic acid	1.0 ml

Phosphomolybdic-Phosphotungstic Acid Solution

Phosphomolybdic acid	5.0 gm
Phosphotungstic acid	5.0 gm
Distilled water	200.0 ml

Aniline Blue Solution

Aniline blue	2.5 gm
Glacial acetic acid	2.0 ml
Distilled water	100.0 ml

1% Glacial Acetic Acid Solution

Glacial acetic acid	1.0 ml

Distilled water	100.0 ml

2-butoxyethanol (ethylene glycol monobutyl ether)

STAINING PROCEDURE:

1. Weigert's iron hematoxylin solution for 20 minutes. Wash in running water 10 minutes.
2. Rinse in distilled water.
3. Biebrich scarlet-acid fuchsin solution for 20 minutes. Save solution.
4. Rinse in distilled water.
5. Phosphomolybdic-phosphotungtic acid for 10 to 15 minutes before aniline blue solution. Discard solution.
6. Aniline blue solution for 10 minutes. Save solution.
7. Rinse in distilled water.
8. Glacial acetic solution for 3 to 5 minutes. Discard solution.
9. Dip in 2-butoxyethanol for 5 dips.
10. Differentiate in 95% alcohol until stain stops flowing from section.
11. Dehydrate in absolute alcohol.
12. Clear in xylene.
13. Mount with Permount or Histoclad.

A3: Immunohistochemical Protocols

Collagen Type I Immunohistochemical Protocol for New Zealand white Rabbit Achilles Tendon

FIXATION: Formalin
TECHNIQUE: paraffin embedded, sectioned at 6-8 μm

SOLUTIONS:

Tris Buffered Saline (pH 8.0) (Wash solution and diluent)

Tris buffered saline (Sigma# T-6664)	1 pkg
Distilled water	to 1000 ml

Trypsin (Digestion)

0.1% solution

Trypsin (Sigma cat# T8128)	0.01 gms
Phosphate buffered Saline	10 ml

20% Donkey serum (Blocking Solution)

Donkey normal sera (Sigma cat#D9663)	0.2 ml
TRIS buffered saline	0.8 ml

Goat monoclonal anti-Type I collagen (Primary antibody) 1: 50

Goat monoclonal anti-type I collagen (SBA cat# 1310-01)	20 μl
TRIS buffered saline	.980 ml

Donkey anti-goat immunoglobulin (Secondary antibody) 1 : 20

Donkey anti-goat IgG (whole molecule) (Sigma cat# G-7767)	50 μl
TRIS buffered saline	.95 ml

Goat Peroxidase-Anti Peroxidase (PAP) 1:200

Goat PAP (Sigma cat#P1901)	20 μl
TRIS buffered saline	3.980 ml

Incubation Medium (AEC)
from alpha smooth muscle actin kit (Sigma cat#IMMH-2)

Distilled water	4 ml
Acetate buffer	2 drops
3% H_2O_2	1 drop
AEC chromogen	1 drop

Filter before use.

Gill's No 3 Hematoxylin Solution (conterstain)

Sigma cat#GHS-3-16

1% Goat Serum (Negative control)

Mouse normal sera (Sigma cat# G9023)	0.1 ml
Phosphate buffered saline	10 ml

STAINING PROCEDURE:

1. Deparaffinize and rehydrate to TBS:

xylene	2 minutes	2X
100% EtOH	1 minute	2X
95% EtOH	1 minute	
80% EtOH	1 minute	
70% EtOH	1 minute	
TBS	5 minute	

2a. Bouin Mordant (Optional):

Soak slides in Bouin fixative (Sigma cat# HT10-1-32) solution for overnight. May enhance the intensity of the stain. Troxel noted that Bouin fixed tissue stained more intensely than formalin fixed tissue.

Rinse under tap water until yellow color disappears.

3. Wipe off excess liquid around sections.
Circle sections with PAP pen (Polysciences).

4. Digestion:

0.1% trypsin solution for 60 minutes (humidifed chamber).

5. Wash in TBS for 3 minutes. (2X)

6. Blot off excess around sections.

7. Blocking solution:

20% donkey serum for 10 minutes.

Wipe slides but DO NOT WASH.

8. Primary antibody or negative control:

Primary (or negative) for overnight.

9. Repeat steps 5 and 6.

10. Secondary antibody.

Secondary antibody for 60 minutes.

11. Repeat steps 5 and 6.

12. PAP "complex".

PAP complex for 60 minutes.

13. Substrate solution:

While waiting for step 13 to complete, prepare substrate solution in provided mixing vial.

14. Repeat steps 5 and 6.

17. Visualization (coloring step):

Substrate solution for 10 minutes, check under microscope for extent of colorization.

Adjust time accordingly.

18. Termination of colorization:

Rinse in distilled water for 3 minutes.

19. Counterstain (optional):

Gill No. 3 hematoxylin solution for 1 minute.

20. Rinse in distilled water.

21. Wash in running tap for 3 minutes.

22. Mount with Aquamount and coverslip.

NOTE:

1. DO NOT allow slides to dry out between steps, will cause excess background staining.
2. AEC oxidation light sensitive, store slides in dark, best, else fading of stain may occur.
3. AEC also alcohol soluble, so make sure counterstain water-based and mounting media water-based.

A3: Immunohistochemical Protocols

Collagen Type III Immunohistochemical Protocol for New Zealand white Rabbit Achilles Tendon

FIXATION: Formalin
TECHNIQUE: paraffin embedded, sectioned at 6-8 μm

SOLUTIONS:

Tris Buffered Saline (pH 8.0) (Wash solution and diluent)

Tris buffered saline (Sigma# T-6664)	1 pkg
Distilled water	to 1000 ml

Trypsin (Digestion)

0.1% solution

Trypsin (Sigma cat# T8128)	0.01 gms
Phosphate buffered Saline	10 ml

20% Donkey serum (Blocking Solution)

Donkey normal sera (Sigma cat#D9663)	0.2 ml
TRIS buffered saline	0.8 ml

Goat monoclonal anti-Type III collagen (Primary antibody) 1: 50

Goat monoclonal anti-type I collagen (SBA cat# 1330-01)	20 μl
TRIS buffered saline	.980 ml

Donkey anti-goat immunoglobulin (Secondary antibody) 1 : 20

Donkey anti-goat IgG (whole molecule) (Sigma cat# G-7767)	50 μl
TRIS buffered saline	.95 ml

Goat Peroxidase-Anti Peroxidase (PAP) 1:200

Goat PAP (Sigma cat#P1901)	20 μl
TRIS buffered saline	3.980 ml

Incubation Medium (AEC)
from alpha smooth muscle actin kit (Sigma cat#IMMH-2)

Distilled water	4 ml
Acetate buffer	2 drops
3% H_2O_2	1 drop
AEC chromogen	1 drop

Filter before use.

Gill's No 3 Hematoxylin Solution (conterstain)
Sigma cat#GHS-3-16

1% Goat Serum (Negative control)

Mouse normal sera (Sigma cat# G9023)	0.1 ml
Phosphate buffered saline	10 ml

STAINING PROCEDURE:

1. Deparaffinize and rehydrate to TBS:

xylene	2 minutes	2X
100% EtOH	1 minute	2X
95% EtOH	1 minute	
80% EtOH	1 minute	
70% EtOH	1 minute	
TBS	5 minute	

2a. Bouin Mordant (Optional):

Soak slides in Bouin fixative (Sigma cat# HT10-1-32) solution for overnight. May enhance the intensity of the stain. Troxel noted that Bouin fixed tissue stained more intensely than formalin fixed tissue.

Rinse under tap water until yellow color disappears.

3. Wipe off excess liquid around sections.
Circle sections with PAP pen (Polysciences).

4. Digestion:

0.1% trypsin solution for 60 minutes (humidifed chamber).

5. Wash in TBS for 3 minutes. (2X)

6. Blot off excess around sections.

7. Blocking solution:

20% donkey serum for 10 minutes.

Wipe slides but DO NOT WASH.

8. Primary antibody or negative control:

Primary (or negative) for overnight.

9. Repeat steps 5 and 6.

10. Secondary antibody.

Secondary antibody for 60 minutes.

11. Repeat steps 5 and 6.

12. PAP "complex".

PAP complex for 60 minutes.

13. Substrate solution:

While waiting for step 13 to complete, prepare substrate solution in provided mixing vial.

14. Repeat steps 5 and 6.

17. Visualization (coloring step):

Substrate solution for 10 minutes, check under microscope for extent of colorization.

Adjust time accordingly.

18. Termination of colorization:

Rinse in distilled water for 3 minutes.

19. Counterstain (optional):

Gill No. 3 hematoxylin solution for 1 minute.

20. Rinse in distilled water.

21. Wash in running tap for 3 minutes.

22. Mount with Aquamount and coverslip.

NOTE:

1. DO NOT allow slides to dry out between steps, will cause excess background staining.
2. AEC oxidation light sensitive, store slides in dark, best, else fading of stain may occur.
3. AEC also alcohol soluble, so make sure counterstain water-based and mounting media water-based.

A3: Immunohistochemical Protocols

α-Smooth Muscle Actin Immunohistochemical Protocol for New Zealand White Rabbit Achilles Tendon

FIXATION: Formalin

TECHNIQUE: paraffin embedded, sectioned at 6-8 μm

SOLUTIONS:

Phosphate buffered saline (pH 7.4) (Wash solution and diluent)

Phosphate buffered saline (Sigma cat# P3813)	1 pkg
Distilled water	to 1000 ml

0.1% Trypsin (Digestion)

Trypsin (Sigma cat# T8128)	0.01 gms
Phosphate buffered Saline	10 ml

3% Hydrogen Peroxide (Endogenous quench)

30% Hydrogen peroxide	1 ml
Distilled water	9 ml

20% Goat serum (Blocking Solution)

Goat normal sera (Sigma cat# G9023)	0.2 ml
Phosphate buffered saline	0.8 ml

Alpha smooth muscle actin kit (Stainin kit)

Sigma cat# IMMH-2

Gill No. 3 Hematoxylin Solution (counterstain)

Sigma cat# GHS-3-16

1% Mouse Serum (Negative control)

Mouse normal sera (Sigma cat# M5905)	0.1 ml
Phosphate buffered saline	10 ml

STAINING PROCEDURE:

1. Deparaffinize and rehydrate to PBS:

xylene	2 minutes	2X
100% EtOH	1 minute	2X
95% EtOH	1 minute	
80% EtOH	1 minute	
70% EtOH	1 minute	
PBS	5 minute	

2. Bouin Mordant (Optional):

Soak slides in Bouin fixative (Sigma cat# HT10-1-32) solution for overnight. May enhance the intensity of the stain. Troxel noted that Bouin fixed tissue stained more intensely than formalin fixed tissue.

Rinse under tap water until yellow color disappears.

3. Wipe off excess liquid around sections.
Circle sections with PAP pen (Polysciences).

4. Digestion:

0.1% trypsin solution for 60 minutes (humidifed chamber).

5. Wash in PBS for 3 minutes. (2X)

6. Blot off excess around sections.

7. Endogenous peroxide quench:

3% H_2O_2 for 5 minutes.

8. Repeat steps 5 and 6.

9. Blocking solution:

20% goat serum for 10 minutes.

Wipe slides but DO NOT WASH.

10. Primary antibody or negative control:

Primary (or negative) for 1 hours.

10. Repeat steps 5 and 6.

12. Secondary antibody.

Biotinylated secondary antibody for 20 minutes.

13. Repeat steps 5 and 6.

14. Biotin-avidin "complex":
    ExtrAvidin-peroxidase labeled reagent for 20 minutes.

15. Substrate solution:
    While waiting for step 13 to complete, prepare substrate solution in provided mixing vial.

16. Repeat steps 5 and 6.

17. Visualization (coloring step):
    Substrate solution for 15 minutes, check under microscope for extent of colorization. Adjust time accordingly.

18. Termination of colorization:
    Rinse in distilled water for 3 minutes.

19. Counterstain (optional):
    Gill No. 3 hematoxylin solution for 1 minute.

20. Rinse in distilled water.

21. Wash in running tap for 3 minutes.

22. Mount with Aquamount and coverslip.

NOTE:
1. DO NOT allow slides to dry out between steps, will cause excess background staining.
2. AEC oxidation light sensitive, store slides in dark, best, else fading of stain may occur.
3. AEC also alcohol soluble, so make sure counterstain water-based and mounting media water-based.

A4: Ultrastructural Staining Protocol

Double staining with uranyl acetate and lead citrate

FIXATION: Post-fixation in 1% osmium tetroxide

TECHNIQUE: epon-embedded, sectioned to ultra-thin (70 nm), affixed to 200 mesh copper grids

SOLUTIONS:

2% Uranyl acetate, aqueous

Uranyl acetate	2 gms
Distilled water	100 ml

Light sensitive. Keep covered and refrigerated.

Reynolds's lead citrate

Lead nitrate	1.33 gms
Sodium citrate	1.76 gms
Distilled water	30 ml

Mix in 50 ml flask for 20 minutes. Add 8.0 ml 1N NaOH and dilute to 50 ml with distilled water. Mix by inversion. Solution ready when completely clear. pH: 12.0
Keep refrigerated. Let come to room temperature before use. Filter before use.

STAINING PROCEDURE:

1. Cover bottom of two glass petri dish with parafilm.
2. Place drops of uranyl acetate onto one of the petri dishes.
3. Place grid with section side down on drop of uranyl acetate. Cover. Protect stain from light by covering petri dish with light-tight box. Stain for 10 minutes.
4. Meanwhile, place drops of filtered lead citrate solution onto petri dish. Add pellets of sodium hydroxide to petri dish to capture released CO_2 gas. Note: Discard first filtered drop.
5. Wash grids in distilled water. Three changes.
6. Blot dry grids on filter paper before proceeding to lead citrate stain.
7. Stain grid with lead citrate solution for 3-5 minutes.
8. Wash grids in distilled water. Three changes.

9. Blot dry on filter paper.
10. Store until ready to view.

References

1. Amadio, P.C., "Tendon and Ligament"; pp. 384-395 in *Wound Healing: Biochemical and Clinical Aspect.* Edited by I. K. Cohen, *et al.* W. B. Saunders Co, Philadelphia, PA, 1992.

2. Amis, A.A., Campbell, J.R., Kempson, S.A., and Miller, J.H., "Comparison of the Structure of Neotendons Induced by Implantation of Carbon or Polyester Fibres," *J Bone Joint Surg*, **66-B** 131-139, 1984.

3. Andreeff, I., Dimoff, G., and Metschkarski, S., "A Comparative Experimental Study on Transplantation of Autogenous and Homogenous Tendon Tissue," *Acta Orthopaedica Scandinavica*, **38** 35-44, 1967.

4. Baur, P.S., Barratt, G., Linares, H.A., Dobrkovsky, M., De La Houssaye, A.J., and Larson, D.L., "Wound Contraction, Scar Contractures and Myofibroblasts: A Classical Case Study," *J Trauma*, **18** [1] 8-22, 1978.

5. Bellows, C.G., Melcher, A.H., and Aubin, J.E., "Contraction and organization of Collagen Gels by Cells Cultured from Periodontal Ligament, Gingiva, and Bone Suggest Functional Differences between Cell Types," *J Cell Sci*, **50** 299-314, 1981.

6. Bellows, C.G., Melcher, A.H., Bhargava, U., and Aubin, J.E., "Fibroblasts Contracting Three-Dimensional Collagen Gels Exhibit Ultrastructure Consistent with Either Contraction of Protein Secretion.," *Journal of Ultrastructural Research*, **78** 178-192, 1982.

7. Best, T.M., Collins, A., Lilly, E.G., Seaber, A.V., and Murrell, G.A.C., "A Functional, Morphological and Biomechanical Study of the Repair Process in Rat Achilles Tendon," *Med Sci Sports Exer*, **23** S139, 1991.

8. Buck, R.C., "Regeneration of Tendon," *Journal of Pathology and Bacteriology*, **66** 1-18, 1953.

9. Buckwalter, J.A., Maynard, J.A., and Vailas, A.C., "Skeletal Fibrous Tissue: Tendon, Joint Capsule, and Ligament"; pp. 387-405 in *The Scientific Basis of Orthopedics.* Edited by J. A. Albright and R. A. Brand. Appleton & Lange, Norwalk, Conn, 1987.

10. Bugg, E.I. and Boyd, B.M., "Repair of Neglected Rupture or Laceration of the Achilles Tendon," *Clin Orthop Relat Res*, **56** 73-75, 1968.

11. Burke, J.F., Yannas, I.V., Quinby, W.C., Bondoc, C.C., and Jung, W.K., "Successful Use of a Physiologically Acceptable Artificial Skin in the Treatment on Extensive Burn Injury," *Ann Surg*, **194** 413-428, 1981.

12. Butler, D.L., Grood, E.S., and Noyes, F.R., "Biomechanics of Ligaments and Tendons"; pp. 125-181 in *Exercise and Sports Science Review.* Edited by R. S. Hutton. Franklin Institute Press, Washington, 1978.

13. Cao, Y., Vacanti, J.P., Ma, X., Paige, K.T., Upton, J., Chowanski, Z., Schloo, B., Langer, R., and Vacanti, C.A., "Generation of Neo-Tendon Using Synthetic Polymers Seeded with Tenocytes," *Transplant Proc*, **26** [6] 3390-3391, 1994.

14. Chamberlain, L.J., "Long Term Functional and Morphological Evaluation of Peripheral Nerves Regenerated through Degradable Collagen Implants"; Master of Science Thesis. Massachusetts Institute of Technology, 1996.

15. Chang, A.S. and Yannas, I.V., "Peripheral Nerve Regeneration"; pp. 125-126 in *Neuroscience (Supplement 2 to the Encyclopedua of Neuroscience).* Edited by B. Smith and G. Adelman. Birkhaüser, Boston, 1992.

16. Chang, A.S.-P., "Electrophysiological Recovery of Peripheral Nerves Regenerated by Biodegradable Polymer Matrix"; Master of Science Thesis. Massachusetts Institute of Technology, 1988.

17. Cheal, E.J., Snyder, B.D., Nunamaker, D.M., and Hayes, W.C., "Trabecular Bone Remodeling around Smooth and Porous Implants in an Equine Patellar Model," *J. Biomechanics*, **20** 1121-1134, 1987.

18. Chen, E.H.-Y., "The Effect of Porosity and Crosslinking of a Collagen Based Artificial Skin on Wound Healing"; Master of Science Thesis. Massachusetts Institute of Technology, 1982.

19. Clancy, W.G., Neidhart, D., and Brand, R.L., "Achilles Tendonitis in Runners: A Report of Five Cases," *Am J Sports Med*, **4** [2] 46-57, 1976.

20. Comnimou, M. and Yannas, I.V., "Dependence of Stress-Strain Nonlinearity of Connective Tissue on the Geometry of Collagen Fibers," *Journal of Biomechanics*, **9** 427-433, 1976.

21. Dagalakis, N., Flink, J., Stasikelis, P., Burke, J.F., and Yannas, I.V., "Design of an Artificial Skin. Part III. Control of Pore Structure," *J Biomed Mater Res*, **14** 511-528, 1980.

22. Dale, W.C. and Baer, E., "Fibre-buckling in Composite Systems: A Model for the Ultrastructure of Uncalcified Collagen Tissues," *Journal of Material Science*, **9** 369-382, 1974.

23. Davis, P.A., Huang, S.J., Ambrosio, L., Ronca, D., and Nicolais, L., "A Biodegradable Composite Artifical Tendon," *Journal of Materials Science: Materials in Medicine*, **3** 359-364, 1992.

24. de Medinaceli, L., Freed, W.J., and Wyatt, R.J., "An Index on the Functional Condition on Rat Sciatic Nerve Based on Measurements Made from Walking Tracks," *Exp Neurol*, **77** 634-643, 1982.

25. de Quervain, M.R., "Crystallization of Water, A Review"; pp. 3-16 in *Freeze Drying and Advanced Food Technology.* Edited by S. A. Goldblith, *et al.* Academic Press Inc, New York, 1975.

26. Derwin, K.A. and Soslowsky, L.J., "Tendon Fascicle Mechanical Properties: A Study Toward Elucidating Structure-Function Relationships in a Transgenic Model"; pp. 28-5, 42nd Annual Meeting, Orthopedic Research Society (Atlanta, Georgia, 1996).

27. Diamant, J., Keller, A., Baer, E., Litt, M., and Arridge, R.G.C., "Collagen; Ultrastructure and its Relation to Mechanical Properties as a Function of Ageing," *Proc. R. Soc. B.*, **180** 293-315, 1972.

28. Doillon, C.J., Silver, F.H., and Berg, R.A., "Fibroblast Growth on a Porous Collagen Sponge Containing Hyaluronic Acid and Fibronectin," *Biomaterials*, **8** 195-200, 1987.

29. Doillon, C.J., Wasserman, A.J., Berg, R.A., and Silver, F.H., "Behaviour of Fibroblasts and Epidermal Cells Cultivated on Analoques of Extracellular Matrix," *Biomaterials*, **9** 91-96, 1988.

30. Dunn, M.G., Liesch, J.B., Tiku, M.L., and Zawadsky, J.P., "Development of Fibroblast-seeded Ligament Analogs for ACL Reconstruction," *J Biomed Mater Res*, **29** 1363-1371, 1995.

31. Dyer, R.F. and Enna, C.D., "Ultrastructural Features of Adult Human Tendon," *Cell Tissue Res*, **168** 247-259, 1976.

32. Enwemeka, C.S., "Inflammation, Cellularity, and Fibrillogenesis in Regeneration Tendon: Implications for Tendon Rehabilitation," *Phys Ther*, **69** 816-825, 1989.

33. Enwemeka, C.S., "Membrane-bound Intracellular Collagen Fibrils in Fibroblasts and Myofibroblasts of Regenerating Rabbit Calcaneal Tendons," *Tissue and Cell*, **23** [2]. 173-190, 1991.

34. Enwemeka, C.S., Spielholz, N.I., and Nelson, A.J., "The Effect of Early Functional Activities on Experimentally Tenotomized Achilles Tendons in Rat," *Am J Phys Med Rehabil*, **67** 264-269, 1988.

35. Faryniarz, D.A., Chaponnier, C., Gabbiani, G., Yannas, I.V., and Spector, M., "Myofibroblasts in the Healing Lapine Medial Collateral Ligament: Possible Mechanisms of Contraction," *J Orthop Res*, **14** 228-237, 1996.

36. Fernando, N.V.P. and Movat, H.Z., "Fibrillogenesis in Regenerating Tendon," *Laboratory Investigations*, **12** 214-229, 1963.

37. Flynn, J.E. and Graham, J.H., "Healing of Tendon Wounds," *American Journal of Surgery*, **109** 315-324, 1965.

38. Frank, C., Amiel, D., Woo, S.L.-Y., and Akeson, W., "Normal Ligament Properties and Ligament Healing," *Clin Orthop Rel Res*, **196** 15-25, 1985.

39. Frank, C., Bray, D., Rademaker, A., Chrusch, C., Sabiston, P., Bodie, D., and Rangayyan, R., "Electron Microscopic Quantification of Collagen Fibril Diameters in the Rabbit Medial Collateral Ligament: a Baseline for Comparison," *Connect Tissue Res*, **19** 11-25, 1989.

40. Frank, C., MacFarlane, B., Edwards, P., Rangayyan, R., Liu, Z.-Q., Walsh, S., and Bray, R., "A Quantitative Analysis of Matrix Alignment in Ligament Scars: A Comparison of Movement Versus Immobilization in an Immature Rabbit Model," *J Orthop Res*, **9** [2] 219-227, 1991.

41. Frank, C., McDonald, D., Bray, D., Bray, R., Rangayyan, R., Chimich, D., and Shrive, N., "Collagen Fibril Diameters in the Healing Adult Rabbit Medial Collateral Ligament," *Connect Tissue Res*, **27** 251-263, 1992.

42. Frank, C., Schachar, N., and Dittrich, D., "Natural History of Healing in the Repaired Medial Collateral Ligament," *J Ortho Res*, **1** 179-188, 1983.

43. Frank, C., Woo, S.L.-Y., Amiel, D., Harwood, F., Gomez, M., and Akeson, W., "Medial Collateral Ligament Healing: A multidisciplinary assessment in rabbits," *Am J Sports Med*, **11** [6] 379-389, 1983.

44. Frank, C.B., Shrive, N.G., and McDonald, D.B., "Collagen Fibril Diameters in Ligament Scars: a Long Term Assessment"; pp. 51-9, 42nd Annual Meeting, Orthopaedic Research Society (Atlanta, Georgia, 1996).

45. Freed, L.E., Marquis, J.C., Nohria, A., Emmanual, J., Mikos, A.G., and Langer, R., "Neocartilage Formation in vitro and in vivo Using Cells Cultured on Synthetic Biodegradable Polymers," *J Biomed Mater Res*, **27** 11-23, 1993.

46. Freed, L.E., Marquis, J.C., Vunjak-Novakovic, G., Emmanual, J., and Langer, R., "Composition of Cell-Polymer Cartilage Implants," *Biotechnology and Bioengineering*, **43** 605-614, 1994.

47. Freed, L.E. and Vunjak-Novakovic, G., "Cultivation of Cell-Polymer Tissue Constructs in Simulated Microgravity," *Biotechnology and Bioengineering*, **46** 306-313, 1995.

48. Freed, L.E., Vunjak-Novakovic, G., Biron, R.J., Eagles, D.B., Lesnoy, D.C., Barlow, S.K., and Langer, R., "Biodegradable Polymer Scaffolds for Tissue Engineering," *Bio/Technology*, **12** 689-693, 1994.

49. Freshney, R.I., *Culture of Animal Cells: A Manual of Basic Technique.*, 2nd ed. pp. 61-62 Wiley-Liss Inc., New York, NY, 1987.

50. Frey, J., Chamson, A., Raby, N., and Rattner, A., "Collagen Bioassay by the Contraction of Fibroblast-populated Collagen Lattices," *Biomaterials*, **16** [2] 139-143, 1995.

51. Garner, W.L., McDonald, J.A., Koo, M., Kuhn, C., and Weeks, P.M., "Identification of the Collagen-Producing Cells in Healing Flexor Tendons," *Plastic Recon Surg*, **83** [5] 875-879, 1989.

52. Gelberman, R., Goldberg, V., An, K.-N., and Banes, A., "Tendon"; pp. 5-40 in *Injury and Repair of the Musculoskeletal Soft Tissue.* Edited by S. L.-Y. Woo and J. A. Buckwalter. American Academy of Orthopaedic Surgeons, Park Ridge, IL, 1988.

53. Gelberman, R.H., Berg, J.S.V., Lundborg, G.N., and Akeson, W.H., "Flexor Tendon Healing and Restoration of the Gliding Surface: An Ultrastructural Study," *J Bone Joint Surg*, **65A** [1] 70-80, 1983.

54. Gleason, T.F., Barmada, R., and Ghosh, L., "Can Carbon Fiber Implants Substitute for Collateral Ligament?," *Clinical Orthopaedic and Related Research*, **191** 275-280, 1984.

55. Goldblith, S.A., Rey, L., and Rothmayr, W.W., Eds., *Freeze Drying and Advanced Food Technology* (Academic Press, London, 1975).

56. Goldstein, J.D., Tria, A.J., Zawadsky, J.P., Kato, Y.P., Christiansen, D., and Silver, F.H., "Development of a Reconstituted Collagen Tendon Prosthesis," *Journal of Bone Joint Surgery*, **71-A** [8] 1183-1191, 1989.

57. Gonzalez, R.I., "Experimental Tendon Repair Within the Flexor Tunnel: Use of Polyethylene Tubes for Improvement of Functional Results in the Dog," *Surgery*, **26** 181-198, 1949.

58. Gown, A.M., "The Mysteries of the Myofibroblast (Partially) Unmasked," *Laboratory Investigation*, **63** [1] 1-3, 1990.

59. Gray, T., "Quantitation in Histopathology"; pp. 641-672 in *Theory and Practice of Histological Techniques*. Edited by J. D. Bancroft and A. Stevens. Churchill Livingstone, New York, 1996.

60. Heimbach, D., Luterman, A., Burke, J., Cram, A., Herndon, D., Hunt, J., Jordan, M., McManus, W., Solem, L., Warden, G., and Zawacki, B., "Artifical Dermis for Major Burns: A Multi-Center Randomized Clinical Trail," *Ann Surg*, **208** 313-320, 1988.

61. Hooper, G., Davies, R., and Tothill, P., "Blood Flow and Clearance in Tendons: Studies with Dogs," *J Bone Joint Surg*, **66-B** 441-443, 1984.

62. Howard, C.B., McKibbin, B., and Rális, Z.A., "The Use of Dexon as a Replacement for the Calcaneal Tendon in Sheep," *Journal of Bone Joint Surgery*, **67-B** [2] 313-316, 1985.

63. Howard, C.B., Winston, I., Bell, W., Mackie, I., and Jenkins, D.H.R., "Late Repair of the Calcaneal Tendon with Carbon Fibre," *J Bone Joint Surg*, **66-B** 206-208, 1984.

64. Ippolito, E., Natali, P.G., Postacchini, F., Accinni, L., and DeMartino, C., "Ultrastructure and Immunochemical Evidence of Actin in the Tendon Cells," *Clin Orthop Relat Res*, **126** 282-284, 1977.

65. Ippolito, E., Natali, P.G., Postacchini, F., Accinni, L., and Martino, C.D., "Morphological, Immunochemical, and Biochemical Study of Rabbit Achilles Tendon at Various Ages," *J Bone Joint Surg*, **62-A** [4] 583-598, 1980.

66. Irving, H., "The Effect of Freeze Drying Temperature on Pore Size in Collagen-GAG Artifical Skin"; Bachelor of Science Thesis. Massachusetts Institute of Technology, 1986.

67. Kastelic, J., Galeski, A., and Baer, E., "The Multicomposite Structure of Tendon," *Connect Tissue Res*, **6** 11-23, 1978.

68. Kato, Y.P., Dunn, M.G., Zawadsky, J.P., Tria, A.J., and Silver, F.H., "Regeneration of Achilles tendon with a Collagen Tendon Prosthesis: Results of a One-year Implantation Study," *J Bone Joint Surg*, **73-A** [4] 561-574, 1991.

69. Kato, Y.P. and Silver, F.H., "Formation of Continuous Collagen Fibres: Evaluation of Biocompatibility and Mechanical Forces," *Biomaterials*, **11** 169-175, 1990.

70. Kessler, I., "The "Grasping" Technique for Tendon Repair," *Hand*, **5** 253-255, 1973.

71. Ketchum, L.D., "Tendon Healing"; pp. 122-153 in *Fundamentals of Wound Management in Surgery: Selected Tissues.* Chirugecom, Inc., New Jersey, 1977.

72. Kleinert, H.E., Schepel, S., and Gill, T., "Flexor Tendon Injuries," *Surg Clin North Am,* **61** 267-286, 1981.

73. Komanowsky, M., "Production of Comminuted Collagen for Novel Applications," *J Am Leather Chem,* **69** 410-411, 1974.

74. Leitner, A., Voigt, C., and Rahmanzadeh, R., "Treatment of Extensive Aseptic Defects in Old Achilles Tendon Ruptures: Methods and Case Reports," *Foot and Ankle,* **13** 176-180, 1992.

75. Litsky, A.S. and Spector, M., "Biomaterials"; pp. 447-486 in *Orthopaedic Basic Science.* Edited by S. R. Simon. American Academy of Orthopaedic Surgeons, Park Ridge, IL, 1994.

76. Loree, H., "A Freeze-Drying Process for Fabrication of Polymeric Bridges for Peripheral Nerve Regeneration"; Master of Science Thesis. Massachusetts Institute of Technology, 1988.

77. Lui, S.H., Yang, R.-S., Al-Shaikh, R., and Lane, J.M., "Collagen in Tendon, Ligament, and Bone Healing: A Current Review," *Clin Orthop Relat Res,* **318** 265-278, 1995.

78. Manske, P.R., Gelberman, R.H., Berg, J.S.V., and Lesker, P.A., "Intrinsic Flexor-Tendon Repair," *J Bone Joint Surg,* **66-A** [3] 385-396, 1984.

79. Manske, P.R. and Lesker, P.A., "Histologic Evidence of Intrinsic Flexor Tendon Repair in Various Experimental Animals," *Clinical Orthopaedic and Related Research,* **182** 297-304, 1984.

80. Mason, M.L. and Allen, H.S., "The Rate of Healing of Tendons. An Experimental Study of Tensile Strength," *Ann Surg,* **113** 424-459, 1941.

81. Mass, D.P. and Tuel, R.J., "Participation of Human Superficialis Flexor Tendon Segments in Repair In Vitro," *J Orthopaedic Research,* **8** 21-34, 1990.

82. Matthews, P. and Richards, H., "The Repair Potential of Digital Flexor Tendon after Repair," *J Bone Joint Surg,* **58-B** 230-236, 1974.

83. Maugh, T.H.I., "A New Treatment for Burn Victims," *SCI,* **217** 1982.

84. McGaw, T., "The Effect of Tension on Collagen Remodelling By Fibroblasts: A Stereological Ultrastructural Study," *Connective Tissue Research,* **14** 229-235, 1986.

85. McMaster, W.C., Kouzelos, J., Liddle, S., and Waugh, T.R., "Tendon Grafting with Glutaraldehyde Fixed Material," *J Biomed Mater Res,* **10** 259-271, 1976.

86. Meislin, R.J., Wiseman, D.M., Alexander, H., Cunningham, T., Linsky, C., Carlstedt, C., Pitman, M., and Casar, R., "A Biomechanical Study of Tendon Adhesion Reduction Using a Biodegradable Barrier in a Rabbit Model," *Journal of Applied Biomaterials,* **1** 13-19, 1990.

87. Mendes, D.G., Angel, D., Grishkan, A., and Boss, J., "Histological Response to Carbon Fibre," *J Bone Joint Surg*, **67-B** 645-649, 1985.

88. Michaeli, D. and McPherson, M., "Immunologic Study of Artificial Skin Used in the Treatment of Thermal Injuries," *J Burn Care Rehabil*, **11** 21-26, 1990.

89. Murrell, G.A.C., III, E.G.L., Goldner, R.D., Seaber, A.V., and Best, T.M., "Effects of Immobilization on Achilles Tendon Healing in a Rat Model," *J Orthop Res*, **12** 582-591, 1994.

90. Murrell, G.A.C., Lilly, E.G., Davies, H., Best, T.M., Goldner, R.D., and Seaber, A.V., "The Achilles Functional Index," *J Orthop Res*, **10** 398-404, 1992.

91. Nystrom, B. and Holmlund, D., "Separation of Tendon Ends after Suture of Achilles tendon," *Acta Orthop Scand*, **54** 620-?, 1983.

92. Orgill, D.P., "The Effects of an Artificial Skin on Scarring and Contraction in Open Wounds"; Doctor of Philosophy Thesis. Massachusetts Institute of Technology, 1983.

93. Parry, D.A.D., Barnes, G.R.G., and Craig, A.S., "A Comparison of the Size Distribution of Collagen Fibrils in Connective Tissues as a Function of Age and a Possible Relation between Fibril Size Distribution and Mechanical Properties," *Proceeding of the Royal Society of London B*, **203** 305-321, 1978.

94. Parry, D.A.D. and Craig, A.S., "Growth and Development of Collagen Fibrils in Connective Tissue"; pp. 34-64 in *Ultrastructure of the Connective Tissue Matrix.* Edited by A. Ruggeri and P. M. Motta. Martinus Nijhoff Publishers, Boston, MA, 1984.

95. Parry, D.A.D., Craig, A.S., and Barnes, G.R.G., "Tendon and Ligament from the horse: an Ultrastructural Study of Collagen Fibrils and Elastic Fibres as a Function of Age," *Proceeding of the Royal Society of London B*, **203** 293-303, 1978.

96. Polysciences, Warrington, PA, JB-4 Embedding Kit Data Sheet No. 123B, 1985.

97. Polysciences, Warrington, PA, Poly/Bed 812 Embedding Media/ DMP-30 Data Sheet #233, 1995.

98. Porter, D.A. and Easterling, K.E., *Phase Transformations in Metals and Alloys.*, ed. Van Nostrand Reinhold (UK) Co. Ltd, Berkshire, England, 1981.

99. Postacchini, F., Accinni, L., Natali, P.G., Ippolito, E., and DeMartino, C., "Regeneration of Rabbit Calcaneal Tendon: A Morphological and Immunochemical Study," *Cell Tissue Res*, **195** 81-97, 1978.

100. Postacchini, F., Natali, P.G., Accinni, L., Ippolito, E., and de Martino, C., "Contractile Filaments in Cells of Regenerating Tendon," *Experimentia*, **3** 957-959, 1977.

101. Potenza, A.D., "Tendon Healing within the Flexor Digital Sheath of the Dog," *J Bone Joint Surg*, **44A** 49-64, 1962.

102. Potenza, A.D., "Concepts of Tendon Healing and Repair"; pp. 18-47 in *Symposium on Tendon Surgery in the Hand.* Edited by American Academy of Orthopaedic Surgeons. CV Mosby Co, St. Louis, 1975.

103. Puddu, G., Ippolito, E., and Postacchini, F., "A Classification of Achilles Tendon Disease," *Am J Sports Med*, **4** [4] 145-150, 1976.

104. Ramappa, A.J., "A Novel Implant for Articular Cartilage Regeneration"; M.D. degree with Honor Thesis. Harvard Medical School, 1996.

105. Rueger, J.M., Siebert, H.R., Wagner, K., and Pannike, A., "Longterm Implantation of a Polyethelene Ligament/ Tendon Allograft in Sheep. Mechanical and Histological Studies"; pp. 135-140 in *Biological and Biomechanical Performance of Biomaterials.* Edited by P. Christel, *et al.* Elsevier Science Publishers B. V., Amsterdam, 1986.

106. Russell, J.E. and Manske, P.R., "Collagen Synthesis During Primate Flexor Tendon Repair In Vitro," *J Orthop Res*, **8** 11-20, 1990.

107. Salamon, A. and Hamori, J., "Present State of Tendon Regeneration. Light and Electron Microscopic Studies of the Regeneration Tendon of the Rat," *Acta Morph Acad Sci Hung [Tomus]*, **14** 7-24, 1966.

108. Schuberth, J.M., "Management of Achilles Tendon Trauma"; pp. 191-218 in *Foot and Ankle Trauma.* Edited by Barry L. Scurran. Churchill Livingston, Inc., New York, 1989.

109. Schuberth, J.M., Dockery, G.L., and McBride, R.E., "Recurrent Rupture of the Tendo Achillis," *J Am Podiatry Assoc*, **74** 157-162, 1984.

110. Shieh, S.-J., Zimmerman, M.C., and Parsons, J.R., "Preliminary Characterization of Bioresorbable and Nonresorbable Synthetic Fibers for the Repair of Soft Tissue Injuries," *J Biomed Mater Res*, **24** 789-808, 1990.

111. Sigma, St. Louis, MO, Alpha-smooth Muscle Actin Kit Instructions, 1996.

112. Skalli, O., Pelte, M.-F., Peclet, M.-C., Gabbiani, G., Gugliotta, P., Bussolati, G., Ravazzola, M., and Orci, L., "α-Smooth Muscle Actin, a Differentiation Marker of Smooth Muscle Cells, Is Present in Microfilamentous Bundles of Pericytes," *J Histochem Cytochem*, **37** [3] 315-321, 1989.

113. Skalli, O., Ropraz, P., Trzeciak, A., Benzonana, G., Gillessen, D., and Gabbiani, G., "A Monoclonal Antibody against α-Smooth Muscle Actin: A New Probe for Smooth Muscle Differentiation," *J Cell Biol*, **103** [6, Pt. 2] 2787-2796, 1986.

114. Skalli, O., Schürch, W., Seemayer, T., Lagacé, R., Montandon, D., Pittet, B., and Gabbiani, G., "Myofibroblasts from Diverse Pathologic Settings are Heterogeneous in Their Content of Actin Isoforms and Intermediate Filament Proteins," *Laboratory Investigation*, **60** [2] 275-285, 1989.

115. Spector, M., Personal Communication, 1996.

116. Stein, S.R. and Luekens, C.A., "Methods and Rationale for Closed Treatment of Achilles Tendon Rupture," *Am J Sports Med*, **4** [4] 162-169, 1976.

117. Stern, R., McPherson, M., and Longaker, M.T., "Histologic Study of Artificial Skin Used in the Treatment of Full-Thickness Thermal Injury," *J Burn Care Rehabil*, **11** 7-13, 1990.

118. Stone, K.R., Rodkey, W.G., Webber, R., McKinney, L., and Steadman, J.R., "Meniscal Regeneration with Copolymeric Collagen Scaffolds: In Vitro and In Vivo Studies Evaluated Clinically, Histologically and Biochemically," *Am J Sports Med*, **20** 104-111, 1992.

119. Stone, K.R., Rodkey, W.R., Webber, R.J., McKinney, L., and Steadman, J.R., "Future Directions: Collagen-Based Protheses for Meniscal Regeneration," *Clinical Orthopaedic and Related Research*, **252** 129-135, 1990.

120. Takai, S., Woo, S.L.-Y., Horibe, S., Tung, D.K.-L., and Gelberman, R.H., "The Effects of Frequency and Duration of Controlled Passive Mobilization on Tendon Healing," *J Orthop Res*, **9** 705-713, 1991.

121. Tauro, J.C., Parsons, J.R., Ricci, J., and Alexander, H., "Comparison of Bovine Collagen Xenografts to Autografts in the Rabbit," *Clin Orthop Relat Res*, **266** 271-284, 1991.

122. Teuffer, A.P., "Traumatic Rupture of the Achilles Tendon," *Orthop Clin North Am*, **5** . 89-93, 1974.

123. Troxel, K.S., "Delay of Skin Wound Contractions by Porous Collagen-GAG Matrices"; Doctor of Philosophy Thesis. Massachusetts Institute of Technology, 1994.

124. Urbaniak, J.R., Cahill, J.D.J., and Mortenson, R.A., "Tendon Suturing Methods: Analysis of Tensile Strengths"; pp. 70-80 in *Symposium on Tendon Surgery in the Hand.* Edited by American Academy of Orthopaedic Surgeons. CV Mosby Co, St. Louis, 1975.

125. Wald, H.L., Sarakinos, G., Lyman, M.D., Mikos, A.G., Vacanti, J.P., and Langer, R., "Cell Seeding in Porous Transplantation Devices," *Biomaterials*, **14** [4] 270-278, 1993.

126. Wasserman, A.J., Kato, Y.P., Christiansen, D., Dunn, M.G., and Silver, F.H., "Achilles Tendon Replacement by a Collagen Fiber Prosthesis: Morphological Evaluation of Neotendon Formation," *Scanning Microscopy*, **3** 1183-1200, 1989.

127. Woo, S.L.-Y., An, K.-N., Arnoczky, S.P., Wayne, J.S., Fithian, D.C., and Myers, D.S., "Anatomy, Biology, and Biomechanics of Tendon, Ligament, and Meniscus"; pp. 45-87 in *Orthopaedic Basic Science.* Edited by S. R. Simon. American Academy of Orthopaedic Surgeons, Park Ridge, Il, 1994.

128. Woo, S.L.-Y., Gomez, M.A., Woo, Y.-K., and Akeson, W.H., "Mechanical Properties of Tendon and Ligaments: II. The Relationships of Immobilization and Exercise on Tissue Remodeling," *BRHLA*, **19** 397-408, 1982.

129. Yannas, I.V., "Regeneration of Skin and Nerve by Use of Collagen Templates"; pp. 87-115 in *Collagen: Volume III, Biotechnology.* Edited by M. E. Nimmi. CRC Press, Inc., Boca Raton, FL, 1988.

130. Yannas, I.V., "Certain Biological Implications of Mammalian Skin Regeneration by a Model Extracellular Matrix"; pp. 131-139 in Fidia Research Series, Vol. 18, *Cutaneous Development, Aging and Repair.* Edited by G. Abatangelo and J. M. Davidson. Liviana Press, Padavo, 1989.

131. Yannas, I.V., "Skin, Regeneration Templates"; pp. 317-334 in Vol. 15, *Encyclopedia of Polymer Science and Engineering.* John Wiley & Sons, Inc, , 1989.

132. Yannas, I.V., "Biologically Active Analogues of the Extracellular Matrix: Artificial Skin and Nerves," *Angew Chem Int Ed Engl*, **29** [1] 20-35, 1990.

133. Yannas, I.V. and Burke, J.F., "Design of an Artificial Skin. I. Basic Design Principles," *J Biomed Mater Res*, **14** 65-81, 1980.

134. Yannas, I.V., Burke, J.F., Gordon, P.L., Huang, C., and Rubenstein, R.H., "Design of an Artificial Skin. II. Control of Chemical Composition," *J Biomed Mater Res*, **14** 107-131, 1980.

135. Yannas, I.V., Burke, J.F., Orgill, D.P., and Skrabut, E.M., "Wound Tissue Can Utilize a Polymeric Template to Synthesize a Functional Extension of Skin," *SCI*, **215** 174-176, 1982.

136. Yannas, I.V., Lee, E., Orgill, D.P., Skrabut, E.M., and Murphy, G.F., "Synthesis and Characterization of a Model Extracellular Matrix that Induces Partial Regeneration of adult Mammalian Skin," *Proc Natl Acad Sci USA*, **86** 933-937, 1989.

137. Yannas, I.V., Orgill, D.P., Silver, J., Norregaard, T.V., Ervas, N.T., and Schoene, W.C., "Regeneration of Sciatic Nerve Across 15 mm Gap by Use of a Polymeric Template"; *Advances in Biomedical Polymers.* Edited by C.G. Gebelein. Plenum Publishing Corp., New York, 1987.